Information Flow In Black Hole Equilibration

by

Juan Hernandez

A thesis
presented to the University of Waterloo
in fulfillment of the
thesis requirement for the degree of
Doctor of Philosophy
in
Physics

Waterloo, Ontario, Canada, 2021

Examining Committee Membership

The following served on the Examining Committee for this thesis. The decision of the Examining Committee is by majority vote.

External Examiner:	Vijay Balasubramanian Professor, University of Pennsylvania
Supervisor:	Robert Myers Professor, Perimeter Institute for Theoretical Physics
Internal Member:	Robert Mann Professor, University of Waterloo
Internal-External Member:	Eduardo Martín-Martínez Associate Professor, University of Waterloo
Committee Member:	Alex Buchel Professor, University of Western Ontario

Author's Declaration

This thesis consists of material all of which I authored or co-authored: see Statement of Contributions included in the thesis. This is a true copy of the thesis, including any required final revisions, as accepted by my examiners.

I understand that my thesis may be made electronically available to the public.

Statement of contributions

This thesis is based on the following publications

- Chapter 2 is based on H. Z. Chen, Z. Fisher, J. Hernandez, R. C. Myers and S.-M. Ruan, *Information Flow in Black Hole Evaporation*, *JHEP* **03** (2020) 152 [1911.03402].
- Chapter 3 is based on H. Z. Chen, Z. Fisher, J. Hernandez, R. C. Myers and S.-M. Ruan, *Evaporating Black Holes Coupled to a Thermal Bath*, *JHEP* **01** (2021) 065 [2007.11658]

Both publications were projects conducted at Perimeter Institute under the supervision of Prof. Rob Myers. I contributed to the analytical and numerical calculations as well as the writing and editing of the articles.

In addition, the following work was produced as a Ph.D. at University of Waterloo but not included in the thesis

- M. Guo, J. Hernandez, R. C. Myers and S.-M. Ruan, *Circuit Complexity for Coherent States*, *JHEP* **10** (2018) 011 [1807.07677]
- A. Bernamonti, F. Galli, J. Hernandez, R. C. Myers, S.-M. Ruan and J. Simón, *First Law of Holographic Complexity*, *Phys. Rev. Lett.* **123** (2019) 081601 [1903.04511]
- E. Caceres, S. Chapman, J. D. Couch, J. P. Hernandez, R. C. Myers and S.-M. Ruan, *Complexity of Mixed States in QFT and Holography*, *JHEP* **03** (2020) 012 [1909.10557]
- A. Bernamonti, F. Galli, J. Hernandez, R. C. Myers, S.-M. Ruan and J. Simón, *Aspects of the first law of complexity*, *Journal of Physics A: Mathematical and Theoretical* **53** (2020) 294002
- J. Hernandez, R. C. Myers and S.-M. Ruan, *Quantum Extremal Islands Made Easy, Part III: Complexity on the brane*, *JHEP* **02** (2021) 173 [2010.16398]
- M. Ammon, S. Grieninger, J. Hernandez, M. Kaminski, R. Koirala, J. Leiber et al., *Chiral hydrodynamics in strong external magnetic fields*, *JHEP* **04** (2021) 078 [2012.09183]

Abstract

We study black hole evaporation and equilibration in the doubly holographic AEM^{4}Z model [1], which consists of a double sided black hole in JT gravity with holographic matter. At t=0, the right side of the black hole is coupled to a bath which consists of the same holographic matter on a half line. Beginning with the evaporation model in which the bath is at zero temperature, we compute the generalized entropy of the left black hole plus different bath intervals using the HRT prescription, and find the corresponding Page curves. By studying the requirements for the Page transition, we study the structure of how the black hole interior is encoded in the Hawking radiation during the evaporation process. We then repeat the analysis with finite temperature baths, and find the importance of the bath purification for reconstruction of the black hole interior past a certain critical temperature.

Acknowledgements

I would like to thank all the people who made this thesis possible.

To begin with, I want to thank my supervisor Rob Myers, for his mentoring, support, encouragement and patience. In addition to working with Rob, I am grateful for the collaborations I was able to be part of these past few years. Thanks to my collaborators Martin Ammon, Alice Bernamonti, Elena Caceres, Shira Chapman, Vincent Chen, Josiah Couch, Zachary Fisher, Federico Galli, Sebastian Grieninger, Minyong Guo, Matthias Kaminski, Roshan Koirala, Julian Leiber, Shan-Ming Ruan, Joan Simon and Jackson Wu. Special thanks to Shan-Ming Ruan with whom I collaborated in most of my projects during my stay at Perimeter, and to Vincent Chen and Zachary Fisher who were also involved in the research from which this thesis is based on.

Many thanks to my friends, family and loved ones for all their love an encouragement. Despite the distance I always felt your presence in my life. Special thanks to my mother Cristina for her unconditional love and unwavering support, and to my sister Sofia who is the strongest person I know and the embodiment of perseverance at the face of adversity. Many thanks to my wonderful friends for all the time and affection they have invested in me. Thanks also to all the new friends I made throughout my stay at Perimeter as well as at different conferences, workshops and schools.

Lastly, thanks to NSERC, the government of Ontario, Perimeter Institute and University of Waterloo for providing funding throughout my studies.

Table of Contents

List of Figures

List of Tables

Chapter 1

Introduction

Over the past few years, our understanding of the black hole information paradox has seen an explosion of progress thanks to exciting new tractable models of black hole evaporation and equilibration [1, 10, 11]. The black hole information paradox is a long standing puzzle in theoretical physics that arose when Hawking first discovered that black holes leak radiation due to quantum fluctuations [12]. Moreover, he calculated that the radiation emitted by a black hole during its evaporation is completely thermal. Hawking's results indicated that black hole evaporation appears to be non-unitary, in stark conflict with the fundamental assumptions of quantum mechanics [13]. This remained an open puzzle for decades, until these new tractable models were discovered and inspired new insights into the structure of information and geometry in quantum gravity. This progress naturally led to the exciting new topic of quantum extremal islands [1] and their relation to the ensemble interpretation of gravity [14, 15]. The goal of this thesis is to summarize some of the lessons that have been learned by studying holographic models of black hole evaporation and equilibration [1, 2, 3, 11].

The remainder of this chapter is organized as follows. We begin in section 1.1 with an introduction and motivation into the subject. In section 1.2, we review some of the necessary background material for the main topic of the thesis. Lastly, we summarize the results and outline the structure of the rest of the thesis in section 1.3.

1.1 From black holes and thermodynamics to information and geometry

Black holes are solutions to Einstein's equations that have a few interesting properties that stand out. One is the existence of a singularity at which the curvature of space-time geometry diverges. The second is an event horizon, which consists of a surface that encloses an inescapable region of space time and shields external observers from seeing the singularity. The first and simplest example of a black hole was discovered by Schwarzschild merely one year after Einstein published his theory of General Relativity. Over the years, more and more generalizations of black hole solutions have been found, adding charge and rotation to the black holes, being in space-times with non-zero cosmological constant, in different numbers of dimensions, and even as solutions of more exotic gravitational theories.

While black holes were originally considered merely a mathematical curiosity, with the advance of technology and improved observational tools, there is an ever growing catalog of real black holes that have been observed. The first indirect evidence of a real black hole was the galactic X-ray source Cygnus X-1 discovered in 1964 [16]. Cygnus X-1 is part of a binary system with the blue supergiant star HDE 226868. Further studies and observations led to it being widely accepted by the astronomical community as a black hole of around 21.2 solar masses [17]. The blue supergiant star provides material for an accretion disk around Cygnus X-1, and this matter falling into the black hole is what produces the large flux of X-rays observed. More recently, the new and exciting field of gravitational-wave astronomy has produced many observations of black hole mergers [18], and just two years ago the Event Horizon Telescope Collaboration produced the first direct image of a black hole: a supermassive black hole of around 6.5 billion solar masses at the center of the supergiant elliptical galaxy Messier 87 [19].

Theoretical studies of black holes have brought to light many interesting insights into quantum field theory in curved spacetime and quantum gravity. A well known example of this is Hawking radiation [12]. The natural space-time coordinates for a static observer far from the black hole are different from the natural coordinates for an observer freely falling though the event horizon. Asymptotically distant observers are in approximately flat spacetime, and the global Minkowski-like coordinates $t, \mathbf{x}$ agree with local rest frame coordinates. On the other hand, for observers close to the black hole, the curvature induced by this massive object distorts the geometry, and local rest frame coordinates agree instead with the Kruskal-Szekeres coordinates $\tilde{t}, \tilde{\mathbf{x}}$. The decomposition of quantum fields in terms of creation and annihilation operators will differ between the two observers, since it depends on the coordinates used. Thus, the *Kruskal vacuum* state for an observer falling though

the horizon is different from the *Boulware vacuum* for an observer far from the black hole. Moreover, by the equivalence principle, the quantum fields in the vicinity of a black hole are in the Kruskal vacuum, which appears to a distant observer as a thermal state. Indeed finding the relation between the two different sets of creation and annihilation operators, it is possible to show that the observer at rest far from the black hole sees particles with a thermal spectrum [20]

$$n(\omega) = \frac{\Gamma_l(\omega)}{\exp\frac{\omega}{T_H} \pm 1} \tag{1.1}$$

being emitted from the black hole. This emission is known as Hawking radiation. Of course, the choice of plus or minus above depends on whether the fields in question are fermions of bosons, and $\Gamma_l(\omega) < 1$ are greybody factors.

A complementary method to find that quantum fields in black hole backgrounds are in a thermal state is to consider regularity of the geometry at the event horizon. A typically spherically symmetric black hole metric with an event horizon at $r = r_h$ will have the following form

$$ds^2 = -f(r)dt^2 + g^{-1}(r)dr^2 + r^2 d\Omega_{d-2}^2\,, \tag{1.2}$$

where both $f(r)$ and $g(r)$ have a first order zero at $r = r_h$. Analytically continuing the metric to Euclidean space-time $\tau = it$ and switching to conical coordinates

$$\rho^2 = \frac{4(r - r_h)}{g'(r_h)}\,, \quad \phi = \frac{1}{2}\sqrt{g'(r_h)f'(r_h)}\tau\,, \tag{1.3}$$

leads to a metric of the form

$$ds^2 = \rho^2 d\phi^2 + d\rho^2 + r(\rho)^2 d\Omega_{d-2}^2 + \cdots\,, \tag{1.4}$$

where we have omitted higher powers of ρ^2. This metric has a conical defect at the event horizon $\rho = 0$ unless ϕ is periodic $\phi \sim \phi + 2\pi$. This in turn implies that the Euclidean time direction must have a period of $4\pi/\sqrt{f'(r_h)g'(r_h)}$, and any quantum fields in a black hole background must be periodic in the Euclidean time direction. The periodicity in Euclidean time corresponds to the quantum fields being at finite temperature with density matrix $\rho \propto \exp(-\beta H)$, with inverse temperature given by $\beta = 1/T = 4\pi/\sqrt{f'(r_h)g'(r_h)}$. The temperature found this way corresponds to the same Hawking temperature T_H calculated in the previous method.

The realization that black holes have a temperature led to interesting insights about what is now known as black hole thermodynamics [12, 20, 21, 22, 23, 24]. A lot of the properties of black holes can be summarized into four laws which have analogues in the corresponding four laws of thermodynamics.

- The zeroth law of black hole thermodynamics states that the surface gravity is constant over the event horizon of a stationary black hole, and is the analogue of thermal equilibrium in standard thermodynamics. This suggests that the surface gravity κ can be interpreted as an analogue of temperature, and indeed the Hawking temperature determined with the methods outlined above is given by $T_H = \frac{\kappa}{2\pi}$.

- The first law states energy conservation, and it relates the change in the mass of the black hole to the change in its area, angular momentum and charge. Among other things, this suggests the area of the event horizon is the analogue of the thermal entropy in standard thermodynamics. Calculating the relation between the change in horizon area and the change in the mass of the black hole fixes the Bekenstein-Hawking entropy as $S_{BH} = \frac{A}{4G}$.

- The second law states that the area of the event horizon can only increase, and further establishes a connection between the area of the event horizon and thermal entropy in standard thermodynamics. There is a generalization of the second law which states that the total entropy of a black hole plus matter system never decreases [25, 26].

- The third law is the analogue of Nernst law, and states that it is impossible to reduce the surface gravity to zero by a finite number of operations.

An interesting feature of black hole thermodynamics is that it relates the entropy of the black hole to its surface area, rather than its volume, as one might naively expect. This is remarkable in the context of the second law of black hole thermodynamics because it implies that there is an upper bound on the entropy of any system in a dynamical gravity theory, and in particular it is bounded by the surface area of a black hole that can be formed by that system [25, 26], independent of any other microscopic details! This remarkable observation is explained by the holographic principle [27, 28, 29]: that the description of a volume of space in a theory of quantum gravity can be thought of as encoded on the (lower-dimensional) boundary of the region. Moreover, the appearance of an entropy term in black hole thermodynamics inspired physicists to properly define and investigate entanglement entropy in quantum field theory and quantum gravity, and together with the concept of holography, led to breakthroughs in our understanding of the nature of space-time in quantum gravity.

A direct consequence of Hawking radiation is that black holes in vacuum will radiate away all of their energy and evaporate into a cloud of thermal radiation [23]. Strikingly, this outcome is independent of the initial state of matter from which the black hole was formed. This means that if one were to start with a pure state of matter that had then

collapsed to form a black hole, after the evaporation of the black hole one would end up with a mixed state of thermal gas. This contradicts one of the main assumptions of quantum mechanics: that time evolution is unitary, and therefore if one begins with a pure state, after time evolution the state should remain pure.

Another way to state this paradox relies on considering the information accessible by measuring the quantum state throughout this process. Before the collapse into a black hole, the state is in one of many possible quantum states with overall energy, charge and angular momentum which will match that of the black hole. Once it collapses to a black hole, by the no-hair theorem, the only parameters needed to characterize the state are the mass, charge and angular momentum of the black hole. After evaporation of the black hole, one is left with Hawking radiation in a grand canonical ensemble with the energy, charge and angular momentum determined by those of the black hole. Therefore, the microscopic details of the initial pure state have been somehow lost. This non-surjective mapping of initial states to final states during black hole formation and evaporation is in contradiction with the unitarity of quantum mechanics. This is because unitarity implies that given a complete set of information about a state on a Cauchy surface, it would be possible to evolve the state to the past or the future and recover all the information of the corresponding state on a different Cauchy surface. But since many initial states before the collapse to a black hole result in the same Hawking radiation after evaporation, it is clearly impossible to determine what initial state gave rise to the Hawking radiation by simply measuring the final state.

The black hole information paradox can be quantitatively described by considering the entropy of the Hawking radiation throughout the evaporation process [30, 31]. The original semiclassical calculation would yield a Hawking entropy curve which begins at zero and increases monotonically as more and more thermal quanta is radiated away from the black hole. The final state would have non-zero entropy, which is an indication that it is now in a mixed state. To recover a unitary evaporation process, the entropy of the Hawking radiation should follow a Page curve, which initially increases until a phase transition occurs and the entropy then begins to decrease back to zero. The time at which this transition occurs is called the Page time.

This surprising paradox has been an active area of investigation for the past few decades [13, 32, 33, 34, 35, 36, 37], and many exotic resolutions have been proposed: from black hole remnants, baby universes and explosions of information at the end of evaporation to the acceptance of the loss of information or the loss of the equivalence principle in the form of firewalls. An indirect resolution was provided by running with a holographic argument [27, 28, 29]. Inspired by the AdS/CFT correspondence (see section 1.2) it was suggested that the quantum gravitational system that undergoes collapse and evaporation

is encoded on, or dual to, a lower dimensional quantum theory at the boundary. Since the lower dimensional quantum theory at the boundary is a standard QFT, then by definition the time evolution is unitary, and information has to be somehow preserved. This line of argument suggests that something subtle was missing in the semiclassical derivations a la Hawking, and that careful considerations of other corrections would restore unitarity and bring a resolution to the paradox. Moreover, in the past couple of years, progress has been sparked through the discovery of tractable holographic models of black hole evaporation. The topic of this thesis is to summarize some of the work that has been done in this area through the use of these doubly holographic models. It is based on two papers [2, 3], which build on the original work [1, 10, 11] that sparked the recent progress in this area.

1.2 Background: holography and all that

In this section we give a quick review of some of the most important concepts needed to study the black hole plus bath models in chapters 2 and 3.

1.2.1 AdS/CFT

The Anti-de Sitter/Conformal Field Theory (AdS/CFT) correspondence [38] is the most well known and widely studied realization of the holographic principle, which states that the degrees of freedom of a gravitational theory in a given volume V are encoded in the boundary ∂V of said volume. This principle was inspired by the aforementioned Bekenstein bound on the entropy of any system in a gravitational theory [25, 26], which comes as a consequence of the second law of black hole thermodynamics [21]. The AdS/CFT correspondence relates gravitational theories in asymptotically AdS space to conformal field theories in one less dimension. We will state it in a "weak" form which, relates a classical supergravity theory to a strongly coupled CFT with many degrees of freedom. A "stronger" version of the AdS/CFT correspondence relates superstring theory or M-theory compactified in $AdS \times X$ with a CFT at general coupling and number of degrees of freedom. Here X is a compact geometry. As will be outlined below, the large number of degrees of freedom in the CFT corresponds to a small string coupling and a corresponding suppression of quantum fluctuations in the bulk. Furthermore, strong coupling in the CFT corresponds to a small string length and therefore leads to a suppression of stringy effects bulk theory. Therefore the "weak" version of the AdS/CFT correspondence follows from the "strong" version by applying a saddle point approximation in the presence of a large number of degrees of freedom and at strong coupling. Concretely, the "weak" AdS/CFT

correspondence relates the generating functional $W[\phi_0]$ for connected n-point functions of the CFT operators $\mathcal{O}$ with sources ϕ_0

$$e^{-W_{CFT}[\phi_0]} = Z_{CFT}[\phi_0] = \left\langle \exp\left(\int d^d x \, \phi_0(x) \mathcal{O}(x) \right) \right\rangle_{CFT} , \tag{1.5}$$

to an asymptotically AdS gravitational action $I_{grav}[\phi]$. That is, it states that $I_{grav}[\phi]$ is related to $W[\phi_0]_{CFT}$ by

$$W_{CFT}[\phi_0] = I_{grav}[\phi]\Big|_{\lim_{z\to 0} \phi(z,x) z^{\Delta - d} = \phi_0(x)} . \tag{1.6}$$

Here, Δ is the dimension of the CFT operator $\mathcal{O}$ and z is the extra holographic direction, such that the asymptotic boundary of AdS is located at $z = 0$. In words, the AdS/CFT correspondence identifies the CFT generating functional in eq. (1.5) with a classical on-shell action on asymptotic Anti-de Sitter subject to the boundary condition that the higher dimensional bulk fields ϕ have boundary values given by ϕ_0. Note that the correspondence stated in eq. (1.6) is a weak version of the AdS/CFT correspondence, which requires a CFT with many degrees of freedom and with strong coupling, which corresponds to a weak string coupling and small string length in the dual string theory, allowing for a saddle point approximation of the log of the string partition function into the classical supergravity action. The prototypical example of the AdS/CFT correspondence relates $\mathcal{N} = 4$ Super Yang-Mills theory with gauge group $SU(N)$ and coupling constant g_{YM} in four spacetime dimensions to type IIB superstring theory with string length l_s and string coupling constant g_s in $AdS_5 \times S^5$ with radius of curvature L. The parameters of these two theories are related by $g^2_{YM} = 2\pi g_s$ and $2g^2_{YM} N = L^4/l^4_s$. In this realization of the AdS/CFT correspondence, it is straightforward to see that the large number of degrees of freedom of the CFT_4 ($N \to \infty$) with fixed L/l_s directly leads to the suppression of quantum effects and allows for the saddle point approximation of the string partition function by a classical string action. Furthermore, at strong t'Hooft coupling $\lambda = g^2_{YM} N$, the stringy effects are also suppressed and one is left with the classical supergravity action on the right hand side of eq. (1.6).

1.2.2 (Holographic) entanglement entropy

The AdS/CFT correspondence relates many important quantities in between the two theories. A central concept studied on both sides of the holographic duality is that of entanglement entropy [39, 40, 41, 42, 43]. Entanglement entropy is a measure of entanglement

of a subset of degrees of freedom in a state. It corresponds to the von Neumann entropy of the reduced density matrix associated with that subset of degrees of freedom.

The von Neumann entropy of a state with density matrix ρ is given by

$$S_{vN} = -\mathrm{Tr}\left(\rho \log \rho\right) , \tag{1.7}$$

and it quantifies how mixed a state is. For example, for a pure state $\rho = |\Psi\rangle\langle\Psi|$, the von Neumann entropy vanishes, while for a maximally mixed state $\rho = \mathbf{I}/|\mathcal{H}|$, the von Neumann entropy is maximized, and is $S_{vN} = \log|\mathcal{H}|$. Here, $|\mathcal{H}|$ is the dimension of the Hilbert space $\mathcal{H}$ in which the state ρ is defined. More generally, any mixed state is given by the density matrix $\rho = \sum_n p_n |\Psi_n\rangle\langle\Psi_n|$ with $|\Psi_n\rangle \in \mathcal{H}$ and $\sum_n p_n = 1$, and the corresponding von Neumann entropy is

$$S_{vN} = -\sum_n p_n \log p_n \, . \tag{1.8}$$

For a given bipartition of the Hilbert space $\mathcal{H} = \mathcal{H}_{\mathcal{A}} \otimes \mathcal{H}_{\mathcal{A}^c}$, the reduced density matrix of the subsystem $\mathcal{A}$ is found by tracing out the degrees of freedom of its complement

$$\rho_{\mathcal{A}} = \mathrm{Tr}_{\mathcal{A}^c} \rho \, , \tag{1.9}$$

and the entanglement entropy of the subregion $\mathcal{A}$ is then

$$S_{\mathcal{A}} = -\mathrm{Tr}_{\mathcal{A}}\left(\rho_{\mathcal{A}} \log \rho_{\mathcal{A}}\right) . \tag{1.10}$$

A simple way to see that entanglement entropy is a measure of entanglement is to calculate it for a product state $|\Psi\rangle = |\Psi_{\mathcal{A}}\rangle \otimes |\Psi_{\mathcal{A}^c}\rangle$, in which there is no correlation between $\mathcal{A}$ and $\mathcal{A}^c$. That is, $\langle \mathcal{O}_{\mathcal{A}} \mathcal{O}_{\mathcal{A}^c}\rangle = \langle \mathcal{O}_{\mathcal{A}}\rangle \langle \mathcal{O}_{\mathcal{A}^c}\rangle$ for any two operators supported in $\mathcal{A}$ and $\mathcal{A}^c$ respectively, *i.e.,* $\mathcal{O}_{\mathcal{A}} = O_{\mathcal{A}} \otimes \mathbb{I}_{\mathcal{A}^c}$ and $\mathcal{O}_{\mathcal{A}^c} = \mathbb{I}_{\mathcal{A}} \otimes O_{\mathcal{A}^c}$, where $\mathbb{I}_{\mathcal{A}}$ is the identity operator in $\mathcal{H}_{\mathcal{A}}$ and similarly $\mathbb{I}_{\mathcal{A}^c}$ is the identity operator in $\mathcal{H}_{\mathcal{A}^c}$. For any product state, the subregion density matrix is pure and the entanglement entropy vanishes

$$\rho_{\mathcal{A}} = |\Psi_{\mathcal{A}}\rangle\langle\Psi_{\mathcal{A}}| \, , \quad S_{\mathcal{A}} = 0 \, . \tag{1.11}$$

Entanglement entropy satisfies a number of interesting properties [44]. For example, for a pure state $|\Psi\rangle \in \mathcal{H}$, the entanglement entropy of a subregion and its complement is the same

$$S_{\mathcal{A}} = S_{\mathcal{A}^c} \, . \tag{1.12}$$

Entanglement entropy also satisfies the subadditivity relation

$$S_{\mathcal{A}\cup\mathcal{B}} \leq S_{\mathcal{A}} + S_{\mathcal{B}} \, , \tag{1.13}$$

and the strong subadditivity condition

$$S_{\mathcal{A}} + S_{\mathcal{B}} \geq S_{\mathcal{A}\cup\mathcal{B}} + S_{\mathcal{A}\cap\mathcal{B}}\,. \tag{1.14}$$

The von Neumann entropy, and similarly the entanglement entropy, can be found by taking the appropriate limit of the Renyi entropies

$$S_n = \frac{1}{1-n}\log\left(\mathrm{Tr}\left(\rho^n\right)\right)\,, \quad S_{vN} = \lim_{n\to 1} S_n\,. \tag{1.15}$$

This is particularly useful in QFT where the Renyi entropies can be defined in terms of path integrals using the replica method. First, the density matrix of a subregion $\mathcal{A}$ of a Cauchy slice defined at $t=0$ can be written as a path integral

$$\left(\rho_{\mathcal{A}}\right)_{\Phi_+\Phi_-} = \int \mathcal{D}\Phi e^{-S_{\mathrm{QFT}}[\Phi]}\delta\left(\Phi_{\mathcal{A}}\Big|_{t=0^-} = \Phi_-\right)\delta\left(\Phi_{\mathcal{A}}\Big|_{t=0^+} = \Phi_+\right)\,, \tag{1.16}$$

where we have split the fields into those in region $\mathcal{A}$ and those outside, *i.e.,* $\Phi = \{\Phi_{\mathcal{A}}, \Phi_{\mathcal{A}^c}\}$. The geometry $\mathcal{B}$ over which the path integral is to be evaluated depends on the state we want to prepare. For example, to prepare the density matrix in the ground state of the QFT in a Cauchy slice Σ, one can do a Euclidean path integral on $\Sigma\times\mathbb{R}$ from $t_E = -\infty$ to $t_E = \infty$, with boundary conditions set at $t_E = 0$ in the subregion $\mathcal{A}$. Another common example is the thermal density matrix, which would be prepared by integrating over the thermal cylinder with period $\beta = 1/T$ in the Euclidean time direction and once again with boundary conditions at $t_E = 0$ in the subregion $\mathcal{A}$. See figure 1.1.

Powers of the density matrix can be calculated by sewing boundary conditions along the subregion $\mathcal{A}$. For example

$$\begin{aligned}\left(\rho_{\mathcal{A}}^2\right)_{\Phi_+\Phi_-} &= \int \mathcal{D}\Phi_x \left(\rho_{\mathcal{A}}\right)_{\Phi_+\Phi_x}\left(\rho_{\mathcal{A}}\right)_{\Phi_x\Phi_-} \\ &= \int \mathcal{D}\Phi^{(1)}\mathcal{D}\Phi^{(2)} e^{-S_{\mathrm{QFT}}[\Phi^{(1)}]-S_{\mathrm{QFT}}[\Phi^{(2)}]} \\ &\quad\times\delta\left(\Phi^{(1)}_{\mathcal{A}}\Big|_{t=0^-} = \Phi_-\right)\delta\left(\Phi^{(1)}_{\mathcal{A}}\Big|_{t=0^+} = \Phi^{(2)}_{\mathcal{A}}\Big|_{t=0^-}\right)\delta\left(\Phi^{(2)}_{\mathcal{A}}\Big|_{t=0^+} = \Phi_+\right)\,.\end{aligned} \tag{1.17}$$

The replica method consists of considering this doubled integral as an integral over a replica manifold, which consists of two copies of the original manifold glued along the subregion $\mathcal{A}$. The trace of an n-th power of the density matrix then consists of a closed path integral over a replica manifold $\mathcal{B}_n$ which consists of n copies of $\mathcal{B}$ glued periodically along the copies of the subregion $\mathcal{A}$. That is,

$$\mathrm{Tr}\,\rho_{\mathcal{A}} = Z[\mathcal{B}]\,, \quad \mathrm{Tr}\left(\rho_{\mathcal{A}}^n\right) = Z[\mathcal{B}_n]\,. \tag{1.18}$$

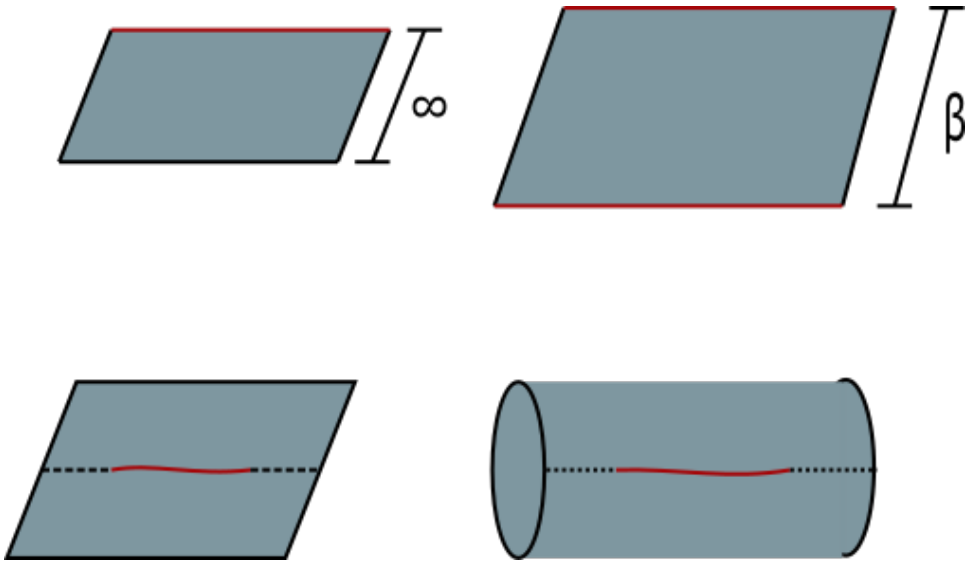

Figure 1.1: Path integrals preparing different states and density matrices. The boundary conditions are at the regions in red. Top left: Euclidean path integral from $t_E = -\infty$ to $t_E = 0$ prepares the ground state $|0\rangle$. Top right: Euclidean path integral from $t_E = 0$ to $t_E = \beta = 1/T$ prepares the thermal density matrix $\rho_\beta = e^{-\beta H}/Z$. Bottom left: gluing the ground state and its CPT conjugate along $\mathcal{A}^c$ gives the reduced density matrix $\mathrm{Tr}_{\mathcal{A}^c}|0\rangle\langle 0|$. Bottom right: gluing the thermal strip along $\mathcal{A}^c$ gives the reduced density matrix $\mathrm{Tr}_{\mathcal{A}^c}\rho_\beta$. The gluing is done by tracing over boundary conditions along the dashed area, representing $\mathcal{A}^c$, and leaving the boundary conditions on the two copies of $\mathcal{A}$ in red as operator indices.

Crucially, since going around $\partial\mathcal{A}$ one full rotation corresponds to jumping to a different copy of the original manifold, it takes a rotation of $2\pi n$ around $\partial\mathcal{A}$ to get to the same point in the replica manifold $\mathcal{B}_n$. That is, there is a conical defect at $\partial\mathcal{A}$ for $n \neq 1$. Furthermore, note that due to the cyclic symmetry of the trace, the replica manifold comes equipped with a $\mathbb{Z}_n$ symmetry, which corresponds to cyclically permuting the different copies of $\mathcal{B}$.

The holographic counterpart to entanglement entropy is given by the Hubeny-Rangamani-Ryu-Takayanagi prescription [41, 42, 45]

$$S_{EE}(\mathbf{R}) = \frac{A(\mathcal{E}_\mathbf{R})}{4G}\,, \tag{1.19}$$

where $\mathcal{E}_\mathbf{R}$ is the HRT surface. The HRT surface is the bulk co-dimension-two extremal surface anchored at $\partial\mathbf{R}$ and homologous to $\mathbf{R}$, with smallest area. That is, for a given region $\mathbf{R}$ of the asymptotic boundary, we consider co-dimension two surfaces in the bulk

anchored at $\partial\mathbf{R}$ on the asymptotic boundary that are smoothly retractable onto $\mathbf{R}$ and find those that extremize the area functional. In the event that there are several candidate HRT surfaces, the one with smallest area is the HRT surface.

Using the AdS/CFT correspondence, the Renyi entropies can be written as a difference of on-shell gravitational actions

$$\begin{aligned} S_n &= \frac{1}{1-n}\log\left(\frac{\mathrm{Tr}\,(\rho_{\mathcal{A}}^n)}{(\mathrm{Tr}\rho_{\mathcal{A}})^n}\right) \\ &= \frac{1}{1-n}\log\left(\frac{Z[\mathcal{B}_n]}{Z[\mathcal{B}]^n}\right) \\ &= \frac{1}{1-n}\left(\log Z[\mathcal{B}_n] - n\log Z[\mathcal{B}]\right) \\ &\approx \frac{1}{n-1}\left(I[\mathcal{M}_n] - n\, I[\mathcal{M}]\right)\,, \end{aligned} \tag{1.20}$$

where $\mathcal{M}$ is an asymptotic AdS manifold with $\partial\mathcal{M} = \mathcal{B}$, and similarly $\mathcal{M}_n$ is a bulk manifold with $\partial\mathcal{M}_n = \mathcal{B}_n$. The bulk manifolds $\mathcal{M}$ and $\mathcal{M}_n$ must satisfy Einstein's equations, and in particular the candidate manifolds $\mathcal{M}'_n$ that inherit the $\mathbb{Z}_n$ replica symmetry of $\mathcal{B}_n$ have codimension two surfaces $\mathbf{e}_n$ anchored at $\partial\mathcal{A}$, which are fixed point surfaces of the $\mathbb{Z}_n$ symmetry. The surface $\mathbf{e}_n$ has an intuitive interpretation when considering the quotient space $\hat{\mathcal{M}}_n = \mathcal{M}_n/\mathbb{Z}_n$ which is found by taking the quotient over the replica symmetry. In the quotient space $\hat{\mathcal{M}}_n$, the surface $\mathbf{e}_n$ has a conical defect which corresponds to a cosmic brane with tension

$$T_n = \frac{1}{4G}\frac{n-1}{n}\,. \tag{1.21}$$

This brane backreacts into the geometry and gives the right singularity, which would correspond to the conical defect of $\mathcal{M}_n$ after the quotient by the replica symmetry. The on-shell action of the replica manifold is n times the on-shell action of the quotient manifold

$$I[\mathcal{M}_n] = n\, I[\hat{\mathcal{M}}_n]\,. \tag{1.22}$$

While Renyi entropies in eq. (1.20) require an integration over the full bulk manifolds $\mathcal{M}$ and $\mathcal{M}_n$, it is convenient to consider the modular entropies

$$\tilde{S}_n = \frac{1}{n^2}\partial_n\left(\frac{n-1}{n}S_n\right)\,, \tag{1.23}$$

which also satisfy $\lim_{n\to 1}\tilde{S}_n = S_{vN}$. Using the modular entropies, we are instead interested in calculating $\partial_n I[\hat{\mathcal{M}}_n]$, which turns out to simply be proportional to the area of the cosmic

brane

$$\partial_n I[\hat{\mathcal{M}}_n] = \frac{A(\mathbf{e}_n)}{4n^2 G}\,. \tag{1.24}$$

Further, using the property in eq. (1.22), we can find

$$\tilde{S}_n = \partial_n I[\hat{\mathcal{M}}_n] = \frac{A(\mathbf{e}_n)}{4n^2 G}\,. \tag{1.25}$$

In the limit $n \to 1$, the cosmic brane has zero tension, the background geometry $\hat{\mathcal{M}}_n = \mathcal{M}$ and the cosmic brane is simply the extremal area surface as proposed in the HRT prescription. In the event that there are several candidate extremal surfaces, the choice of the minimal area candidate is justified by the saddle point approximation $\log Z[\mathcal{B}_n] \approx -I[\mathcal{M}_n]$, which picks out the saddle with smallest on-shell action, and correspondingly the dominant saddle corresponds to the geometry for which the cosmic brane $\mathbf{e}_n$ has smallest area. In the limit $n \to 1$ this corresponds to picking the extremal surface $\lim_{n\to 1} \mathbf{e}_n = \mathcal{E}_{\mathbf{R}}$ that has smallest area, which agrees with the HRT prescription.

1.2.3 Generalized entropy and quantum extremal surfaces

The HRT prescription is a leading saddle-point approximation in large number of effective degrees of freedom c_{eff} for the entanglement entropy of the subregion $\mathcal{A}$. It corresponds to the leading $1/c_{eff}$ computation for the entanglement entropy which can be done with the bulk classical gravity dual. Generally one would expect subleading corrections in $1/c_{eff}$ that correspond to loop corrections to the entanglement entropy [43, 46, 47]

$$S_{\mathcal{A}} = c_{eff} S_{\mathcal{A}}^{saddle} + S_{\mathcal{A}}^{1-loop} + \mathcal{O}(c_{eff}^{-1})\,. \tag{1.26}$$

In the bulk perspective, truncating the $1/c_{eff}$ expansion corresponds to taking the classical limit of the quantum gravity dual to the boundary QFT. It was argued in [46, 47] that the 1-loop correction to the entanglement entropy corresponds to the regulated contribution arising from the entanglement entropy of bulk modes given a bipartition with separating surface anchored at $\partial\mathcal{A}$ at the boundary

$$S_{\mathcal{A}} = \frac{A(\mathcal{E}_{\mathcal{A}})}{4G} + S_{\Sigma_{\mathcal{A}}}^{bulk} + \mathcal{O}(G)\,, \tag{1.27}$$

where $\Sigma = \Sigma_{\mathcal{A}} \cup \Sigma_{\mathcal{A}}^c$ is a bipartition of the Cauchy slice Σ separated by the surface $\mathcal{E}_{\mathcal{A}}$ analogue to the HRT surface. This can be argued as follows. The $1/c_{eff}$ expansion in the CFT corresponds to an expansion in powers of the Newton constant G in the bulk quantum

gravity theory. To obtain the leading order corrections to the entanglement entropy, it is therefore sufficient to work perturbatively in G, so that we can work with quantum fields in a rigid background. The entanglement entropy of $\mathcal{A}$ is then calculated by the entanglement entropy of the bulk fields on a subregion $\Sigma_{\mathcal{A}}$ of a Cauchy slice Σ that is bipartitioned by an extremal surface $\mathcal{E}_{\mathcal{A}}$. Because of the short range entanglement, one might expect a large contribution proportional to the area of the separating surface $\mathcal{E}_{\mathcal{A}}$ and then the subleading correction would correspond to the regulated entanglement entropy of the bulk quantum fields in $\Sigma_{\mathcal{A}}$, leading to eq. (1.27). The surface in eq. (1.27) is a quantum extremal surface (QES) that extremizes the generalized entropy

$$S_{\mathcal{A}}^{gen} = \frac{A(\mathcal{E}_{\mathcal{A}})}{4G} + S_{\Sigma_{\mathcal{A}}}^{bulk} . \tag{1.28}$$

Just like in the HRT prescription, if more than one candidate QES exists, it is the one with smallest generalized entropy that dominates.

At first one might expect the QES to be perturbatively close to the HRT surface since the entanglement entropy in eq. (1.19) and the generalized entropy in eq. (1.28) differ by quantum corrections which are suppressed by a factor of G. However, an important insight that led to progress in understanding the black hole information paradox, and more generally brought insights into our understanding of quantum gravity, is that there are situations in which certain parameters (like the time of the evaporation) can be taken large enough that the two contributions become comparable, and the QES can be located far away from the HRT surface [10, 11]. This is indeed the case for the black hole + bath models we will be discussing in chapters 2 and 3 after the Page time.

1.3 Summary

In the few past years, new models of black hole evaporation [1, 10, 11] have given fresh insight into one of the longest-standing puzzles in quantum gravity, the black hole information paradox [13, 34, 35, 36, 48, 49, 37]. The black hole information paradox is essentially the problem that in Hawking's famous calculation, black hole evaporation appears non-unitary, in conflict with the standard rules of quantum mechanics. A black hole may be formed in the collapse of a pure quantum state, however, the evaporation process appears to leave only thermal Hawking radiation in a mixed state. That is, quantum information seems to be destroyed by this process. The newly constructed models, however, have convincingly demonstrated for the first time the entropy decreases after the Page time and unitarity is maintained in quantum gravity. Although the models are semiclassical, they

exhibit novel saddle points, first observed in [10, 11], which take into account large corrections from quantum fields and produce a Page curve consistent with unitary evaporation. This result represents the first major progress toward resolving the famous paradox in many years.

The model of Almheiri, Engelhardt, Marolf and Maxfield [11] examines black holes in two-dimensional Jackiw-Teitelboim (JT) gravity theory coupled to conformal matter. Later, Almheiri, Mahajan, Maldacena and Zhao [1] made an apparently small but important modification: instead of only assuming conformal symmetry for the bulk matter, they also assume that the matter theory is holographic. We will use the initials of the original paper (AEMM) to denote the original model, and the initials of both papers combined (AEM^{4}Z) to denote the model with holographic matter.

We now give a brief description of the setup for both models. One begins with a two-sided equilibrium black hole, which is a solution of JT gravity coupled to a CFT in two-dimensional anti-de Sitter (AdS_2) spacetime and which has a holographic description in terms of a thermofield double state of two entangled quantum mechanical systems [50]. We denote the latter as QM_L and QM_R – see the top illustrations in figure 1.2. At some finite time, we couple the right boundary system QM_R to a heat bath, which consists of a copy of the same two-dimensional CFT prepared in a thermal state on a half-line. This corresponds to allowing the black hole to evaporate by changing the asymptotic boundary conditions with a 'joining quench' to a nongravitational region containing the same CFT. That is, at time zero, the asymptotic boundary on one side is joined to a semi-infinite interval $[0, \infty)$. The conformal matter in the latter space acts as an auxiliary bath system, which absorbs the Hawking radiation emitted from the evaporating black hole. Conversely, for a bath with non-zero temperature, there is thermal radiation from the bath falling into the black hole. The balance between the temperatures of the black hole and the bath determine whether the black hole evaporates and cools to the bath's temperature, or it grows and heats up from a hotter bath.

The two-dimensional AEMM model of [11] doesn't specify the type of CFT in AdS_2 and the bath, and reproduces many expected features of semiclassical black hole evaporation. In particular, the model reproduces the information paradox for the Hawking radiation, *i.e.,* the entropy of the Hawking radiation absorbed by the bath appears to grow without bound. However, the entropy of the black hole, *i.e.,* of QM_R,[1] undergoes a Page transition. That is, the QM_R entropy initially rises to track the increasing entropy of the bath, but then there is a sharp transition to a phase where it decreases again. This rise and fall of

[1]Of course, the entanglement entropy of QM_L remains fixed at the Bekenstein-Hawking entropy of the initial eternal black hole.

the black hole entropy are characteristic of the behaviour exhibited by the classic Page curve [30, 31]. This novel transition occurs in this holographic model (and in the model described by [10]) as a result of the existence of a new class of QESs just inside the event horizon of the evaporating black hole. These surfaces are in fact the minimal solutions at late times, and thus delineate the true boundary of the entanglement wedge of the dual QM_{R} theory.

This AEMM model [11] was then extended with an extra layer of holography by [1]. In the AEM^{4}Z variant, the matter theory in the bulk and bath is chosen to be itself a holographic CFT (coupled to JT gravity in the bulk). This theory is itself the boundary theory of a dual AdS_3 bulk – see the third illustration in figure 1.2. The JT gravity theory resides on a Planck brane suspended in an asymptotically AdS_3 bulk. The latter can be thought of as a Randall-Sundrum brane [51, 52], which cuts off the asymptotic AdS_3 geometry at a finite radius, but it is also engineered as a Dvali-Gabadadze-Porrati brane [53], in that the brane carries an intrinsic gravity action (confined to one lower dimension), *i.e.,* the JT action. Since the CFT is defined on manifolds with boundary (a boundary conformal field theory, or BCFT), the bulk also contains a second class of branes on which the AdS space ends: end-of-the-world (ETW) branes [54]. The dynamics of this model can be solved analytically, including the gravitational backreaction and the von Neumann entropy of the Hawking radiation. One can study the entropy of the black hole or its complementary subsystem (containing the Hawking radiation) as a function of time, using the Engelhardt-Wall prescription [55] (see also [56]) for calculating von Neumann entropy – a generalization of the Hubeny-Ryu-Rangamani-Takayanagi (HRT) prescription [57, 58] to incorporate quantum corrections. As was outlined in section 1.2, the important distinction between the HRT prescription and the Engelhardt-Wall prescription is that the former computes entropy using codimension-two surfaces with stationary areas, whereas the latter asks us to instead find minimal values of the generalized entropy defined in eq. (1.28)

$$S_{\mathrm{gen}} = \frac{A}{4G_{\mathrm{N}}\hbar} + S_{\mathrm{bulk}} \ . \tag{1.29}$$

That is, to leading order in $G_{\mathrm{N}}\hbar$, this quantity is simply the area A,[2] but the functional receives a quantum correction S_{bulk} given by the entropy of quantum fields of the spatial region outside the surface. The surface that extremizes S_{gen} is referred to as the quantum extremal surface (QES). In the AEM^{4}Z model, the calculation of the generalized entropy is purely geometric using holography in the AdS_3 bulk. That is, assuming the bath system is described by a holographic CFT_2, S_{bulk} can be found using the HRT prescription in the

[2]Note that in the following we examine two-dimensional JT gravity where the Bekenstein-Hawking contribution is replaced by $\phi/(4G_N\hbar)$, where ϕ denotes the value of the dilaton evaluated on the QES.

AdS_3 dual, while the Bekenstein-Hawking term becomes an additional boundary contribution (from the JT gravity) for HRT surfaces ending in the gravitational region, *i.e.,* on the Planck brane – see [59, 60] for further discussion.

Recovering a unitary Page curve for old black holes is a major step towards resolving the information paradox. It indicates that the semiclassical gravity path integral knows more about unitarity than previously believed. This result is surprising from the perspective of the two-dimensional theory. In particular, the above phase transition indicates that at late times, the standard calculation of the von Neumann entropy of the Hawking radiation is incorrect because of gravitational effects. Instead, one must modify the usual prescription for computing the entropy with the so-called 'island formula' [1], which accounts for the contributions of quantum extremal islands (QEIs). The QEIs are gravitational regions that may contribute to reducing the (entanglement) entropy of a non-gravitational region by creating new stationary points for the generalized entropy, *i.e.,* the sum of the gravitational and matter entropies. In particular, for a QEI, a change in area from perturbing the boundary of a QEI is exactly compensated for with an equal and opposite change in the entropy of the quantum fields inside the island. The HRT prescription in the three-dimensional bulk theory implies that the correct generalized entropy in the two-dimensional theory should be computed by including these islands, whenever they exist, to the entangling region, if doing so results in a smaller entropy. In the present context, the phase transition where the QEIs appear corresponds to the time when the bath encodes (part of) the black hole interior, a manifestation of the ER = EPR principle [61]. See [2, 3, 15, 59, 60, 62, 63, 64, 65, 66, 67, 68, 69, 70, 71, 72, 73, 74, 75, 76, 77, 78, 79, 80, 81, 82, 83, 84, 85, 86, 87, 88, 89, 90, 91, 92, 93, 94, 95, 96] for recent explorations on the island formula in different black hole geometries and [14, 97, 98, 99, 100, 101, 102, 103, 104, 105, 106, 107, 108, 109, 110, 111, 112, 113, 114, 115, 116, 117] for more associated studies on information paradox and Page curve from various perspectives.

The AEMM and AEM^{4}Z models are clearly rich with new physics, and with fascinating implications for quantum gravity. Chapter 2 is based on work done on the evaporating AEM^{4}Z model [2], where we begin to investigate how the black hole interior is encoded in the bath. The approach is straightforward: we start by considering the entire bath (plus QM_L) as our entangled subsystem. We then systematically excise various subregions of the bath from our entangling region, each time studying the corresponding entanglement wedge in the three-dimensional dual. We perform the excisions such that the system always sits at the transition where the entanglement wedge of the remaining bath in combination with QM_Lbegins to include the interior of the black hole. By identifying the Page transition for these various 'hole-y' subregions of the bath, we can find which regions of the bath are important for encoding the black hole interior. In this simple case, we find that the late

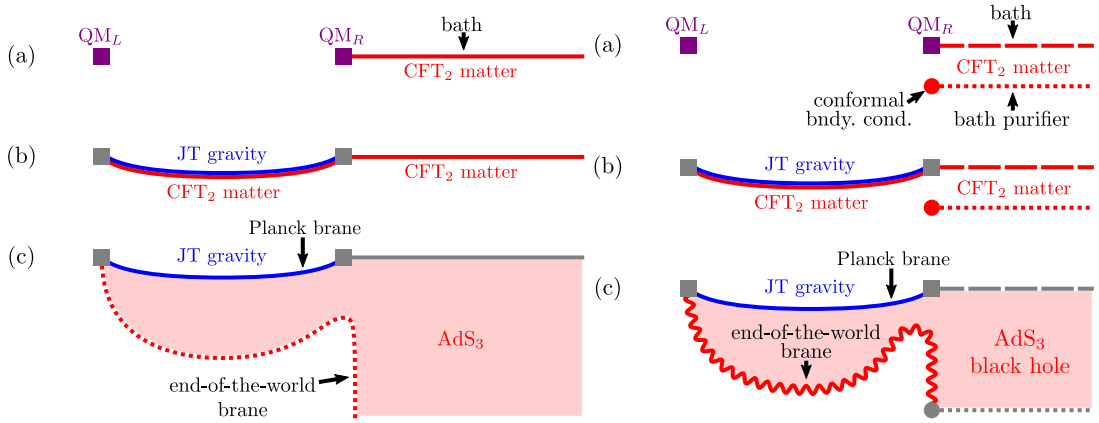

Figure 1.2: In the AEM^{4}Z model, the holographic principle is invoked twice, resulting in three different pictures of the same physical system. In the top picture, there are two quantum mechanics systems (QM_L and QM_R) as well as a field theory (CFT_2) state prepared on the half-line. The middle picture includes the 2D holographic geometry (JT gravity) dual to the entangled state of QM_L and QM_R. The last picture contains the doubly-holographic description, with a bulk AdS_3 dual to the matter in the middle picture. The figure to the left illustrates the three holographic layers of the evaporating model, in which the QM_R system is coupled to a zero temperature bath. To the right, we illustrate the equilibrating model in which the bath is prepared in a thermal state. In the doubly-holographic description, the thermofield double state of the bath plus its purifier, is replaced by an AdS_3 black hole.

radiation contains somewhat redundant information to reconstruct the black hole interior, and the early time radiation is more important; a similar effect was observed recently in [94, 97]. We also study the limiting case where we excise a large number of subintervals in the bath. By repeating this process ad infinitum, the remaining bath has a fractal structure. In this way, we implement the überholography of [118], and we can determine the support of the black hole interior encoding in the bath.

In chapter 3, we study the dynamics of coupling the initial equilibrium black hole to a bath BCFT that is initially in a finite non-zero temperature state instead, and is based on [3]. Similar situations were studied in [62, 70], but we do not make the assumption that the black hole and bath are initially at the same temperature. We study the resulting dynamics numerically and analytically. As in [62], we find that the quantum extremal surfaces can lie outside the black hole horizon, and correspondingly the QEIs can include part of the exterior of the black hole. For thermal baths with a temperature around

the same temperature as the initial black hole, the late time QES is already outside the horizon around the Page time. On the other hand, with arbitrary bath temperatures, the late time QES are initially inside of the event horizon and eventually cross the event horizon, remaining outside for the rest of the equilibration process. Similar to our analysis in chapter 2, we compute the Page curve for the dynamic black hole coupled with a thermal bath at arbitrary temperatures or equivalently, that of the complementary subsystem to the black hole, *i.e.,* the QM_{L} together with (parts of) the bath and its purification. Taking the bath to be at finite temperature changes the flow of quantum information in important ways. The bath has its own purification and thus must be accounted for in the computation of the generalized entropy. We study the role of the purification in altering the flow of quantum information as the black hole and bath exchange radiation.

Outline. In section 2.1, we review the AEM^{4}Z model. In particular, we show that there are three phases that the entanglement entropy evolves through after the quench. We study the entanglement properties of the holographic model in section 2.2, removing increasingly large entangling segments from the bath. We explain how the information encoding the interior of the black hole is encoded in the CFT via an increasingly refined boundary-bath operator algebra. In section 2.3, we conclude with a discussion of our calculations and future directions.

In section 3.1, we review the AEM^{4}Z model and set up the model for a black hole in contact with an auxiliary bath at finite temperature, finding the generalized entanglement entropy of various different intervals during the equilibration process. The equilibrium case, *i.e.,* the black hole temperature immediately after the quench matches that of the bath, is analyzed in section 3.2, and we find the constraints for finite bath intervals, together with QM_{L}, to recover the black hole interior. Interestingly, the purification of the bath is essential for the reconstruction of the black hole interior. The case of general temperatures is studied in section 3.3, and the results smoothly interpolate between the evaporating case of chapter 2 and the equilibrium case in section 3.2.

Chapter 2

Evaporation model

In this chapter, we review the AEM^{4}Z model [1, 11] for black hole evaporation and describe the salient quantitative results for the quantum extremal surfaces and generalized entropies. We also examine numerical solutions in certain instances to compare with our analytical approximations.

The process described in section 1.3 involves a quantum quench where the QM_R system is connected to the bath, as well as the subsequent evaporation of the black hole on the Planck brane. In the three-dimensional bulk description, the quench involves connecting the corresponding end-of-the-world (ETW) branes and letting them fall into the AdS_3 geometry. Similarly, the black hole evaporation is described by the dynamics of the joint between the Planck brane and the asymptotic AdS_3 boundary.

In principle, the problem of finding quantum extremal surfaces for the extremely dynamical bulk geometry described above seems an intimidating one. However, this difficulty is mitigated by several simplifying features in the AEM^{4}Z model.[1] First, the theory in the first holographic description (panel (b) in figure 1.2) is a *two-dimensional* boundary CFT (BCFT). Hence in the dual description, after an analytic continuation, the entire evolution can be conformally mapped to the vacuum state in the upper half-plane (UHP), *i.e.,* with a simple boundary running along the real axis. Given this configuration and turning to the second holographic description (panel (c) in figure 1.2), we exploit the fact that *holographic* BCFTs have relatively simple expressions for the entanglement entropy, *e.g.,* see eq. (2.20). Lifting this result back to the two-dimensional description (b), the remainder of the anal-

[1] Certainly, one of the simplifying features is that the evaporating black hole is constructed in the two-dimensional JT model, which means any candidate QES is simply a point and its extremality is easily tested by taking ordinary derivatives, *e.g.,* see eqs. (2.32).

ysis involves undoing the previous conformal transformations. That is, we are essentially following the analysis of [11], but the key difference is that we have a specific formula for the entanglement entropy determined by the holographic BCFT. This also allows us to consider more complicated situations, *e.g.,* multiple intervals, in the two-dimensional description in a straightforward way.

When, as in [11], we consider the entanglement entropy of QM_{R}, or alternatively its purification, the bath plus QM_{L}, we find the entropy evolves through three phases, which are sketched in figure 2.1 – see also the spacetime diagram of the two-dimensional boundary in figure 2.2. These three phases are as follows:

a) Quench Phase: This is a short period after the bath and QM_{R} systems are joined, in which the entanglement entropy rapidly rises. The three-dimensional description involves the HRT surface having two separate components. The first is anchored to the bifurcation surface of the initial eternal black hole on the Planck brane and falls straight down into the AdS_3 bulk to terminate on the ETW brane (which is stationary at this point). Similarly, the second connects QM_{R} to the ETW brane where the new connection was made and where it quickly falls into the bulk. Hence the rapid rise in the entanglement entropy is entirely due to the stretching of this second component of the HRT surface.

b) Scrambling Phase: The transition to this phase occurs on a thermal time scale (see eq. (2.47)). The entanglement entropy shows some transient behaviour at the beginning of this phase, *e.g.,* depending on the precise choice of parameters, the entropy may initially decrease, as shown in figure 2.2. However, after roughly the scrambling time (see eq. (2.54)), the entanglement entropy begins to grow linearly as the bath steadily absorbs more and more Hawking radiation from the black hole (or from QM_{R}). The gradual increase in entropy is consistent with the heuristics from efficient scrambling systems where only a small but increasing amount of the radiation can be decoded before the Page transition [119]. During this phase, the corresponding HRT surface consists of a single geodesic that connects QM_{R} to a point very close to the bifurcation surface of the initial black hole (see figure 2.2). In particular, it connects boundary points on opposite sides of the shock wave propagating into the Planck brane.

c) Late-Time Phase: In this phase, the entanglement entropy decreases, as required by the late time behaviour of the Page curve. Of course, the bath continues to absorb Hawking radiation and so this decrease indicates there must be correlations between the Hawking quanta emitted at early and late times. In this phase, the corresponding HRT

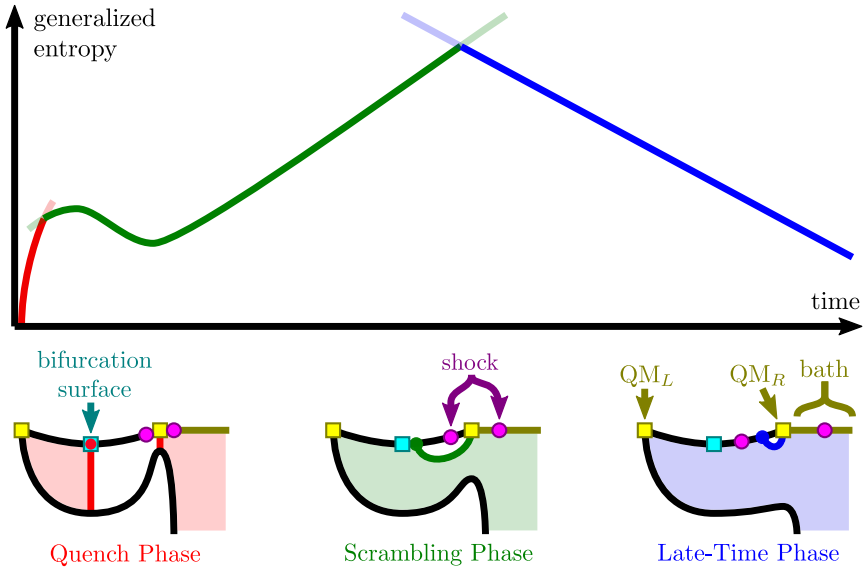

Figure 2.1: A cartoon illustration of the three phases for the entanglement entropy of QM_R or QM_L+bath, after the quench where QM_R is connected to the bath. The darker colors indicate the true generalized entropy, while the lighter colors indicate the general shape of each of the branches slightly beyond the regime where it provides the minimal value for the generalized entropy. Below the plot is a sketch of the shape of the extremal surfaces in AdS_3 which contribute to the generalized entropy in each phase.

surface again consists of a single component, but now the geodesic connects QM_R to the new QES behind the event horizon of the evaporating black hole – see figure 2.2. Hence these geodesics are distinguished from the previous class since the two boundary points which they connect both lie to the future of the shock wave.

2.1 Setup and Page curve

The AEM^{4}Z model consists of an AdS_2 black hole in JT gravity, dual to a Hartle-Hawking state of two copies of a one-dimensional quantum mechanics theory [1, 11]. At Lorentzian time $t = 0$, we perform a quantum quench on the CFT, joining it to a field theory vacuum state defined on the half-line $\sigma > 0$. In the bulk, Hawking radiation can now escape to the bath and land on the asymptotic null infinity $\mathscr{I}^+$ of the flat space bath region, and the black hole thus evaporates. Additionally, the quench results in two shockwaves, one propagating into the black hole and one into the bath, corresponding to the propagation of

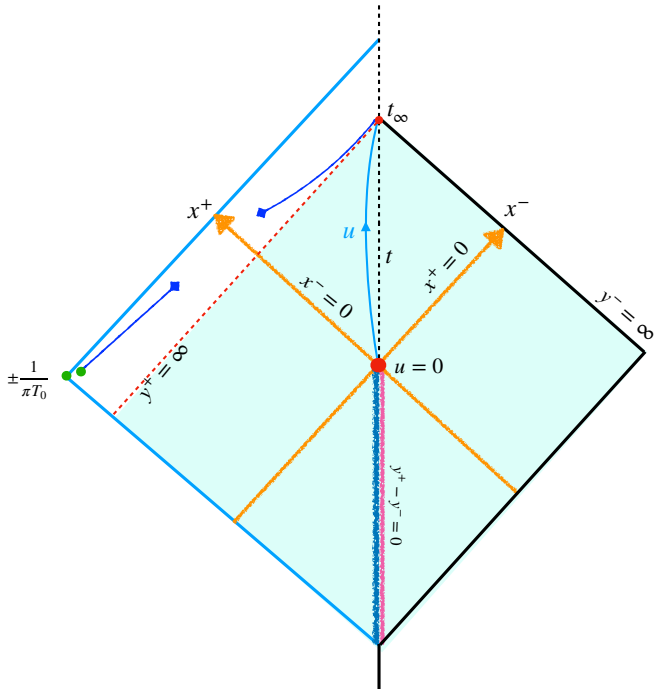

Figure 2.2: In the AEM^{4}Z model, the AdS_2 black hole is coupled to bath along the boundary $\sigma = 0$ at time $\tau = 0 = t$. This results in the shock indicated by the yellow solid line. The evolution of quantum extremal surfaces is indicated by the solid blue curve. The first phase transition occurs when the QES jumps from the green point at $x^\pm = (\pi T_0)^{-1}$ to the other green point, and the second (Page) phase transition happens at the jump between the blue blocks. In this final phase, the QES tracks close to the new horizon. The regime of applicability of this semi-classical model breaks down at very late times, with $u \gtrsim k^{-1} \log \frac{T_1}{k}$. After times of this order, quantum effects of the near extremal black hole cannot be neglected and therefore the final moments of the evaporation are not captured by the present analysis.

a large amount of energy arising from the joining quench. The energy of these shockwaves E_S should be thought of as one of the UV scales for the model. The spacetime diagram of the coupled system is shown in figure 2.2.

The two-dimensional gravity solution is locally AdS_2, described by the Poincaré metric

$$ds^2_{\text{AdS}} = -\frac{4\,L^2_{\text{AdS}}}{(x^+ - x^-)^2} dx^+ dx^- \qquad (x^\pm = t \pm s)\,. \tag{2.1}$$

Note that the Poincaré depth coordinate is denoted s, so that the (unregulated) asymptotic boundary is at $s = 0$. Further, we will generally set the AdS curvature scale $L_{AdS} = 1$ in the following. Meanwhile, the bath is represented by a flat Minkowski half-space:

$$ds^2_{\text{bath}} = -dy^+ dy^- \qquad (y^\pm = u \mp \sigma)\,. \tag{2.2}$$

where σ denotes the spatial coordinate.[2] These two spaces are to be glued along their respective boundaries, *i.e.,* $\sigma = 0$ in the bath region and $s \sim \epsilon \approx 0$ in the AdS_2 space, where ϵ is an IR cutoff in the AdS_2 bulk. After this quench, energy can flow freely through the boundary from one space to the other. The $x^\pm$ coordinates can be extended to cover the bath, and the $y^\pm$ coordinates can be extended to cover a Rindler patch of the AdS.

To prepare the corresponding bulk quantum state, we Wick rotate to Euclidean signature. The Euclidean coordinates and Lorentzian coordinates are related by $x^- \to -x$, $x^+ \to \bar{x}$. This state can be mapped to the vacuum of the CFT in the upper half plane (UHP) $\text{Im}\{z\} \geq 0$ by a local Weyl rescaling

$$\begin{aligned} ds^2_{\text{AdS}} &\longrightarrow \Omega(x^+, x^-)^2 ds^2_{\text{AdS}} = \frac{dz d\bar{z}}{\epsilon^2}\,, \\ ds^2_{\text{bath}} &\longrightarrow \Omega'(y^+, y^-)^2 ds^2_{\text{bath}} = \frac{dz d\bar{z}}{\epsilon^2}\,. \end{aligned} \tag{2.3}$$

Explicitly,

$$\Omega = \frac{x^+ - x^-}{2\epsilon}\sqrt{z'(x)\bar{z}'(\bar{x})}\,, \quad \Omega' = \frac{1}{\epsilon}\sqrt{z'(y)\bar{z}'(\bar{y})}\,. \tag{2.4}$$

Before the quench, the reparameterization function $f(u)$ relating the x and y coordinates (*i.e.,* $x = f(y)$) is given by the solution of a black hole with temperature T_0 in JT gravity, *i.e.,*

$$f(u) = \frac{1}{\pi T_0}\tanh(\pi T_0 u) \qquad (u < 0), \tag{2.5}$$

[2] Our unconventional choice in defining $y^\pm$ ensures that moving further into the bath corresponds to moving towards larger positive σ. That is, σ is positive in the bath, while s is positive in AdS.

where we identify the physical time on the boundary with the coordinate t via the inverse function $u = f^{-1}(t)$. The quench occurs at $u = 0$. The quench introduces a localized positive energy shock followed by a flux of energy:[3]

$$\langle T_{x^-x^-}\rangle = E_{\rm S}\,\delta(x^-) - \frac{c}{24\pi}\{y^-, x^-\}\Theta(x^-)\,. \tag{2.6}$$

After the quench, consistency of the change in black hole energy with this flow of energy between the AdS and bath systems demands that f satisfies the following equation

$$\{f(u), u\} = -2(\pi T_1)^2 e^{-ku}\,, \tag{2.7}$$

where T_1 is the temperature of the black hole after the initial shock of energy $E_{\rm S}$ falls in, so that $E_S \equiv \frac{\phi_r \pi}{4G_{\rm N}}\,(T_1^2 - T_0^2)$. The solution was found in [11] to be

$$f(u) = \frac{1}{\pi T_1}\frac{I_0\left[\frac{2\pi T_1}{k}\right]K_0\left[\frac{2\pi T_1}{k}e^{-ku/2}\right] - I_0\left[\frac{2\pi T_1}{k}e^{-ku/2}\right]K_0\left[\frac{2\pi T_1}{k}\right]}{I_1\left[\frac{2\pi T_1}{k}\right]K_0\left[\frac{2\pi T_1}{k}e^{-ku/2}\right] + I_0\left[\frac{2\pi T_1}{k}e^{-ku/2}\right]K_1\left[\frac{2\pi T_1}{k}\right]}\,. \tag{2.8}$$

where $k \ll T_1$ is a constant that determines the relative strength of backreaction compared to the entropy:

$$\frac{c}{12} = k\frac{\bar{\phi}_r}{4G_{\rm N}}\,. \tag{2.9}$$

After the quench, the horizon shifts, corresponding to the change in temperature. The new horizon corresponds to $x^+ = t_\infty$, where

$$t_\infty = f(u=\infty) = \frac{1}{\pi T_1}\frac{I_0\left[\frac{2\pi T_1}{k}\right]}{I_1\left[\frac{2\pi T_1}{k}\right]} = \frac{1}{\pi T_1} + \frac{k}{4\left(\pi T_1\right)^2} + O\left(k^2\right)\,. \tag{2.10}$$

After taking the limit of very large E_S, the map to the UHP is achieved by the piecewise-Möbius map [11]

$$z = \begin{cases} \left(\frac{12\pi}{c}E_S\right)^{-2}\frac{i}{f(y)} & \text{for } y > 0, \\ -iy & \text{for } y < 0, \end{cases} \tag{2.11}$$

or equivalently in terms of x coordinates,

$$z = \begin{cases} \left(\frac{12\pi}{c}E_S\right)^{-2}\frac{i}{x} & \text{for } x > 0\,, \\ if^{-1}(-x) & \text{for } x < 0\,. \end{cases} \tag{2.12}$$

[3]The Schwarzian is defined as $\{f(u), u\} = \frac{2f'f''' - 3f''^2}{2f'^2}$.

We are looking for the quantum corrections to the entanglement wedge of $\mathrm{QM_R}$. This means we need to evaluate the generalized entropy (1.29), which in JT gravity means the function

$$S_{\text{gen}}(x^+, x^-) = \frac{\phi}{4G_{\text{N}}} + S_{\text{bulk}}\,, \tag{2.13}$$

where

$$\phi = \phi_0 + \frac{\phi_r(x^+, x^-)}{\epsilon}\,, \tag{2.14}$$

is the value of the dilaton. The large constant contribution from ϕ_0 is related to the divergences associated to the short range entanglement across the end points of an interval. The spacetime-dependent ϕ_r takes the value $\bar{\phi}_r$ at the boundary where AdS and the bath are joined.

We solve the quantum extremal surfaces, *i.e.,* the codimension-two surfaces (points) that minimize the generalized entropy. Before the quench, the dilaton profile is given by the simple static solution

$$\phi = 2\bar{\phi}_r \frac{1 - (\pi T_0)^2\, x^+ x^-}{x^+ - x^-} = 2\bar{\phi}_r \pi T_0 \coth\left(\pi T_0 (y^+ - y^-)\right)\,, \tag{2.15}$$

where we used the reparameterization function for the static black hole with temperature T_0 in eq. (2.5). After the quantum quench, the AdS_2 geometry is modified due to the backreaction. Since 2D gravity is topological, this corresponds to a modification of the boundary. Alternatively, we can consider the AdS_2 geometry as fixed and account for the backreaction by having the dilaton profile change. After the shock $x^- > 0$, the new solution is

$$\phi = 2\bar{\phi}_r \frac{1 - (\pi T_0)^2\, x^+ x^- + \frac{k}{2} I(x^+, x^-)}{x^+ - x^-}\,, \tag{2.16}$$

where

$$I = \int_0^{x^-} (x^+ - t)(x^- - t)\{u, t\} dt \tag{2.17}$$

is the contribution due to the presence of stress-energy exchange through the boundary [120, 121].

In the original iteration of the AEM^{4}Z model [11], no assumptions are made about the bulk BCFT. The calculation of the entanglement entropy can then be carried out using replica techniques [122, 123, 124]. In terms of the conformal cross-ratio

$$\eta \equiv \frac{(z_1 - \bar{z}_1)(z_0 - \bar{z}_0)}{(z_1 - \bar{z}_0)(z_0 - \bar{z}_1)}, \tag{2.18}$$

the entanglement entropy of an interval with endpoints z_0 and z_1 in a two-dimensional BCFT with boundary at $z - \bar{z} = 0$ is

$$S_{\text{UHP}} = \frac{c}{6} \log \left(\frac{|z_0 - z_1|^2}{\delta^2} \eta \right) + \log \mathcal{F}(\eta). \tag{2.19}$$

Here, δ is a UV cutoff and $\mathcal{F}(\eta)$ is a function which depends on the theory living on the boundary defect. In the limit $\eta \to 1$, we are in the OPE limit, whence $\mathcal{F}(1) = 1$; in the opposite limit $\eta \to 0$, we instead have $\mathcal{F}(0) = g^2$, where $\log g$ is the Affleck-Ludwig boundary entropy [125].

For our purposes, however, we wish to work with the holographic model described in [1]. In this case, the matter theory is a holographic BCFT. Thus, we can imagine the JT gravity theory plus bath system as living on the boundary of a new, asymptotically-AdS_3 bulk. Because of the boundary defects, there is a dynamical ETW brane hanging into the space [126, 127]. After the quench, the ETW brane detaches from the asymptotic boundary (where the JT gravity and bath are connected) and falls into the bulk.

A particularly convenient aspect of the holographic model is that the entanglement entropy is now determined simply using the Hubeny-Rangamani-Ryu-Takayanagi prescription [57, 43]. In this setup, this simply means evaluating the length of the minimal geodesic homologous to the entangling region. In this case, the HRT surfaces are allowed to end on the ETW brane.

In this case, the entanglement entropy of one interval reduces to

$$S_{\text{UHP}} = \begin{cases} \frac{c}{6} \log \left(\frac{|z_1 - z_0|^2}{\delta^2} \right) & \text{for } \eta > \eta_* \\ \frac{c}{6} \log \left(\frac{|z_1 - \bar{z}_1|}{\delta} \cdot \frac{|z_0 - \bar{z}_0|}{\delta} \right) + 2 \log g & \text{for } \eta < \eta_* \end{cases} \tag{2.20}$$

where $\eta_* = (1 + g^{12/c})^{-1}$ is the value of the cross-ratio at which the transition between families of HRT surfaces occurs.[4] Without loss of generality for our purposes, we take $g = 1$ from now on, so that $\eta_* = 1/2$. We will discuss the role of g in more detail in section 2.3.

Figure 2.3 illustrates the two families of bulk geodesics in the two different branches contained in eq. (2.20) (with $\log g = 0$). The $\eta \geq \frac{1}{2}$ branch corresponds to a single geodesic stretching between the two endpoints, while the $\eta \leq \frac{1}{2}$ branch corresponds to two geodesics (one from each endpoint) terminating on the ETW brane. This formula matches

[4] The transition value η_* for the conformal cross ratio is precisely that for which the entropy given by the two channels in eq. (2.20) are equal.

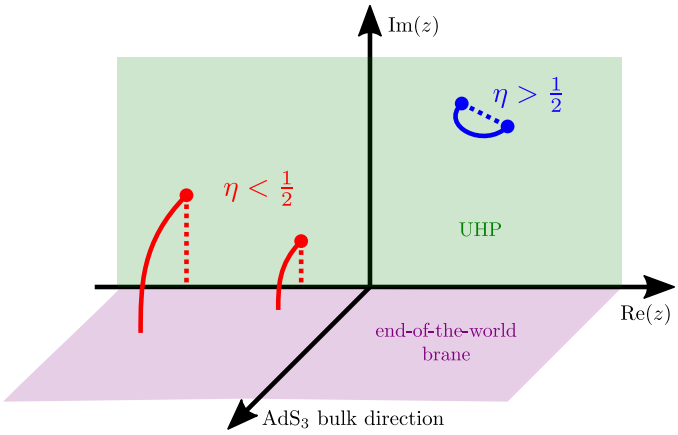

Figure 2.3: The entanglement entropy for an interval in a holographic BCFT on the upper half-plane has two branches. The dominant branch is determined by the cross ratio η defined in eq. (2.18). The ETW brane is anchored at $\mathrm{Im}(z) = 0$. The case illustrated here corresponds to a tensionless ETW brane in the bulk, or alternatively $\log g = 0$ in the BCFT. As shown for this case, the ETW brane lies at right angle to the AdS$_3$ boundary. For other choices of $\log g$, the ETW brane will be tensionful and intersect the UHP at some other angle.

with CFT calculations in the large c limit; the phase transition between the two branches follows from the universality of the four-point function on the full plane in a holographic theory [128, 129].

Employing this holographic formula (2.20) for the entropy of an interval on the upper half-plane, we can find the bulk entropy we need by taking the conformal transformation to the physical coordinate system. Because of the conformal invariance, this reduces to the answer on the upper half-plane, except for the transformation of the cutoff at each endpoint:

$$S_{\text{bulk}} = S_{\Omega^{-2}g} = S_{\text{UHP}} - \frac{c}{6}\sum_{x_i\in\partial} \log \Omega(x_i) \tag{2.21}$$

where the sum runs over all the endpoints of the intervals.

Note that all of the entanglement entropies that we calculate in the following are formally UV divergent, because of the UV cutoff δ appearing in eq. (2.20). However, in any of our analyses, we are also comparing different branches with the same number of endpoints in the bath and so these δ contributions do not play a role. Hence in any expressions that are explicitly shown in equations or plotted in the figures, we simply subtract $\frac{c}{6}\log(L_{AdS}/\delta)$ for each of the endpoints. Of course, in the holographic description, these UV divergences

Parameter	L_{AdS}	k	T_1	T_0	c	ϵ	ϕ_0	$\bar{\phi}_r$
Value	1	$\frac{1}{4096}$	$\frac{1}{\pi}$	$\frac{63}{64\pi}$	4096	$\frac{1}{4096}$	0	$\frac{1}{4096^2}$

Table 2.1: Baseline parameters for this work. Unless otherwise specified, all of our figures are generated using these values for the parameters. These parameters were chosen to remain consistent throughout all our numerical analysis, but the results are robust. Varying any of the parameters produces qualitatively similar results to those shown here.

appear because of the infinite length appearing when the HRT geodesics extend to the AdS_3 boundary. A similarly large length appears when these bulk geodesics terminate on the Planck brane. In this case, the divergences are absorbed by the gravitational contribution in the generalized entropy (2.13). In particular, these divergences are associated with renormalizing the coupling to the topological Einstein term in the JT action, *i.e.,* $\phi_0/4G_{\text{N}}$ [1, 11].[5]

We now review the results in [2, 11] and find the quantum extremal surfaces. Finding these surfaces requires computing the generalized entropy for an interval with one point in the AdS_2 and another point on the boundary. We assume the simple holographic results for bulk entropy, where we found a small change in the behavior of the quantum extremal surface before the shock relative to the results of [11]. Unless otherwise specified, we will use the parameters in table 2.1 as our baseline parameters in all of our numerics.

Before the shock, the possible contributions to generalized entropy are also divided into two different phases according to the position of endpoints. After the shock, the cross-ratio is fixed to be 1 at leading order in E_S^{-2}, as in [11].

Finding the phase transitions

Consider a bulk region defined by the interval between two points, $x^{\pm}_{\text{QES}}$ and $x^{\pm}_1$. (More correctly, consider the domain of dependence of this interval.) As a warm-up, we take x_0 to lie in the bulk and x_1 to be near the boundary. In this case we can relabel the point x_1 in terms of the proper time u along the boundary,

$$t = f(u) = \frac{x_1^+ + x_1^-}{2}\,, \quad z = \frac{x_1^+ - x_1^-}{2} = \epsilon f'(u)\,. \tag{2.22}$$

[5]For details on how this occurs in general dimensions, refer to the appendix of [130].

Phase	Range of η	Position relative to shock
Quench	$[0, \frac{1}{2})$	Straddling ($x^-_{\text{QES}} \leq 0$)
Scrambling	$[\frac{1}{2}, 1)$	Straddling ($x^-_{\text{QES}} \leq 0$)
Late-Time	≈ 1	Above ($x^-_{\text{QES}} \geq 0$)

Table 2.2: A summary of the range of parameters determining the phase of the von Neumann entropy. In Lorentzian coordinates, $\eta = x_1^+(x^+_{\text{QES}} - x^-_{\text{QES}})/[x^+_{\text{QES}}(x_1^+ - x^-_{\text{QES}})]$.

From the above holographic formula for entanglement entropy with two points, we can fix the choice of bulk entropy by taking account of the cross-ratio decided by the position of AdS_2 point, giving

$$S_{\text{bulk}} = \begin{cases} \frac{c}{6}\log\left(\frac{|z_1-\bar{z}_1|\cdot|z_{\text{QES}}-\bar{z}_{\text{QES}}|}{\Omega_1\Omega_{\text{QES}}\delta^2}\right) & \text{for } \eta \in [0, \frac{1}{2}) \\ \frac{c}{6}\log\left(\frac{|z_1-z_{\text{QES}}|\cdot|\bar{z}_1-\bar{z}_{\text{QES}}|}{\Omega_1\Omega_{\text{QES}}\delta^2}\right) & \text{for } \eta \in [\frac{1}{2}, 1] \end{cases} \tag{2.23}$$

The first formula (where $\eta < \frac{1}{2}$) is only applicable when the bulk endpoint lies before the shock with $x^-_{\text{QES}} < 0$. In this formula, the entropy factorizes into contributions from the two endpoints. (For an idea of what the $\eta < \frac{1}{2}$ region looks like, consult figure 2.4.)

The second formula (where $\eta \geq \frac{1}{2}$) holds both before and after the shock. However, because the map from the upper half plane to the physical coordinates depends on whether the interval straddles the shock or lies to its future, the formulas for the bulk entropy will still depend on this distinction.

In total, we end up with the following bulk von Neumann entropy formulas for the three phases defined in table 2.2:

$$S_{\text{bulk, quench}} = \frac{c}{6}\log\left(\frac{24\pi E_S}{\epsilon c}\frac{ut}{\sqrt{f'(u)}}\right), \tag{2.24}$$

$$S_{\text{bulk, scrambling}} = \frac{c}{6}\log\left(\frac{24\pi E_S}{\epsilon c}\frac{ux^-_{\text{QES}}\left(t - x^+_{\text{QES}}\right)}{(x^+_{\text{QES}} - x^-_{\text{QES}})\sqrt{f'(u)}}\right), \tag{2.25}$$

$$S_{\text{bulk, late-time}} = \frac{c}{6}\log\left[\frac{2\left(u - y^-_{\text{QES}}\right)\left(x^+_{\text{QES}} - t\right)}{\epsilon\left(x^+_{\text{QES}} - x^-_{\text{QES}}\right)}\sqrt{\frac{f'(y^-_{\text{QES}})}{f'(u)}}\right]. \tag{2.26}$$

With these ingredients in place, we can find the generalized entropy in each of the three phases,

$$S_{\text{gen}} = \frac{\phi}{4G_{\text{N}}} + S_{\text{bulk}}, \tag{2.27}$$

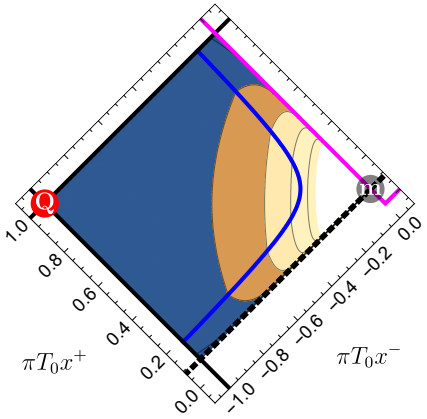

(a) Quench Phase.

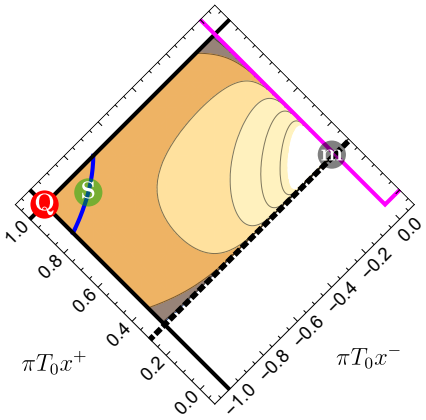

(b) A new extremum (point S) emerges, but is non-minimal.

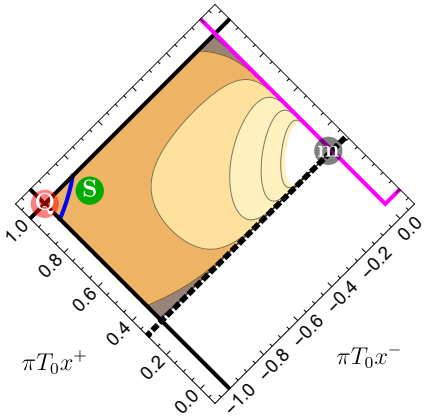

(c) Transition to Scrambling Phase.

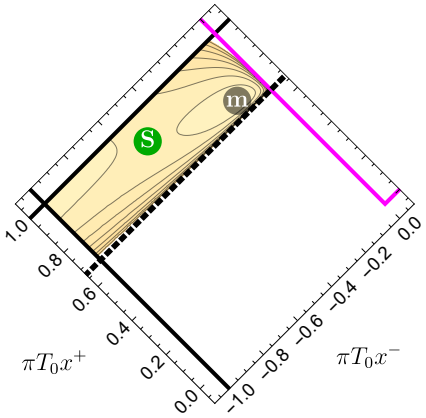

(d) Instant before Page transition.

Figure 2.4: Motion of QES and other (non-minimal) extrema in the Quench and Scrambling Phases. The sub-figures show contour plots of generalized entropy as a function of x_{QES} in the region bounded by the initial black hole horizon (solid black lines), a past null ray (dotted black line) emanating from the point x_1 on the AdS-bath boundary, and the shock (magenta lines); dark blue and bright yellow shading indicate low and high generalized entropies respectively. The blue curve marks points for which $\eta = 1/2$. Three extrema of generalized entropy are shown: the bifurcation point (Q), a saddle point (S), and a maximum point (m). The QES (opaque point) in the Quench and Scrambling Phases is given respectively by Q and S. In order to make various qualitative features visible in this figure, we have chosen parameters differing from the baselines listed in table 2.1; here, $\epsilon = \frac{1}{16}$, $c = 16$, $k = \frac{1}{16}$, $T_0 = \frac{2}{3\pi}$, $T_1 = \frac{1}{\pi}$, $\phi_0 = 0$, and $\phi_r = \frac{1}{256}$.

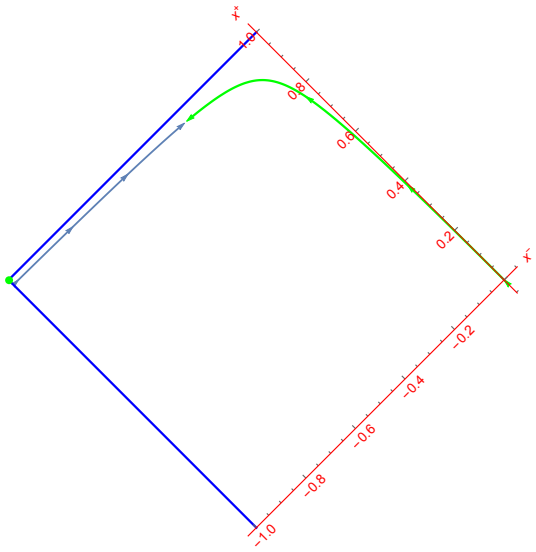

Figure 2.5: The time evolution of quantum extremal surfaces. The arrow indicates the direction of the flow. The blue line is the physical solution we considered in our analysis. It starts at the bifurcation point and ends at a point away from shock. The green one is another branch of the solution with larger entropy. Here, we choose a large k to make the deviation from the horizon more obvious when plotted.

and find the quantum extremal surfaces which are stationary points of this equation, using

$$\partial_+ S_{\text{gen}} = 0\,, \qquad \partial_- S_{\text{gen}} = 0. \tag{2.28}$$

where we abbreviate $\partial_\pm$ to mean $\partial_{x^\pm_{QES}}$ to simplify the notation.

Quantum extremal surfaces at early times

It is easy to minimize the generalized entropy in the quench phase, because the bulk von Neumann entropy in this phase is independent of x_{QES}. The problem reduces to finding the saddle point of the dilaton, which is of course the bifurcation surface of the original (temperature T_0) black hole at

$$x^\pm_{\text{QES}} = \pm\frac{1}{\pi T_0}\,. \tag{2.29}$$

Even though the quantum extremal surface is fixed to the bifurcation surface, the generalized entropy still evolves with time, and is given by

$$S_{\text{gen, quench}} = \frac{\bar{\phi}_r}{4G_{\text{N}}}\left(2\pi T_0 + 2k\log\left(\frac{24E_S}{\epsilon c}\frac{ut}{\sqrt{f'(u)}}\right)\right) \qquad (\eta \leq \tfrac{1}{2}). \tag{2.30}$$

This solution is relevant only when

$$t \leq \frac{1}{3\pi T_0}. \tag{2.31}$$

Now we consider the scrambling phase. The quantum extremal surfaces in this phase are found by solving the equations

$$0 = \frac{4G_{\text{N}}}{\bar{\phi}_r}\partial_+ S_{\text{gen}} = \frac{2((\pi T_0 x^-_{\text{QES}})^2 - 1)}{(x^+_{\text{QES}} - x^-_{\text{QES}})^2} + 2k\frac{x^-_{\text{QES}} - t}{(t - x^+_{\text{QES}})(x^+_{\text{QES}} - x^-_{\text{QES}})}\,, \tag{2.32}$$

$$0 = \frac{4G_{\text{N}}}{\bar{\phi}_r}\partial_- S_{\text{gen}} = \frac{2(1 - (\pi T_0 x^+_{\text{QES}})^2)}{(x^+_{\text{QES}} - x^-_{\text{QES}})^2} + \frac{2kx^+_{\text{QES}}}{x^-_{\text{QES}}(x^+_{\text{QES}} - x^-_{\text{QES}})}\,. \tag{2.33}$$

An exact solution[6] for $x^{\pm}_{\text{QES}}$ can easily be found. Using these exact solutions, we plot the generalized entropy in this phase in figure 2.6. An approximate solution (using a small-k expansion) is

$$x^+_{\text{QES}}(t) = \frac{1}{\pi T_0} - \frac{k}{\pi^2 T_0^2} + \frac{k^2\,(3\pi T_0 t - 1)}{2\pi^3 T_0^3\,(\pi T_0 t - 1)} + \mathcal{O}(k^3) < \frac{1}{\pi T_0}\,, \tag{2.34}$$

$$x^-_{\text{QES}}(t) = -\frac{1}{\pi T_0} - \frac{k\,(\pi T_0 t + 1)}{\pi^2 T_0^2\,(\pi T_0 t - 1)} + \frac{k^2\,(\pi T_0 t + 1)}{2\pi^3 T_0^3\,(\pi T_0 t - 1)} + \mathcal{O}(k^3)\,, \tag{2.35}$$

The small k expansion is a good approximation for this early-time regime and we need to consider more and more orders of k when we move to later time region. From the k expansion, we can also derive the leading contributions to generalized entropy for $uT_1 = \mathcal{O}(1)$ as

$$\begin{aligned} S_{\text{gen, scrambling}} \approx \frac{\bar{\phi}_r}{4G_{\text{N}}}\Bigg[&2\pi T_0 + 2k\pi T_1 u + 2k\log\left(\frac{24\pi E_S}{\epsilon c}\frac{u}{2\pi T_0}\right) \\ &+ 2k\log\left(\frac{T_0\left(2e^{-2\pi T_1 u} - 1\right) + T_1}{2T_1}\right)\Bigg] + \mathcal{O}(k^2)\,, \end{aligned} \tag{2.36}$$

[6]The above equations actually have several branches of solutions. Here we only take the solutions satisfying the constraints. Even still there is another solution, shown in figure 2.5 in green, which satisfies the constraints but with larger generalized entropy. This occurs because of the factor of $\log x^-_{\text{QES}}$ in the entropy of the scrambling phase; the solution lies close to the shock located at $x^-_{\text{QES}} = 0$.

keeping the first two orders in k. The first line is the dominant term in this approximation, because the second line is order $\mathcal{O}\left(k \log\left(\frac{T_1-T_0}{T_1}\right)\right)$. The above approximation captures the behavior of generalized entropy at early time in the scrambling phase. We also note the contribution from dilaton is almost constant up to a linear increase of order k^2:

$$\frac{\phi}{\bar{\phi}_r} \approx 2\pi T_0 + \frac{k^2\left(\pi T_0 t + 1\right)}{\pi T_0\left(1 - \pi T_0 t\right)} + \mathcal{O}\left(k^3\right) , \tag{2.37}$$

which is negligible at early times ($\pi T_0 t \ll 1$).

For later times, closer to the Page time, we need to push the above approximation to next order. The next order correction to the dilaton takes the form

$$\frac{\phi}{\bar{\phi}_r} \approx 2\pi T_0 + \frac{k^2}{\pi T_0}\frac{2T_1}{T_1 - T_0} + \mathcal{O}\left(k^3\right) . \tag{2.38}$$

which is not negligible when $T_1 - T_0$ is order k. Similarly, the bulk terms are corrected at order $k^n/(T_1 - T_0)^{n-1}$. For example, we can find the linearized generalized entropy as

$$\begin{aligned} S_{\text{gen, scrambling}} \approx \frac{\bar{\phi}_r}{4G_{\text{N}}}\Bigg[2\pi T_0 + 2k\pi T_1 u + 2k\log\left(\frac{24\pi E_S}{\epsilon c}\frac{u}{2\pi T_0}\frac{T_1 - T_0}{2T_1}\right) \\ + \frac{1}{2}k^2\left(-\pi T_1 u^2 + \frac{5}{\pi\left(T_0 - T_1\right)} + u\right)\Bigg] + \mathcal{O}(k^2) . \end{aligned} \tag{2.39}$$

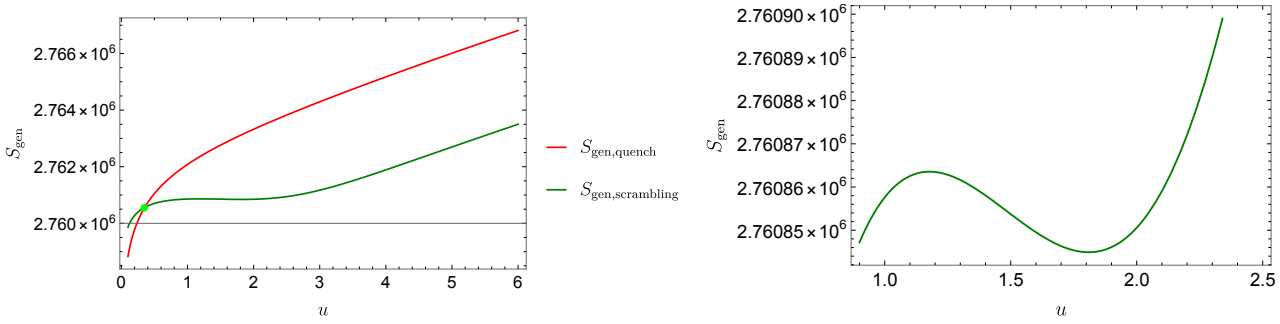

Figure 2.6: The generalized entropy from full solutions. The green curve is derived from (2.25) with exact solutions of (2.32). The red one represents the generalized entropy with endpoint at bifurcation point. The green point in the left plot indicates the point u_{QS} where $S_{\text{gen,scrambling}} = S_{\text{gen,quench}}$.

This approximation highlights that the growth of generalized entropy as a function of proper time u in the regime $1/\pi T_1 \ll u < k^{-1}$ is approximately linear, as shown in

figure 2.6. This linear growth is dominated by the second term, which comes from the bulk entropy term in eq. (2.13). However, at later times, the terms that we dropped at small k become important. Fortunately, it is easy to find that the evolution in the x^+ direction at late time is very small. We can therefore make use of the approximation

$$x^+_{\rm QES}(t) \approx x^+_{\rm QES}(t_\infty) > t_\infty\,, \qquad t \approx t_\infty\,. \tag{2.40}$$

and various terms in the generalized entropy will be close to a constant decided by its value at t_∞. For example,

$$\log\left(\frac{1}{x^+_{\rm QES}-x^-_{\rm QES}}\right) \approx -\log\left(\frac{2}{\pi T_0}+\frac{2k}{(\pi T_0)^2(\pi T_0 t_\infty-1)}\right)\,. \tag{2.41}$$

In order to get a simple expression for the generalized entropy, we define the following constant

$$\kappa = \frac{2(1-\pi T_0 x^+_{\rm QES})(\pi T_0 x^-_{\rm QES}+1)}{x^+_{\rm QES}-x^-_{\rm QES}} + 2k\log\left(\frac{\pi T_1 x^-_{\rm QES}(t-x^+_{\rm QES})}{x^+_{\rm QES}-x^-_{\rm QES}}\right)\Bigg|_{t\to t_\infty}\,, \tag{2.42}$$

and rewrite the entropy for very late u as

$$S_{\text{gen, scrambling}} \approx \frac{\bar{\phi}_r}{4G_{\rm N}}\left[2\pi T_0 + 2k\log\left(\frac{24\pi E_S}{\epsilon c}\frac{u}{\pi T_1\sqrt{f'(u)}}\right)+\kappa\right]\,, \tag{2.43}$$

The evolution of generalized entropy is dominated by the derivative term, which can be approximated by

$$\log\frac{1}{\sqrt{f'(u)}} \approx \frac{2\pi T_1}{k}\left(1-e^{-ku/2}\right) - \frac{1}{2}\log\left(4\pi T_1 t_\infty\right) + \frac{ku}{4} + \mathcal{O}(ke^{ku})\,. \tag{2.44}$$

For the late-time region $ku < 1$, the above term leads to a linearly increasing entropy

$$\begin{aligned} S_{\text{gen, scrambling}} \approx \frac{\bar{\phi}_r}{4G_{\rm N}}\Bigg[&2\pi(T_0+T_1 ku) + 2k\log\left(\frac{24\pi E_S}{\epsilon c}\frac{u}{2\pi T_1}\right) \\ &- \frac{\pi T_1}{2}k^2u^2 + \frac{k^2}{2}u + \kappa\Bigg]\,, \end{aligned} \tag{2.45}$$

as show in figure 2.6. Physically, we can understand this linear increase of entropy as the increase of entanglement between the Hawking quanta and their partners left behind the event horizon. For very late times $u > k^{-1}$, one can see from the above formula in eq. (2.43)

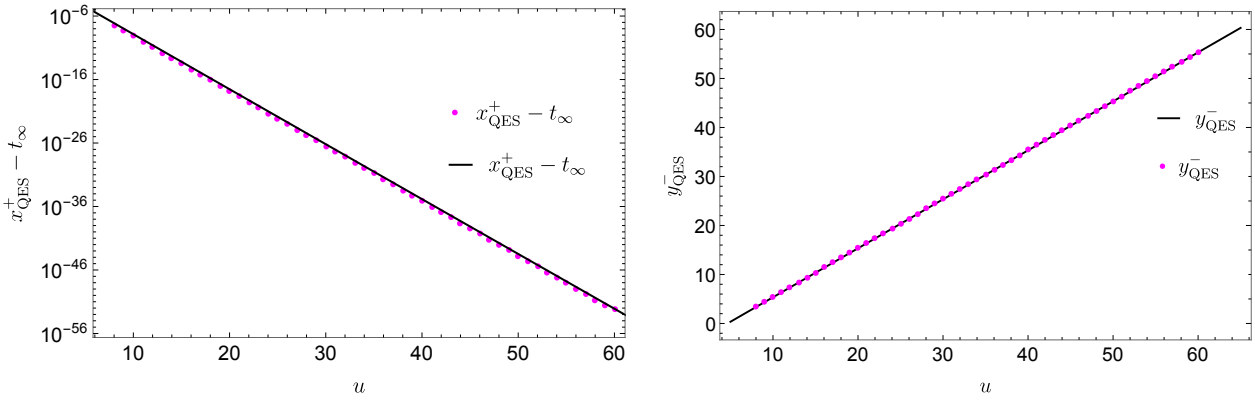

Figure 2.7: The numerical solutions $x^+_{\rm QES}, y^-_{\rm QES}$ from eqs. (2.48) is presented by the dotted lines. Note that the left plot is a log plot. The solid line is the linear approximation from (2.52).

that the linear dependence on time u breaks down and the entropy is dominated by the logarithmic term.

Having located the candidates for the quantum extremal surfaces in each phase using eq. (2.24), the next step is to compare their generalized entropies and pick the minimal solution. Using the approximations described above, we can find the transition occurs at

$$\log t_{\rm QS} \approx \log\left(\frac{x^-_{\rm QES}(t_{\rm QS} - x^+_{\rm QES})}{x^+_{\rm QES} - x^-_{\rm QES}}\right) + \frac{k\,(\pi T_0 t_{\rm QS} + 1)}{2\pi T_0\,(1 - \pi T_0 t_{\rm QS})} + \dots\,, \tag{2.46}$$

which gives the approximate solution

$$t_{\rm QS} \equiv f(u_{\rm QS}) \approx \frac{1}{3\pi T_0} - \frac{4k}{9\pi^2 T_0^2} + \frac{7k^2}{27\pi^3 T_0^3} + \dots\,. \tag{2.47}$$

Quantum extremal surfaces at later times

If the bulk endpoint is located in the region after the shock (*i.e.*, if $x^+_{\rm QES} \geq 0$), then the bulk entropy is in its late-time phase. The position of the QES is found by solving the

following two equations

$$0 = \frac{4G_{\rm N}}{\bar{\phi}_r}\partial_+ S_{\rm gen} = \frac{2(\pi T_1 x^-_{\rm QES})^2 - 2 - k\int_0^{x^-_{\rm QES}}(x^-_{\rm QES}-t)^2\{u,t\}\,dt}{(x^+_{\rm QES}-x^-_{\rm QES})^2} + 2k\left(\frac{1}{x^+_{\rm QES}-t} - \frac{1}{x^+_{\rm QES}-x^-_{\rm QES}}\right), \tag{2.48a}$$

$$0 = \frac{4G_{\rm N}}{\bar{\phi}_r}\partial_- S_{\rm gen} = \frac{2 - 2(\pi T_1 x^+_{\rm QES})^2 + k\int_0^{x^-_{\rm QES}}(x^+_{\rm QES}-t)^2\{u,t\}\,dt}{(x^+_{\rm QES}-x^-_{\rm QES})^2} + 2k\left(\frac{1}{x^+_{\rm QES}-x^-_{\rm QES}} - \frac{1}{(u-y^-_{\rm QES})f'(y^-_{\rm QES})} + \frac{f''(y^-_{\rm QES})}{2(f'(y^-_{\rm QES}))^2}\right). \tag{2.48b}$$

The integral terms in eqs. (2.48) are due to the stress-energy exchange through the boundary between the bath and the AdS_2 bulk, and make it hard to find the analytic solutions for these equations. Therefore, we first turn to numerics. Numerical solutions for the position of the QES are presented in figure 2.7, and the corresponding generalized entropy is shown in figure 2.8.

From the numerical plot, it is interesting to find that around the Page time, the two branches both display linear behavior. For the solution before the Page time, the linearity can be seen in the small k expansion in (2.36). The post-Page time analysis is performed in the original paper [11] by carefully dealing with the integral terms with the Schwarzian. The key idea is we can use the approximation for $f(u)$ around small k for fixed ku, specifically

$$\log\left(\frac{t_\infty - f(u)}{2t_\infty}\right) \sim -\frac{4\pi T_1}{k}\left(1 - e^{-\frac{k}{2}u}\right) + O\left(ke^{\frac{k}{2}u}\right). \tag{2.49}$$

Keeping only the leading terms in the QES equations ($\partial_\pm S_{\rm gen} = 0$), we arrive at these simple equations

$$0 \approx 4\pi T_1 \frac{e^{-\frac{k}{2}y^-_{\rm QES}}}{t_\infty - x^-_{\rm QES}} - \frac{2k}{x^+_{\rm QES}-t}, \tag{2.50}$$

$$0 \approx 4\pi T_1 (t_\infty - x^+_{\rm QES})e^{-\frac{k}{2}y^-_{\rm QES}} + \frac{k}{2}(t_\infty - x^-_{\rm QES}), \tag{2.51}$$

and solving at the same order,

$$x^+_{\rm QES} = \frac{4}{3}t_\infty - \frac{1}{3}t + \mathcal{O}(k(t_\infty - t)), \tag{2.52}$$

$$y^-_{\rm QES} = u - u_{\rm HP} + \frac{k}{2}\left(u_{\rm HP} - \frac{1}{2\pi T_1}\right)(u_{\rm HP} - u) + \mathcal{O}(k^2), \tag{2.53}$$

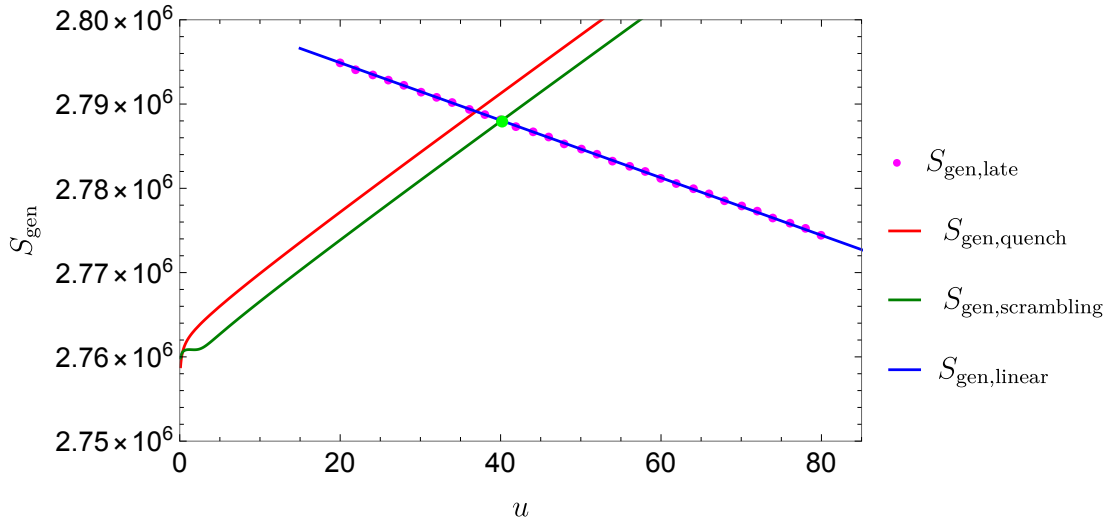

Figure 2.8: The dotted pink line shows the numerical results for generalized entropy with endpoint after the shock. The Page time and the first transition at the early time are both indicated by the green point in this plot. The solid red line is derived from the linear approximation, *i.e.,* eq. (2.60). The difference between analytical and numerical results is approximately constant, due to the constant error from the approximation of the dilaton term.

where we define the delay of y^- in time direction as

$$u_{\rm HP} = \frac{1}{2\pi T_1} \log\left(\frac{8\pi T_1}{3k}\right) , \tag{2.54}$$

which is (to leading order) the Hayden-Preskill scrambling time [119], as explained in [11]. Note that the quantum extremal surface after the shock $(x^+_{\rm QES}, y^-_{\rm QES})$ lies close to but behind the new horizon located at $x^+ = t_\infty$.

The above linear solution captures the leading-order behavior of the QES and the generalized entropy. In figure 2.7, we compare this analytic approximation to the numerical solution. We can find an approximation for the generalized entropy[7]

$$S_{\rm bulk} \approx \frac{c}{6}\left(\log\left(\frac{8u_{\rm HP}}{3\epsilon}\right) - \pi T_1 u_{\rm HP} + \frac{k}{4}u_{\rm HP}\right) + \mathcal{O}(k^2) , \tag{2.55}$$

[7]Compared to [11], here we added the contributions from bulk terms and also two sub-leading corrections for dilaton which are ignored in [11].

$$\phi \approx 2\bar{\phi}_r \left(\frac{1-(\pi T_1)^2 x^+_{\rm QES} x^-_{\rm QES} + \frac{k}{2} I\left(x^+_{\rm QES}, x^-_{\rm QES}\right)}{t_\infty - x^-_{\rm QES}} \right) \left(1 - \frac{x^+_{\rm QES} - t_\infty}{t_\infty - x^-_{\rm QES}}\right) + \mathcal{O}(k^2 \log k)\,, \tag{2.56}$$

$$I\left(t_\infty, x^-\right) \approx \frac{2}{k}\left((\pi T_1 t_\infty)^2 - 1\right) + \frac{t_\infty - x^-}{2}\left(\log\left(\frac{t_\infty - x^-}{t_\infty}\right) - 1\right)\,. \tag{2.57}$$

For times much smaller than k^{-1} we can further simplify these expressions by taking the limit

$$\begin{aligned} \log\left(\frac{t_\infty - f(u)}{t_\infty - f(y^-)}\right) &\sim \frac{4\pi T_1}{k}\left(e^{-\frac{k}{2}u} - e^{-\frac{k}{2}y^-}\right) + O\left(k e^{\frac{k}{2}u}\right) \approx 2\pi T_1 (y^- - u)\,, \\ \log\left(\frac{f'(y^-)}{f'(u)}\frac{t_\infty - f(u)}{t_\infty - f(y^-)}\right) &\approx \log\left(e^{\frac{k}{2}(u-y^-)}\right) = \frac{k}{2}(u - y^-)\,. \end{aligned} \tag{2.58}$$

Using these approximations, we find the entropy from the dilaton contribution decreases linearly

$$\phi \approx \bar{\phi}_r \left(2\pi T_1 - k\pi T_1 (u - u_{\rm HP}) - \frac{k}{2}\log 2e\right)\,, \tag{2.59}$$

and we find the generalized entropy decreases linearly with time

$$S_{\rm linear} \approx \frac{\bar{\phi}_r}{4G_{\rm N}}\left[2\pi T_1 - k\pi T_1 (u - u_{\rm HP}) + k\log\left(\frac{8k u^2_{\rm HP}}{3\sqrt{2e}\epsilon^2 \pi T_1}\right) + \mathcal{O}(k^2 \log(k))\right]\,, \tag{2.60}$$

where the first two terms are derived from the dilaton term which lead to the linear decrease of the entropy around the Page time, and the extra constant terms are contributions from the bulk entropy.

The linear formula given above matches the numerical results shown in figure 2.8. As shown in this figure, when the time is larger than the Page time $u_{\rm Page}$, the endpoint of QES jumps from the point before the shock to that after the shock.

From the approximations in eqs. (2.60) and (2.39), we can find the approximate Page time

$$\begin{aligned} u_{\rm Page} \approx \frac{2}{3}\frac{T_1 - T_0}{T_1 k} + \frac{u_{\rm HP}}{3} + \frac{k}{6\pi T_1}\frac{5}{(T_1 - T_0)\pi} \\ + \frac{2}{3\pi T_1}\log\left(\sqrt{\frac{8k\pi T_1}{3\sqrt{2e}}}\frac{u_{\rm HP}}{u^0_{\rm P}}\frac{c}{6\pi E_{\rm S}}\frac{T_0}{T_1 - T_0}\right) + \mathcal{O}(T_1 - T_0)\,, \end{aligned} \tag{2.61}$$

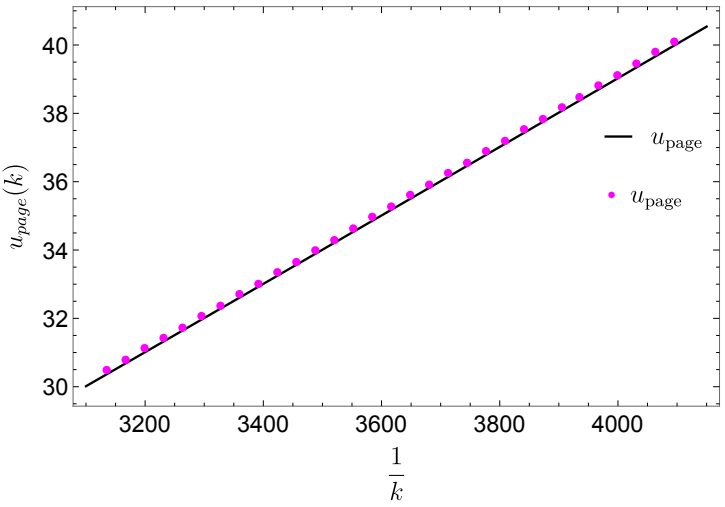

Figure 2.9: The Page time for fixed temperatures T_0 and T_1, as a function of k^{-1}. The dots are derived from numerical results without any approximation and the solid line is the approximate Page time defined in (2.61).

where we have defined[8]

$$u_{\text{P}}^0 = \frac{2}{3}\frac{T_1 - T_0}{T_1 k} + \frac{u_{\text{HP}}}{3} \tag{2.62}$$

as the leading-order approximation to u_{Page}. A comparison with numerical results is given in figure 2.9.

2.2 Structure of information

As was shown in section 2.1, the evaporating model we are considering exhibits two phase transitions. Each phase corresponds to a different location for the quantum extremal surface inside the new horizon. An important consequence of these transitions is that the entanglement wedge of QM_{L}+bath contains a bigger region of the bulk geometry after each phase transition. In particular, there is an area inside the black hole that is contained in the entanglement wedge after the transitions, but not before. This is illustrated in figure 2.10. By entanglement wedge reconstruction [10, 131, 132, 133, 134, 135, 136], this implies that after some time, QM_{L} plus the bath contain information about the interior

[8]Here we have kept the $\frac{k}{T_1 - T_0}$ term, which may be order one for some choices for parameters.

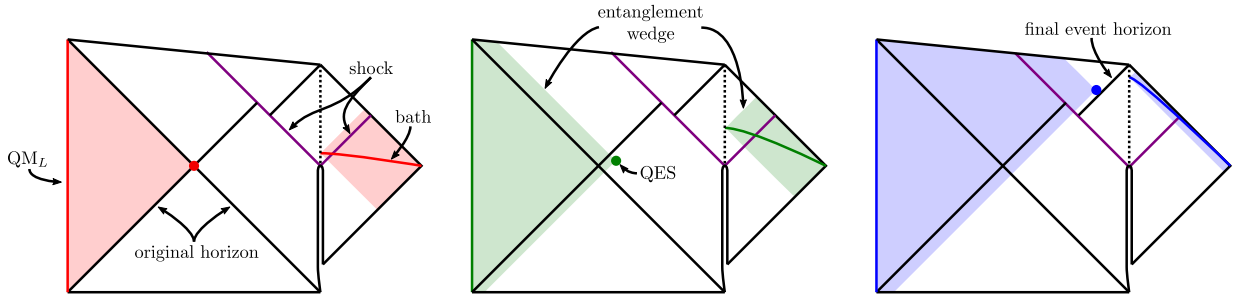

Figure 2.10: Entanglement wedges for the three phases of evolution. The quench phase is in red, the scrambling phase in green and the late-time phase in blue.

of the black hole.[9] In this section, we investigate how much of the bath is essential to keep in order to still reconstruct the black hole interior. For concreteness we will focus on the Page transition in which the quantum extremal surface jumps across the infalling shock, because this transition allows much more of the interior to be reconstructed; but a qualitatively similar story occurs for the first transition, in which the extremal surface jumps from the bifurcation point to a point perturbatively close to it.

Before the evaporation begins, the black hole interior cannot be reconstructed from only the $\mathrm{QM_L}$ or the $\mathrm{QM_R}$ system since it is not contained in the entanglement wedge of either. On the other hand, the combination of the $\mathrm{QM_L}$ and $\mathrm{QM_R}$ is enough to reconstruct the entire bulk geometry. This implies that the information required to reconstruct the interior of the black hole is shared between the two sides of the black hole. One can also ask what is the entanglement wedge of $\mathrm{QM_R}$ (or $\mathrm{QM_L}$)+bath before evaporation begins, but the answer is trivial because there is no entanglement between the two: it is the entanglement wedge of $\mathrm{QM_R}$ ($\mathrm{QM_L}$) plus the empty set. After the Page time, enough evaporation has taken place and the quantum extremal surface of $\mathrm{QM_R}$ is located after the shock perturbatively close to the apparent horizon. The entanglement wedge of $\mathrm{QM_R}$ is *smaller* than it was before evaporation began: $\mathrm{QM_R}$ has *lost* part of the information required to reconstruct some of the bulk geometry it was originally encoding before the evaporation. On the other hand, the entanglement wedge of the complement, the $\mathrm{QM_L}$ plus the bath, *gained* information encoding part of the interior of the black hole. This reflects the fact that some of the initial entanglement between $\mathrm{QM_L}$ and $\mathrm{QM_R}$ has been

[9] In the present example the black hole interior is relatively calm and undisturbed. However, entanglement wedge reconstruction [131, 132, 133, 134, 135, 136] indicates that the bath + $\mathrm{QM_L}$ system would know about disturbances falling into the black hole. This would hold at least for small amounts of matter falling in, as long as the entanglement structure is perturbatively stable. However, we note that the perturbative stability of the entanglement structure of this setup has not yet been rigorously studied.

transferred to the bath by the Hawking radiation so that $\mathrm{QM_L}$+bath can reconstruct a portion of the black hole interior. In this section, we set out to study the structure of where the information necessary to reconstruct the black hole interior is encoded during the evaporation process.

2.2.1 Early-time protocol: forgetting the late-time radiation

Our first modification of the AEM^{4}Z model as described in section 2.1 is to move the endpoint $y_1^\pm$ of the bulk interval into the bath region. This corresponds to omitting the late-time Hawking radiation from the entanglement wedge of $\mathrm{QM_L}$+bath. In this regime, we will have $y_1^\pm > 0$.

We parameterize the distance from a bath point to the AdS boundary by specifying the coordinate distance σ_1 from the boundary to the bath, *i.e.,* we set $y_1^\pm = u \mp \sigma_1$. Similar to eq. (2.24), we can identify three phases of the von Neumann entropy of the interval in the bulk, which we label the same way: the quench phase, the scrambling phase, and the late-time phase. The most important difference is in the Lorentzian cross-ratio, where we must now account for the fact that the endpoints are not fixed on the boundary

$$\eta = \frac{f(y_1^+)(x_{\mathrm{QES}}^+ - x_{\mathrm{QES}}^+))}{x_{\mathrm{QES}}^+(f(y_1^+) - x_{\mathrm{QES}}^-)} \tag{2.63}$$

The phase boundary between the quench and scrambling phases still lies at $\eta = \frac{1}{2}$. The entropy functions in each phase now read

$$S_{\text{bulk, quench}} = \frac{c}{6}\log\left(\frac{24\pi E_S}{\epsilon c}\frac{y_1^- f(y_1^+)}{\sqrt{f'(y_1^+)}}\right), \tag{2.64}$$

$$S_{\text{bulk, scrambling}} = \frac{c}{6}\log\left(\frac{24\pi E_S}{\epsilon c}\frac{y_1^- x_{\mathrm{QES}}^- \left(f(y_1^+) - x_{\mathrm{QES}}^+\right)}{(x_{\mathrm{QES}}^+ - x_{\mathrm{QES}}^-)\sqrt{f'(y_1^+)}}\right), \tag{2.65}$$

$$S_{\text{bulk, late-time}} = \frac{c}{6}\log\left[\frac{2\left(y_1^- - y_{\mathrm{QES}}^-\right)\left(x_{\mathrm{QES}}^+ - f(y_1^+)\right)}{\epsilon\left(x_{\mathrm{QES}}^+ - x_{\mathrm{QES}}^-\right)}\sqrt{\frac{f'(y_{\mathrm{QES}}^-)}{f'(y_1^+)}}\right]. \tag{2.66}$$

The location of the corresponding quantum extremal surface $x_{\mathrm{QES}}^\pm$ is found by minimizing the generalized entropy ($\partial_\pm S_{\mathrm{gen}} = 0$). Before we move to finding the solutions, let's first comment on the effect of taking the point x_1 into the bath region, *i.e.,*

$$y_1^\pm = u \mp \sigma_1\,. \tag{2.67}$$

It is obvious this operation has nontrivial effect on the location of the quantum extremal surface and bulk entropy because the entropy in the three cases all depend on both $y_1^{\pm}$. However, the effect from y_1^- only appears in $S_{\rm gen}$ as a term like

$$\begin{cases} \frac{c}{6}\log\left(y_1^-\right) & \text{for} \quad x^-_{\rm QES} < 0 < t < x^+_{\rm QES}\,, \\ \frac{c}{6}\log\left(y_1^- - y^-_{\rm QES}\right) & \text{for} \quad 0 < x^-_{\rm QES} < t < x^+_{\rm QES}\,. \end{cases} \tag{2.68}$$

If the above contribution is negligible, it is easy to claim that the effect from moving the endpoint to the bath corresponds to a reparameterization, changing u to $u - y_0$. At leading order, this is what happens, as we will now explain.

As before, the bulk entropy in the quench phase is independent of the location of the quantum extremal surface. Again the dilaton term is minimized at the bifurcation point $x^{\pm} = \pm\frac{1}{\pi T_0}$, so this is the location of the quantum extremal surface in the quench phase. The generalized entropy in this quench ($\eta \leq \frac{1}{2}$) phase reads

$$S_{\text{gen, quench}} = \frac{\bar{\phi}_r}{4G_{\rm N}}\left(2\pi T_0 + 2k\log\left(\frac{24\pi E_S}{\epsilon c}\frac{y_1^- f(y_1^+)}{\sqrt{f'(y_1^+)}}\right)\right)\,. \tag{2.69}$$

which reduces to the AdS-boundary case when we take the limit $y^{\pm} \sim u$ or $\sigma_1 \to 0$, as expected. The cross-ratio region $\eta \leq \frac{1}{2}$ that defines the quench phase is equivalent to

$$f(y_1^+) \leq \frac{1}{3\pi T_0}\,, \qquad y_1^+ = u - \sigma_1 \leq f^{-1}(\frac{1}{3\pi T_0})\,. \tag{2.70}$$

The location of the quantum extremal surface in the scrambling phase and with $\sigma_1 > 0$ is delayed with respect to the $\sigma_1 = 0$ solution, because the solutions to the extrema equations ($0 = \partial_{\pm} S_{\rm gen}$), which read

$$0 = \frac{(\pi T_0 x^-_{\rm QES})^2 - 1}{x^+_{\rm QES} - x^-_{\rm QES}} + k\frac{x^-_{\rm QES} - f(y_1^+)}{f(y_1^+) - x^+_{\rm QES}}\,, \tag{2.71}$$

$$0 = \frac{1 - (\pi T_0 x^+_{\rm QES})^2}{x^+_{\rm QES} - x^-_{\rm QES}} + k\frac{x^+_{\rm QES}}{x^-_{\rm QES}} \tag{2.72}$$

only depend on $f(y_1^+)$. The location is similar to eq. (2.34) after making the replacement $u \to y_1^+$, $t \to f(y_1^+)$, *i.e.*,

$$x^{\pm}_{\rm QES} = x^{\pm}_{\rm QES}(f(y_1^+))\,. \tag{2.73}$$

Although the location of the quantum extremal surface is simply delayed by σ_1, the generalized entropy still has the non-trivial term from $\log y_1^-$ as we claimed before:

$$S_{\text{gen, scrambling}} \approx \frac{\bar{\phi}_r}{4G_{\text{N}}}\left[2\pi T_0 + 2k\log\left(\frac{24\pi E_S}{\epsilon c}\frac{u+\sigma_1}{\pi T_1\sqrt{f'(u-\sigma_1)}}\right)+\kappa\right], \tag{2.74}$$

where κ is defined in eq. (2.42) and we have assumed $\eta \geq \frac{1}{2}$ and $u \gg 1$. This extra term is still sub-leading, with the full generalized entropy dominated by the linear growth at early times $u \ll \frac{1}{k}$.

Similar to the $\sigma_1 = 0$ case, the transition between the quench and scrambling phases happens at the point where

$$S_{\text{gen, scrambling}} = S_{\text{gen, quench}} \qquad \longleftrightarrow \qquad y^+_{\text{QS}} = u_{\text{QS}}\,. \tag{2.75}$$

where the equivalence is exact because of the cancellation of $\log y^-$ in $S_{\text{gen,scrambling}} - S_{\text{gen,quench}}$. Just like the $\sigma_1 = 0$ case considered in section 1.2, the quantum extremal surface is at the bifurcation point until u_{AB} and then jumps to $x^{\pm}(y^+)$ in eq. (2.34). This marks the transition between the quench phase and the scrambling phase.

In the late time phase, the quantum extremal surface is located after the shock, and the extremum equations $0 = \partial_{\pm} S_{\text{gen}}$ can be expanded into first order in k to read

$$0 \approx 2\pi T_1 \frac{e^{-\frac{k}{2}y^-_{\text{QES}}}}{t_\infty - x^-_{\text{QES}}} - \frac{k}{x^+_{\text{QES}} - f(y_1^+)}\,, \tag{2.76}$$

$$0 \approx 4\pi T_1 (t_\infty - x^+_{\text{QES}}) e^{-\frac{k}{2}y^-_{\text{QES}}} + \frac{k}{2}(t_\infty - x^-_{\text{QES}})\,. \tag{2.77}$$

This leads to the linear solution

$$x^+_{\text{QES}} = \frac{4}{3}t_\infty - \frac{1}{3}f(y_1^+) + \mathcal{O}(k(t_\infty - f(y_1^+)))\,, \tag{2.78}$$

$$y^-_{\text{QES}} = y_1^+ - u_{\text{HP}} + \frac{k}{2}\left(u_{\text{HP}} - \frac{1}{2\pi T_1}\right)\left(u_{\text{HP}} - y_1^+\right) + \mathcal{O}(k^2)\,. \tag{2.79}$$

The generalized entropy in the late time phase is given by eq. (2.39)

$$S_{\text{linear}} \approx \frac{\bar{\phi}_r}{4G_{\text{N}}}\left[2\pi T_1 - k\pi T_1(u - \sigma_1 - u_{\text{HP}}) + k\log\left(\frac{8k(u_{\text{HP}}+2\sigma_1)^2}{\sqrt{2e}3\epsilon^2(\pi T_1)}\right) + \mathcal{O}(k^2\log(k))\right]. \tag{2.80}$$

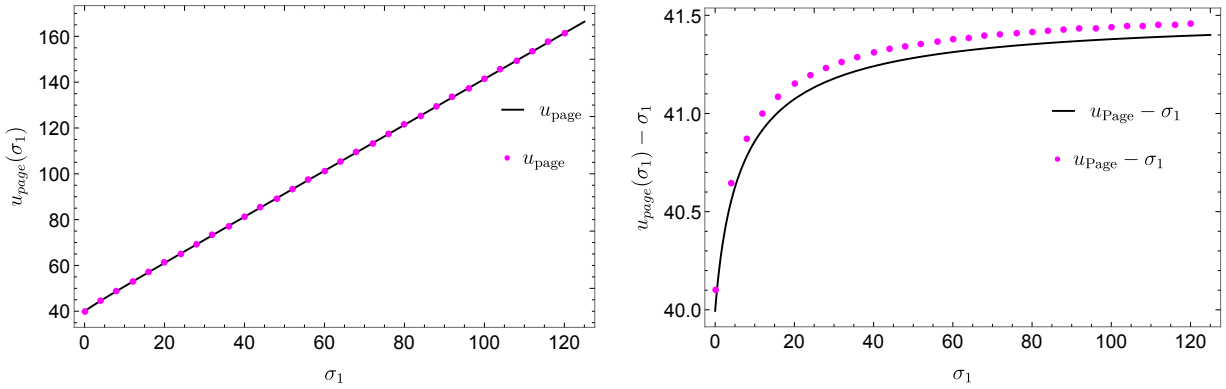

Figure 2.11: Left: The numerical results for u_{Page} on the dependence on σ_1 and the comparison with analytical result defined in (2.81). Right: $u_{\text{Page}} - \sigma_1$

With the new approximations (2.80), we can also define the Page time for this late-radiation-excised bath with fixed δ as

$$u_{\text{Page}}(\sigma) \approx \frac{2}{3}\frac{T_1 - T_0}{T_1 k} + \frac{u_{\text{HP}}}{3} + \sigma + \frac{2}{3\pi T_1}\log\left(\sqrt{\frac{8k\pi T_1}{3\sqrt{2e}}}\frac{(u_{\text{HP}} + 2\sigma)}{(u_{\text{P}}^0 + 2\sigma)}\frac{c}{6\pi E_S}\frac{T_0}{T_1 - T_0}\right) + \frac{k}{6\pi T_1}\frac{5}{(T_1 - T_0)\pi} + \mathcal{O}(T_1 - T_0)\,, \tag{2.81}$$

with the crossing condition $S_{\text{linear}} = S_{\text{gen, scrambling}}$. It is clear that it is just the $u_{\text{Page}} + \sigma$ with corrections from one log term which is decreasing with the increase of σ. As a final check, in figure 2.11 we compare the numerical results for the Page time with the analytical approximation.

Time evolution of σ_{Page}

Armed with the approximate solution (2.81), we can fix a time slice u after the Page time and ask how far into the bath we need to move to arrive at the Page transition. To fix the notation, we will say that this happens at

$$y^{+}_{\text{Page}} \equiv u - \sigma_{\text{Page}}\,, \tag{2.82}$$

We can thus consider the evolution of the distance of the second endpoint to AdS boundary σ_{Page} such that

$$u - \sigma_{\text{Page}} - u_{\text{Page}} = \frac{2}{3\pi T_1}\left(\log\left(\frac{u_{\text{HP}} + 2\sigma_{\text{Page}}}{u_{\text{HP}}}\right) - \log\left(\frac{u_{\text{Page}} + 2\sigma_{\text{Page}}}{u_{\text{Page}}}\right)\right)\,, \tag{2.83}$$

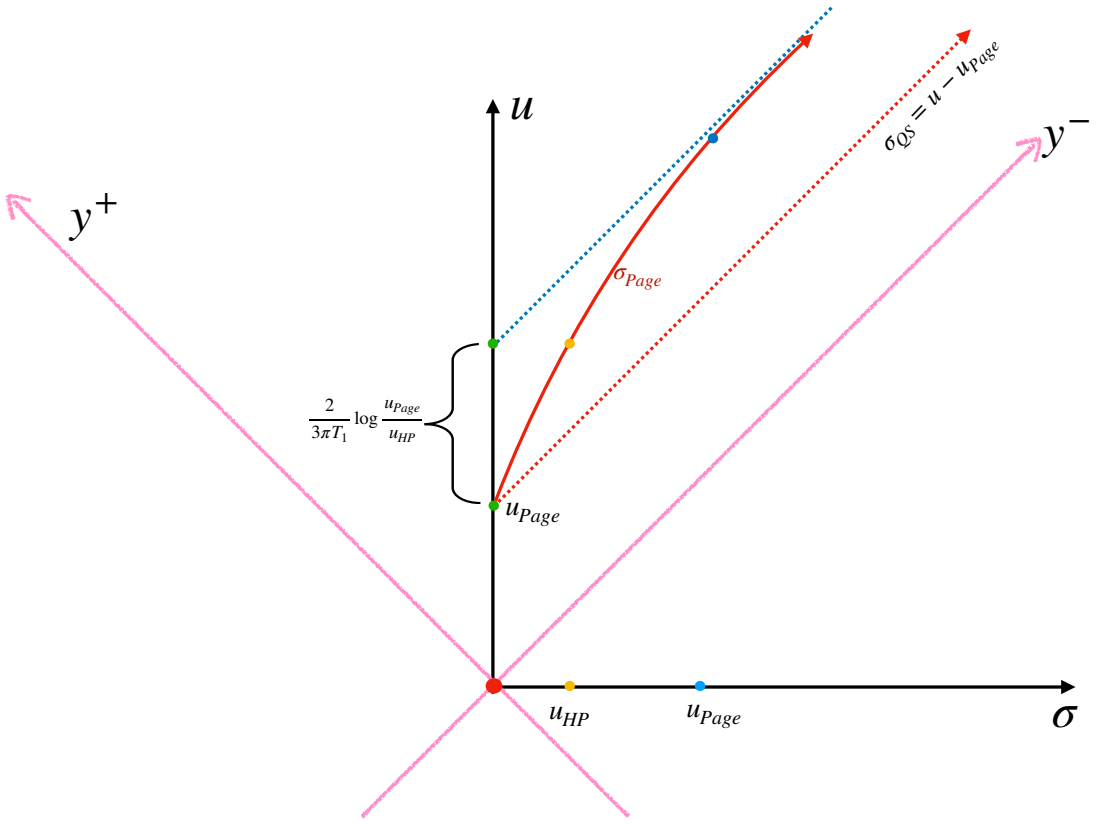

Figure 2.12: The red line indicates the evolution of $\sigma_{\rm Page}$. It starts from the boundary point at $u = u_{\rm Page}$ and evolves with time u. For very late times, it approaches another null surface with shift $\frac{2}{3\pi T_1}\log\left(\frac{u_{\rm Page}}{u_{\rm HP}}\right)$.

which is derived from the approximation of $y^+_{\rm Page}$ and $u_{\rm Page}$. It is still hard to solve the above equation for $\sigma_{\rm Page}$. However, let's first comment on its speed with respect to u, *i.e.*,

$$\partial_u \sigma_{\rm Page} = \left(1 + \frac{4}{3\pi T_1}\frac{u_{\rm Page} - u_{\rm HP}}{(u_{\rm HP} + 2\sigma_{\rm Page})(u_{\rm Page} + 2\sigma_{\rm Page})}\right)^{-1} < 1\,, \tag{2.84}$$

which approaches 1 when $\sigma_{\rm Page} \to \infty$. In order to get insight on the simple form of $\sigma_{\rm Page}$, we consider three different regions for $\sigma_{\rm Page}$ using the separation of scales: $\frac{1}{\pi T_1} \ll u_{\rm HP} \ll u_{\rm Page}$.

First of all, if we start from a small $\sigma_{\rm Page}$, it is easy to find for $\sigma < u_{\rm HP}$

$$\sigma_{\rm Page}(\sigma) \simeq \left(1 + \frac{4}{3\pi T_1}\frac{u_{\rm Page} - u_{\rm HP}}{u_{\rm Page} u_{\rm HP}}\right)^{-1}(u - u_{\rm Page})\,, \tag{2.85}$$

where the coefficient is a little bit smaller than one. Then we can move to the middle region with the approximate solution for $u_{\rm HP} < \sigma < u_{\rm Page}$:

$$\sigma_{\rm Page} \simeq \left(1 - \frac{4}{3\pi T_1 u_{\rm Page}}\right)^{-1} \left(u - u_{\rm Page} - \frac{2}{3\pi T_1} \log \frac{u_{\rm HP} + 2(u - u_{\rm Page})}{u_{\rm HP}}\right). \tag{2.86}$$

Note that although the coefficient looks larger than 1, it is easy to check that with the logarithmic correction, the velocity in this region still satisfies $\partial_u \sigma_{\rm Page} < 1$.

Finally we arrive at the region with $\sigma_{\rm Page} > u_{\rm Page}$, one can still find a linear result when $u_{\rm Page} < \sigma$:

$$\sigma_{\rm Page} \simeq u - u_{\rm Page} - \frac{2}{3\pi T_1} \log\left(\frac{u_{\rm Page}}{u_{\rm HP}}\right) + \frac{u_{\rm Page} - u_{\rm HP}}{3\pi T_1 (u - u_{\rm Page})}. \tag{2.87}$$

So we can find that the evolution of $\sigma_{\rm Page}$ is time-like. However in this regime it quickly approaches a null line as the last term decays as $u - u_{\rm Page}$ grows. We note that the third term above represents a (small) finite shift of the asymptotic line above the simple leading approximation $y^+_{\rm QES} \simeq u - u_{\rm Page}$. We show a sketch of the evolution of $y^+_{\rm QES}$ in figure 2.12, summarizing our results here.

In closing here, we comment that a similar but even simpler conclusion applies to the transition between the quench and scrambling phases. Recall that this transition occurs at $u = u_{\rm QS}$ defined in eq. (2.47). Then on later time slices, we push σ_1 into the bath and define $\sigma_{\rm QS}$ in analogy with $y^+_{\rm QES}$, *i.e.*, $\sigma_{\rm QS}$ is the value of σ on a constant u slice where the transition between the quench and scrambling branches occurs. From eq. (2.75), it is straightforward to show that $\sigma_{\rm QS}$ *exactly* satisfies the simple relation

$$\sigma_{\rm QS} = u - u_{\rm QS}\,. \tag{2.88}$$

Importance of the early radiation

So far we have seen how much of the later radiation can be discarded while still being able to reconstruct the interior of the black hole with the remaining radiation + $\rm QM_L$. This was done by starting at some time slice after the Page time and removing an interval of the bath starting from the AdS-bath juncture until the generalized entropy of the late-time branch matches the entropy of the scrambling branch. That is, we found the point $x_1^+ = f(y_1^+)$ in the bath such that

$$S_{\rm QES'-1} = S_{\rm QES-1}\,, \tag{2.89}$$

where $x^+_{\rm QES'}$ is at the extrema of the generalized entropy with one endpoint before the shock, and $x^+_{\rm QES}$ is at the extrema of the generalized entropy with both endpoints after the shock.

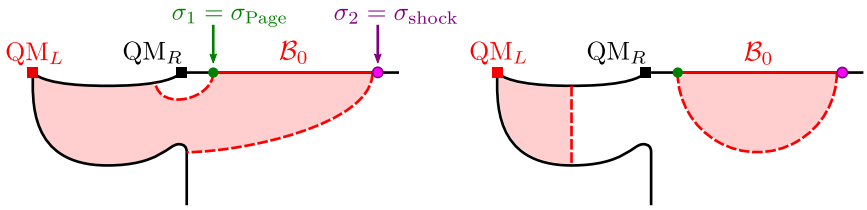

Figure 2.13: The smallest connected bath interval $\mathcal{B}_0$ that, together with the QM_L, still has enough information to reconstruct the black hole interior is the one in which the generalized entropy in the two channels depicted are equal.

This allows us to remove part of the bath close to AdS that is not essential for black hole interior reconstruction. We can now ask the question of how much of the early-radiation regime of the bath we can remove while still keeping information about the black hole interior. That is, we consider a bath interval $\mathcal{B}_0 = [\sigma_1 = y^+_{\text{QES}}(u), \sigma_2]$ on a constant time slice u, and ask how close can we move σ_2 to the initial endpoint while still being able to reconstruct the black hole interior. Unsurprisingly, we must place σ_2 near the shockwave falling into the bath, since more distant points are out of causal contact with the quench point. However, we will also find that σ_2 must be positioned slightly to the right of the shock, *i.e.,* we need to keep all of the early radiation.

As above, consider an interval of the bath $\mathcal{B}_0 = [\sigma_1 = y^+_{\text{QES}}(u), \sigma_2]$, and then in terms of the null coordinates, the endpoints are positioned at $y_1^\pm = u \mp \sigma_{\text{Page}}$ and $y_2^\pm = u \mp \sigma_2$. Now we ask for the smallest of σ_2 such that

$$S^{\text{gen}}_{\text{QES}''} + S_{1-2} = S^{\text{gen}}_{\text{QES}-1} + S_2 \tag{2.90}$$

where $x_{\text{QES}''}$ is at the bifurcation point and x_{QES} is at the extrema of the late time generalized entropy. This is illustrated in figure 2.13

We begin by assuming that y_2 is close to spacelike infinity of the bath, so that $y_2^- > 0$, $y_2^+ < 0$, and see how much closer to AdS we can bring it without losing the information required to reconstruct the interior of the black hole. After the coordinate transformation (2.12) and the Weyl rescaling required to bring to the evaporating black hole model,

we find the generalized entropy for these two channels is

$$S^{\rm gen}_{\rm QES''} + S_{1-2} = \frac{c}{6}\log\left(\frac{24\pi E_S}{c\epsilon^2}\frac{-y_2^+ x_1^+ (y_2^- - y_1^-)}{\sqrt{f'(y_1^+)}}\right) + \frac{\phi(x_{\rm QES''})}{4G_N}\,, \tag{2.91}$$

$$S^{\rm gen}_{\rm QES-1} + S_2 = \frac{c}{6}\log\left(\frac{2}{\epsilon^2}\frac{(y_1^- - y^-_{\rm QES})(x^+_{\rm QES} - x_1^+)(y_2^- - y_2^+)\sqrt{f'(y^-_{\rm QES})}}{(x^+_{\rm QES} - x^-_{\rm QES})\sqrt{f'(y_1^+)}}\right) + \frac{\phi(x_{\rm QES})}{4G_N}\,. \tag{2.92}$$

The value of the dilaton at the bifurcation $x_{\rm QES''}$ is

$$\phi(x_{\rm QES''}) = \phi_0 + 2\pi T_0 \bar{\phi}_r\,. \tag{2.93}$$

The dilaton at the extremal point $x_{\rm QES}$ is given by eq. (2.59) to first order in k. The position x_0 of the extremal surface in eq. (2.52) to leading order in k is

$$x^+_{\rm QES} \approx t_\infty\,, \quad y^-_{\rm QES} \approx y_1^+ - u_{HP}\,. \tag{2.94}$$

Using the leading order in eq. (2.49) and its derivative

$$\frac{f'(u)}{t_\infty - f(u)} \approx 2\pi T_1\,, \tag{2.95}$$

we find $\Delta S^{\rm gen} = S^{\rm gen}_{\rm QES''} + S_{1-2} - S^{\rm gen}_{\rm QES-1} - S_2$ is

$$\begin{aligned}\frac{4G_N}{\bar{\phi}_r}\Delta S^{\rm gen} = &\left(2\pi(T_0 - T_1) + k\pi T_1(3y_1^+ + u_{HP}) + \frac{k}{2}\log 2e\right)\\ &+ 2k\log\left(\frac{6\pi E_S}{c}\frac{-y_2^+ x_1^+ (y_2^- - y_1^-)}{(y_1^- - y_1^+ + u_{HP})(y_2^- - y_2^+)}\right) + \mathcal{O}(k^2)\,,\end{aligned} \tag{2.96}$$

where we have used $\frac{\bar{\phi}_r}{4G_N} = \frac{c}{12k}$.

The very large negative $\frac{c\pi}{6k}(T_0 - T_1)$ term is offset by the $\frac{c\pi}{4k}T_1 y_1^+$ term because we are choosing $y_1^+ = u_{\rm Page}(\sigma_{\rm Page}) - \sigma_{\rm Page}$ where $u_{\rm Page}$ can be read off eq. (2.81). Plugging the value of $y_1^\pm$ and $y_2^\pm$, we find

$$\frac{4G_N}{\bar{\phi}_r}\Delta S^{\rm gen} = 2k\log\left(\frac{8}{3\sqrt{\pi T_1 t_\infty}}\frac{T_0}{T_1 - T_0}\frac{(\sigma_2 - u_{\rm Page})(\sigma_2 - \sigma_{\rm Page})}{(2\sigma_{\rm Page} + u_P^0)(2\sigma_2)}\right) + \mathcal{O}(k^2)\,, \tag{2.97}$$

where we have used $u_{\rm Page} = u_{\rm Page}(\sigma_{\rm Page})$ to simplify the equation and once again u_P^0 in eq. (2.62) is the leading order approximation to $u_{\rm Page}$. The $(T_1 - T_0)(u_P^0 + 2\sigma_{\rm Page})$ term in

the denominator is small, and the only term that can offset this to bring the argument of the logarithm close to one is $y_2^+ = \sigma_2 - u_{\text{Page}}$. But this requires us to anchor the end of the bath interval a distance $\sim (T_1 - T_0)u/T_1$ to the right of the shock. The takeaway from this calculation is that we can remove most of the bath behind the shock. This should be expected because these intervals do not capture any of the radiation of the evaporating black hole, so they should not be essential for interior reconstruction.

We can now consider what happens when the point x_2 crosses the shock, and see if we can remove any more of the bath interval. This would amount to removing some of the early radiation after the evaporation began. In terms of the calculation, the difference now is that $x_2^+ > 0$ and therefore $\bar{z} = \left(\frac{12\pi}{c}E_S\right)^{-2}\frac{i}{x^+}$ so that the expressions for the generalized entropies of the two channels in eqs. (2.91) and (2.92) are now

$$\begin{aligned} S^{\text{gen}}_{\text{QES}''} + S_{1-2} &= \frac{c}{6}\log\left(\frac{2}{\epsilon^2}\frac{(x_1^+ - x_2^+)(y_2^- - y_1^-)}{\sqrt{f'(y_1^+)f'(y_2^+)}}\right) + \frac{\phi(x_{\text{QES}''})}{4G_N}\,, \\ S^{\text{gen}}_{\text{QES}-1} + S_2 &= \frac{c}{6}\log\left(\frac{24\pi E_S}{c\epsilon^2}\frac{y_2^- x_2^+ (y_1^- - y^-_{\text{QES}})(x^+_{\text{QES}} - x_1^+)\sqrt{f'(y^-_{\text{QES}})}}{(x^+_{\text{QES}} - x^-_{\text{QES}})\sqrt{f'(y_1^+)f'(y_2^+)}}\right) + \frac{\phi(x_{\text{QES}})}{4G_N}\,. \end{aligned} \tag{2.98}$$

Using the position of the extremal surface in eq. (2.52), the approximation in eq. (2.49) and plugging the positions of the endpoints y_1 and y_2 the difference in the entropies of the two channels ΔS^{gen} is

$$\frac{4G_N}{\bar{\phi}_r}\Delta S^{\text{gen}} = 2k\log\left(\left(\frac{c}{12\pi E_S}\right)^2 \frac{8\pi T_1}{3\sqrt{\pi T_1 t_\infty}}\frac{T_0}{T_1 - T_0}\frac{(x_1^+ - x_2^+)(\sigma_2 - \sigma_{\text{Page}})}{(u_{\text{Page}} + \sigma_2)x_2^+(2\sigma_{\text{Page}} + u_P^0)}\right) + \mathcal{O}(k^2)\,. \tag{2.99}$$

The term in the denominator $\left(\frac{12\pi E_S}{c}\right)^2(T_1 - T_0)(u_P^0 + 2\sigma_{\text{Page}}) \sim E_S^4 k/c^2 T_1^3$ is very large and needs to be canceled by the separation y_2^+ of the point y_2 from the shock. Taking the ansatz $y_2^+ = d\,\eta$ with

$$\eta = \left(\frac{c}{12\pi E_S}\right)^2 \frac{8\pi T_1}{3(u_P^0 + 2\sigma_{\text{Page}})\sqrt{\pi T_1 t_\infty}}\frac{T_0}{T_1 - T_0} \lesssim \left(\frac{cT_1}{6E_S}\right)^4 \frac{\pi T_1}{k} \ll 1\,, \tag{2.100}$$

we find that $y_2^- = 2u_{\text{Page}} - d\,\eta$ and $x_2^+ = y_2^+ + \mathcal{O}((y_2^+)^3) = d\eta + \mathcal{O}(\eta^3)$. Solving for $\Delta S^{\text{gen}} = 0$ then gives

$$d = x_1^+\frac{u_{\text{Page}} - \sigma_{\text{Page}}}{2u_{\text{Page}}} - x_1^+\frac{u_{\text{Page}} - \sigma_{\text{Page}}}{2u_{\text{Page}}}\frac{u_{\text{Page}}(x_1^+ + 2u_{\text{Page}}) + \sigma_{\text{Page}}(x_1^+ - 2u_{\text{Page}})}{4u_{\text{Page}}^2}\eta + \mathcal{O}(\eta^2)\,. \tag{2.101}$$

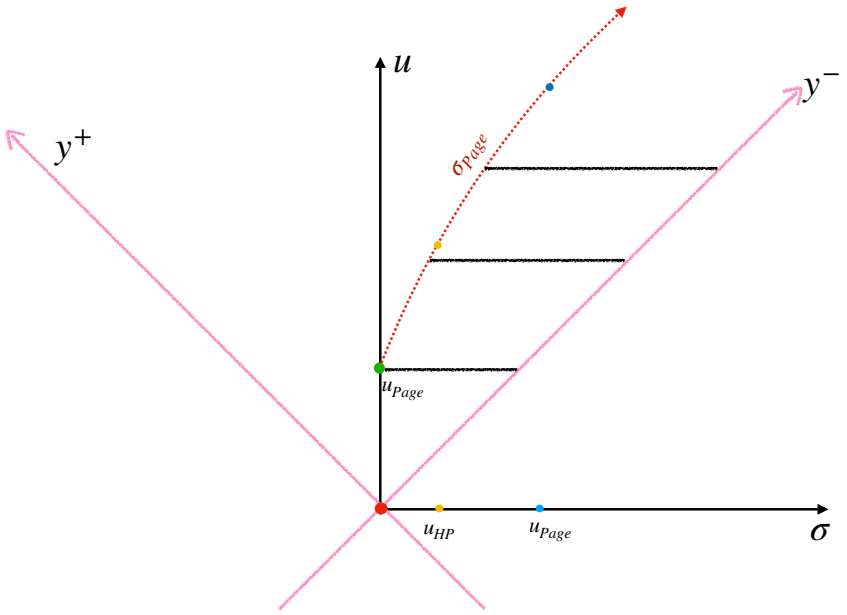

Figure 2.14: Smallest connected intervals that, together with $\mathrm{QM_L}$, are able to reconstruct a part of the black hole interior. The left endpoint σ_{Page} follows the path illustrated in figure 2.12, while the right endpoint is anchored very close to the shockwave, as described by eq. (2.102).

Hence we find that the right endpoint must indeed anchored very close to the shock wave (at $y^+_{\mathrm{shock}} = 0$). That is,

$$y_2^+ = x_1 \, \frac{u_{\mathrm{Page}} - \sigma_{\mathrm{Page}}}{2\, u_{\mathrm{Page}}} \, \eta \sim \left(\frac{cT_1}{6E_S} \right)^4 \frac{\pi T_1}{k} \ll t_\infty \, . \tag{2.102}$$

Figure 2.14 shows the smallest connected intervals that are able to reconstruct a portion of the black hole interior.

2.2.2 Late-time protocol: forgetting the early-time radiation

In section 2.2.1, we asked the question of how much of the bath is required to reconstruct the interior of the black hole in combination with $\mathrm{QM_L}$while focusing on the Hawking radiation emitted at early times. A different approach is to ask how much of the early-time radiation can we ignore but still keep the ability to reconstruct the interior of the

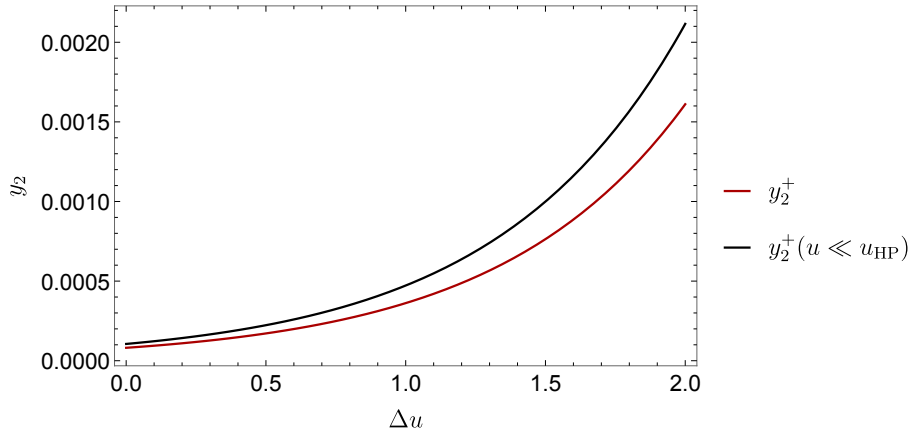

Figure 2.15: The time evolution of y_2^+ with dependence on $\Delta u = u - u_{\rm Page}$. The red line is derived from the direct numerical calculation, while the blue line represents eq. (2.106).

black hole. Concretely, we can anchor $\sigma_1 = 0$ for times later than $u_{\rm Page}$ and see how small σ_2 can be while still keeping the recoverability of the black hole interior. The two competing channels are the same as the ones in the early-time protocol, and are illustrated in figure 2.13. The difference is that the left endpoint of the bath interval is now anchored at the AdS-bath junction, *i.e.*, $\sigma_1 = 0$, and the right endpoint is no longer anchored at the shock, *i.e.*, $\sigma_2 < \sigma_{\rm shock}$.

As in eq. (2.90), we need to consider the equivalence condition,

$$S^{\rm gen}_{\rm QES''} + S_{1-2} - S^{\rm gen}_{\rm QES-1} - S_2 = 0 \tag{2.103}$$

with the new endpoints, which is equivalent to

$$\begin{aligned} &2k \log\left(\frac{12\pi E_S}{c}\frac{f(y_2^+)y_2^-}{\left(t - f(y_2^+)\right)\sigma_2}\right) \\ &= 2\pi T_0 - \frac{\phi(x^\pm_{\rm QES})}{\bar{\phi}_r} + 2k\log\left(\frac{(x^+_{\rm QES} - x^-_{\rm QES})}{(y_1^- - y^-_{\rm QES})(x^+_{\rm QES} - x_1^+)\sqrt{f'(y^-_{\rm QES})}}\right), \end{aligned} \tag{2.104}$$

where the dilaton is derived in eq. (2.59) and the bulk entropy on the right hand side is as in eq. (2.55). The above equation can not be solved analytically in general, and so we examine different regimes of $\Delta u \equiv u - u_{\rm Page}$.

When Δu is smaller than the Hayden-Preskill scrambling time $u_{\rm HP}$, the distance of the right endpoint of the bath interval to the shock y_2^+ is still very small. This is shown in the

plateau region in the beginning of figure 2.16. For $y_2^+ \ll t_\infty$, we can use[10]

$$\begin{aligned} x_2^+ = f(y_2^+) &\approx t_\infty \tanh\left(\frac{y_2^+}{t_\infty}\right) , \\ \log\left(\frac{f(y_2^+)y_2^-}{\left(t-f(y_2^+)\right)\sigma_2}\right) &\approx \log\frac{y_2^+}{t_\infty} + \log 2 + \frac{y_2^+}{2u} + \frac{y_2^+}{t_\infty} \approx \log\frac{y_2^+}{t_\infty} + \log 2\,. \end{aligned} \tag{2.105}$$

Solving for $\Delta S = 0$ then leads to the solution

$$\begin{aligned} y_2^+(u) \approx \frac{ct_\infty}{2^{23/4}\pi E_{\rm S} u_{\rm HP}} \exp\Bigg[&\frac{1}{4} + \frac{\pi(T_0-T_1)}{k} + \frac{\pi T_1}{2}\left(3u+u_{\rm HP}\right) \\ &+ \frac{k}{8}\left(-\frac{1}{\pi T_1} + (3-2\pi T_1 u_{\rm HP})(u-u_{\rm HP})\right)\Bigg] , \end{aligned} \tag{2.106}$$

for $u \lesssim u_{\rm HP}$. As expected, we find an exponential increase of $y_2^+(u)$ for early times. The comparison with numerical results are shown in figure 2.15.

We now move on to later times, when Δu is of the order of the Page time, but still less than $\mathcal{O}(k^{-1}\log k)$. The above approximation of eq. (2.105) will break down. For times with Δu comparable to the Page time we find numerically that the separation increases linearly with Δu, as can be seen in figure 2.16. We now proceed to show this linear behavior analytically. Using the results of section 2.1 in eqs.(2.59) and (2.55), the only new terms we need to consider are

$$\begin{aligned} \log\left(\frac{f(y_2^+)y_2^-}{\left(t-f(y_2^+)\right)\sigma_2}\right) &\approx \log\left(\frac{u+\sigma_2}{2\sigma_2}\right) + \frac{4\pi T_1}{k}\left(1-e^{-\frac{k}{2}(u-\sigma_2)}\right) , \\ \log\left(\sqrt{f'(u)}\right) &\approx \log 2 + \frac{k}{8\pi T_1} - \frac{ku}{4} - \frac{2\pi T_1}{k}(1-e^{-\frac{ku}{2}}) , \end{aligned} \tag{2.107}$$

where we have taken the approximation $f(y_+^-) \approx t_\infty$ for $u-\sigma \gg t_\infty$, which is satisfied in the region with linear behavior. We also note that the $\log\left(\frac{u+\sigma_2}{2\sigma_2}\right)$ is a small contribution because of the log function and σ also increases with u. Furthermore, if we take the small ku expansion again and keep the liner terms, this approximation leads us to the following solution

$$\sigma_2\,(u) = \frac{T_1-T_0}{2T_1 k} + \frac{1}{4}\,(u-u_{\rm HP}) + \frac{1}{2\pi T_1}\log\left(\frac{16E_S\pi u_{\rm HP}(u+\bar\sigma_2)}{(2e)^{1/4}c\bar\sigma_2}\right) - \frac{k}{8}u_{\rm HP}^2 + \mathcal{O}(k)\,, \tag{2.108}$$

[10] This approximation only works for small y_2^+. In previous sections, we dealt with times u of the order of the Page time or larger, and then (2.49) is a much better approximation.

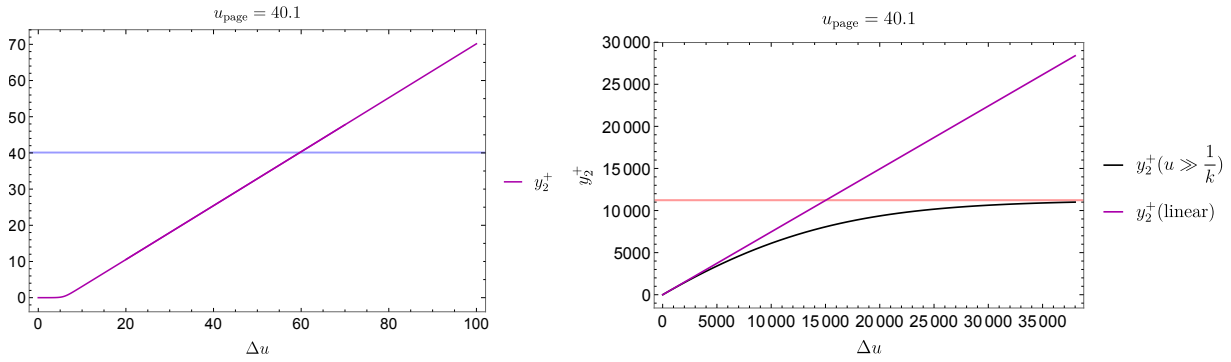

Figure 2.16: The time evolution of y_2^+ with dependence on $\Delta u = u - u_{\text{Page}}$. Left: The numerical results from the full linear generalized entropy. The horizontal line indicates the $y_2^+ = u_{\text{Page}}$. Right: Black curve shows the results with exponential dilaton term. The horizontal line represents the limit of y_2^+ defined in (2.112).

where $\bar{\sigma}_2 = \frac{T_1 - T_0}{2T_1 k} + \frac{1}{4}(u - u_{\text{HP}})$ is the leading order term of $\sigma_2(u)$.[11] It is straightforward to add higher k corrections to this approximation, but we only need the first order terms to show that σ_2 depends almost linearly in u for Δu of the order of the Page time and up to $\mathcal{O}(k^{-1})$. Thus, in this regime, we find a linear evolution for the distance of the endpoint of the bath interval to the shock:

$$y_2^+(u) = u - \sigma_2(u) \simeq \frac{3}{4}(u - u_{\text{Page}})\,, \tag{2.109}$$

where the slope is fixed to be $\frac{3}{4}$ at leading order, and we have ignored the correction of order $\mathcal{O}(k)$.[12] The linear behavior is illustrated in figure 2.17.

For very late times of $\mathcal{O}(k^{-1})$, the small ku approximation in *e.g.,* eq. (2.60) breaks down. This is due to the breakdown of the dilaton approximation in eq. (2.59). The correct expression for times of $\mathcal{O}(k^{-1})$ is

$$\phi \approx \bar{\phi}_r \left(2\pi T_1 e^{-\frac{k}{2} y_{\text{QES}}^-} - \frac{k}{2} \log 2e \right) . \tag{2.110}$$

Correspondingly, the linear decrease of generalized entropy is replaced by a much slower exponential decrease. Using the improved dilaton contribution in eq. (2.110), as well as

[11] The u dependence inside the log is very small, since for Δu much larger than u_{Page} we have $\log \frac{(u+\sigma_2)}{\sigma} \approx \log 5$.

[12] The approximation is in $\partial_u y_2^+(u) \approx \frac{1}{4} e^{-\frac{k}{2}(y_{\text{QES}}^- - y_2^+)} \partial_u y_{\text{QES}}^- + \frac{1}{2} e^{-\frac{k}{2}(u - y_2^+)}$, reducing to $\frac{3}{4}$ when u is order u_{Page} and to 0 for $ku \gg 1$.

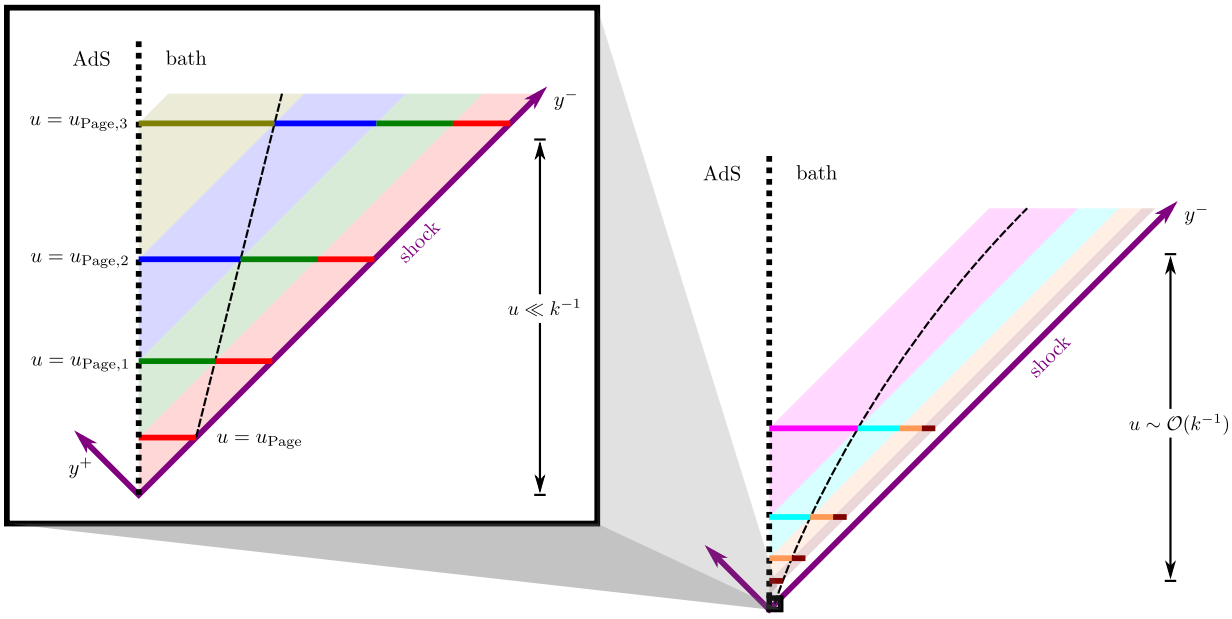

Figure 2.17: The dotted line in the right figure illustrates the evolution of $y_2^{\pm}$ with respect of time u. The left figure is the linear region with the approximation of y_2^+ described by eq. (2.109).

the approximation in eq. (2.107), we can solve eq. (2.104) numerically and plot the results in figure 2.16. Focusing on the large u limit, we can give an approximation for the surface y_2^+ at very late time with $u \gg k^{-1}$

$$y_2^+ \approx \frac{2}{k} \log \left(\frac{16\pi T_1}{4\pi T_1(2T_1 - T_0) + 4k \log\left(\frac{16 E_{\text{S}} \pi u_{\text{HP}}}{c}\right) - k(1 + 4\pi T_1 u_{\text{HP}} - \log 8) - 2\pi T_1 k^2 u} \right) . \tag{2.111}$$

This surface is becoming null for very large u. In an approximation that holds up to late times of order $u \sim \mathcal{O}(k^{-1} \log \frac{T_1}{k})$,[13] the asymptotic behaviour is

$$y_2^+ \simeq \frac{2}{k} \log \left(\frac{4T_1}{2T_1 - T_0} \right) + \mathcal{O}(1) . \tag{2.112}$$

We observe that the order-one correction above is also a constant. However, u-dependent terms appear on the right-hand side at order k.

[13]Note that we can not simply take u to infinity to derive this leading order behaviour because the semi-classical model will break down in the late-late-time regime with $u \gg k \log \frac{T_1}{k}$. Here we assume $u \sim y^-_{\text{QES}}$ approaches the very late-time limit. However, this formula (2.112) does not hold for $u \to \infty$.

Before closing here, let us also comment on the late-time protocol applied to the quench-scrambling phase transition. The calculation to find the behavior of the right endpoint with $u > u_{\rm QS}$ is similar to the one for the Page transition carried earlier in this section. However, the result is that as we increase the time up to the Page time, the distance of the right point to the shock $y_2^+(u)$ starts from a very small value *i.e.,* $\sigma_{\rm shock} - \sigma_2 \sim \left(\frac{cT_1}{6E_S}\right)^2 t_\infty \ll t_\infty$ and then *decreases* exponentially for $u_{\rm QS} < u < u_{\rm Page}$. That is, the left boundary very quickly approaches the null curve defined by the shock, *i.e.,* $\sigma_2 \simeq u$. This contrasting behavior originates from the increase of bulk entropy in scrambling phase, *i.e.,* the linear term in eqs. (2.36) and (2.39).

2.2.3 Redundancy of the encoding

In examining the holographic entanglement and the corresponding entanglement wedge for $\mathrm{QM_L}$+bath in section 2.2.1, we found that the information needed to reconstruct the interior of the black hole is encoded in a region in the bath extending from $y^+_{\rm QES} \simeq u - u_{\rm Page}$ to $\sigma_{\rm shock} = u$ on a given time slice u in the bath.[14] However, as may be expected for holography [137, 138, 139], we will see that this encoding is redundant, here and in the next subsection. In this subsection, we examine the question of removing a smaller interval from the shortest connected bath interval that can still recover the black hole interior.[15] While in the following two subsections we will be working with the early-time protocol in mind for concreteness, the results in this subsection are qualitatively similar if we started from the shortest connected intervals in the late-time protocol of section 2.2.2, and in fact the main conclusion of subsection 2.2.3 in eqs. (2.122) and (2.127) is quantitatively the same.

Let us denote the bath interval described above as $\mathcal{B}_0 = \left[y^+_{\rm QES}, \sigma_{\rm shock}\right]$. Now we ask how large a hole $\mathcal{H}_1$ can we remove from $\mathcal{B}_0$ while still preserving recoverability of the black hole interior? The desired configuration of HRT surfaces is sketched in the top left illustration of figure 2.18. We are now left with two disjoint intervals in the bath $B_{1,1} = [\sigma_1 = y^+_{\rm QES}, \sigma_2]$ and $B_{1,2} = [\sigma_3, \sigma_4 = \sigma_{\rm shock}]$, which combined with $\mathrm{QM_L}$ are still able to reconstruct the black hole interior. To determine the allowed size and position of the hole, *i.e.,* to determine the allowed values of σ_2 and σ_3, we must compare the contributions of the different HRT surfaces. For example, the desired configuration (in the top left of figure 2.18) is given by

$$S_{\rm QES-1,2-3,4} = S_{\rm QES-1} + S_{2-3} + S_4\,, \tag{2.113}$$

[14] Recall that $y^\pm \equiv u \mp \sigma$, so that increasing positive σ corresponds to moving further into the bath.

[15] If one is favorably inclined to puns, one might call this process "lyft"ing, since we are on our way to überholography.

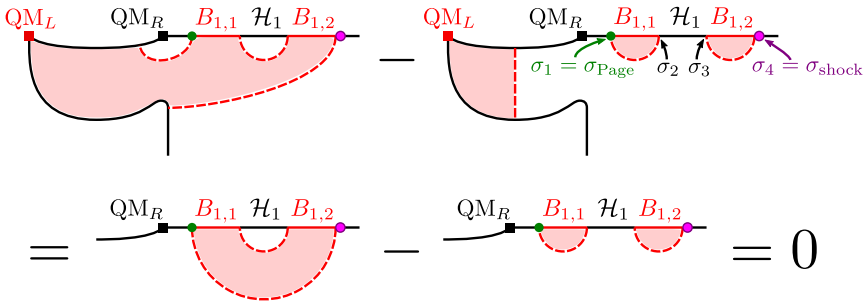

Figure 2.18: Excising the largest possible hole $\mathcal{H}_1$ from the smallest possible interval $\mathcal{B}_0 = B_{1,1} \cup \mathcal{H}_1 \cup B_{1,2}$ of the bath such that recoverability of the black hole interior is preserved. Minimizing of $\mathcal{B}_0$ *i.e.,* setting $\sigma_1 = y^+_{\rm QES}$, allows us to equate the difference in generalized entropies of the first line with the differences in von Neumann entropies in the second line; maximization of $\mathcal{H}_1$ is determined by the equality of latter branches.

where we have indicated the contributions of the separate components of the HRT surface on the right. For example, S_4 is the contribution of the geodesic connecting y_4 to the ETW brane, while $S_{\rm QES-1}$ corresponds to the generalized entropy which includes the length of the geodesic connecting σ_1 to the QES and also the dilaton contribution at the latter point. Now the competing configuration that limits the size of the hole is shown in the top right illustration of figure 2.18, and the corresponding holographic entropy is given by

$$S_{\rm QES',1-2,3-4} = S_{\rm QES'} + S_{1-2} + S_{3-4}\,. \tag{2.114}$$

In this case, QES$'$ indicates that the quantum extremal surface is distinct from that appearing in eq. (2.113). In fact, in this configuration, QES$'$ corresponds to the bifurcation surface of the original black hole on the Planck brane.

A priori it may seem that comparing the entropies in eqs. (2.113) and (2.114) will require some numerical analysis. However the present comparison is simplified because we have chosen $\sigma_1 = y^+_{\rm QES}$. This point marks the precise transition between two competing sets of HRT surfaces, as illustrated in figure 2.13. Hence at this precise point, we have

$$S_{\rm QES-1} + S_4 = S_{\rm QES'} + S_{1-4}\,. \tag{2.115}$$

Substituting this expression into eq. (2.113) and taking the difference then yields

$$S_{\rm QES-1,2-3,4} - S_{\rm QES',1-2,3-4} = S_{1-4} + S_{2-3} - S_{1-2} - S_{3-4}\,, \tag{2.116}$$

as illustrated by the bottom illustration of figure 2.18. Note that the latter (2.116) is controlled entirely by the positions of the points in the bath, which are fixed, *i.e.,* the

transition between the two branches in the top of figure 2.18 is completely independent of the physics on the Planck brane, *i.e.,* of QES and QES′.[16]

Hence in eq. (2.116), we are simply comparing the lengths of the corresponding HRT surfaces. This comparison can be made in terms of the z coordinates, where the transition occurs at

$$\frac{|z_2 - z_3|^2}{|z_4 - z_3|^2} \frac{|z_4 - z_1|^2}{|z_2 - z_1|^2} = 1\,, \tag{2.117}$$

or in the $y^{\pm}$ coordinates, where

$$\frac{y_3^- - y_2^-}{y_4^- - y_3^-} \frac{f(y_2^+) - f(y_3^+)}{f(y_3^+) - f(y_4^+)} \frac{y_4^- - y_1^-}{y_2^- - y_1^-} \frac{f(y_1^+) - f(y_4^+)}{f(y_1^+) - f(y_2^+)} = 1\,. \tag{2.118}$$

Now, of course, the width of our hole $\mathcal{H}_1$, *i.e.,* $|\sigma_3 - \sigma_2|$, depends on how it is positioned within the original interval $\mathcal{B}_0 = \left[y^+_{\rm QES}, \sigma_{\rm shock}\right]$. As an example, in figure 2.19, we consider $\mathcal{B}_0$ with $y^+_{\rm QES} = 0$, *i.e.,* $u = u_{\rm Page}$,[17] and explore the maximum width of the interval that can be removed as a function of the center of the interval. In the figure, we see that the optimal choice, *i.e.,* the largest hole, is when we position the hole at the center of $\mathcal{B}_0$. In the figure, we see that in this optimal configuration, we can remove approximately 10% of the region $\mathcal{B}_0$. The width of the hole shrinks rapidly as σ_c approaches either $y^+_{\rm QES}$ or $\sigma_{\rm shock}$ – see further comments below. We can interpret this shrinking as indicating that the information in both the early Hawking radiation (near the shock) and the later radiation (near $y^+_{\rm QES}$) are very important in reconstructing the black hole interior.

The resulting plot in the left panel of figure 2.19 is almost symmetric about the midpoint. The small asymmetry (shown in the right panel) is due to the nonlinearities of the mapping $f(y_i^+)$. Interestingly, this asymmetry is eliminated if we use the small k approximation:[18] $f(u) \simeq \frac{1}{\pi T_\infty} \tanh\left(\pi T_\infty u\right)$ where $T_\infty = \frac{1}{\pi t_\infty} = I_1\left[\frac{2\pi T_1}{k}\right]/I_0\left[\frac{2\pi T_1}{k}\right]$. With this approximation, the identity $\tanh(x) - \tanh(y) = \mathrm{sech}(x)\,\mathrm{sech}(y)\sinh(x-y)$ can be used to simplify eq. (2.118) as

$$\frac{y_3^- - y_2^-}{y_4^- - y_3^-} \frac{\sinh(y_2^+ - y_3^+)}{\sinh(y_3^+ - y_4^+)} \frac{y_4^- - y_1^-}{y_2^- - y_1^-} \frac{\sinh(y_1^+ - y_4^+)}{\sinh(y_1^+ - y_2^+)} = 1\,. \tag{2.119}$$

[16] However, if instead, σ_1 was placed closer to the end of the bath (*i.e.,* closer to $\mathrm{QM_R}$), then eq. (2.115) would no longer hold and comparing eqs. (2.113) and (2.114) would no longer be as simple.

[17] Note that there is no real loss of generality with this choice. Moving to a later time slice simply shifts the parameters to $u' = u_{\rm Page} + \Delta u$, $y^{+\,\prime}_{\rm QES} \simeq \Delta u$ and $\sigma'_{\rm shock} = u_{\rm Page} + \Delta u$, which corresponds to just shifting $y^-_{1,2}$ by a constant while leaving $y^+_{1,2}$ unchanged. However, we observe that eq. (2.118) is invariant under a constant shifts in y^- and so our analysis here would be unchanged.

[18] For the parameters in table 2.1, the difference between the full $f(u)$ and this approximation is less that an fraction of a percent, *i.e.,* $|f(u) - f_{\rm approx}(u)|/|f(u)| \lesssim 0.0015\%$.

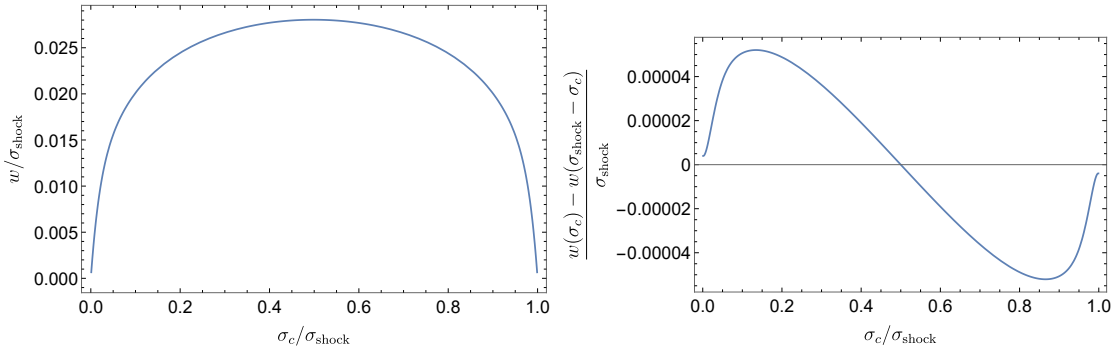

Figure 2.19: To the left, maximum width w of the hole $\mathcal{H}_1$ removed from the bath region $\mathcal{B}_0$ as a function of the center of the interval σ_c. To the right, asymmetry in the maximum width about $\sigma_c = \sigma_{\rm shock}/2$. Here we consider the time slice $u = u_{\rm Page}$ so that $\mathcal{B}_0 = [y^+_{\rm QES} = 0, \sigma_{\rm shock} = u_{\rm Page}]$.

Further, for the example shown in figure 2.19,[19] we then substitute $y_1^\pm = u_{\rm Page}$, $y_2^\pm = u_{\rm Page} \mp (\sigma_c - w/2)$, $y_3^\pm = u_{\rm Page} \mp (\sigma_c + w/2)$ and $(y_4^+, y_4^-) = (0, 2u_{\rm Page})$, which yields

$$\frac{w}{u_{\rm Page} - \sigma_c - w/2} \frac{\sinh w}{\sinh(u_{\rm Page} - \sigma_c - w/2)} \frac{u_{\rm Page}}{\sigma_c - w/2} \frac{\sinh u_{\rm Page}}{\sinh(\sigma_c - w/2)} = 1\,. \tag{2.120}$$

Clearly, the resulting expression is invariant under $\sigma_c \to u_{\rm Page} - \sigma_c$, *i.e.,* the corresponding plot is exactly symmetric about the midpoint $\sigma_c = u_{\rm Page}/2$. Hence in this approximation, the importance of the information in both the early and later Hawking radiation is equally weighted for the reconstruction of the black hole interior.

In closing this section, we note that the initial and final slopes of the curve in the left panel of figure 2.19 are universal for holographic CFTs. This is because the question of how large a hole can be exciseded near the endpoint of an interval without triggering a phase transition is one which probes the UV entanglement structure. To see this, let us, without loss of generality, take in the RHS of eq. (2.116) the endpoints, σ_2 and σ_3, of the hole to be very close to the endpoint $\sigma_1 = y^+_{\rm QES}$. Maximizing the size of the hole to the verge of triggering the transition between the two branches amounts to setting the RHS of eq. (2.116) to zero. In the limit of the hole tending towards the point σ_1, we have $S_{1-4} = S_{3-4}$; moreover, the dependence of S_{3-4} on point σ_3 is extremely weak relative to the dependence of S_{1-2} and S_{2-3} on the location and size of the hole. Thus, we find that $S_{1-2} \sim S_{2-3}$ for maximally-sized holes close to σ_1. Since these latter entropies probe short distances, this relation gives the same constraint on points $\sigma_{1,2,3}$ as in the vacuum

[19] Again, the general result corresponds to shifting all the points to the left by $\Delta u = u - u_{\rm Page}$.

case, *i.e.*, $|\sigma_1 - \sigma_2| \sim |\sigma_2 - \sigma_3|$. This corresponds to slopes of $\pm 2/3$ at the endpoints of figure 2.19, *i.e.*, near σ_1, we have $w \simeq \frac{2}{3}(\sigma_c - \sigma_1)$ while near σ_4, $w \simeq \frac{2}{3}(\sigma_4 - \sigma_c)$. These results might be contrasted with the largest holes that can be removed from $\mathcal{B}_0$ in these limits, *i.e.*, $w < 2(\sigma_c - \sigma_1)$ and $w < 2(\sigma_4 - \sigma_c)$. This comparison gives a quantitative measure that the w is indeed shrinking *rapidly* near the endpoints of $\mathcal{B}_0$, as commented above.

Überholography

Having considered removing a single hole from the bath region $\mathcal{B}_0 = \left[y^+_{\text{QES}}, \sigma_{\text{shock}}\right]$, it is natural to generalize our analysis to arbitrarily many holes. Specifically, one may ask: what is the smallest total length of disconnected regions in $\mathcal{B}_0$ needed, in conjunction with QM_L, to reconstruct the interior of the black hole? In fact, by an iterative process where, at each step, a hole is punched into each connected region in this bath region, this total length can be reduced arbitrarily close to zero. This procedure was designated 'überholography', where a bulk region is encoded in a subset of the boundary with lower (fractal) dimension than the dimension of the boundary [118].

We illustrate this process in figure 2.20a. We begin, as in section 2.2.1, with the smallest interval $\mathcal{B}_0$ on a constant time slice of the bath such that the black hole interior can be recovered from QM_L and $\mathcal{B}_0$. For concreteness, we have positioned the first endpoint $\min(\mathcal{B}_0) = \sigma_{\text{Page}}$ at the AdS-bath boundary in figure 2.20 — we find qualitatively similar results when this endpoint is chosen inside the bath. In the first round of the iterative process, we punch a maximally-sized hole $\mathcal{H}_1$ into the initial interval $\mathcal{B}_0$ while preserving recoverability of the black hole interior, as discussed in section 2.2.3. What remains is the union $\mathcal{B}_1 = \mathcal{B}_0 \setminus \mathcal{H}_1 = B_{1,1} \cup B_{1,2}$ of two intervals $B_{1,1}, B_{1,2}$. Before proceeding to the inductive step, we emphasize again that the task of maximizing $\mathcal{H}_1$ can be reduced into a simple problem that involves comparing channels of the Von Neumann entropy of the disconnected region $\mathcal{B}_1$, as written in eq. (2.116) and illustrated in the first equality of figure 2.18. A similar reduction can be made in all further iterative steps of the hole-punching procedure, so that we need only consider Von Neumann entropy channels of the surviving region $\mathcal{B}_n$ in the bath.[20]

Due to the maximization of the hole $\mathcal{H}_1$, the two channels shown in the last line of figure 2.18 give the same entropy. For the inductive step, it is simplest to consider the second channel shown. Since, in this channel, the entanglement wedges for $B_{1,1}$ and $B_{1,2}$

[20] Indeed, the problem would be identical to the vacuum case considered in [118] save for the conformal transformation taking z to x, y coordinates.

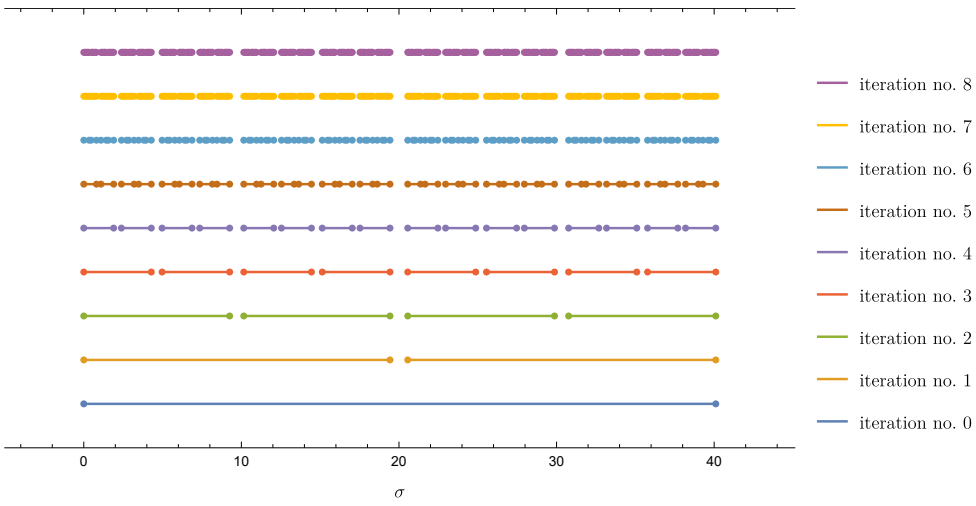

(a) Interval of the bath needed to reconstruct black hole interior, iteratively hole-punched.

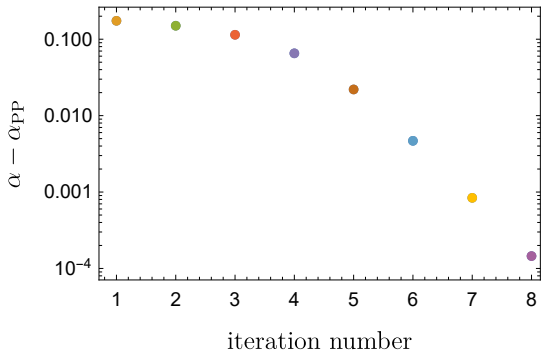

(b) Parameter α, defined in eq. (2.121), which, in the infinite iteration limit, gives the fractal dimension of the bath region needed to recover the black hole interior.

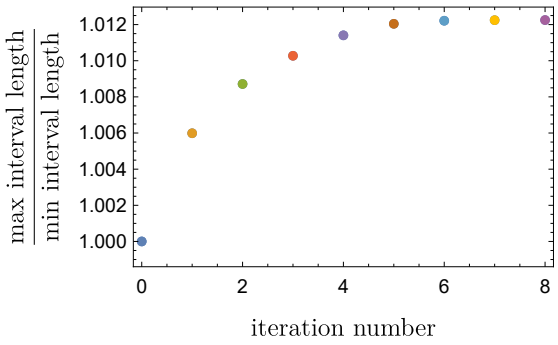

(c) Ratio between the maximal and minimal lengths of connected intervals after each iteration.

Figure 2.20: Iterative process of punching maximally-sized holes into the interval of the bath needed (together with QM_L) to reconstruct the black hole interior. Here, the original interval of the bath under consideration stretches from the AdS-bath boundary to the shock on the time slice corresponding to the Page time on the boundary.

are disconnected, we may separately consider punching maximally-sized holes in $B_{1,1}$ and $B_{1,2}$. Thus, the process described in the previous paragraph can be repeated, now with $B_{1,1}$ or $B_{1,2}$ taking the place of $\mathcal{B}_0$. Indeed, this procedure may be performed iteratively: given a disconnected region $\mathcal{B}_n = B_{n,1} \cup \cdots \cup B_{n,2^n}$ composed of intervals $B_{n,m}$, we may punch a maximally-sized hole $H_{n+1,m}$ into each $B_{n,m}$ while maintaining recoverability of the the black hole interior; the result is a smaller region $\mathcal{B}_{n+1} = \mathcal{B}_n \setminus \mathcal{H}_{n+1}$, where $\mathcal{H}_{n+1} = H_{n+1,1} \cup \cdots \cup H_{n+1,2^n}$.

At each step, we may define the quantities

$$r_n = \frac{|\mathcal{B}_n|}{|\mathcal{B}_{n-1}|}, \qquad \alpha_n = \frac{\log 2}{\log \frac{2}{r_n}} \tag{2.121}$$

describing the rate at which the total length $|\mathcal{B}_n|$ of the region in the bath shrinks over iterations. In figure 2.20b, we plot α_n, showing that it approaches the constant value

$$\alpha_\infty = \alpha_{\text{PP}} \equiv \frac{\log 2}{\log(\sqrt{2}+1)} \approx 0.786 \tag{2.122}$$

obtained for the CFT vacuum in [118]. Thus, we find that the region $\mathcal{B}_\infty$ of the bath needed, with QM_L, to recover the black hole interior exhibits uberholography — it has zero total length. Moreover, as we shall show momentarily, α_∞ gives the fractal dimension $d(\mathcal{B}_\infty)$ of $\mathcal{B}_\infty$. Hence, we see that $\mathcal{B}_\infty$ has the same fractal dimension $\alpha_\infty = \alpha_{\text{PP}}$ as for uberholography in the vacuum case. The universality of α_{PP} may be explained by the fact that the UV entanglement excised by uberholography is determined predominantly by the vacuum entanglement structure. Explicitly, for our case, despite the conformal transformation from eq. (2.117) to eq. (2.118), for small interval sizes, eq. (2.118) still reads as though it were comparing vacuum entropy channels:

$$\frac{|y_2 - y_3|^2 |y_1 - y_4|^2}{|y_3 - y_4|^2 |y_1 - y_2|^2} + \mathcal{O}\left(f'' \cdot (\text{distance between points})\right) = 1. \tag{2.123}$$

It is straight-forward to show that α_∞ gives the dimension of $\mathcal{B}_\infty$ by making use of the fact that the ratio $\frac{\max_m |B_{n,m}|}{\min_m |B_{n,m}|}$ of maximal and minimal lengths of the consituents of $\mathcal{B}_n$ approaches a constant in the infinite iteration limit $n \to \infty$, as verified in figure 2.20c. Recall that the (Minkowski) dimension of the set $\mathcal{B}_\infty$ is defined to be

$$d(\mathcal{B}_\infty) \equiv \lim_{\epsilon \to 0} \frac{\log N(\epsilon)}{\log(1/\epsilon)}, \tag{2.124}$$

where $N(\epsilon)$ is the minimal number of ϵ-diameter balls (in this case, ϵ-length intervals) needed to cover $\mathcal{B}_\infty$. For any small ϵ, it is possible to find the first iteration $n = n^+(\epsilon)$ such that $\max_m |B_{n,m}| \leq \epsilon$ and also the last iteration $n = n^-(\epsilon)$ such that $\epsilon \leq \min_m |B_{n,m}|$. Since $\max_m |B_{n,m}|$ and $\min_m |B_{n,m}|$ differ only by a constant factor in the $n \to \infty$ limit, it follows that

$$n^\pm \sim \frac{\log(\epsilon)}{\log(r_{n^\pm}/2)} \tag{2.125}$$

where $r_n/2$ gives the factor by which the average length of single intervals shrinks over the nth iteration. By monotonicity in $N(\epsilon)$, we also have

$$2^{n^-} \leq N\left(\min_m |B_{n^-,m}|\right) \leq N(\epsilon) \leq N\left(\max_m |B_{n^+,m}|\right) \leq 2^{n^+}. \tag{2.126}$$

Using eqs. (2.125) and (2.126), we have from eq. (2.124) and the definition (2.122) of α_∞,

$$d(\mathcal{B}_\infty) = \alpha_\infty \tag{2.127}$$

as claimed. Eqs. (2.122) and (2.127) are the main results of this subsection. Lastly, we emphasize once again that despite the fact that we have started from the shortest connected intervals of the early-time protocol, the results are the same if we start from the shortest connected intervals of the late-time protocol of section 2.2.2.

More redundancy and efficiency of the encoding

With the late time protocol introduced in section 2.2.2, we found that we can reconstruct the black hole interior with the bath interval $\widetilde{\mathcal{B}}_1 = [\sigma_1 = 0, \sigma_2 = \sigma_{\text{Turn}}(u)]$, where σ_{Turn} is the minimum value of σ_2 defined by eq. (2.109), *i.e.*,

$$\sigma_{\text{Turn}} = (1-\gamma)\, u + \gamma\, u_{\text{Page}}\,, \quad \gamma = \frac{3}{4} \tag{2.128}$$

where γ receives corrections at order k which only become relevant at times of order k^{-1}, and which slowly change the slope to zero at very late times of order $k^{-1} \log \frac{T_1}{k}$. Therefore σ_{Turn} defines a time-like boundary for the endpoints of these minimal intervals, as shown in figure 2.17. Assuming the information flows at the speed of light,[21] this result points to a redundancy of the encoding of the black hole interior. That is, the black hole interior is encoded in the Hawking radiation emitted over many finite time intervals, but at times

[21] As indicated by the evolution of y^+_{QES} in section 2.2.1.

much later than the Page time u_{Page}. In general, if we begin to collect the radiation at an arbitrary time $u_{\text{initial}} > u_{\text{Page}}$ and we can reconstruct the black hole interior with radiation collected (at $\sigma_1 = 0$) in the time interval $[u_{\text{initial}}, u_{\text{final}}]$ with

$$u_{\text{final}} = \frac{u_{\text{initial}}}{\gamma} + u_{\text{Page}} \,. \tag{2.129}$$

This time u_{final} is determined by the intersection of the null ray entering the bath at u_{initial} with the curve σ_{Turn}, such that all of the information flowing into the bath in the above time interval is captured in the interval $[0, \sigma_{\text{Turn}}(u_{\text{initial}})]$ on this final time slice.

As a concrete example, we can discard all of the Hawking radiation emitted before u_{Page}, but we are still able to reconstruct the black hole interior by collecting the radiation emitted in $u \in [u_{\text{Page}}, u_{\text{Page},1}]$ where $u_{\text{Page},1} - u_{\text{Page}} = u_{\text{Page}}/\gamma$. Further, this process can be repeated again, *i.e.,* we discard the radiation before $u_{\text{Page},1}$ but the black hole interior is recovered if we collect the subsequent radiation up to a time $u_{\text{Page},2}$. Repeating the process repeatedly, one finds that

$$u_{\text{Page},n} - u_{\text{Page},n-1} = \frac{u_{\text{Page}}}{\gamma^n} \,. \tag{2.130}$$

Since $\gamma < 1$, these intervals are becoming longer and longer. This suggests that while the information about the black hole interior is still encoded in the radiation collected at later times, the density of this information becomes less dense at much later times. That is, the encoding of the information is becoming less efficient at later times – see further comments in section 2.3.

These results depend on the simple linear growth of σ_{Turn} in eq. (2.128). However, we also showed above that this behaviour breaks down at late times, with this boundary approaching a null curve (2.112) at very late times – see figure 2.17. This means that the size of the successive intervals, *i.e.,* $u_{\text{Page},n} - u_{\text{Page},n-1}$, would grow even more quickly than the geometric behaviour shown in eq. (2.130). With the final asymptotic expansion of σ_{Turn} following a null curve, we would conclude that for times beyond

$$u_{\text{max}} \simeq \frac{2}{k} \log\left(\frac{4T_1}{2T_1 - T_0}\right) \,, \tag{2.131}$$

we could never collect enough information to reconstruct the black hole interior. This conclusion should be tempered by the fact that our semi-classical understanding of the AEM^{4}Z model will break down at times of order $u \gtrsim k^{-1} \log \frac{T_1}{k}$. Combining eq. (2.131) with the expressions for $u_{\text{Page},n}$ following from eq. (2.128),[22] suggests a finite redundancy

[22] Explicitly, one finds that $u_{\text{Page},n} = \frac{1-\gamma^{n+1}}{\gamma^n\,(1-\gamma)}\, u_{\text{Page}}$.

of the encoding of the black hole interior in the Hawking radiation with

$$n_{\max} \simeq \frac{\log\left(2u_{\text{Page}}/k\right)}{\log\gamma}\,. \tag{2.132}$$

More precisely, the black hole information is encoded in a finite number of distinct time intervals roughly given by eq. (2.132).

Of course, there is nothing special about these intervals $[u_{\text{Page},n+1}, u_{\text{Page},n}]$. As indicated in eq. (2.129), we can reconstruct the black hole interior with radiation collected in general time intervals $[u_{\text{initial}}, u_{\text{final}}]$, beginning at any arbitrary $u_{\text{initial}} > u_{\text{Page}}$. Further, on the time slice $u = u_{\text{final}}$, we could remove intermediate segments between $\sigma_1 = 0$ and $\sigma_2 = u_{\text{final}} - u_{\text{initial}}$ as in section 2.2.3 or even implement the überholography process as in section 2.2.3. Of course, this indicates that the reconstruction of the black hole interior does not require all of the radiation in the time interval $[u_{\text{initial}}, u_{\text{final}}]$. Rather, the überholography process suggests collecting the radiation on some fractal subset of this time interval. All of these considerations certainly point to a remarkable redundancy in time for the encoding in the Hawking information of information about the black hole interior. It would be interesting to understand if and how this pattern of redundancies is manifest in other models of black hole evaporation.

2.3 Discussion

In this chapter, we examined the flow of information in black hole evaporation as described by the AEM^{4}Z model [1, 11]. This model involves two systems: JT gravity coupled to a two-dimensional holographic CFT, and an infinite bath, comprised of the same holographic CFT on a half-line. The former is prepared as an eternal black hole, which is dual to a thermofield-double state entangling QM_L and QM_R, while the bath is prepared in its vacuum state. These two systems are connected by a quantum quench, and the subsequent evolution of the entanglement entropy of QM_L+bath subsystem exhibits three phases: the quench phase, in which the QES on the Planck brane is fixed at the bifurcation surface of the initial black hole; the scrambling phase, in which the QES moves slowly away from this bifurcation surface; and the late-time phase, in which QES is just behind the event horizon of the evaporating black hole.

In the example of the eternal AdS_2 black hole with reflecting boundary conditions at the asymptotic boundary, the QES for QM_L (or QM_R) alone will be the bifurcation surface. Hence the information in this subsystem can be used to reconstruct the exterior region on

the left (or right) side of the black hole. That is, the entanglement wedge for $\mathrm{QM_L}$ is the entire region outside of the left event horizon, as shown in the left plot in figure 2.10. Considering the information flow after the quench, since the position of the QES for the $\mathrm{QM_L}$+bath subsystem is fixed in the initial quench phase, the Hawking radiation is carrying negligible information into the bath. That is, any information about the black hole interior would only be at order one in the large c expansion of the holographic CFT.[23]

The onset of the scrambling phase marks the time when the Hawking radiation begins to contain information about the interior. In the scrambling phase, the information flow is detected by the QES, and is order c, but Hawking radiation absorbed by the bath only carries enough information for $\mathrm{QM_L}$+bath to reconstruct a small additional region behind the horizon of the left side (and to the past of the shockwave), as illustrated in the middle plot in figure 2.10. However, once the black hole has passed the Page transition and entered into the late-time phase, the QES jumps to be behind the right event horizon (and to the future of the shockwave), and so the bath has acquired enough information for $\mathrm{QM_L}$+bath to reconstruct a much larger portion of the black hole interior (see the right plot in figure 2.10).

Let us comment on the HRT surfaces and the encoding of the black hole interior in the late-time phase (see figure 2.1). We note that in this regime, the black hole interior provides a classic example of the quantum error correcting encoding that is characteristic of holography [138, 137]. We are considering three subsystems of the boundary, $\mathrm{QM_L}$, $\mathrm{QM_R}$ and the bath. In this configuration the information about the black hole interior cannot be recovered from any one of these subsystems; however, combining any two of them allows us to reconstruct the interior information. In our discussion, the focus was on the combination $\mathrm{QM_L}$+bath, but a quick examination of the HRT surfaces in figure 2.1 shows that it is also included in the entanglement wedges of either $\mathrm{QM_L}$+$\mathrm{QM_R}$ or $\mathrm{QM_R}$+bath.

However, the above discussion is not complete. Eventually, on a time scale much larger than those considered here, the bath on its own will make a Page transition. Initially, the bath is in the analog of the quench phase with the HRT surface sketched in the left panel of figure 2.21. It then makes a transition to a late-time phase with the HRT surfaces sketched in the right panel, where a quantum extremal island [1] has formed. Here we implicitly assume a large intrinsic gravitational entropy for the JT model, *i.e.,* we are assuming that $S_0 = \phi_0/(4G_\mathrm{N}) \gg 1$ in eq. (2.13).[24] This contribution to the generalized entropy adds a heavy penalty for HRT surfaces that end on the Planck brane, and so it

[23] In the analysis of [11] for a general CFT, the QES already begins to move away from the bifurcation surface during the quench phase. Of course, there is also a smooth cross-over between the quench and scrambling phases in their model.

[24] A standard assumption is that $\phi_0 \gg \phi_r/\epsilon$ in the spacetime regions of interest [120] – see eq. (2.13).

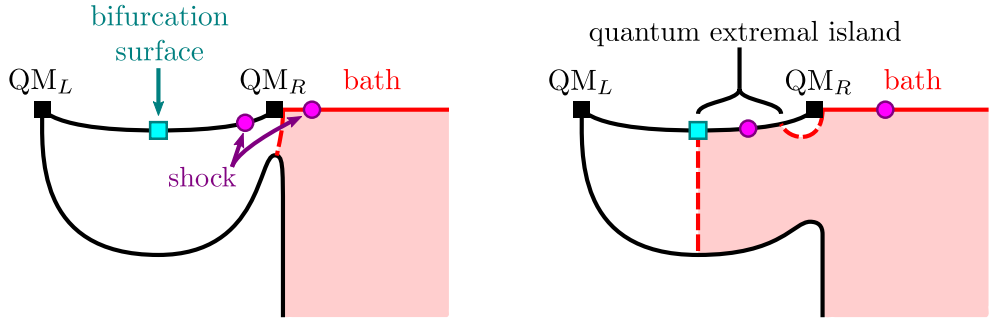

Figure 2.21: Quench (left) and late-time (right) phases for the entropy of the bath.

would delay the onset of the late-time phase and the appearance of the quantum extremal island. Note that the transitions in the main text (for the entropy to QM$_{\rm L}$+bath), one is always comparing branches where a single HRT geodesic ends on the Planck brane and so S_0 did not play a role. Further, one can argue that if $S_0 \gtrsim \Delta S$ (the change in the black hole entropy generated by the shock wave, *i.e.,* in going from T_0 to T_1), then the branch corresponding to the scrambling phase never dominates and so the Page transition corresponds to going directly from the quench branch to the late-time branch. Of course, in the latter phase with the quantum extremal island, the bath by itself now encodes sufficient information to reconstruct a portion of the black hole interior. The fact that this other Page transition takes place much later suggests that early-time scrambling is important for the reconstruction of the black hole interior, as suggested in [10]. It would be interesting to repeat the detailed analysis that we have performed in this chapter considering just the bath on its own.

As the QM$_{\rm L}$+bath system continues to evolve beyond the Page time, the wedge region grows relatively slowly as the bath continues to absorb more Hawking radiation. That is, the information carried by the radiation coming after the Page transition is less important for the reconstruction of the black hole interior. Eventually, one expects the entanglement wedge of the QM$_{\rm L}$+bath subsystem to extend to the right boundary of the AdS$_2$ geometry at t_∞ (where the dilaton vanishes), but we can not trust the model to these very late times. However, a more appropriate comment might be to say that the information is less densely encoded in the late-time radiation – see further comments below.

In this late-time phase, we found in section 2.2.1 that the information needed to reconstruct the black hole interior propagates at nearly the speed of light into the bath. That is, (a large portion of) the black hole interior could be reconstructed using the Hawking radiation captured on the time slice $u = u_{\rm Page}$ between $\sigma_1 = 0$ and $\sigma_2 = u_{\rm Page}$, together with QM$_{\rm L}$. However, on a later time $u > u_{\rm Page}$, we could reproduce essentially the same

reconstruction using the Hawking radiation captured between $\sigma_1 = y^+_{\rm QES} \simeq u - u_{\rm Page}$ and $\sigma_2 = \sigma_{\rm shock} = u$ instead.[25] Of course, this is consistent with the information being carried into the bath by massless right-moving quasi-particles in the two-dimensional CFT [129]. Similar behaviour was also recently observed in [97]. Of course, as shown in eq. (2.87) (see also figure 2.12), there are corrections to $y^+_{\rm QES}$ in the small k expansion. However, the corrected (timelike) boundary still rapidly approaches a (slightly) shifted null ray. In section 2.2.1, we also showed that the early Hawking radiation is extremely important in the above reconstruction protocol. That is, the right boundary σ_2 of the bath region must be extremely close to the shockwave, *i.e.*, $\sigma_{\rm shock} - \sigma_2 \sim \left(\frac{cT_1}{6E_S}\right)^4 \frac{\pi T_1}{k} \ll t_\infty$ as in eq. (2.102).

The importance of the early and late time Hawking radiation in this protocol was examined more closely in section 2.2.3, where we considered removing an intermediate interval from the bath region – see figure 2.13. As shown in figure 2.19, the size of the intermediate interval is maximal when it is at the center and quickly decreases as this interval approaches either the shockwave or the boundary $y^+_{\rm QES}$. This is indicative of a clear separation of the radiation into early and late pieces. Of course, the process of systematically removing intermediate intervals from the bath region can be continued, cutting out smaller and smaller subregions, as discussed in section 2.2.3. Repeating this process ad infinitum, following [118], we produce a fractal structure which, in combination with $\rm QM_L$, contains enough information to reconstruct the interior of the black hole. It is interesting that the (Minkowski) dimension characterizing this fractal matches that found for the CFT vacuum in [118]. This match arises because the very small intervals only probe the correlations of the CFT deep in the UV, and these must match in both settings.

In section 2.2.2, we considered a different reconstruction procedure that focused on the later radiation by anchoring the bath interval at $\sigma_1 = 0$. We found that the minimal size $\sigma_2 = \sigma_{\rm Turn}$ for which the information in $\rm QM_L$+bath still allowed us to reconstruct a large portion of the black hole interior follows a time-like boundary, as shown in figure 2.17. Using eq. (2.128), we found a redundancy with the information about the black hole interior being encoded in the Hawking radiation emitted in the time intervals $[u_{{\rm Page},n+1}, u_{{\rm Page},n}]$ after the Page time $u_{\rm Page}$.

Of course, this redundancy is consistent with the Hayden-Preskill thought experiment [119]. The latter indicates that if a few qubits are dropped into an old black hole, the information can be recovered after the scrambling time by combining (essentially) the same number of qubits from the subsequent radiation with (all of) the early Hawking radiation.

[25] Of course, it is reasonable to expect that no information about the black hole interior is encoded in the bath beyond the position of the shockwave, since this portion of the bath is not in causal contact with the quench point.

However, the radiated qubits need not be those radiated immediately after the scrambling time, but rather can be collected from the subsequent radiation at any time – see also [140, 141]. From this perspective, the initial eternal black hole at temperature T_0 plays the role of the old black hole and early radiation, *i.e.,* QM_{R} is the old black hole while QM_{L} plays the role of the early radiation. The black hole is 'rejuvenated' by dropping in the shock wave and the information can be recovered after u_{Page}, which then plays the role of the scrambling time in this discussion. However, as noted above, the information need not be collected immediately after the Page time but in any sufficiently large interval after u_{Page}. This analogy might be made more precise by regarding the shock wave as a 'heavy diary', as discussed in [10] – see also [142].

Of course, as indicated by eq. (2.130), or more generally by eq. (2.129), the length of the time interval needed to collect sufficient information grows at later times. We suggested that this indicates the encoding is becoming less dense or less efficient at later times. However, the temperature of the black hole is (slowly) falling, and so one might wonder if the reduction in the flux of Hawking radiation accounts for this effect. However, the flux flowing into the bath (at $\sigma_1 = 0$) is given by $T_{y^+y^+}(u) \sim T_1^2 e^{-ku}$, as shown in eq. (2.7). Hence this reduction only becomes noticeable on time scales of order $u \sim 1/k$. A simple calculation shows that an interval $[0, \sigma_2]$ needed to capture a fixed amount of Hawking radiation, as counted by energy or number of quanta (*i.e.,* E/T_{eff}), barely exhibits any growth at early times, *i.e.,* in the regime where eq. (2.130) is valid.[26] Hence the reduction of Hawking radiation over time does not explain the growth of σ_{Turn}, and the natural explanation is once again that the redundant encoding of information simply becomes less efficient over time. However, we should note that the different time intervals are not reconstructing precisely the same interior region. Rather the latter also grows with time, and so this way partially account for the growth in σ_{Turn}.

We also note that the reduction of the Hawking flux, *i.e.,* $T_{y^+y^+}(u) \sim T_1^2 e^{-ku}$, is a central factor in the nonlinear behaviour in the growth of σ_{Turn} found at time scales of order $u \sim 1/k$, as shown in figure 2.17. More directly in our calculations, the reduction in the corresponding gravitational entropy (2.110) on the QES produces this effect. As a result, $\sigma_{\mathrm{Turn}}(u)$ approaches a null ray, as shown in eq. (2.112), in this nonlinear regime. We then infer that the information in the Hawking radiation is too depleted beyond u_{max} – see eq. (2.131) – to collect enough quanta to reconstruct the black hole interior. Of course, our semi-classical understanding of the AEM^{4}Z model breaks down at times of order $u \gtrsim k^{-1} \log \frac{T_1}{k}$, and so nonperturbative effects may still allow for such a reconstruction.

In wrapping up this discussion, we reiterate that there is a remarkable redundancy in the

[26] Our conclusion assumes $(T_1 - T_0)/T_1 \ll 1$ and uses $u_{\mathrm{Page}} \sim (T_1 - T_0)/(k\, T_1)$ from eq. (2.61).

encoding of the black hole interior in the Hawking radiation. In section 2.2.3, we explicitly showed that the interior information was still available after numerous subintervals were gouged out of the initial parcel of radiation emitted between the quench and u_{Page}, to the point where it was reduced to a fractal structure. The reconstruction was also possible with the radiation collected (at $\sigma_1 = 0$) in the interval $[u_{\text{initial}}, u_{\text{final}}]$, beginning at any arbitrary $u_{\text{initial}} > u_{\text{Page}}$ and with u_{final} given by eq. (2.129). Again, the überholography approach could again be applied to perforate any such interval with holes. It would, of course, be interesting to understand if this pattern of redundancies appears in other models of black hole evaporation.

In closing, we observe that our analysis in section 2.2 focused on the Page transition between the scrambling and late-time transitions. However, this discussion can easily be extended to the first transition between the quench and scrambling phases, corresponding to the onset of scrambling, and the results are more or less the same. One important difference is that the trajectory for the σ_{QS} analog of σ_{Page} in section 2.2.1 is null for all times, unlike the trajectory of σ_{Page} which asymptotes towards a null path as is shown in figure 2.12. As was noted towards the end of section 2.2.2, the position of the σ_{Turn} in the quench-to scrambling phase transition shows different behaviour from the σ_{Turn} of the Page transition. In particular, as we increase the time from u_{QS} up to the Page time u_{Page}, the distance of the right point to the shock $y_2^+(u)$ starts from a very small value *i.e.,* $\sigma_{\text{shock}} - \sigma_2 \sim \left(\frac{cT_1}{6E_S}\right)^2 t_\infty \ll t_\infty$ and then *decreases* exponentially. It was noted that the contrasting behavior originates from the increase of bulk entropy in the scrambling phase, *i.e.,* the linear term in eqs. (2.36) and (2.39).

Furthermore, in our discussion, for simplicity we set the boundary entropy to zero, *i.e.,* $\log g = 0$ in eq. (2.20). This choice does not affect the Page transition in any way, as we have said. The reason is that neither of the two competing geodesics terminates on the end-of-the-world brane in this case. However, the first (quench-to-scrambling) transition will be shifted if we choose $\log g \neq 0$. On the scrambling phase branch, bulk geodesic connects a boundary point in the bath to the QES on the Planck brane. However, in the quench phase, the HRT surfaces are comprised of two geodesics terminating on the ETW brane. Therefore, the corresponding generalized entropy would be increased by a term $4 \log g$. If we consider figure 2.6, then the transition time would move to an even earlier time (assuming that $\log g > 0$).

Chapter 3

Equilibration model

As explained in section 1.3, the AEM^{4}Z model [1] has three holographic descriptions – see figure 1.2. The boundary perspective describes the system as two quantum mechanical systems $\mathrm{QM_L}$ + $\mathrm{QM_R}$ in a thermofield double (TFD) state that is connected to a bath via a quantum quench. In the present analysis, the bath consists of two copies of a two-dimensional holographic CFT on a half-line, which is initially prepared in an independent TFD state, with a temperature T_b. After the quench, the system evolves towards a new equilibrium between the quantum mechanical and bath systems, during which three different phases are distinguished by the position of the quantum extremal surface. The TFD in $\mathrm{QM_L}$ + $\mathrm{QM_R}$ is dual to a two-dimensional black hole in JT gravity, and this gravitational region also supports the same holographic CFT matter as appears in the bath. The third description replaces the holographic CFT with a three-dimensional AdS bulk and in particular, the TFD is replaced by a $\mathrm{AdS_3}$ black hole geometry. From this bulk perspective, the joining quench [143, 144] connecting the systems has a holographic description as an end-of-the-world brane pinching off the $\mathrm{AdS_2}$/bath boundary and falling into $\mathrm{AdS_3}$ spacetime.[1]

The three phases of the equilibration process are illustrated in figure 3.1. The QES

[1] We would like to point out that the roles of the end-of-the-world branes and Planck brane are quite different. The latter supports the JT gravity (as well as the holographic CFT) and plays a crucial role in the appearance of the island phase. The interested reader is referred to references [59, 60] for a detailed discussion of the explicit construction from the viewpoint of bulk spacetime, including the renormalization on the brane theory. The end-of-the-world branes appear in the $\mathrm{AdS_3}$ bulk construction since the two-dimensional dual theory is a boundary CFT living on the upper-half-plane (viewed in the appropriate conformal frame) [126, 145]. The details of the bulk dynamics of these branes through the joining quench is described in [143, 144].

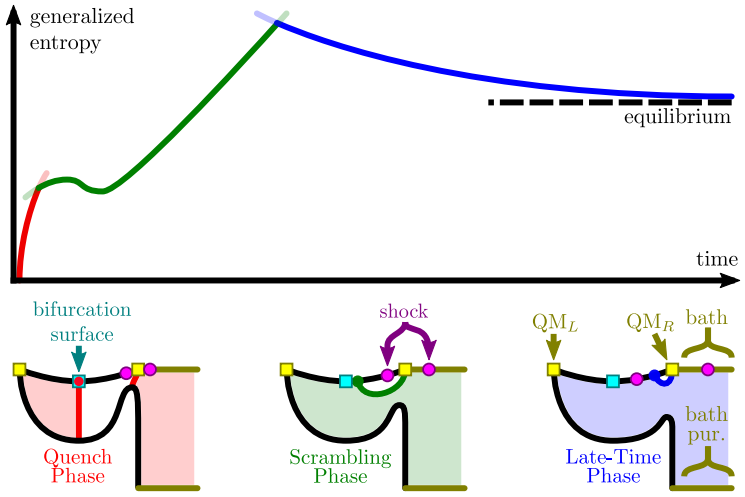

Figure 3.1: A cartoon illustration of the three phases for the entanglement entropy of QM_R or of QM_L, (a semi-infinite interval in) the thermal bath, and the (entire) bath purifier, after the quench where QM_R is connected to the bath. The darker colors indicate the true generalized entropy, while the lighter colors indicate the general shape of each of the branches slightly beyond the regime where it provides the minimal value for the generalized entropy. Below the plot is a sketch of the shape of the extremal HRT surfaces in AdS_3 which contribute to the generalized entropy in each phase.

remains at the bifurcation surface during the quench phase. At the transition to the scrambling phase, the QES shifts outwards by a very small distance. The generalized entropy in these two phases increases, consistent with the original information loss calculations. However, at the Page transition, the QES is instead located at a new minimum outside of the infalling shock. The generalized entropy at the Page transition then begins to asymptote towards the expected entropy of a black hole in equilibrium with the bath, completing a correct Page curve of the equilibration process. In the example shown in figure 3.1, the temperature of the bath is less than that of the black hole so the entropy decreases in the late time phase, similarly to the evaporating black hole. Note that a bath with temperature greater than that of the black hole instead heats up the black hole, giving a Page curve as in figure 3.10.

The central quantity necessary for studying the Page curve and the behaviour of the extremal surface throughout the equilibration process is the generalized entanglement entropy S_{gen}. Similar to previous work in the evaporating AdS_2 black hole in JT gravity [11],

we break the process of calculating the generalized entropy into three steps:[2]

- Calculating the von Neumann entropy of the CFT matter S_{vN}
- Calculating the backreaction of the quench onto the dilaton ϕ
- Extremizing the resulting $S_{\text{gen}} = \frac{\phi}{4G_{\text{N}}} + S_{\text{vN}}$

Conveniently, these steps are very similar to the evaporating model in chapter 2, the only change coming from the details of the time reparametrization function in eq. (3.29) and the extra conformal transformation in eq. (3.18) required to map the vacuum on upper half plane to our quenched system. We now proceed to carry out each one of these steps in the rest of this chapter.

3.1 Setup at finite temperature

3.1.1 Entropy of holographic CFT$_2$

To calculate the von Neumann entropy of the CFT matter, we proceed in a similar way to chapter 2 and map the corresponding quantum state to the vacuum of the CFT on the upper half plane by a local Weyl rescaling and a coordinate transformation. The details of the required coordinate transformation will be explained in section 3.1.3, but for now, we simply specify that we will be working in Poincaré coordinates for the AdS$_2$ spacetime

$$ds^2_{\text{AdS}} = -\frac{4L^2_{\text{AdS}}}{(x^+ - x^-)^2} dx^+ dx^- \,, \quad (x^\pm = t \pm s) \,, \tag{3.1}$$

and in flat coordinates for the bath

$$ds^2_{\text{bath}} = -\frac{L^2_{\text{AdS}} dy^+ dy^-}{\epsilon^2} \,, \quad (y^\pm = u \mp \sigma) \,. \tag{3.2}$$

The two spaces are glued together at one-dimensional boundary with $\sigma = -\epsilon$, $s = \epsilon f'$, $g_{uu} = \frac{L^2_{\text{AdS}}}{\epsilon^2}$ where ϵ corresponds to the UV cutoff in the dual boundary theory, and f is the

[2]Note that we have adapted the notation in eq. (1.29) to our specific system, in which the area of the HRT surface is given by the value of the dilaton. Further, we specify that the quantum corrections S_{out} are given by the von-Neumann entropy S_{vN} of the CFT matter on either side of the bipartition.

coordinate reparametrization function $x = f(y)$, given below in eq. (3.29).[3] As before, we simply set $L_{\text{AdS}} = 1$ for the rest of the chapter.

The CFT matter state can then be mapped to the CFT vacuum via the local Weyl rescaling

$$\begin{aligned} ds^2_{\text{AdS}} &\to \Omega(x^+, x^-)^2 ds^2_{\text{AdS}} = dz d\bar{z}\,, \\ ds^2_{\text{bath}} &\to \Omega'(y^+, y^-)^2 ds^2_{\text{bath}} = dz d\bar{z}\,, \end{aligned} \tag{3.3}$$

where

$$\Omega = \frac{x^+ - x^-}{2}\sqrt{z'(x)\bar{z}'(\bar{x})}\,, \quad \Omega' = \epsilon\sqrt{z'(y)\bar{z}'(\bar{y})}\,, \tag{3.4}$$

where we have introduced the Euclidean coordinates $x = -x^-$, $\bar{x} = x^+$ and similarly for y and $\bar{y}$. The coordinate transformations relating the x, y and z coordinates in eqs. (3.18), (3.21) and (3.29) are all derived in section 3.1.3. In the rest of this subsection, we focus on deriving the von Neumann entropy of the CFT matter in the z coordinates.

To begin, one can consider the von Neumann entropy of a finite interval with one end-point being the boundary of the BCFT and the other $(z, \bar{z})$ residing in the interior. Equivalently, this is the entropy for the semi-infinite interval beginning at $(z, \bar{z})$ and extending to infinity. This can be calculated using twist operator one-point functions in the upper half plane, but by the method of images, the latter resembles a two-point function of a CFT on the entire plane. Correspondingly, the von Neumann entropy resembles that of an interval with length $-i(z - \bar{z})$:

$$S_{\text{1pt}} = \frac{c}{6}\log[-i(z - \bar{z})] + \log g \tag{3.5}$$

where $\log g$ is the Affleck-Ludwig boundary entropy [125].

The entanglement entropy of an interval in a two-dimensional CFT in the presence of a conformal boundary at $z - \bar{z} = 0$ is [122, 123, 146, 124]

$$S_{\text{2pt}} = \frac{c}{6}\log\left(|z_1 - z_2|^2\eta\right) + \log G(\eta)\,, \tag{3.6}$$

where $\eta = \frac{(z_1-\bar{z}_1)(z_2-\bar{z}_2)}{(z_1-\bar{z}_2)(z_2-\bar{z}_1)}$ is the conformally invariant cross ratio and $G(\eta)$ is an undetermined function that depends on the theory and boundary conditions. The $G(\eta)$ function has two limits that can be determined by either a bulk OPE or an operator-boundary expansion:

[3] In section 3.2.3, we also introduce analogous coordinates $\tilde{y}^\pm = \tilde{u} \pm \tilde{\sigma}$ for the purification of the bath. These are related to $x^\pm$ in eq. (3.73), which is then the analog of eq. (3.13).

$G(\eta \to 1) = 1$ from the OPE limit, and $G(\eta \to 0) = g^2$ from the operator-boundary expansion.

Once again, we adopt the holographic framework describing boundary conformal field theory (BCFT) [126, 127]. In this setup, the JT gravity plus bath system lives on the boundary of an AdS_3 geometry. From this bulk perspective, the boundary defect at the moment of quenching anchors an end-of-the-world (ETW) brane hanging into the holographic direction. After the quench, the ETW brane detaches from the asymptotic boundary and falls off into the bulk. For this system, the entanglement entropy is determined using the Ryu-Takayanagi prescription [43], *i.e.,* for a two-dimensional CFT on the asymptotic AdS boundary, the entanglement entropy is simply given by evaluating the bulk length of the corresponding geodesics connecting the end-points on the boundary, with the added possibility of having geodesics ending at the ETW brane. In the z coordinates, this corresponds to evaluating the length of the geodesics connecting the end-points in a flat asymptotic boundary of AdS_3 with the possibility of having geodesics ending at a flat ETW brane intersecting the asymptotic boundary at $z - \bar{z} = 0$ at an angle determined by the boundary entropy $\log g$. In this case, eq. (3.6) reduces to the following simple form

$$S_{2\text{pt}} = \begin{cases} \frac{c}{3} \log\left(|z_1 - z_2|\right) & \text{if } \eta > \eta_* \\ \frac{c}{6} \log\left(|z_1 - \bar{z}_1||z_2 - \bar{z}_2|\right) + 2\, \log g & \text{if } \eta < \eta_* \end{cases}, \tag{3.7}$$

where $\eta_* = \frac{1}{1+g^{12/c}}$ is the value of the conformal cross ratio at which the transition between HRT surfaces occur. Let us note that with the simple choice $g = 1$ (*i.e.,* $\log g = 0$ and a tensionless ETW brane), the latter simplifies to $\eta_* = 1/2$. Equivalently, the $G(\eta)$ function for a holographic BCFT is given by

$$G(\eta) = \theta(\eta - \eta_*)\, \eta^{-c/6} + \theta(\eta_* - \eta)\, \frac{g^2}{(1-\eta)^{c/6}}\,. \tag{3.8}$$

It is straightforward to verify that $G(\eta \to 1) = 1$ and $G(\eta \to 0) = g^2$. For simplicity, we take the case of zero boundary entropy $g = 1$ (and $\eta^* = 1/2$) in the following. As was noted in chapter 2, for a general g, the quench to scrambling phase transition gets shifted, while the Page transition remains unaffected.

The von Neumann entropies in eqs. (3.5) and (3.7) correspond to intervals of the vacuum of the BCFT. To find the von Neumann entropies of the CFT matter in our black hole equilibration model, we simply have to include the effect of the local Weyl transformation in eq. (3.3). Under a Weyl transformation $g_{\mu\nu} \to \Omega^{-2} g_{\mu\nu}$, the transformation of twist

operators induces the following transformation on entropy:

$$S_{\Omega^{-2}g} = S_g - \frac{c}{6} \sum_{\text{endpoints}} \log \Omega(\text{endpoint}). \tag{3.9}$$

The above transformation may be interpreted as resulting from the rescaling of UV cutoffs with respect to which the entropy is defined.

3.1.2 Jackiw-Teitelboim gravity

The brane perspective of the AEM^{4}Z model – see figure 1.2b – describes the system as a black hole in two-dimensional JT theory coupled to holographic conformal matter that is connected to a bath with a joining quench, and allowed to evaporate. We refer the reader to chapter 2 for a more detailed discussion of this description. In this subsection, we summarize the essential parts of our analysis.

The dynamics of the black hole and CFT matter are governed by the action

$$I = \frac{1}{16\pi G_{\text{N}}} \left[\int_{\mathcal{M}} d^2x \sqrt{-g}\, \phi \left(R + \frac{2}{L_{\text{AdS}}^2} \right) + 2 \int_{\partial\mathcal{M}} \phi_b K \right] + I_{\text{top}} + I_{\text{CFT}}\,, \tag{3.10}$$

where

$$I_{\text{top}} = \frac{\phi_0}{16\pi G_{\text{N}}} \left[\int_{\mathcal{M}} d^2x \sqrt{-g}\, R + 2 \int_{\partial\mathcal{M}} K \right] \tag{3.11}$$

is a topological term, which provides a large constant contribution $S_0 = \frac{\phi_0}{4G_{\text{N}}}$ to the entropy of the black hole. The last term in eq. (3.10) is the action of the holographic CFT matter to which JT gravity is coupled.

The dilaton equation of motion imposes the geometry to be locally AdS_2 with radius L_{AdS}, as described by the metric in eq. (3.1). The metric equations of motion give the coupling of the dilaton to the CFT stress tensor

$$\begin{aligned} 2\partial_{x^+}\partial_{x^-}\phi + \frac{4\phi}{(x^+ - x^-)^2} &= 16\pi G_{\text{N}} \langle T_{x^+x^-} \rangle\,, \\ -\frac{\partial_{x^+}\left((x^+ - x^-)^2 \partial_{x^+}\phi\right)}{(x^+ - x^-)^2} &= 8\pi G_{\text{N}} \langle T_{x^+x^+} \rangle\,, \\ -\frac{\partial_{x^-}\left((x^+ - x^-)^2 \partial_{x^-}\phi\right)}{(x^+ - x^-)^2} &= 8\pi G_{\text{N}} \langle T_{x^-x^-} \rangle\,. \end{aligned} \tag{3.12}$$

Before the quench, the CFT matter is in the vacuum of the generator of t translations (see eq. (3.1)) *i.e.*, $\langle T_{x^+x^+}\rangle = \langle T_{x^-x^-}\rangle = \langle T_{x^+x^-}\rangle = 0$,[4] however, this can also be seen as a TFD state for the generator of u translations (see eq. (3.2)). Here we have continued the y coordinates into a Rindler patch of AdS_2 with

$$x^{\pm} = \frac{1}{\pi T_0} \tanh\left(\pi T_0 y^{\pm}\right) . \tag{3.13}$$

The dilaton profile is given by

$$\phi = 2\bar{\phi}_r \frac{1-(\pi T_0)^2 x^+x^-}{x^+-x^-} = 2\bar{\phi}_r \pi T_0 \coth\left(\pi T_0\left(y^+-y^-\right)\right) . \tag{3.14}$$

After the quench, the dilaton receives a contribution from the back-reaction of the matter stress tensor

$$\phi = \bar{\phi}_r \frac{2-2\left(\pi T_1\right)^2 x^+x^- + kI_0}{x^+-x^-} , \tag{3.15}$$

where

$$I_0 = -\frac{24\pi}{c}\int_0^{x^-} dt\,(x^+-t)(x^--t)\,\langle T_{x^-x^-}(t)\rangle , \tag{3.16}$$

accounts for the matter back-reaction and $k = \frac{cG_N}{3\bar{\phi}_r}$ controls the strength of the back-reaction, which we take to be very small. The dilaton profile in eqs. (3.14) and (3.15) give the leading contribution to the generalized entanglement entropy. The details of the dilaton profile after the quench in eq. (3.15) and the resulting generalized entropy are calculated in section 3.1.3.

3.1.3 Coupling to a thermal bath

The setup which we wish to consider is very similar to the one studied in chapter 2: a two-sided AdS_2 black hole prepared at some temperature T_0 coupled by a joining quench to a bath consisting of a CFT on a half-line. Again, the key difference will be that our bath will be at some finite temperature T_b, rather than zero temperature as in chapter 2. The corresponding Penrose diagram is shown in figure 3.2. Up until an initial time, we imagine

[4] In principle, we should have one non-zero component $\langle T_{x^+x^-}\rangle = \frac{c}{12\pi(x^+-x^-)^2}$ due to the trace anomaly. But this extra term can be absorbed by shifting the value of the dilaton field as $\tilde{\phi} = \phi - \frac{cG_N}{3}$ – see discussion in [59, 60]. So we simply ignore the trace anomaly in the following.

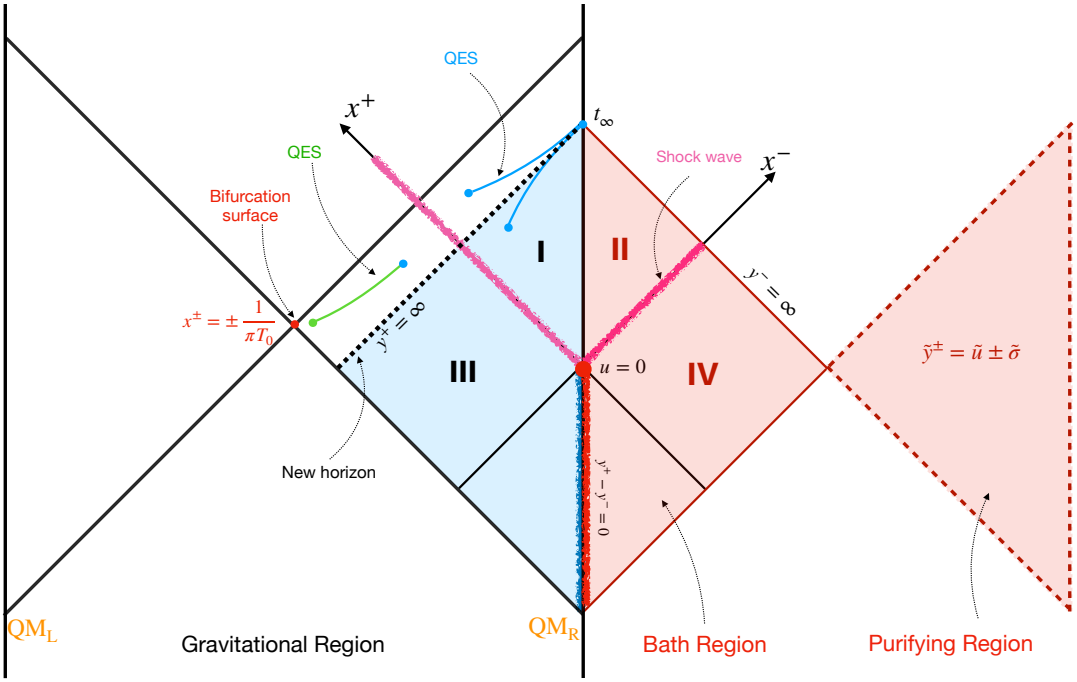

Figure 3.2: The Penrose diagram for the AdS_2 black hole coupled with a thermal bath and its purification in flat spacetime at time $u = 0$. The (thick) pink lines are the shock waves propagating into the gravitating and bath regions, which are generated by this joining quench. The bifurcation surface of the initial equilibrium black hole is indicated by the red dot. The new horizon is indicated by the black dashed line, *i.e.*,$y^+ = \infty$. Note that only the blue and red shaded regions are covered by the $y^\pm, \tilde{y}^\pm$ coordinates, respectively. The evolution of quantum extremal surface in three phases is presented by the corresponding colored curves, as indicated in figure 3.1.

two decoupled systems. Firstly, we have the AdS_2 black hole solution[5] of JT gravity with the metric and dilaton profile in eqs. (3.1) and (3.14), respectively. This gravitating region also supports the same two-dimensional CFT as appears in the bath region. The right side of this black hole will have a boundary given by an IR cutoff introduced by the JT boundary particle. Additionally, we have a separate bath system supporting an identical CFT_2 (but in a different state), prepared on a half-line $\sigma = \frac{y^- - y^+}{2} > -\epsilon$ on the flat spacetime (3.2). The boundaries in the two systems initially impose reflecting boundary conditions. But, at some initial time $u = t = 0$, we perform a joining quench. This is done by identifying $\sigma = -\epsilon$ in the bath with the AdS_2 IR cutoff surface, allowing CFT matter to flow freely across the now transparent division between the AdS_2 and bath systems. The details of this gluing are specified by the trajectory $t = f(u)$ – that is, we identify the time parameter of the AdS_2 boundary with the time coordinate of the bath. Further demanding that the induced metrics along the AdS_2 and bath boundaries match to leading order in ϵ, we have

$$x^{\pm} = f(y^{\pm}) \tag{3.17}$$

along the gluing. For convenience, we shall further extend the above equality to hold everywhere, so that we may alternatively describe patches of AdS_2 and the bath using either $x^{\pm}$ or $y^{\pm}$ coordinates. Later in this section, we will determine the trajectory $t = f(u)$ of the JT boundary particle by tracking the exchange of energy between the AdS_2 and bath systems.

While we have described the physical evolution of the system above, it is practically useful also to consider a Euclidean preparation of the CFT state at $u = t = 0$. Thus, we imagine preparing the CFT in a Hartle-Hawking state on the JT black hole with a path integral over Euclidean AdS_2 (with an appropriate dilaton profile). Similarly, we prepare the CFT in the bath (and the purifying copy) in a thermofield state with a path integral on Euclidean half-spaces. (The details will be elaborated below.) Both systems have reflecting boundary conditions, except in an infinitesimal neighborhood of $iu = it = 0$, where the two spacetimes are joined. The size of this neighborhood provides a regulator for the shock energy E_S produced by the joining quench — recall that removing the vacuum entanglement along an entangling surface (in this case, the point at the AdS-bath boundary) produces an infinite amount of energy. This construction produces the CFT state at $u = t = 0$, from which analytic continuation provides the correct Lorentzian evolution according to the joined Hamiltonian. We note that this joined evolution, obtained by analytic continuation, does not match the physical decoupled evolution of the AdS and bath systems to the past

[5]Note that an appropriate choice of coordinates, *e.g.,* those spanning the trajectory of the JT boundary particle, furnishes a pure AdS_2 with Rindler horizons — we are treating the AdS_2 spacetime as a black hole in the usual sense for JT gravity [121, 147, 120].

of the point of the joining quench. In particular, we expect the time-reversal symmetry of the Euclidean path integral to carry over to Lorentzian time upon analytic continuation; in contrast, the physical Lorentzian evolution is manifestly not time-reversal symmetric due to the change in boundary conditions at the quench. However, results obtained by analytic continuation will be adequate for our purposes as we are primarily interested in the Lorentzian physics beyond the past light-cone of the quench point where the AdS_2 and bath boundaries are joined.

Our point of departure from chapter 2 lies with the generalization to thermal baths prepared at finite temperature. To put the bath at a finite temperature T_b, we take the Euclidean y coordinates for the bath and identify $y \sim y + \frac{i}{T_b}$.[6] We still take the bath to be the half-space $\frac{y+\bar{y}}{2} \leq \epsilon$. As expected for a thermal state, this results in a non-zero stress tensor expectation value in y coordinates. Although the x coordinates of AdS_2 are stitched to the y coordinates of the bath (*i.e.*, $x = f(y)$), it will nonetheless be convenient in the following to introduce a conformal transformation after which the stress tensor becomes trivial. This can be achieved by transforming the thermal half-cylinder, with coordinates y, to the left half-plane,[7] with coordinates Y, via

$$Y = \frac{1}{\pi T_b} \tanh(\pi T_b y). \tag{3.18}$$

This is simply the composition of an exponential map $y' = e^{2\pi T_b y}$ taking the thermal half-cylinder to a unit disk, and a Mobius map $Y = \frac{1}{\pi T_b} \frac{y'-1}{y'+1}$ pushing a point on the boundary of the disk to ∞.

It will be useful, *e.g.*, to make use of the entropy formula (3.9), to write down another map that maps the joint system of AdS, with Poincare coordinates x, and the bath, with Euclidean coordinates y or equivalently the coordinates Y found above, to the upper half

[6] Note that this identification makes T_b the temperature associated with the unit time-like vector in the geometry $dyd\bar{y}$, as opposed to the physical geometry $\frac{L^2_{AdS} dyd\bar{y}}{\epsilon^2}$. In the doubly holographic language of Figure 1.2c, the former is the CFT metric of the asymptotic boundary of AdS_3 while the latter is the induced metric on a cutoff surface which becomes the asymptotic boundary in the $\epsilon \to 0$ limit. Similarly, in (3.13), T_0 describes a temperature with respect to the parametric time $u = \frac{y^+ + y^-}{2}$ of the boundary particle, which does not correspond to a unit vector in the AdS_2 geometry (3.1).

[7] Strictly speaking, we should take the bath to be the half-space $\frac{y+\bar{y}}{2} \leq \epsilon$ and (3.18) would map this region to the plane minus a large disk in the right half-plane. Similarly, Euclidean preparation of the AdS_2 system, in the $x, \bar{x}$ coordinates analytically continued from (3.13), does not occur on a full Euclidean Poincaré AdS_2, but rather on a large disk-like subregion. Note that the stress tensor still vanishes in these subregions of the $dYd\bar{Y}$ and $\frac{2dxd\bar{x}}{x+\bar{x}}$ geometries, since a flat disk (or its complement) is related to a flat half-plane by a Mobius transformation. (The rescaling of $dxd\bar{x}$ by the Poincaré Weyl factor $\frac{2}{x+\bar{x}}$ does not introduce an extra anomalous contribution to the stress tensor.)

plane, with coordinates $z, \bar{z}$. Just prior to coupling the AdS and bath systems, the AdS system is in the Hartle-Hawking state with vanishing stress tensor in x coordinates. Meanwhile, by construction, the stress tensor of the bath vanishes in the Y coordinates. Finally, the stress tensor in the half-plane with coordinates z must also vanish. By demanding that the conformal anomalies of the map from x and Y to z vanish respectively in AdS and the bath, together with boundary conditions, fixes this map. Following [11], we choose boundary conditions such that the AdS_2 space is mapped to the region $(0, iz_0)$ and the bath to $(iz_0, i\infty)$. The map is piecewise-Mobius:

$$z = \begin{cases} \frac{-iz_0^2}{x-iz_0} & x > 0\,, \\ z_0 - iY & x < 0\,. \end{cases} \tag{3.19}$$

The discontinuity at $z = z_0$ produces the shock wave contributions to the stress tensor components $\langle T_{xx}\rangle = E_S\,\delta(x)$ and $\langle T_{\bar{x}\bar{x}}\rangle = E_S\,\delta(\bar{x})$, with

$$E_S \simeq \frac{c}{12\pi(-iz_0)}. \tag{3.20}$$

In the limit $E_S \to \infty$ (*i.e.*, $-iz_0 \to 0$), the map (3.19) becomes

$$z = \begin{cases} (\frac{12\pi}{c}E_S)^{-2}\frac{i}{x} & x > 0\,, \\ -iY & x < 0\,. \end{cases} \tag{3.21}$$

The next step is to determine f by demanding the conservation of energy between the AdS and bath systems [147, 11]:

$$\partial_u E(u) = f'(u)^2(T_{x^-x^-} - T_{x^+x^+}). \tag{3.22}$$

From the conformal anomaly associated with the Weyl transformation (3.21), *i.e.*,

$$\langle T_{xx}\rangle = \left(\frac{dz}{dx}\right)^2 \langle T_{zz}\rangle - \frac{c}{24\pi}\{z, x\}\,, \tag{3.23}$$

we can find that the stress tensor in the AdS region satisfies[8]

$$\begin{aligned} \langle T_{x^\pm x^\pm}(x^\pm)\rangle_{\text{AdS}} =& E_S\,\delta(x^\pm) - \frac{c}{24\pi}\,\{Y^\pm, x^\pm\}\,\Theta\big(\mp x^\pm\big) \\ =& E_S\,\delta(x^\pm) - \frac{c}{24\pi}\,\Theta\big(\mp x^\pm\big)\left[\{y^\pm, x^\pm\} - 2\left(\frac{\pi T_{\text{b}}}{f'(y^\pm)}\right)^2\right], \end{aligned} \tag{3.24}$$

[8]This result does not apply in the causal past of the junction point. Further, note that the Schwarzian is defined by $\{f(y), y\} \equiv \frac{f'''}{f'} - \frac{3}{2}\left(\frac{f''}{f'}\right)^2$.

where we have used the Schwarzian composition rule

$$\{Y,x\} = \{y,x\} + \left(\frac{dy}{dx}\right)^2 \{Y,y\}. \tag{3.25}$$

For completeness, from eq. (3.21), we also write the stress tensor in the bath region:

$$\langle T_{y^\pm y^\pm}(y^\pm)\rangle_{\text{bath}} = E_S\,\delta(y^\pm) - \frac{c}{24\pi}\left[\Theta\big(\pm y^\pm\big)\,\{x^\pm, y^\pm\} - \Theta\big(\mp y^\pm\big)\,2(\pi T_{\text{b}})^2\right]. \tag{3.26}$$

As mentioned below eq. (3.19), the δ-function contributions in eqs. (3.24) and (3.26) may be interpreted as the positive-energy shockwaves produced by the quench. The Schwarzian terms have a similar simple interpretation: $T_{x^-x^-} \sim -\frac{c}{24\pi}\{y^-, x^-\} < 0$ describes a negative energy flux from the bath experienced by the black hole, while $T_{y^+y^+} \sim -\frac{c}{24\pi}\{x^+, y^+\} > 0$ describes a positive energy flux from the black hole experienced by the bath. Considering for simplicity the $T_{\text{b}} = 0$ case, note that the quanta described by these fluxes are the result of vacuum fluctuations in their native geometries. In particular, on the initial time slice, these quanta register as vanishing stress-energy, which is to be expected in the Hartle-Hawking vacuum of AdS_2 and the flat half-space vacuum. It is only when these quanta cross over the AdS_2-bath interface that they register as non-vanishing stress energy. Finally, in the case of nonvanishing bath temperature $T_{\text{b}} > 0$, the last terms in eqs. (3.24) and (3.26) can be interpreted as the contribution to the stress-energy of the bath's thermal radiation.

To determine the f function, we next note that the ADM energy of the AdS_2 JT system

$$E(u) = -\frac{\bar{\phi}_r}{8\pi G_{\text{N}}}\{f(u),u\}. \tag{3.27}$$

can also be expressed in terms of the Schwarzian of f. We have, from solving eq. (3.22), the Schwarzian equation

$$\{f(u),u\} = -2\pi^2\left[T_{\text{b}}^2 + (T_1^2 - T_{\text{b}}^2)e^{-ku}\right], \quad \text{with} \quad k \equiv \frac{cG_{\text{N}}}{3\bar{\phi}_r} \ll 1, \tag{3.28}$$

where once again T_1 is the temperature of the black hole after the initial shock of energy E_{s} falls in, so that $E_S \equiv \frac{\phi_r \pi}{4G_{\text{N}}}(T_1^2 - T_0^2)$.

From the initial conditions $f(0) = 0, f'(0) = 1, f''(0) = 0$, we can solve this differential equation to obtain the map between y and x:[9]

$$f(u,T_b) = \frac{2}{ka}\,\frac{I_\nu(a)\,K_\nu(ae^{-ku/2}) - K_\nu(a)\,I_\nu(ae^{-ku/2})}{I'_\nu(a)\,K_\nu(ae^{-ku/2}) - K'_\nu(a)\,I_\nu(ae^{-ku/2})} \tag{3.29}$$

[9]We note that the same differential equation appears in the analysis of [70], although differences arise since their work involves different boundary conditions for $f(u)$.

where

$$a = \frac{2\pi}{k}\sqrt{T_1^2 - T_{\rm b}^2} \qquad \text{and} \qquad \nu = \frac{2\pi T_{\rm b}}{k}\,. \tag{3.30}$$

The above function is also well-defined and always real for complex a, *i.e.*, $T_1 < T_{\rm b}$.

Given the map (3.21) and the function f, we may compute the von Neumann entropy of various intervals in the AdS-bath system by applying the transformation rule (3.9) to the formulas (3.5) or (3.6) for entropy of intervals in a half-plane.

First, we divide the spacetime of interest into four regions according to

$$x^{\pm} \in \begin{cases} \text{I} & \text{post-shock in AdS}\,, \quad x^+ \geq x^- \geq 0\,, \\ \text{II} & \text{post-shock in bath}\,, \quad x^- \geq x^+ \geq 0\,, \\ \text{III} & \text{pre-shock in AdS}\,, \quad x^+ \geq 0 \geq x^-\,, \\ \text{IV} & \text{pre-shock in bath}\,, \quad x^- \geq 0 \geq x^+\,. \end{cases} \tag{3.31}$$

Applying the entropy transformation rule (3.9) to eq. (3.5) with these Weyl factors and the form (3.21) of the map, we obtain the following formulas for the von Neumann entropy computed with a single twist operator at $x^{\pm}$:

$$S_{\rm 1pt}(x^{\pm}) = \log g + \frac{c}{6}\log \begin{cases} \frac{24E_S}{cT_{\rm b}}\frac{x^+\sinh(\pi T_{\rm b} y^-)\sqrt{f'(y^-)}}{x^+ - x^-}\,, & x^{\pm} \in \text{I}\,, \\ \frac{12E_S}{c\epsilon T_{\rm b}}\frac{x^+\sinh(\pi T_{\rm b} y^-)}{\sqrt{f'(y^+)}}\,, & x^{\pm} \in \text{II}\,, \\ 2\,, & x^{\pm} \in \text{III}\,, \\ \frac{\sinh[\pi T_{\rm b}(y^- - y^+)]}{\pi\epsilon T_{\rm b}}\,, & x^{\pm} \in \text{IV}\,. \end{cases} \tag{3.32}$$

Note that in the pre-shock cases, we recover the expected entropy formulas in AdS and a thermal half-line. In particular, if we take $\frac{y^- - y^+}{2} \to \sigma_{\rm IR}$ for some IR cutoff $\sigma_{\rm IR}$, we get the entropy of the whole thermal half-line:

$$S_{\frac{1}{2}\text{-line}} = \log g + \frac{c}{6}\left[2\pi T_{\rm b}\sigma_{\rm IR} + \log\left(\frac{1}{2\pi\epsilon T_{\rm b}}\right)\right]. \tag{3.33}$$

Of course, these three terms are interpreted as: the boundary entropy, the thermal entropy of the CFT at temperature $T_{\rm b}$, and the log divergent contribution associated with the endpoint of the interval.

We obtain entropy formulas derived from two-point function by transforming eq. (3.6):

$$S_{\rm 2pt}\left(x_1^\pm \in {\rm II}, x_2^\pm\right) = \log G(\eta) + \frac{c}{6}\log\begin{cases} \frac{2}{\pi\epsilon T_{\rm b}}\frac{\sinh[\pi T_{\rm b}(y_2^- - y_1^-)](x_1^+ - x_2^+)}{x_2^+ - x_2^-}\sqrt{\frac{f'(y_2^-)}{f'(y_1^+)}}\,, & x_2^\pm \in {\rm I}\,, \\ \frac{1}{\pi\epsilon^2 T_{\rm b}}\frac{-\sinh[\pi T_{\rm b}(y_1^- - y_2^-)](x_1^+ - x_2^+)}{\sqrt{f'(y_1^+)f'(y_2^+)}}\,, & x_2^\pm \in {\rm II}\,, \\ \frac{24E_S}{c\epsilon T_{\rm b}}\frac{\sinh(\pi T_{\rm b} y_1^-)x_1^+ x_2^-(x_1^+ - x_2^+)}{x_2^+(x_1^+ - x_2^-)\sqrt{f'(y_1^+)}}\,, & x_2^\pm \in {\rm III}\,, \\ \frac{12\pi E_S}{c\epsilon^2}\frac{-x_1^+ Y_2^+(Y_2^- - Y_1^-)\eta}{\sqrt{f'(y_1^+)}} & \\ \quad\times\cosh(\pi T_{\rm b} y_1^-)\cosh(\pi T_{\rm b} y_2^+)\cosh(\pi T_{\rm b} y_2^-)\,, & x_2^\pm \in {\rm IV}\,, \end{cases} \tag{3.34}$$

where the cross-ratio is determined by

$$\eta(x_1^\pm \in {\rm II}, x_2^\pm) = \begin{cases} \frac{Y_1^-(Y_2^- - Y_2^+)}{Y_2^-(Y_1^- - Y_2^+)}\,, & x_2^\pm \in {\rm IV}\,, \\ \frac{x_1^+(x_2^+ - x_2^-)}{x_2^+(x_1^+ - x_2^-)}\,, & x_2^\pm \in {\rm III}\,, \\ 1\,, & x_2^\pm \in {\rm I}, {\rm II}\,. \end{cases} \tag{3.35}$$

(3.36)

Note that this agrees with eq. (3.30) of [11] in the limit when $T_{\rm b} \to 0$ and the $x_1^\pm$ endpoint is taken to the AdS-bath boundary. With the holographic formula (3.8) for G, the pre-shock cases of (3.34) with $x_1^\pm \in {\rm II}$ become[10]

$$S_{\rm 2pt} = \begin{cases} S_{\rm 1pt}(x_1^\pm) + S_{\rm 1pt}(x_2^\pm)\,, & \text{if } \eta \le \eta^* \\ \frac{c}{6}\log\left(\frac{24E_S}{c\epsilon T_{\rm b}}\frac{(x_2^+ - x_1^+)x_2^-\sinh(\pi T_{\rm b} y_1^-)}{(x_2^+ - x_2^-)\sqrt{f'(y_1^+)}}\right)\,, & \text{if } \eta > \eta^*,\ x_2^\pm \in {\rm III}\,, \\ \frac{c}{6}\log\left(\frac{12E_S}{c\pi\epsilon^2 T_{\rm b}^2}\frac{x_1^+\sinh(\pi T_{\rm b} y_2^+)\sinh[\pi T_{\rm b}(y_1^- - y_2^-)]}{\sqrt{f'(y_1^+)}}\right)\,, & \text{if } \eta > \eta^*,\ x_2^\pm \in {\rm IV}\,. \end{cases} \tag{3.37}$$

3.2 Thermal equilibrium

From eq. (3.28), we see that the main effect of a finite temperature $T_{\rm b} > 0$ for the bath is that the black hole does not evaporate completely, but rather equilibriates with the bath.

[10] The x_2 dependence of the bulk entropy is identical to that found for a bath with vanishing temperature, *e.g.*, see eqs. (2.64) and (2.65). This immediately implies that the position of the quantum extremal surfaces in the quench and scrambling phases are the same as for the $T_{\rm b} = 0$ case.

That is, it tends towards a stationary black hole with temperature $T_{\rm b}$, for which

$$\{f(y), y\} = -\,2\pi^2 T_{\rm b}^2\,. \tag{3.38}$$

Indeed, when $T_1 = T_{\rm b}$, the black hole does not change at all and instead, after consuming the shock, the black hole remains a stationary black hole at temperature $T_1 = T_{\rm b}$. In this case, f takes same form as for the eternal black hole solution

$$f(y) = \frac{1}{\pi T_1}\,\tanh(\pi T_1 y)\,. \tag{3.39}$$

Note that, from eq. (3.18), we then have $x = Y$ which agrees with the intuition that the radiation emitted by the bath mimics the radiation that would have been reflected from the AdS boundary in the Hartle-Hawking state had the bath not been attached. In this section we focus on the special case in which the black hole and the bath are in thermal equilibrium $T_1 = T_b$ after the quenching.

For the equilibrium case, the formulas (3.32), (3.34), and (3.37) become simple. More explicitly, the one-point function (3.32) reduces to

$$S_{\rm 1pt}(x^\pm) = \log g + \frac{c}{6}\log\begin{cases} \frac{24\pi E_S}{c}\frac{x^+x^-}{x^+-x^-}\,, & x^\pm \in {\rm I}\,,\\ \frac{12\pi E_S}{c\epsilon}\frac{x^+x^-}{\sqrt{[1-(\pi T_1 x^+)^2][1-(\pi T_1 x^-)^2]}}\,, & x^\pm \in {\rm II}\,,\\ 2\,, & x^\pm \in {\rm III}\,,\\ \frac{x^- - x^+}{\epsilon\sqrt{[1-(\pi T_1 x^+)^2][1-(\pi T_1 x^-)^2]}}, & x^\pm \in {\rm IV}\,. \end{cases} \tag{3.40}$$

According to the position of endpoints x_1, x_2, the entanglement entropy based on two-point function reads

$$S_{\rm 2pt}\,(x_1, x_2) = \begin{cases} S_{\rm 1pt}(x_1^\pm) + S_{\rm 1pt}(x_2^\pm)\,, & \text{if } \eta \le \eta^* \\ \frac{c}{6}\log\left\{\frac{24\pi E_S}{c\epsilon}\frac{x_1^- x_2^-(x_1^+ - x_2^+)}{(x_2^+ - x_2^-)\sqrt{[1-(\pi T_1 x_1^+)^2][1-(\pi T_1 x_1^-)^2]}}\right\}\,, & \text{if } \eta > \eta^*,\ x_2^\pm \in {\rm III}, \\ \frac{c}{6}\log\left\{\frac{12\pi E_S}{c\epsilon^2}\frac{x_1^+ x_2^+(x_1^- - x_2^-)}{\sqrt{[1-(\pi T_1 x_1^+)^2][1-(\pi T_1 x_1^-)^2][1-(\pi T_1 x_2^+)^2][1-(\pi T_1 x_2^-)^2]}}\right\}\,, & \text{if } \eta > \eta^*,\ x_2^\pm \in {\rm IV}, \end{cases} \tag{3.41}$$

for $x_1^\pm \in \text{I}$ and also

$$S_{2\text{pt}} = \log G(\eta) + \frac{c}{6}\log\begin{cases} \frac{2}{\epsilon}\frac{(x_1^+-x_2^+)(x_2^--x_1^-)}{(x_2^+-x_2^-)\sqrt{[1-(\pi T_1 x_1^+)^2][1-(\pi T_1 x_1^-)^2]}}\,, & x_2^\pm \in \text{I}\,, \\ \frac{1}{\epsilon^2}\frac{-(x_1^+-x_2^+)(x_1^--x_2^-)}{\sqrt{[1-(\pi T_1 x_1^+)^2][1-(\pi T_1 x_1^-)^2][1-(\pi T_1 x_2^+)^2][1-(\pi T_1 x_2^-)^2]}}\,, & x_2^\pm \in \text{II}\,, \\ \frac{24\pi E_S}{c\epsilon}\frac{x_1^+x_1^-x_2^-(x_1^+-x_2^+)}{x_2^+(x_1^+-x_2^-)\sqrt{[1-(\pi T_1 x_1^+)^2][1-(\pi T_1 x_1^-)^2]}}\,, & x_2^\pm \in \text{III}\,, \\ \frac{12\pi E_S}{c\epsilon^2}\frac{-x_1^+x_2^+(x_2^--x_1^-)\eta}{\sqrt{[1-(\pi T_1 x_1^+)^2][1-(\pi T_1 x_1^-)^2][1-(\pi T_1 x_2^+)^2][1-(\pi T_1 x_2^-)^2]}}\,, & x_2^\pm \in \text{IV}\,, \end{cases} \tag{3.42}$$

when $x_1 \in \text{II}$. As noted below eq. (3.32), the before-shock single-twist entropy formulas are the standard ones in AdS and the thermal half-line, which are invariant under translations in time $u = \frac{y^+ + y^-}{2}$. For the thermal case at hand, the two-twist formulas, with both twists inserted to the future of the shock, are also time-translation invariant. This can be made manifest by writing those cases of (3.42) in $y^\pm$ coordinates:

$$S_{2\text{pt}}\left(x_1^\pm \in \text{II}\right) = \frac{c}{6}\log\begin{cases} \frac{2\sinh[\pi T_1(y_2^+-y_1^+)]\sinh[\pi T_1(y_1^--y_2^-)]}{\pi T_1\epsilon\sinh[\pi T_1(y_2^+-y_2^-)]}\,, & x_2^\pm \in \text{I}\,, \\ \frac{\sinh[\pi T_1(y_2^+-y_1^+)]\sinh[\pi T_1(y_1^--y_2^-)]}{(\pi T_1\epsilon)^2}\,, & x_2^\pm \in \text{II}\,. \end{cases} \tag{3.43}$$

Moreover, the above is also invariant under 'time-reversal' $u_1 - u_2 \leftrightarrow -(u_1 - u_2)$. These properties will be helpful in finding the late-time QES. Indeed, eq. (3.43) is the same entropy formula as for an eternally-coupled black hole and bath system, as studied in [62]. For simplicity, we shall take $g = 1$ and $\eta^* = 1/2$ in the following sections.

In the following sections, we apply the RT formula to the calculation of entropy for various subregions in the full system consisting of QM_L, QM_R, the thermal bath, and an auxiliary system purifying the bath. We begin in Section 3.2.1 by considering the entropy of QM_L, the bath system, and the purifier, recovering the Page curve, discussed previously in Section 3.1 and illustrated in figure 3.1 — the corresponding bulk RT surfaces are also shown in figure 3.3a. Next, in Section 3.2.2, we trace out the majority of the bath, as shown in figure 3.3b, finding that only a finite bath interval of some minimal length is required to recover the black hole interior. Finally, in Section 3.2.3, we evaluate the importance of the bath's purifier. In particular, we find that if the purifier is completely traced out, as shown figure 3.3c, the black hole interior can no longer be recovered, regardless of the size of the bath interval that one can access; at the very least, a finite interval of the purifier is required, as shown in figures 3.3d and 3.4.

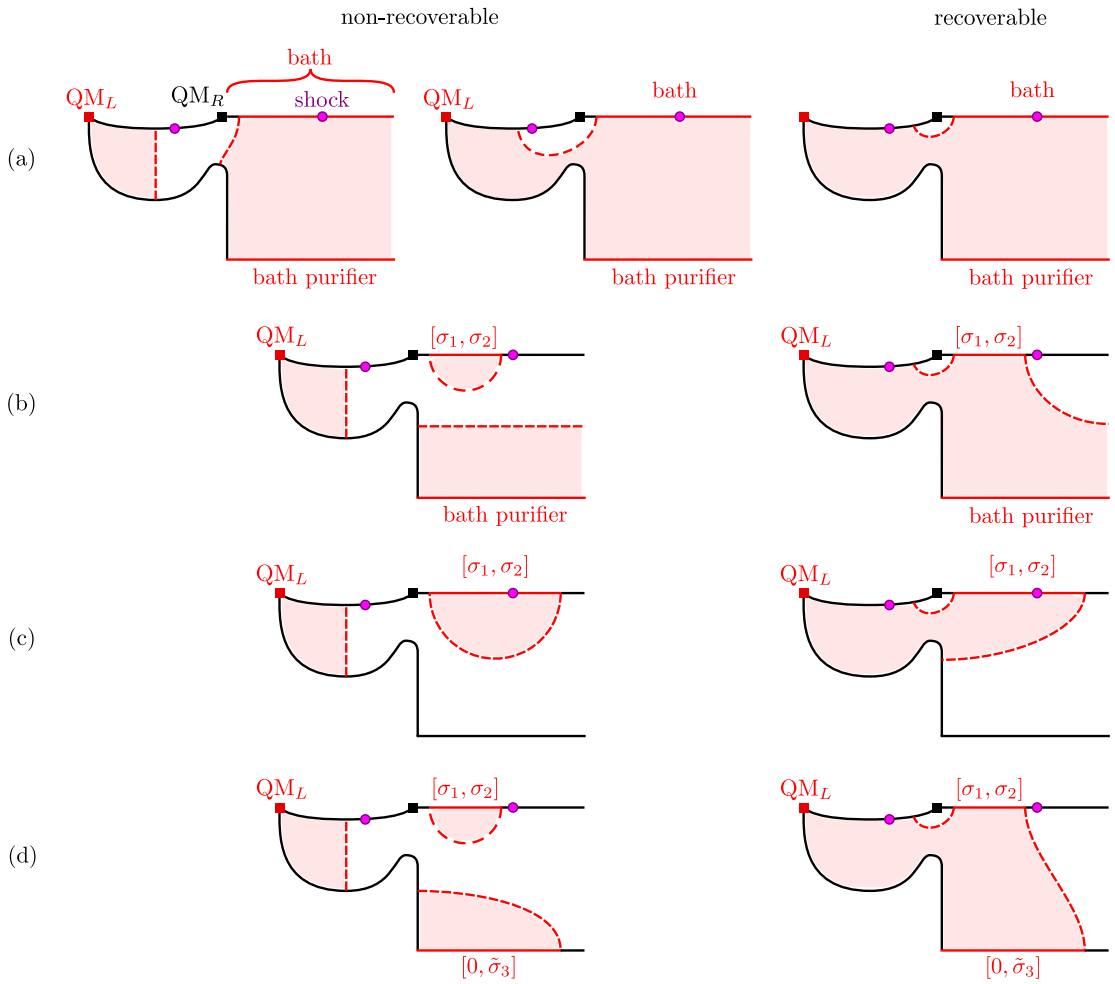

Figure 3.3: Competing channels computing the generalized entropy of various subsystems (solid red) and the corresponding bulk RT surfaces (dashed red) and entanglement wedges (light red). In each case, the R-channel where the black hole interior is recoverable or reconstructible is shown on the left. On the right, we show the N-channel where the interior is non-recoverable or non-reconstructible. The corresponding generalized entropies for these channels are denoted S_{R} and S_{N}, respectively. In the top row (a), we consider the generalized entropy of QM_{L}, the thermal bath, and the bath's purifier. In row (b), we keep only a finite interval $[\sigma_1, \sigma_2]$ of the bath. In row (c), we further trace out the purifier. Finally, in row (d), we include a finite interval $[0, \tilde{\sigma}_3]$ of the purifier. Note that in this last case, we can also vary $\tilde{u}_3$, the time slice of the purifier interval, and we find the minimal $\tilde{\sigma}_3$ depends on $\tilde{u}_3$ — see section 3.2.3.

3.2.1 Semi-infinite interval of the bath

First, we consider the evolution of (generalized) entropy for the subsystem consisting of QM_{L}, a semi-infinite interval of the bath with endpoint $x_1^{\pm}$ after the shock, and the purifier of the bath. The corresponding HRT surfaces and the time evolution are illustrated in figure 3.1, and we shall find three phases for the generalized entropy, corresponding to different portions of a Page curve. Note that, tracing out the purifier would also produce an infinite thermal entropy for the semi-infinite bath interval, *i.e.,* the infinite entanglement entropy between the semi-infinite interval and the purifier.

Initially, in the quench phase, the QES in the gravitating region simply sits at the bifurcation surface of the original eternal black hole geometry,

$$x_{\mathrm{QES}}^{\pm} = \pm\frac{1}{\pi T_0}\,. \tag{3.44}$$

The corresponding generalized entropy is obtained by summing the Bekenstein-Hawking entropy

$$S_{\mathrm{BH}}(T_0) = \frac{c(\phi_0 + 2\pi T_0\phi_r)}{12k\phi_r} \tag{3.45}$$

and the von Neumann entropy (3.41) evaluated holographically with endpoints $x_1^{\pm}$ and $x_{\mathrm{QES}}^{\pm}$, which picks out the $\eta < \eta^* = 1/2$ channel:

$$S_{\mathrm{gen}} = S_{\mathrm{BH}}(T_0) + S_{1\mathrm{pt}}(\mathrm{AdS}) + S_{1\mathrm{pt}}(x_1^{\pm})\,, \tag{3.46}$$

with $S_{1\mathrm{pt}}(\mathrm{AdS})$ and $S_{1\mathrm{pt}}(x_1^{\pm})$ given by eq. (3.32). Note that, in the $\eta < \eta^*$ channel, the von Neumann entropy (3.41) (and more generally eq. (3.37)) has no dependence on $x_2^{\pm}$; this justifies a posteriori choosing the QES to simply be the classical one at the bifurcation point. This was also the case in the zero-temperature bath case in chapter 2.

Transitioning to the scrambling phase, the QES jumps from the bifurcation point to another saddle of generalized entropy, which is still located before the shock but now with $\eta > \eta^* = 1/2$. Since the $x_2^{\pm}$ dependence of eq. (3.41) (and more generally eq. (3.37)) in this channel is also identical to the zero temperature case in chapter 2, we obtain the same QES:

$$x_{\mathrm{QES}}^{+} = \frac{1}{\pi T_0}\left[1 - \frac{k}{\pi T_0} + O\left(\frac{k^2}{T_0^2}\right)\right] \tag{3.47}$$

$$x_{\mathrm{QES}}^{-} = \frac{1}{\pi T_0}\left[-1 + \frac{k}{\pi T_0}\frac{1+\pi T_0 x_1^{+}}{1-\pi T_0 x_1^{+}} + O\left(\frac{k^2}{T_0^2}\right)\right]. \tag{3.48}$$

Evaluating eq. (3.41) for this QES, one finds

$$S_{\text{gen}} - S_{\text{BH}}(T_0) \sim \frac{c}{6} \log \left\{ \frac{12 E_S}{c\epsilon T_0} \frac{x_1^-(1-\pi T_0 x_1^+)}{\sqrt{[1-(\pi T_1 x_1^+)^2][1-(\pi T_1 x_1^-)^2]}} \right\}. \tag{3.49}$$

Comparing eq. (3.49) with the $\eta < \eta^*$ channel of eq. (3.41), we find that the quench-to-scrambling transition occurs at the same point as in the zero-temperature bath case:

$$x_1^+ \sim \frac{1}{3\pi T_0}. \tag{3.50}$$

Note that this is essentially the instant at which the bifurcation point (3.44) reaches $\eta = \eta^* = 1/2$. At later times, eq. (3.49) exhibits a growth linear in the physical time $u = \frac{y_1^+ + y_1^-}{2}$:

$$S_{\text{gen}} - S_{\text{BH}}(T_0) \sim \frac{c}{6} \left\{ \log \left[\frac{3E_S(T_1 - T_0)}{c\epsilon \pi T_0 T_1^2} \right] + 2\pi T_1 u \right\} \tag{3.51}$$

with

$$x_1^\pm = \frac{1}{\pi T_1} \left[1 + O\left(\frac{k}{T_1} \right) \right]. \tag{3.52}$$

We note that this growth has a rate double that of the zero-temperature bath case. Physically, this can be explained by the fact that, in addition to absorbing radiation from the AdS black hole, the semi-infinite interval of the bath is also sending radiation into the black hole which itself (and the purifier of the bath) purifies.

Finally, there is a transition to the late-time phase, with the QES jumping to a saddle point after the shock in AdS. As noted around eq. (3.43), the relevant post-shock two-point entropy formula is the same as if the black hole and bath were eternally coupled. Since the after-shock AdS geometry is also the same as for an eternal black hole, the late-time generalized entropy is identical to the eternally coupled case studied in [62]. This matching with the eternally-coupled case suggests that, by the Page time, the black hole and bath have reached equilibrium.

As in the eternally-coupled case, time translation invariance (in u) simplifies the determination of the QES. In particular, the QES must be on the same time-slice as $\frac{y_1^+ + y_1^-}{2} = u_1$:

$$u_{\text{QES}} = u_1. \tag{3.53}$$

Hence, it remains only to determine the spatial location of the QES. Substituting eq. (3.53) into the entropy formula (3.43) with $y_1^\pm = u \mp \sigma_1$ gives

$$S_{\text{gen}} = \frac{c}{12k} \left[\frac{\phi_0}{\phi_r} - 2\pi T_1 \coth(2\pi T_1 \sigma_{\text{QES}}) \right] + \frac{c}{6} \log \left[\frac{2\sinh^2[\pi T_1(\sigma_1 - \sigma_{\text{QES}})]}{\pi T_1 \epsilon \sinh(-2\pi T_1 \sigma_{\text{QES}})} \right], \tag{3.54}$$

in agreement with eq. (19) in [62]. By setting the σ_{QES}-derivative of eq. (3.54) to zero, we find

$$-\sigma_{\text{QES}} = \sigma_1 + \frac{1}{2\pi T_1}\log\left(\frac{2\pi T_1}{k}\right) + \frac{1}{T_1}O\left(\frac{k}{T_1}\right), \tag{3.55}$$

reproducing eq. (21) in [62]. Hence the QES sits outside of the black hole horizon.

As an aside, time translation invariance permits a natural measure of proper distance between the QES and the horizon along a constant time slice. Using eq. (3.55), we have in units of L_{AdS}:

$$\int_{\frac{\tanh(-\pi T_1\sigma_{\text{QES}})}{\pi T_1}}^{\frac{1}{\pi T_1}} \frac{ds}{s} = \frac{ke^{-2\pi T_1\sigma_1}}{\pi T_1} + O\left[\left(\frac{k}{T_1}\right)^2\right], \tag{3.56}$$

from which we see that the QES is an order k/T_1 proper distance outside the horizon.[11]

Using the location of the QES given by eqs. (3.53) and (3.55), we can evaluate the generalized entropy of the late time phase. Again, by similarity to the eternally coupled case, this is a constant:

$$S_{\text{gen}}(T_1, \sigma_1) \sim S_{\text{BH}}(T_1) + \frac{c}{6}\left[\log\left(\frac{1}{\pi T_1\epsilon}\right) + 2\pi T_1\sigma_1\right], \tag{3.57}$$

Interestingly, the above von Neumann part of the generalized entropy matches the entropy obtained from placing a twist operator at a large separation σ_1 from the boundary of a thermal half-line (see eq. (3.33)) plus $S_{\text{1pt}}(\text{AdS})$. Comparing with the generalized entropy given by eq. (3.51) for the scrambling phase, we see that the transition between the scrambling and late time phases occurs when y_1^+ reaches a Page time of

$$y^+_{\text{Page}} \approx \frac{1}{2k}\left(1 - \frac{T_0}{T_1}\right) - \frac{1}{2\pi T_1}\log\left[\frac{3E_S(T_1 - T_0)}{cT_0T_1}\right]. \tag{3.58}$$

For later use, we note that more exact formulas may be obtained in the late time phase in the simple case where $x_1^\pm$ is placed on the boundary of AdS_2, *i.e.,* we consider the entanglement wedge of QM_{L} plus the entire bath and its purifier. As in chapter 2, we can ignore the correction from the position of the cut-off surface and set $x_1^+ = x_1^- = t =$

[11] By measuring the distance (3.56) between the QES and the horizon along a constant Killing time slice, we have implicitly extended the after-shock geometry to before the shock. The bifurcation surface of the final stationary black hole does not actually exist in the physical spacetime.

$f(u) = \frac{1}{\pi T_1} \tanh(\pi T_1 u)$. With this simplification, one can exactly solve, in $x^{\pm}$ coordinates, the equations

$$\begin{aligned} k\left(x^+ - x^-\right)^2 \left(\frac{1}{x^+ - x_1^+} - \frac{1}{x^+ - x^-}\right) &= 1 - \left(\pi T_1 x^-\right)^2, \\ k\left(x^+ - x^-\right)^2 \left(\frac{1}{x^+ - x^-} - \frac{1}{x_1^- - x^-}\right) &= \left(\pi T_1 x^+\right)^2 - 1, \end{aligned} \tag{3.59}$$

obtained from minimization of the late-time generalized entropy. These admit two trivial solutions $x^{\pm}_{\rm QES} = \pm\frac{1}{\pi T_1}$ and two non-trivial ones. Because of the constraints $x^+_{\rm QES} > x^-_{\rm QES} > 0$, the only relevant solution for the position of QES reads

$$\begin{aligned} x^+_{\rm QES}(t) &= \frac{\sqrt{k^2 + \pi^2 T_1^2}\left((\pi T_1 t)^2 - 1\right) + k\left((\pi T_1 t)^2 + 1\right)}{\pi^2 T_1^2\left(\pi^2 T_1^2 t^2 + 2kt - 1\right)}, \\ x^-_{\rm QES}(t) &= \frac{\sqrt{k^2 + \pi^2 T_1^2}\left((\pi T_1 t)^2 - 1\right) + k\left((\pi T_1 t)^2 + 1\right)}{\pi^2 T_1^2\left(-\pi^2 T_1^2 t^2 + 2kt + 1\right)}. \end{aligned} \tag{3.60}$$

As a consistency check, we can use the time map $t = \frac{1}{\pi T_1}\tanh(\pi T_1 u)$ and find our solution (3.60) for QES satisfies eq. (3.53):

$$\frac{1}{2}\left(y^+_{\rm QES} + y^-_{\rm QES}\right) \equiv \frac{1}{2\pi T_1}\operatorname{arctanh}\left(\pi T_1 x^+_{\rm QES}\right) + \frac{1}{2\pi T_1}\operatorname{arctanh}\left(\pi T_1 x^-_{\rm QES}\right) = u\,. \tag{3.61}$$

Noting that the above solution of QES is not always physical, we need to impose the restrictions on parameters k, t as

$$\begin{aligned} \pi^2 T_1^2 t^2 + 2kt - 1 &> 0\,, \\ \sqrt{k^2 + \pi^2 T_1^2}\left((\pi T_1 t)^2 - 1\right) + k\left((\pi T_1 t)^2 + 1\right) &> 0\,, \end{aligned} \tag{3.62}$$

which implies t is very close to t_∞, *i.e.,* late time phase.[12] Moreover, it is straightforward to show $x^{\pm}_{\rm QES}(t_\infty) = t_\infty = \frac{1}{\pi T_1}$ and the simple monotonic behavior due to the fact

$$\frac{dx^+_{\rm QES}(t)}{dt} = \frac{2k}{\pi^2 T_1^2 t\left(t\sqrt{k^2 + \pi^2 T_1^2} + 2\right) + \sqrt{k^2 + \pi^2 T_1^2} + k(1 - t^2\pi^2 T_1^2)} > 0\,, \tag{3.63}$$

[12] This is why the small k expansion does not work for $x^-_{\rm QES}$ at late time phase because we have another much smaller value $(1 - \pi T_1 t)$ except for k. For example, $1 - \tanh(\pi T_1 u)|_{\pi T_1 u = 10} \approx 4 \times 10^{-35}$ does not depend on k and is much smaller than k at late time phase.

from which we verify that the QES is located outside the horizon, as described around eq. (3.56). (Note that any apparent spatial motion of the QES is purely an artifact of the choice of coordinates here – due to time translation invariance in u, the QES is spatially stationary in $\sigma = \frac{y^- - y^+}{2}$, as indicated in eq. (3.55).) So this is the first difference with the case under zero temperature bath where the QES is located inside the horizon. With the exact solution, one can obtain the generalized entropy

$$S_{\text{gen,late}}(T_1) = \frac{\bar{\phi}}{2G_{\text{N}}}\left(\sqrt{k^2+\pi^2T_1^2} - k\log\left[\epsilon\left(k+\sqrt{k^2+\pi^2T_1^2}\right)\right]\right), \tag{3.64}$$

where the first term is the thermal entropy of a one-sided black hole with temperature T_1 and the second term describes the von Neumann entropy of bulk matter with the same temperature. It is obvious that the above generalized entropy is exactly constant, indicating this is a thermal equilibrium state.

3.2.2 Finite interval of the bath

In this section, we consider the question of whether the interior of the black hole can be recovered by a finite-sized interval in the bath, together with QM_{L} and the bath's purifier. We shall write the endpoints of the finite bath interval as $y_1^{\pm} = u \mp \sigma_1$ and $y_2^{\pm} = u \mp \sigma_2$ where $\sigma_1, \sigma_2 \geq -\epsilon$.

To begin, we consider the case where we have access to the entire purifier for the thermal bath — this is illustrated in Figure 3.3a. (In Section 3.2.3, we shall see that the purifier is crucial for recovering the black hole interior.) To stand a chance of recovering the black hole interior, we take $y_1^+ \geq y_{\text{Page}}^+$, with y_{Page}^+ given in eq. (3.58). We also take $y_2^{\pm}$ to be in the bath to the future of the shock, as we will see that this is sufficient to recover the black hole interior.

The two competing channels of generalized entropy in the holographic limit, corresponding to recoverability and non-recoverability of the black hole interior, are[13]

$$S_{\text{R}} = S^{\text{gen}}_{\text{QES}-1} + S_{2-\text{IR}}, \qquad S_{\text{N}} = S^{\text{gen}}_{\text{QES}''} + S_{1-2} + S_{\frac{1}{2}\text{-line}}, \tag{3.65}$$

where S_i^{gen}, S_i denote generalized and von Neumann entropies calculated with a single twist operator at $x_i^{\pm}$, while S_{i-j}^{gen}, S_{i-j} denote generalized and von Neumann entropies

[13]There is in fact another channel where the black hole interior is recoverable, $S^{\text{gen}}_{\text{QES}-1} + S_2 + S_{\frac{1}{2}\text{-line}}$, but comparison of this with S_{N} in eq. (3.65) reduces to a problem where the purifier of the bath has been traced out — we deal with this case later in this section.

of the interval with endpoints $x_i^{\pm}, x_j^{\pm}$. Further, subscripts QES, QES$''$ and IR denote the late-time QES associated to $y_1^{\pm}$, the (original) bifurcation point, and the IR point at $\sigma = \frac{y^- - y^+}{2} = \sigma_{\text{IR}}$, respectively. Recall that the entropy $S_{\frac{1}{2}\text{-line}}$ of the thermal half-line is given in eq. (3.33). The entropy $S_{2-\text{IR}}$, like $S_{\frac{1}{2}\text{-line}}$, is IR divergent as $\sigma_{\text{IR}} \to \infty$; below, these divergences cancel in the differences of the entropies in the distinct channels.

To determine whether the black hole interior is recoverable, we ask whether $S_{\text{R}} < S_{\text{N}}$, or equivalently,

$$\begin{aligned} 0 &> S_{\text{R}} - S_{\text{N}} \\ &\approx \frac{c}{6}\Bigg\{ \frac{\pi(T_1 - T_0)}{k} + 2\pi T_1 \sigma_1 \\ &\quad + \log\left[\frac{3E_S}{c\pi T_1^2} \frac{x_2^+(1-\pi T_1 x_2^-)\sqrt{[1-(\pi T_1 x_1^+)^2][1-(\pi T_1 x_1^-)^2]}}{(x_2^- - x_1^-)(x_1^+ - x_2^+)} \right] \Bigg\}, \end{aligned} \tag{3.66}$$

where we have used eq. (3.57) to approximate $S^{\text{gen}}_{\text{QES}-1}$, eq. (3.46) for the one-point generalized entropy at the bifurcation point, and eq. (3.33) for the entropy of the thermal half-line. The remaining entropies were obtained from the appropriate cases in eqs. (3.42) and (3.41). (Recall we are taking here $y_2^{\pm}$ to the future of the shock.) Since we have $y_1^{\pm}, y_2^- \gg \frac{1}{\pi T_1}$, we may use the following approximations,

$$x_1^{\pm} \approx \frac{1}{\pi T_1}\left(1 - 2e^{-2\pi T_1 y_1^{\pm}}\right), \qquad x_2^- \approx \frac{1}{\pi T_1}\left(1 - 2e^{-2\pi T_1 y_2^-}\right). \tag{3.67}$$

In this limit of large $y_1^{\pm}, y_2^- \gg \frac{1}{\pi T_1}$, the RHS of eq. (3.66) becomes

$$S_{\text{R}} - S_{\text{N}} \approx \frac{c}{6}\left\{ \frac{\pi(T_1 - T_0)}{k} - 4\pi T_1 \sigma_2 + \log\left[\frac{6E_S}{cT_1} \frac{1}{(e^{-2\pi T_1 \sigma_1} - e^{-2\pi T_1 \sigma_2})^2} \right] \right\}. \tag{3.68}$$

Hence, the recoverability of the black hole interior is equivalent to $\sigma_2 - \sigma_1 > \Delta_{\text{turn}}$, where

$$\Delta_{\text{turn}} \approx \frac{1}{4\pi T_1}\left[\frac{\pi(T_1 - T_0)}{k} + \log\left(\frac{6E_S}{cT_1} \right) \right]. \tag{3.69}$$

Comparing terms in eqs. (3.58) and (3.69) leading order in k, note that $\Delta_{\text{turn}} \approx y^+_{\text{Page}}/2$.

3.2.3 Importance of the bath's purifier

As hinted earlier, the purifier of the bath is crucial to the reconstruction of the black hole interior. Let us briefly attempt a similar calculation to the above, now additionally tracing

out this purifier. The generalized entropy for $\mathrm{QM_L}$ and an interval of the bath from $y_1^\pm$ to $y_2^\pm$ then has the competing channels – see figure 3.3

$$S_{\mathrm{R}} = S^{\mathrm{gen}}_{\mathrm{QES}-1} + S_2, \qquad\qquad S_{\mathrm{N}} = S^{\mathrm{gen}}_{\mathrm{QES}''} + S_{1-2}, \tag{3.70}$$

as illustrated in Figure 3.3c. Recall that the R-channel corresponds to the channel in which the interior of the black hole is recoverable, while in the N-channel the interior is non-recoverable. Now, we take $y_2^\pm$ to the past of the shock, since we shall momentarily show that, even as the interval is extended by taking $\sigma_2 = \frac{y_2^- - y_2^+}{2}$ arbitrarily large, the N-channel with entropy S_{N} will nonetheless remain favorable.[14] Using the formulas (3.57) for $S^{\mathrm{gen}}_{\mathrm{QES}-1}$, (3.46) for $S^{\mathrm{gen}}_{\mathrm{QES}''}$, (3.32) for S_2, and (3.34) for S_{1-2}, we have

$$S_{\mathrm{R}} - S_{\mathrm{N}} \approx \frac{c}{6}\Bigg\{\frac{\pi(T_1 - T_0)}{k} + 2\pi T_1\sigma_1 + \log\left[\frac{c}{24\pi^2 T_1 E_S}\frac{(x_2^+ - x_2^-)\sqrt{[1-(\pi T_1 x_1^+)^2][1-(\pi T_1 x_1^-)^2]}}{x_1^+ x_2^+ (x_2^- - x_1^-)}\right]\Bigg\}. \tag{3.71}$$

Using again the $y_1^\pm, y_2^- \gg \frac{1}{\pi T_1}$ approximations (3.67), we find

$$S_{\mathrm{R}} - S_{\mathrm{N}} \approx \frac{c}{6}\Bigg\{\frac{\pi(T_1 - T_0)}{k} + 2\pi T_1\sigma_1 + \log\left(\frac{cT_1}{12\pi E_S}\right) + \log\left[\frac{x_2^+ - x_2^-}{T_1 x_1^+ x_2^+ (e^{-2\pi T_1\sigma_1} - e^{-2\pi T_1\sigma_2})}\right]\Bigg\}. \tag{3.72}$$

On the RHS, the first three terms sum to a large positive number (note that the third term, though negative, scales like the logarithm of the first term). Moreover, the logarithm of the last term is bounded from below by $\log\pi$. It follows that $S_{\mathrm{R}} > S_{\mathrm{N}}$. We thus conclude that when the purifier of the bath is traced out, no matter how large an interval of the bath one has access to, the N-channel is favorable and the black hole interior cannot be recovered.

[14] If one attempts a similar exercise with $y_2^\pm$ after the shock, then naively one finds with our entropy formulas that when this endpoint is placed at $O(c/E_S)$ away from the shock, it is possible for $S^{\mathrm{gen}}_{\mathrm{rec}} < S^{\mathrm{gen}}_{\text{non-rec}}$. However, this is an artifact of the fact that our setup is incapable of probing distances of such small scales. Since extending the interval of the bath can only increase the entanglement wedge, the argument presented in the main text precludes the possibility of the black hole interior being recovered from shorter intervals which stop to the future of the shock.

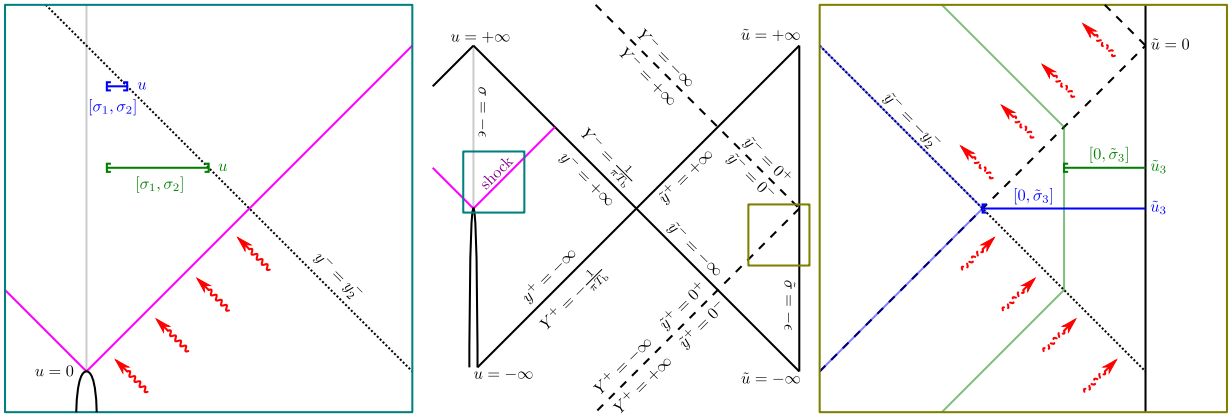

Figure 3.4: The bath and purifier subsystems. The central panel shows a Penrose diagram of various coordinate patches of the bath and purifier subsystems. The left panel shows two examples, sharing the same y_2^-, of an interval $[\sigma_1, \sigma_2]$ of the bath system after the Page time: the shorter blue interval is just barely above the critical length Δ_{turn} needed to recover the black hole interior; the green interval is much longer. Red wavy lines show thermal radiation leaving the bath prior to $y^- = y_2^-$. The right panel shows the corresponding intervals $[0, \tilde{\sigma}_3]$ needed in conjunction with the bath intervals (plus QM_{L}) to recover the black hole interior. The phase boundaries of $\tilde{\sigma}_3$ for recoverability is shown in light blue and green. The dashed wavy lines show the thermal quanta of the purifier that are most entangled with the radiation marked in the left panel.

A natural follow-up question is whether the black hole interior can be recovered when one can only access a finite portion of the bath's purifier at various times. We shall take the joint system of the bath and its purifier to be in a thermofield double state. Furthermore, we introduce a new set of coordinates $\tilde{y}^{\pm} = \tilde{u} \pm \tilde{\sigma}$ for the purifier of the bath, where $\tilde{u}$ and $\tilde{\sigma}$ are analogous to the u and σ coordinates of the bath. These coordinates for the purifier are related to the coordinates we have been using thus far by

$$Y^{\pm} = -\frac{1}{\pi T_1} \coth(\pi T_1 \tilde{y}^{\pm}). \tag{3.73}$$

Note that while $\pi T_1 Y^{\pm} \in (-1, 1)$ provides a coordinate chart that includes the bath, the coordinate chart of $(\pi T_1 Y^{\pm})^{-1} \in (-1, 1)$ includes the purifier of the bath. Moreover, we have

$$\pi T_1 \tilde{y} = -\pi T_1 y + \frac{i\pi}{2}, \qquad\qquad d\tilde{y}^+ d\tilde{y}^- = dy^+ dy^- \tag{3.74}$$

so that there is no additional Weyl transformation that must be applied to our entropy formulas when endpoints are moved from the bath to its purifier. (Specifically, in eqs. (3.40), (3.42), and (3.41), end-points in the purifier of the bath should be treated as though they were simply in the bath and to the past of the shock.) The coverage of the $Y, y, \tilde{y}$ coordinates in the bath and purifier subsystems are summarized in the middle panel of Figure 3.4.

We may then repeat the analysis of Section 3.2.2, now pushing the IR endpoint to a point $\tilde{y}_3^{\pm}$ in the bath's purifier. That is, we consider whether the black hole interior can be recovered from QM_{L}, an interval of the bath with endpoints $y_1^{\pm} = u \mp \sigma_1$ and $y_2^{\pm} = u \mp \sigma_2$, and an interval of the bath's purifier stretching from an endpoint $\tilde{y}_3^{\pm} = \tilde{u}_3 \pm \tilde{\sigma}_3$ to the boundary $\tilde{\sigma} = 0$ — see figure 3.4. In general, we shall find that the size of the purifier interval required to recover the black hole interior will depend on the time $\tilde{u}_3$ at which the interval is selected.

From Sections 3.2.1 and 3.2.2, we see that, to have a chance of recovering the black hole interior, we should take $y_1^+ > y_{\mathrm{Page}}^+$ and $\sigma_2 - \sigma_1 > \Delta_{\mathrm{turn}}$ with y_{Page}^+ and Δ_{turn} given in eqs. (3.58) and (3.69). For simplicity, we take $y_2^{\pm}$ to the future of the shock. The relevant generalized entropies for the R- and N-channels are,

$$S_{\mathrm{R}} = S^{\mathrm{gen}}_{\mathrm{QES}-1} + S_{2-3}\,, \qquad\qquad S_{\mathrm{N}} = S^{\mathrm{gen}}_{\mathrm{QES}''} + S_{1-2} + S_3\,, \tag{3.75}$$

as illustrated in Figure 3.3d. Relating to the problem treated in Section 3.2.2, where $\tilde{y}_3^{\pm}$ is pushed to the IR, in comparing S_{R} and S_{N}, we have the extra contribution

$$S_{\mathrm{R}} - S_{\mathrm{N}} - [S_{\mathrm{R}} - S_{\mathrm{N}}]_{\tilde{\sigma}_3 \to +\infty} = \frac{c}{6} \log\left[\frac{2\pi T_1 x_3^+ (-x_2^- + x_3^-)}{(1 - \pi T_1 x_2^-)(x_3^+ - x_3^-)}\right]. \tag{3.76}$$

From eq. (3.68), we see that

$$[S_{\rm R} - S_{\rm N}]_{\tilde{\sigma}_3 \to +\infty} \approx -\frac{2\pi c T_1}{3}(\sigma_2 - \sigma_1 - \Delta_{\rm turn}). \tag{3.77}$$

Applying the approximation (3.67) for x_2^-, we find that the condition $S_{\rm R} \leq S_{\rm N}$ for the recoverability of the black hole interior translates to

$$\pi T_1 - (x_3^-)^{-1} \lesssim \frac{\pi T_1 \left[1 - 2e^{-4\pi T_1(\sigma_2 - \sigma_1 - \Delta_{\rm turn})}\right] - (x_3^+)^{-1}}{e^{2\pi T_1(u - \sigma_2 + 2\sigma_1 + 2\Delta_{\rm turn})}}. \tag{3.78}$$

The RHS, giving the maximal separation of $(x_3^-)^{-1}$ from past null infinity line $(x^-)^{-1} = \pi T_1$ of the bath's purifier, is largest when $(x_3^+)^{-1}$ sits on the future null infinity line $(x^+)^{-1} = -\pi T_1$. Here,

$$\pi T_1 - (x_3^-)^{-1}\big|_{(x_3^+)^{-1} = -\pi T_1} \lesssim \frac{2\pi T_1 \left[1 - e^{-4\pi T_1(\sigma_2 - \sigma_1 - \Delta_{\rm turn})}\right]}{e^{2\pi T_1(u - \sigma_2 + 2\sigma_1 + 2\Delta_{\rm turn})}}. \tag{3.79}$$

We see that even this is exponentially suppressed (note $u - \sigma_2 + 2\sigma_1 + 2\Delta_{\rm turn} \geq 2\Delta_{\rm turn}$ with $\Delta_{\rm turn}$ given in eq. (3.69)). In contrast, with appropriate $\sigma_2 - \sigma_1 > \Delta_{\rm turn}$, $(x_3^+)^{-1}$ can be pushed far from the future null infinity value $-\pi T_1$; the largest separation is achieved when $(x_3^-)^{-1}$ sits on past null infinity:

$$\pi T_1 + (x_3^+)^{-1}\big|_{(x_3^-)^{-1} = \pi T_1} \lesssim 2\pi T_1 \left[1 - e^{-4\pi T_1(\sigma_2 - \sigma_1 - \Delta_{\rm turn})}\right]. \tag{3.80}$$

It is also instructive to consider the condition (3.78) in terms of the spatial interval length $\tilde{\sigma}_3$ taken in the purifier. As we elaborate below, due to the step-like nature of the tanh function in f, the constraint (3.78) becomes a piece-wise linear constraint on $\tilde{\sigma}_3$ as a function of $\tilde{u}_3$ with interpolation between the pieces on scales of order πT_1^{-1}.

Let us consider first the case $\sigma_2 - \sigma_1 - \Delta_{\rm turn} \ll (4\pi T_1)^{-1}$. Then, both eqs. (3.79) and (3.80) are small so that we are in the regime

$$\pi T_1 - (x_3^-)^{-1} \approx 2\pi T_1 e^{2\pi T_1 \tilde{y}_3^-}, \qquad \left(\tilde{y}_3^- \ll -\frac{1}{2\pi T_1}\right), \tag{3.81}$$

$$\pi T_1 + (x_3^+)^{-1} \approx 2\pi T_1 e^{-2\pi T_1 \tilde{y}_3^+}, \qquad \left(\tilde{y}_3^+ \gg \frac{1}{2\pi T_1}\right). \tag{3.82}$$

Note that the bounds given by the RHS's of eqs. (3.79) and (3.80) are complementary in the following sense: if $\pi T_1 - (x_3^-)^{-1}$ is much smaller than the RHS of eq. (3.79), then

eq. (3.78) reduces to the constraint that $\pi T_1 + (x_3^+)^{-1}$ is less than approximately the RHS of eq. (3.80); on the other hand, if $\pi T_1 + (x_3^+)^{-1}$ is much smaller than the RHS of eq. (3.80), then eq. (3.78) reduces to $\pi T_1 - x_3^-$ being smaller than approximately the RHS of eq. (3.79). Considering eqs. (3.81) and (3.82), the interpolation between these two cases occurs on scales of order $(\pi T_1)^{-1}$ in $\tilde{y}_3^\pm$. We thus find a piecewise null phase boundary for $\tilde{y}_3^\pm$:

$$\tilde{\sigma}_3 \gtrsim -\frac{1}{2\pi T_1}\log[4\pi T_1(\sigma_2-\sigma_1-\Delta_{\text{turn}})] + \begin{cases} -\tilde{u}_3 & \text{if } \tilde{u}_3 \lesssim -\frac{y_2^-}{2} \\ \tilde{u}_3 + y_2^- & \text{if } \tilde{u}_3 \gtrsim -\frac{y_2^-}{2} \end{cases}, \tag{3.83}$$

with interpolation between the pieces occurring on scales of order $(\pi T_1)^{-1}$ in $\tilde{u}_3$. We see that as $\sigma_2 - \sigma_1$ approaches the minimum interval length Δ_{turn} of the bath required for recovery of the black hole interior, $\tilde{\sigma}_3$ diverges logarithmically.

Next, we consider the case where $\sigma_2 - \sigma_1 - \Delta_{\text{turn}} \gg (4\pi T_1)^{-1}$. Now, the RHS of eq. (3.80) need not be small, opening the possibility for a new regime where

$$\pi T_1 - (x_3^+)^{-1} \approx 2\pi T_1 e^{2\pi T_1 \tilde{y}_3^+} \qquad \left(\tilde{y}_3^+ \ll -\frac{1}{2\pi T_1}\right) \tag{3.84}$$

but

$$-\tilde{y}_3^+ \lesssim \sigma_2 - \sigma_1 - \Delta_{\text{turn}} \tag{3.85}$$

so that the bound (3.80) is not yet saturated. Inserting eq. (3.84) into eq. (3.78), we obtain the phase boundary in an intermediate regime between eqs. (3.79) and (3.80). This phase boundary, at the conclusion of this intermediate regime, *i.e.,* when eq. (3.85) is saturated, ends deep in the region where eq. (3.84) holds. Finally, plugging eq. (3.84) into eq. (3.80), we obtain a phase boundary in the complement of eq. (3.85). Altogether, we find

$$\tilde{\sigma}_3 \gtrsim \begin{cases} -\tilde{u}_3 - 2(\sigma_2-\sigma_1-\Delta_{\text{turn}}) & \text{if } \tilde{u}_3 + \frac{y_2^-}{2} < -(\sigma_2-\sigma_1-\Delta_{\text{turn}}) \\ \frac{y_2^-}{2} - (\sigma_2-\sigma_1-\Delta_{\text{turn}}) & \text{if } \left|\tilde{u}_3 + \frac{y_2^-}{2}\right| < \sigma_2-\sigma_1-\Delta_{\text{turn}} \\ \tilde{u}_3 + y_2^- - 2(\sigma_2-\sigma_1-\Delta_{\text{turn}}) & \text{if } \tilde{u}_3 + \frac{y_2^-}{2} > \sigma_2-\sigma_1-\Delta_{\text{turn}} \end{cases}, \tag{3.86}$$

with interpolation on the thermal scale.[15] We see that the intermediate case gives the smallest possible region of the purifier needed for reconstruction of the black hole interior.

[15] Eq. (3.86) can be condensed into

$$2\tilde{\sigma}_3 \gtrsim |\tilde{y}_3^+| + |y_2^- + \tilde{y}_3^-| + y_2^- - 4\,(\sigma_2 - \sigma_2 - \Delta_{\text{turn}})\,, \tag{3.87}$$

which is similar to the general T_{b} result in eq. (3.211) with $\delta\sigma_2 \to \sigma_2 - \sigma_1 - \Delta_{\text{turn}}$ and $T_{\text{b}} = T_{\text{eff}} = T_1$. As noted around eq. (3.211), the assumptions leading to the general result are more constraining.

For the blue and green bath intervals illustrated in the left panel of figure 3.4, the approximate phase boundary (3.86) is highlighted respectively in light blue and light green in the right panel of figure 3.4 and examples of minimal-length purifier intervals are shown in opaque blue and green. The blue case illustrates the phase boundary given by eq. (3.86) for a bath interval just large enough for eq. (3.86) to be valid (as opposed to eq. (3.83)) — in this limit, the intermediate piece of eq. (3.86) vanishes. The green case, on the other hand, has a much larger bath interval. As illustrated in Figure 3.4, eq. (3.86) has the interpretation of giving the interval of the purifier needed to capture quanta entangled with out-going thermal bath radiation emitted between times $y^- = 0$ and $y^- = y_2^-$. When the bath interval length $\sigma_2 - \sigma_1$ is barely a few thermal lengths greater than the critical value Δ_{turn} (blue case), nearly all of these quanta must be accessible in the purifier. For much longer bath intervals (green case), fewer purifier quanta are necessary. We shall comment further on this in Section 3.4.

3.3 Non equilibrium T_b

In the previous section, we analyzed the two-dimensional black hole coupled to a bath system with temperature $T_{\text{b}} = T_1$, which together formed a system in thermal equilibrium as soon as the Page time was reached. Compared to the results from the evaporating black hole with zero temperature in chapter 2, we found qualitatively different behavior in the evolution of the generalized entropy – and, of course, the role of purification of the bath. In this section, we consider coupling the black hole with temperature T_1 after the shock is absorbed into a thermal bath with a general temperature T_{b}. The black hole and bath evolve to reach an equilibrium where the black hole temperature matches T_{b}. However, the black hole will decrease or increase in size (and entropy) depending on whether $T_{\text{b}} < T_1$ or $T_{\text{b}} > T_1$. The evolution of the (effective) black hole temperature is shown in figure 3.5 for several cases.

As was explained in section 3.1.3, the Schwarzian equation (3.28) can be solved for arbitrary bath temperature to find the time-map function $f(u)$ in eq. (3.29) which reduces to the $T_{\text{b}} = 0$ result of chapter 2 by taking $\nu = 0$.[16] Taking the limit $ku \to \infty$, one can

[16] We note that for numerical purposes, the following form of the time-map function

$$f(u, T_b) = \frac{2}{k} \frac{I_\nu(a)\, K_\nu(ae^{-\frac{ku}{2}}) - K_\nu(a)\, I_\nu(ae^{-\frac{ku}{2}})}{I_\nu(ae^{-\frac{ku}{2}})\,(aK_{\nu-1}(a) + \nu K_\nu(a)) + K_\nu(ae^{-\frac{ku}{2}})\,(aI_{\nu-1}(a) - \nu I_\nu(a))}\,, \tag{3.88}$$

is easier to deal with than the expression in eq. (3.29). Note that similar expressions appear in [70].

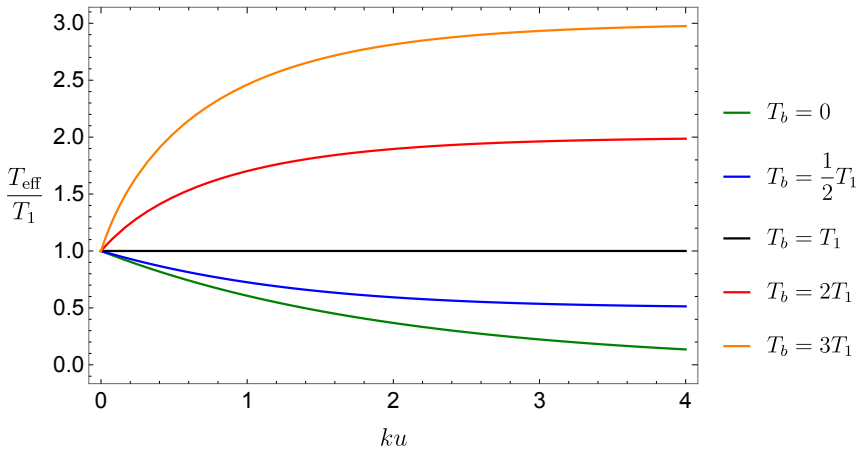

Figure 3.5: The time dependence of effective temperature of black hole, which simply parametrizes the dynamical behavior of black hole.

also define the end of the proper time

$$t_\infty = \frac{2}{k}\frac{I_\nu(a)}{aI_{\nu-1}(a) - \nu I_\nu(a)} = \frac{2}{ka}\frac{I_\nu(a)}{I'_\nu(a)}\,, \tag{3.89}$$

which is also the final position of the QES, *i.e.*, $x^{\pm}_{\rm QES}|_{u\to\infty} = t_\infty$. We now stress some important facts about the above map function from coordinate time t to proper (physical) time u. First, the function $f(u, T_{\rm b})$ is well defined and real for $T_{\rm b} \leq T_1$ and also $T_{\rm b} \geq T_1$. Secondly, it is also invariant under the following rescaling

$$T_1 \to \alpha T_1\,, \quad T_{\rm b} \to \alpha T_{\rm b}\,, \quad k \to \alpha k\,, \quad u \to \frac{u}{\alpha}\,, \quad \frac{\bar{\phi}_r}{G_{\rm N}} \to \frac{\bar{\phi}_r}{\alpha^2 G_{\rm N}}\,. \tag{3.90}$$

In other words, the independent dimensionless parameters in the model are

$$T_1 L_{\rm AdS}\,, \quad \frac{T_{\rm b}}{T_1}\,, \quad ku\,, \quad \frac{k}{T_1}\,, \tag{3.91}$$

besides of $\frac{\phi_r}{G_{\rm N}}$. We simply take the radius of AdS as the standard scale by choosing $L_{\rm AdS} = 1$ and all other parameters can be considered to be normalized by T_1. From an energetic point of view, it is clear that $T_{\rm b} = T_1$ is a critical temperature for the thermal bath, where the black hole will neither lose nor absorb energy. From the energy flow equation (3.27) and Schwarzian equation (3.28), we can define an effective temperature

$$T_{\rm eff}(u; T_{\rm b}) = \sqrt{T_{\rm b}^2 + (T_1^2 - T_{\rm b}^2)\, e^{-ku}}\,, \tag{3.92}$$

which parametrizes the ADM mass of the dynamical black hole at time u by

$$E(u) = \frac{\bar{\phi}_r \pi}{4G_{\rm N}} T_{\rm eff}^2(u)\,. \tag{3.93}$$

Recalling the energy flux (3.24) on the physical boundary $x^- \approx t$, *i.e.,*

$$\langle T_{x^-x^-}\rangle = E_S\,\delta(t) + \frac{c\pi}{12}\frac{1}{(f'(u))^2}\left(T_{\rm b}^2 - T_{\rm eff}^2(u)\right)\,, \tag{3.94}$$

we can explain the above three terms as the contributions from the shock wave, thermal radiation from the coupled bath system at temperature $T_{\rm b}$, and Hawking radiation escaped from the dynamical black hole. As expected, we can also understand the effective temperature as the measure for the temperature of Hawking radiation at time u. For later use, we also show the numerical plot for the time evolution of effective temperature with various $T_{\rm b}$ in figure 3.5.

For $T_{\rm b} < T_1$, the black hole loses energy via the absorption of Hawking radiation by the bath and evaporates to a smaller black hole with lower temperature $T_{\rm b}$, which is similar to the model with $T_{\rm b} = 0$ as described in chapter 2. Conversely, a black hole coupled with a higher temperature bath $T_{\rm b} > T_1$ absorbs radiation from the bath and approaches another equilibrium state with temperature $T_{\rm b}$ when $ku \gg 1$. In both cases, for $ku \to \infty$, the system thermalizes and shows similar qualitative features to the equilibrium case $T_{\rm b} = T_1$. In summary, we have the three different dynamical behaviors in the two-dimensional gravity setup: an evaporating black hole when $T_{\rm b} < T_1$; a growing black hole when $T_{\rm b} > T_1$; and equilibrium when $T_{\rm b} = T_1$. Note that these outcomes are independent of the temperature of the original black hole, *i.e.,* T_0.

However, diving into the details of the QES and the flow of information, we will see there are different critical temperatures determining the position of the QES relative to the final event horizon, as will be explained in section 3.3.1. For this analysis, we approximate the equations for the generalized entropy and find the approximate solutions for the QES. Making a small k expansion with **fixed** ku, one can find the following approximation for

$f(u)$:[17]

$$\frac{f(u)}{t_\infty} \approx \tanh\left(\frac{2\pi}{k}\left(T_1 - T_{\rm eff} - T_{\rm b}\log\left(\frac{T_1+T_{\rm b}}{T_{\rm b}+T_{\rm eff}}\right) + \frac{ku}{2}T_{\rm b}\right)\right), \tag{3.96}$$

which reduces to the equilibrium case with $f(u) = \frac{1}{\pi T_1}\tanh(\pi T_1 u)$ after taking $T_{\rm b} = T_1$. Hence the above simplified form approximates the map-function $f(u)$ even for $T_{\rm b} \geq T_1$. From the asymptotic expansion in eq. (3.95), one can also obtain the approximation for the upper bound of physical time

$$t_\infty \approx \frac{1}{\pi T_1} + \frac{k}{4\pi^2 T_1^4}\left(T_1^2 - T_{\rm b}^2\right) + \mathcal{O}(k^2)\,. \tag{3.97}$$

Let us remark that one can further derive several simpler and useful approximations

$$\begin{aligned}
\log\left(\frac{t_\infty - f(u)}{2t_\infty}\right) &\sim -\frac{4\pi}{k}\left(T_1 - T_{\rm eff} - T_{\rm b}\log\left(\frac{T_1+T_{\rm b}}{T_{\rm b}+T_{\rm eff}}\right) + \frac{ku}{2}T_{\rm b}\right), \\
f'(u) &\sim 2\pi T_{\rm eff}\left(t_\infty - f(u)\right), \\
\{u, f(u)\} = -\frac{1}{(f'(u))^2}\{f(u), u\} &\sim \frac{1}{2(t_\infty - f(u))^2},
\end{aligned} \tag{3.98}$$

which will be used many times in the following analysis. It is also easy to find that all the above approximations reduce to the same forms used in chapter 2 after taking $T_{\rm b} = 0$. The above approximations are still complicated due to the appearance of $T_{\rm eff}(u, T_{\rm b})$, but we can further simplify the above results if we focus on times at the order of the Page time by taking the early-time limit $ku \ll 1$ (**linear region**).[18] In the linear regime, the effective temperature $T_{\rm eff} \sim T_1$ and we find the following linear approximations

$$\begin{aligned}
\log\left(\frac{t_\infty - f(u)}{2t_\infty}\right) &\sim -2\pi T_1 u + \mathcal{O}\left(ku^2\right) \\
\log\left(\frac{1}{f'(u)}\right) &\sim 2\pi T_1 u - \log\left(4\pi T_1 t_\infty\right),
\end{aligned} \tag{3.99}$$

[17] In order to do this analytically, we use the series expansions of Bessel functions [148]

$$\begin{aligned}
&K_\nu(\nu z) \underset{\nu\to\infty}{\sim} \sqrt{\frac{\pi}{2\nu}}\left(\frac{e^{-\nu\eta}}{(1+z^2)^{1/4}} + \mathcal{O}(\frac{1}{e^{\eta\nu}\nu})\right), \quad I_\nu(\nu z) \underset{\nu\to\infty}{\sim} \sqrt{\frac{1}{2\pi\nu}}\left(\frac{e^{\nu\eta}}{(1+z^2)^{1/4}} + \mathcal{O}(\frac{e^{\eta\nu}}{\nu})\right) \\
&\text{with} \qquad \eta = \sqrt{1+z^2} + \log\frac{z}{1+\sqrt{1+z^2}}\,.
\end{aligned} \tag{3.95}$$

[18] Later, we will find that most of our most analytic approximations (at leading order) in the linear region present linear behaviors in time. One can consider some transition point $ku \sim \frac{1}{\#}$ as the endpoint for the linear region.

where the leading-order contributions are not sensitive to the temperature of the bath $T_{\rm b}$ because the black hole does not evaporate very much in this phase. We are also interested in the **late-time region** with $e^{ku} \gg 1$ where we need the following approximations[19]

$$\begin{aligned}\log\left(\frac{t_\infty - f(u)}{2t_\infty}\right) &\sim \frac{4\pi}{k}\left(T_{\rm b} - T_1 + T_{\rm b}\log\left(\frac{T_1+T_{\rm b}}{2T_{\rm b}}\right) - \frac{ku}{2}T_{\rm b} + \frac{T_1^2 - T_{\rm b}^2}{4T_{\rm b}}e^{-ku}\right)\,,\\ \log\left(\frac{1}{f'(u)}\right) &\sim \frac{1}{k}\left(2\pi T_{\rm b}ku - 4\pi\left(T_{\rm b} - T_1 + T_{\rm b}\log\left(\frac{T_1+T_{\rm b}}{2T_{\rm b}}\right)\right)\right) - \log\left(4\pi T_{\rm b}t_\infty\right)\,.\end{aligned} \tag{3.100}$$

Finally, we note that the coefficient of the linear term changes to $2\pi T_{\rm b}$, which is expected because the temperature of the black hole at late time ($e^{ku} \gg 1$) is close to $T_{\rm b}$. In addition to these analytic approximations, we also performed numerical calculations for all the results as the double-check for these approximations in the following analysis. For convenient comparisons with the results at $T_{\rm b} = 0$, all numerical plots are done by choosing the numerical parameters listed in table 2.1, which are the same as those chosen in chapter 2.

3.3.1 QES and Page curve

In the following section, we first consider the generalized entropy of the subsystem $\mathrm{QM_R}$, which is the same with that of subsystem consisting of $\mathrm{QM_L}$, the thermal half-line and another half-line containing the purification. That is, we would like to find the position of the QES, *i.e.*, $x^{\pm}_{\rm QES}$, in the late-time phase when we anchor the endpoint $x_1^{\pm}$ on the boundary between AdS and flat spacetime. The generalized entropy reads

$$\begin{aligned}S_{\rm gen,late}(T_{\rm b}) =& \frac{\bar{\phi}_r}{4G_{\rm N}}\left[2\frac{1-(\pi T_1)^2 x^+_{\rm QES}x^-_{\rm QES} + \frac{k}{2}I\left(x^+_{\rm QES}, x^-_{\rm QES}; x^-_{\rm QES}\right)}{x^+_{\rm QES} - x^-_{\rm QES}}\right.\\ &\left. + 2k\log\left(\frac{2}{\epsilon}\frac{\sinh\left(\pi T_{\rm b}\left(y_1^- - y^-_{\rm QES}\right)\right)}{\pi T_{\rm b}}\frac{\left(x^+_{\rm QES} - x_1^+\right)}{\left(x^+_{\rm QES} - x^-_{\rm QES}\right)}\sqrt{\frac{f'(y^-_{\rm QES})}{f'(y_1^+)}}\right)\right]\,,\end{aligned} \tag{3.101}$$

with the integral term defined as

$$\begin{aligned}I(x^+, x^-; x) &= \int_0^x \left(x^+ - t\right)\left(x^- - t\right)\left(\{u,t\} - 2\left(\frac{\pi T_{\rm b}}{f'(u)}\right)^2\right)dt\,,\\ \text{with}\qquad \{u,t\} - 2\left(\frac{\pi T_{\rm b}}{f'(u)}\right)^2 &= \left(\frac{1}{f'(u)}\right)^2 2\pi^2\left(T_1^2 - T_{\rm b}^2\right)e^{-ku}\,.\end{aligned} \tag{3.102}$$

[19] Note that the $ku \to \infty$ and the $T_{\rm b} \to 0$ limits of eq. (3.95) do not commute.

In order to minimize the generalized entropy, we need to solve the differential equations $\partial_\pm S_{\rm gen} = 0$. Explicitly, we have

$$
\begin{aligned}
0 &= 2\left(\pi T_1 x^-_{\rm QES}\right)^2 - 2 - kI\left(x^-_{\rm QES}, x^-_{\rm QES}; x^-_{\rm QES}\right) + 2k\left(x^+_{\rm QES} - x^-_{\rm QES}\right)^2\left(\frac{1}{x^+_{\rm QES} - x^+_1} - \frac{1}{x^+_{\rm QES} - x^-_{\rm QES}}\right), \\
0 &= 2 - 2\left(\pi T_1 x^+_{\rm QES}\right)^2 + kI\left(x^+_{\rm QES}, x^+_{\rm QES}; x^-_{\rm QES}\right) \\
&\quad + 2k\left(x^+_{\rm QES} - x^-_{\rm QES}\right)^2\left(\frac{\pi T_{\rm b}}{\tanh\left(\pi T_{\rm b}(y^-_{\rm QES} - y^-_1)\right)}\frac{1}{f'\left(y^-_{\rm QES}\right)} + \frac{1}{x^+_{\rm QES} - x^-_{\rm QES}} + \frac{1}{2}\frac{f''(y^-_{\rm QES})}{\left(f'(y^-_{\rm QES})\right)^2}\right).
\end{aligned}
\tag{3.103}
$$

To solve these equations, we will need the approximation for the time-map function $f(u)$ in eq. (3.96) (and it's subsequent limits in eqs. (3.98), (3.99) and (3.100)), but we still need to carefully deal with the integral term that originates from the backreaction of the dilaton in the JT gravity. From the late time limit of eq. (3.103) we find

$$
I_\infty \equiv I(t_\infty, t_\infty; t_\infty) = \frac{2}{k}\left((\pi T_1 t_\infty)^2 - 1\right), \tag{3.104}
$$

which is the leading-order contribution to the integral at late times because the position of QES should be located near t_∞, *i.e.*, $x^+_{\rm QES} \sim t_\infty \sim t \sim x^-_{\rm QES}$. As before, we start from considering the generalized entropy of the subsystem consisting of $\mathrm{QM_L}$ and the whole bath (with its purification) by taking x_1 on the conformal boundary of AdS

$$
x^+_1 \approx t \approx x^-_1 \qquad \left(i.e., y^+_1 \approx u \approx y^-_1\right), \tag{3.105}
$$

where we ignored the correction at the order $\mathcal{O}(\epsilon f'(u))$.[20]

Turn on the temperature of bath

From the intuition derived from studying the $T_{\rm b} = 0$ case in chapter 2, we expect the position of the QES after the Page time to satisfy

$$
0 < x^+_{\rm QES} - t_\infty < t_\infty - t \ll t_\infty - x^-_{\rm QES} \ll t_\infty\,. \tag{3.106}
$$

[20]Recall the point on AdS boundary at proper time u is defined by $t = f(u) = \frac{x^+_1 + x^-_1}{2}, s = \frac{x^+_1 - x^-_1}{2} \approx \epsilon f'(u)$.

We will therefore solve the extremal equations (3.103) by expanding around t_∞. With the help of the approximations in eqs. (3.98), we can approximate the integral

$$\begin{aligned} &I\left(x^-_{\rm QES}, x^-_{\rm QES}; x^-_{\rm QES}\right) \sim I_\infty - (t_\infty - x^-_{\rm QES})\partial_- I\left(x^-_{\rm QES}, x^-_{\rm QES}; x^-_{\rm QES}\right) \\ &\sim \frac{2}{k}\left((\pi T_1 t_\infty)^2 - 1\right) + (t_\infty - x^-_{\rm QES})\log\left(\frac{t_\infty - x^-_{\rm QES}}{t_\infty}\right)\left(1 - \frac{T_{\rm b}^2}{T^2_{\rm eff}(v_{\rm QES})}\right) . \end{aligned} \tag{3.107}$$

where for $\partial_- I\left(x^-_{\rm QES}, x^-_{\rm QES}; x^-_{\rm QES}\right) \equiv \frac{dI\left(x^-_{\rm QES}, x^-_{\rm QES}; x^-_{\rm QES}\right)}{dx^-_{\rm QES}}$, we used the approximation

$$\int_0^{x^-_{\rm QES}} 2\left(x^-_{\rm QES} - t\right)\left(\{u,t\} - 2\left(\frac{\pi T_{\rm b}}{f'(u)}\right)^2\right) dt \approx \int_0^{x^-_{\rm QES}} \frac{\left(t_\infty - t + x^-_{\rm QES} - t_\infty\right)}{(t_\infty - t)^2}\left(1 - \frac{T_b^2}{T^2_{\rm eff}(u)}\right) dt\,. \tag{3.108}$$

However, it is not easy to perform the above integral of t due to the appearance of time u. Instead, we apply the mean value theorem and find

$$\begin{aligned} \partial_- I\left(x^-_{\rm QES}, x^-_{\rm QES}; x^-_{\rm QES}\right) &\approx \int_0^{x^-_{\rm QES}} \frac{1}{(t_\infty - t)}\left(1 - \frac{T_b^2}{T^2_{\rm eff}(u)}\right) dt \\ &\approx -\left(1 - \frac{T_{\rm b}^2}{T^2_{\rm eff}(v_{\rm QES})}\right)\log\left(\frac{t_\infty - x^-_{\rm QES}}{t_\infty}\right) , \end{aligned} \tag{3.109}$$

where $v_{\rm QES} \in \left[0, y^-_{\rm QES}\right]$ is referred to as the middle value for the t integral from 0 to $x^-_{\rm QES}$. Similarly, we can obtain the other integral $I\left(x^+_{\rm QES}, x^+_{\rm QES}; x^-_{\rm QES}\right)$ by

$$\begin{aligned} &\int_0^{x^-_{\rm QES}} \left((t_\infty - x^+_{\rm QES})^2 - 2(t_\infty - x^+_{\rm QES})(t_\infty - t) + (t_\infty - t)^2\right)\left(\{u,t\} - 2\left(\frac{\pi T_{\rm b}}{f'(u)}\right)^2\right) dt\,, \\ &\sim (t_\infty - x^+_{\rm QES})\log\left(\frac{t_\infty - x^-_{\rm QES}}{t_\infty}\right)\left(1 - \frac{T_{\rm b}^2}{T^2_{\rm eff}(v_{\rm QES})}\right) + I_\infty - \frac{1}{2}(t_\infty - x^-_{\rm QES})\left(1 - \frac{T_{\rm b}^2}{T^2_{\rm eff}(y^-_{\rm QES})}\right) , \end{aligned} \tag{3.110}$$

where we have ignored the first integral at the order $\mathcal{O}((x^+_{\rm QES} - t_\infty)^2)$, used the mean value theorem for the second integral again with the **same** middle value $v_{\rm QES}$ as before and considered the third integral as a function of $x^-_{\rm QES}$ with its Taylor expansion around $x^-_{\rm QES} \sim t_\infty$ as

$$\int_0^{x^-_{\rm QES}} (t_\infty - t)^2\left(\{u,t\} - 2\left(\frac{\pi T_{\rm b}}{f'(u)}\right)^2\right) dt \sim I_\infty - \frac{1}{2}(t_\infty - x^-_{\rm QES})\left(1 - \frac{T_{\rm b}^2}{T^2_{\rm eff}(y^-_{\rm QES})}\right) . \tag{3.111}$$

Although we cannot decide the middle value for any $y^-_{\rm QES}$, it is easy to find $T_{\rm eff}(v_{\rm QES}) \sim T_1$ at the linear region with $ku \ll 1$.

Combining our assumptions (3.106) and the approximations of the integrals in eqs. (3.107) and (3.110), we can approximate the equations for QES by much simpler forms

$$\begin{aligned}
&\frac{4\pi T_1}{t_\infty - x^-_{\rm QES}}\left(\pi T_1 t_\infty + \frac{k}{4\pi T_1}\log\left(\frac{t_\infty - x^-_{\rm QES}}{t_\infty}\right)\left(1 - \frac{T_{\rm b}^2}{T_{\rm eff}^2(v_{\rm QES})}\right)\right) \approx \frac{2k}{x^+_{\rm QES} - t}\,,\\
&4\pi T_1\left(x^+_{\rm QES} - t_\infty\right)\left(\pi T_1 t_\infty + \frac{k}{4\pi T_1}\log\left(\frac{t_\infty - x^-_{\rm QES}}{t_\infty}\right)\left(1 - \frac{T_{\rm b}^2}{T_{\rm eff}^2(v_{\rm QES})}\right)\right) \approx \frac{k}{2}\left(t_\infty - x^-_{\rm QES}\right)\Gamma_{\rm eff}(y^-_{\rm QES})\,,
\end{aligned} \tag{3.112}$$

where we have defined

$$\Gamma_{\rm eff}(y^-_{\rm QES}) \equiv \left(1 - \frac{T_{\rm b}}{T_{\rm eff}(y^-_{\rm QES})}\right)^2\,, \tag{3.113}$$

and only keep the leading-order contributions. The non-negative coefficient $\Gamma_{\rm eff}$ approaches zero as the black hole reaches thermal equilibrium with the bath. For later use, we also present the numerical plot for $\Gamma_{\rm eff}$ for various temperature in figure 3.8.

With the above equations, it is straightforward to find the solutions, *i.e.,* the location of QES

$$\begin{aligned}
x^+_{\rm QES} &\approx t_\infty + \frac{\Gamma_{\rm eff}}{4 - \Gamma_{\rm eff}}\left(t_\infty - t\right)\,,\\
x^-_{\rm QES} &\approx t_\infty - \frac{8\pi T_1}{k(4 - \Gamma_{\rm eff})}\left(t_\infty - t\right)\left(\pi T_1 t_\infty + \frac{k}{4\pi T_1}\log\left(\frac{t_\infty - x^-_{\rm QES}}{t_\infty}\right)\left(1 - \frac{T_{\rm b}^2}{T_{\rm eff}^2(v_{\rm QES})}\right)\right)\,.
\end{aligned} \tag{3.114}$$

Assuming the time delay $u - y^-_{\rm QES}$ is not large (*i.e.,* $k(u - y^-_{\rm QES}) \ll 1$), one can use the approximation

$$\begin{aligned}
\log\left(\frac{t_\infty - f(y^-_{\rm QES})}{t_\infty - f(u)}\right) &\approx -\frac{4\pi}{k}\left(T_{\rm eff}(u) - T_{\rm eff}(y^-_{\rm QES}) - T_{\rm b}\log\left(\frac{T_{\rm b} + T_{\rm eff}(u)}{T_{\rm b} + T_{\rm eff}(y^-_{\rm QES})}\right) - \frac{k}{2}(u - y^-_{\rm QES})\right)\\
&\sim 2\pi T_{\rm eff}(y^-_{\rm QES})(u - y^-_{\rm QES}) \sim 2\pi T_{\rm eff}(u)(u - y^-_{\rm QES})\,,
\end{aligned} \tag{3.115}$$

and further simplify the position of the QES to

$$\begin{aligned} y^-_{\rm QES} &\approx u - u_{\rm HP} \\ u_{\rm HP} &= \frac{1}{2\pi T_{\rm eff}(u)} \log\left[\frac{8\pi T_1}{k(4-\Gamma_{\rm eff}(u))}\left(1+\frac{k}{4\pi T_1}\log\left(\frac{t_\infty - t}{t_\infty}\right)\left(1-\frac{T_{\rm b}^2}{T_{\rm eff}^2(v_{\rm QES})}\right)\right)\right] , \end{aligned} \tag{3.116}$$

where the second term can be understood as the Hadyen-Preskill time. It is noted that the time scale $u_{\rm HP}$ is not constant in general because the black hole is also dynamical. For $T_{\rm b} = 0$, the solutions reduce to

$$y^-_{\rm QES}(T_{\rm b}=0) \approx u - \frac{1}{2\pi T_1 e^{-\frac{k}{2}u}} \log\left(\frac{8\pi T_1 e^{-\frac{k}{2}u}}{3k}\right) , \tag{3.117}$$

which is in agreement with the results of chapter 2.[21] Similarly to the zero temperature bath case, the QES moves towards the horizon at $x^+ = t_\infty$. However, we want to stress the importance of the role of the non-zero factor $\Gamma_{\rm eff}$ that captures the speedup of the equilibration process because the thermal bath also emits radiation to the AdS region when $T_{\rm b} \neq 0$.

Furthermore, we can also compare our new solutions with the explicit and linear solution found in chapter 2. Focusing on the Page transition within the linear region, we can further simplify the results for the position of QES and explicitly obtain

$$\begin{aligned} x^+_{\rm QES} &\approx t_\infty + \frac{\Gamma_0}{4-\Gamma_0}(t_\infty - t) , \qquad \Gamma_0 = \left(1-\frac{T_{\rm b}}{T_1}\right)^2 , \\ y^-_{\rm QES} &\approx u - \frac{1}{2\pi T_1}\log\left(\frac{8\pi T_1}{k(4-\Gamma_0)}\right) , \qquad ku \ll 1 \text{ (linear region)} , \end{aligned} \tag{3.118}$$

where we can rewrite the time delay

$$u_{\rm HP}(ku \ll 1) = \frac{1}{2\pi T_1}\log\left(\frac{8\pi T_1}{k\left(4-(1-T_{\rm b}/T_1)^2\right)}\right) , \tag{3.119}$$

as the Hadyen-Preskill time in linear region. It is also easy to check that the above results are reduced to the linear results presented in chapter 2 by setting $T_{\rm b} = 0$, *i.e.*, $\Gamma_{\rm eff} = 1$.

[21] Here we explicitly write the right side as a function of time u which should be understood as the leading-order contribution. To be more precise, we can also use $e^{\frac{k}{2}y^-_{\rm QES}}$ rather than $e^{\frac{k}{2}u}$.

After finding the position of the QES, we are able to consider the evolution of the generalized entropy (3.101). The generalized entropy is dominated by the classical area term from the dilaton

$$\begin{aligned}\phi &\approx 2\bar{\phi}_r\left(\frac{1-(\pi T_1)^2 x^+_{\rm QES}x^-_{\rm QES}+\frac{k}{2}I\left(t_\infty,x^-_{\rm QES};x^-_{\rm QES}\right)}{t_\infty-x^-_{\rm QES}}\right)\left(1-\frac{x^+_{\rm QES}-t_\infty}{t_\infty-x^-_{\rm QES}}\right)\\ &\sim \frac{2\bar{\phi}_r}{t_\infty-x^-_{\rm QES}}\left[1-\left(\pi T_1 t_\infty\right)^2-(\pi T_1)^2 t_\infty\left(x^+_{\rm QES}-t_\infty\right)-(\pi T_1)^2 t_\infty(x^-_{\rm QES}-t_\infty)\right.\\ &\quad\left.+\frac{k}{2}\left(I_\infty+\frac{(t_\infty-x^-_{\rm QES})}{2}\left(1-\frac{T_{\rm b}^2}{T^2_{\rm eff}(v_{\rm QES})}\right)\log\left(\frac{t_\infty-x^-_{\rm QES}}{t_\infty}\right)\right)\right]\\ &\sim \bar{\phi}_r\left(2(\pi T_1)^2 t_\infty+\frac{k}{2}\left(1-\frac{T_{\rm b}^2}{T^2_{\rm eff}(v_{\rm QES})}\right)\log\left(\frac{t_\infty-x^-_{\rm QES}}{t_\infty}\right)-\frac{k\Gamma_{\rm eff}(y^-_{\rm QES})}{4}\right),\end{aligned} \tag{3.120}$$

which is approximated by the value of dilaton on the horizon at $x^+_{\rm QES}=t_\infty$. Recall that $\Gamma_{\rm eff}(y^-_{\rm QES})$ is given in eq. (3.113). Comparing the area term (without divergences associated with short range entanglement)

$$S_{\phi_{\rm QES}}=\frac{\phi}{4G_{\rm N}}\sim\frac{c}{12k}\left(2\pi T_1+\frac{k}{2}\left(1-\frac{T_{\rm b}^2}{T^2_{\rm eff}(v_{\rm QES})}\right)\log\left(\frac{t_\infty-x^-_{\rm QES}}{t_\infty}\right)\right), \tag{3.121}$$

with the time delay in position of QES, *i.e.*, eq. (3.116), we can rewrite the time shift as

$$u_{\rm HP}\approx\frac{1}{2\pi T_{\rm eff}(u)}\log\left(\frac{S_{\phi_{\rm QES}}}{c}\right)+\mathcal{O}(1)\approx\frac{1}{2\pi T_{\rm eff}(u)}\log\left(\frac{S(u)-S_0}{c}\right), \tag{3.122}$$

where we have restored the extremal entropy $S_0\equiv\frac{\phi_0}{4G_{\rm N}}$ (see (3.10)) in the complete entropy $S(u)$ of our dynamical black hole. Here we can explain the entropy $S(u)$ as the density of state at time u and take S_0 as the ground state entropy associated with the value ϕ_0. As discussed in [11], the time delay $u_{\rm HP}$ appearing in $y^-_{\rm QES}$ can be understood as the Hayden-Preskill time.

Page transition

The subleading term of the generalized entropy is the bulk entropy

$$\begin{aligned}\frac{4G_{\rm N}}{\bar{\phi}_r}S_{\rm bulk}&=\left(2k\log\left(\frac{2}{\epsilon}\frac{\sinh\left(\pi T_{\rm b}\left(u-y^-_{\rm QES}\right)\right)}{\pi T_{\rm b}}\frac{(x^+_{\rm QES}-t)}{(x^+_{\rm QES}-x^-_{\rm QES})}\sqrt{\frac{f'(y^-_{\rm QES})}{f'(u)}}\right)\right)\\ &\sim 2k\left(\log\left(\frac{8}{(4-\Gamma_{\rm eff})\epsilon}\frac{\sinh\left(\pi T_{\rm b}u_{\rm HP}\right)}{\pi T_{\rm b}}\right)-\pi T_{\rm eff}u_{\rm HP}+\frac{ku_{\rm HP}}{4T^2_{\rm eff}}(T_1^2-T_{\rm b}^2)e^{-ku}\right),\end{aligned} \tag{3.123}$$

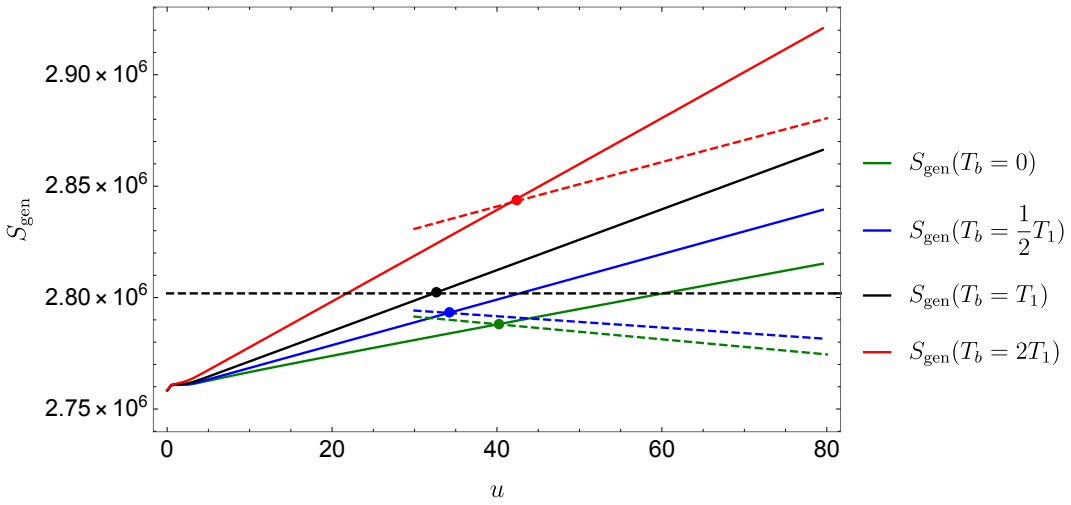

Figure 3.6: The Page curve of generalized entropy around Page transition from scrambling phase to late-time phase for different bath temperatures. The solid lines represent the analytical results at the scrambling phase and the dashed lines indicate the numerical results for the late-time phase which are also approximated by solutions (3.114) and their approximate generalized entropy (3.124). Note that the black dashed line shows the generalized entropy at equilibrium case, which is the constant given in eq. (3.64).

which remains constant in the linear region with $ku \ll 1$. As expected, it also reproduces the results in chapter 2 after fixing $T_{\rm b} = 0$. In order to derive the Page time, we can also explicitly write generalized entropy at late time phase in the **linear region**

$$S_{\rm gen,late}(ku \ll 1) \approx \frac{\bar{\phi}_r}{4G_{\rm N}} \left[2\pi T_1 - k\pi T_1 \left(1 - \frac{T_{\rm b}^2}{T_1^2}\right)(u - u_{\rm HP}) \right.$$
$$\left. + 2k \log\left(\frac{8}{(4-\Gamma_0)\epsilon} \frac{\sinh(\pi T_{\rm b} u_{\rm HP})}{\pi T_{\rm b}} \right) - 2k\pi T_{\rm eff} u_{\rm HP} + \mathcal{O}(k^2 \log k) \right], \tag{3.124}$$

which displays linear decrease (increase) of the generalized entropy after the Page transition for $T_{\rm b} < T_1$ ($T_{\rm b} > T_1$). Given the fact that the time delay $u_{\rm HP}$ is a constant when $T_{\rm b} = T_1$, it is obvious that the entropy $S_{\rm gen,late}$ also reduces to a constant when $T_{\rm b} = T_1$ (see eq. (3.116)), which is the same as the result derived in eq. (3.64) for the equilibrium case. Shortly before the Page time, we can obtain the generalized entropy in the scrambling phase with $1 \ll \pi T_1 u$ and $ku \ll 1$ by

$$S_{\rm gen,scrambling} \approx \frac{\bar{\phi}_r}{4G_{\rm N}} \left(2\pi T_0 + 2k \log\left(\frac{24\pi E_s}{\epsilon c} \frac{\sinh \pi(T_{\rm b} u)}{\pi T_{\rm b}} \frac{1}{\sqrt{f'(u)}} \right) + \kappa \right)$$
$$\approx \frac{\bar{\phi}_r}{4G_{\rm N}} \left(2\pi T_0 + 2k\pi(T_{\rm b} + T_1)u + 2k \log\left(\frac{12E_s}{\epsilon c T_{\rm b}} \right) + \frac{k^2 u}{2} \left(1 - \frac{T_{\rm b}^2}{T_1^2}\right)(1 - u\pi T_1) + \kappa \right). \tag{3.125}$$

where we put all other contributions in $S_{\rm Bulk}$ into κ which approaches a constant when $t = f(u) \to t_\infty$.[22] The leading-order terms of the generalized entropy in the scrambling phase (3.125) are a constant related to the entropy of the original black hole and two linearly increasing terms, *i.e.,* $2k\pi(T_1 + T_{\rm b})$, due to the entanglement of radiation escaping from the non-zero temperature bath and black hole, respectively. Because the temperature of black hole is approaching $T_{\rm b}$, we will show later that the linear increase is replaced by a $2k\pi(T_{\rm b} + T_{\rm b})$ term.[23] As a result, the generalized entropy at the scrambling phase increases indefinitely while that of the late time phase asymptotes to the entropy of a black hole with temperature $T_{\rm b}$, we expect there is a phase transition (Page transition) between them

[22] The analysis for the scrambling phase is similar to that in chapter 2. See the section 2.1 for more details.

[23] Technically, this is due to the approximations for $\log \frac{1}{\sqrt{f'(u)}}$ for different time regions, see (3.99) and (3.100).

when $S_{\text{gen,scrambling}} = S_{\text{gen,linear}}$. This transition occurs at the Page time

$$u_{\text{Page}}(T_{\text{b}}) \approx \frac{2}{4-\Gamma_0}\frac{T_1-T_0}{kT_1} + \frac{1-\frac{T_{\text{b}}^2}{T_1^2}}{4-\Gamma_0}u_{\text{HP}} + \mathcal{O}(1)\,, \tag{3.126}$$

which decreases with the increase of T_{b} for $T_{\text{b}} < T_1$, reaches a minimum at $T_{\text{b}} = T_1$ and then increases for larger T_{b}. In contrast, the generalized entropy at the Page time

$$S_{\text{gen}}(u_{\text{Page}}) \approx \frac{\bar{\phi}_r}{4G_{\text{N}}}2\pi\left(T_0 + \frac{2(T_1-T_0)}{3-\frac{T_{\text{b}}}{T_1}} + \cdots\right)\,, \tag{3.127}$$

increases with the increase of T_{b}. These linear behaviors are explicitly shown in the figure 3.6. As a comparison, we represent the Page transition at linear region with $T_{\text{b}} \geq T_1$.

Lastly, we add that the expressions for the Page time in eq. (3.126) and the Page entropy in eq. (3.127) diverge for $T_{\text{b}} \to 3T_1$. This is an artifact of approximating the coefficient Γ_{eff} defined in eq. (3.113) by $\Gamma_0 = \left(1-\frac{T_{\text{b}}}{T_1}\right)^2$. However, if we include the subleading terms in Γ_{eff}, we find that both of these quantities remain finite. We return to discuss this point in section 3.3.1.

Approach to Equilibrium

For the equilibrium situation studied in [62], the QES sat outside of the horizon, resulting in part of the quantum extremal island being located outside the black hole. The same behaviour was found in section 3.2 – see eq. (3.55) – where the bath temperature matches that of the black hole after it has absorbed the shockwave. Therefore in the present case where the two temperatures do not match, we still expect that as the black hole approaches its final equilibrium, *i.e.,* in the late time phase with $T_{\text{eff}} \approx T_{\text{b}}$, the QES will move outside of horizon at some critical temperature.[24]

Ultimately, we wish to track the position of the QES for a black hole as a function of boundary time u starting with a temperature T_1 and the bath at some fixed temperature T_{b}. However, the analysis is simplified by asking how with fixed u and T_1, the position of the QES moves as we vary the bath temperature T_{b}. With this approach, we can find different phases according to the position of QES as a function of the boundary time u

- Inside horizon $\qquad T_{c_1}(u) < T_{\text{b}} < T_{c_2}(u)\,,$

[24] Similar behaviour was found in [70].

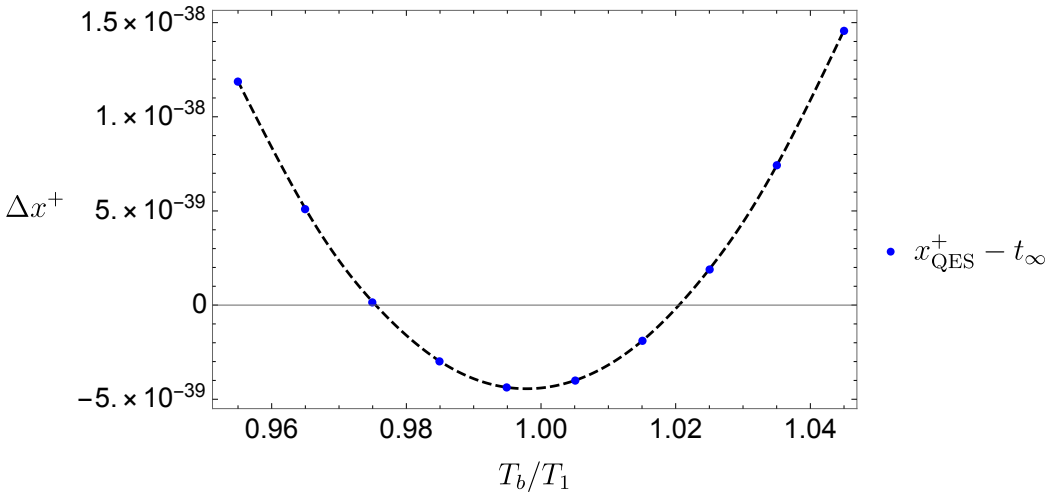

Figure 3.7: The numerical results from solving QES equations for the deviation of QES from horizon, *i.e.*, $\left(x^+_{\rm QES}-t_\infty\right)$, at a fixed time slice $u=40$ (after Page transition) with different bath temperatures $T_{\rm b}$. For T_b very close to T_1, the extremal surface lies outside of the event horizon, in agreement with the analysis of section 3.3.1

.

- On the horizon $\qquad T_{\rm b}=T_{c_1}(u)$ or $T_{\rm b}=T_{c_2}(u)\,,$
- Outside horizon $\qquad T_{\rm b}<T_{c_1}(u)$ or $T_{\rm b}>T_{c_2}(u)\ \ ,$

where the critical temperatures $T_{c_1}(u)$ and $T_{c_2}(u)$ will be derived in the following – see eq. (3.133).

If we extend the position (3.114) of the QES to the equilibrium case with $\Gamma_{\rm eff}=0$, we find the QES is located on the horizon at $x^+=t_\infty$, which is not what we found in section 3.2. Recalling the simplified solutions for QES (3.112), it is obvious that the non-negative term on the right-hand side, *i.e.*,

$$\frac{k}{2}\left(t_\infty-x^-_{\rm QES}\right)\Gamma_{\rm eff}(y^-_{\rm QES})\,, \tag{3.128}$$

implies we always have $x^+_{\rm QES}\geq t_\infty$. The solution to this puzzle is simple: all the approximations used in the previous analysis for the QES are based on the assumptions in eq. (3.106), which are invalid when $T_{\rm b}$ is extremely near T_1. Technically speaking, it is traced back to the fact that $\Gamma_{\rm eff}=\left(1-\frac{T_{\rm b}}{T_{\rm eff}}\right)^2$ around this narrow region suppresses the leading-order

contribution. In order to find the critical temperature for the transition of QES, we need to track the (some) sub-leading contributions which compete with the leading-order terms when $\Gamma_{\text{eff}} \sim k$. Although it is not easy to perform the integral I to next order, we can determine these corrections by perturbing from the equilibrium case at $T_{\text{b}} = T_1$ because the critical temperature should satisfy $T_1 - T_c \sim \sqrt{k}$. In other words, we can approach the critical temperature from regular T_{b} and from $T_1 = T_{\text{b}}$ and look for all necessary corrections.

Instead of directly solving the QES equations for the equilibrium case, we can approximate the two equations (3.59) with $x_1^{\pm} = t$ by

$$\begin{aligned} 4\pi T_1(t_\infty - x^-_{\text{QES}})\left(1 + \frac{x^-_{\text{QES}} - t_\infty}{t_\infty}\right) &\approx 2k\left(t_\infty - x^-_{\text{QES}}\right)^2\left(\frac{1}{x^+_{\text{QES}} - t} - \frac{1}{t_\infty - x^-_{\text{QES}}}\right) , \\ \longrightarrow \qquad x^+_{\text{QES}} - t &\sim \frac{k}{2\pi T_1}\left(t_\infty - x^-_{\text{QES}}\right) , \end{aligned} \tag{3.129}$$

and

$$\begin{aligned} 4\pi T_1\left(x^+_{\text{QES}} - t_\infty\right) &\approx 2k\left(x^+_{\text{QES}} - x^-_{\text{QES}}\right)^2\left(\frac{1}{t_\infty - x^-} - \frac{x^+_{\text{QES}} - t_\infty}{(t_\infty - x^-_{\text{QES}})^2} - \frac{1}{t_\infty - x^-} + \frac{t - t_\infty}{(t_\infty - x^-_{\text{QES}})^2}\right) < 0 \\ &\approx 2k\left(t - x^+_{\text{QES}}\right) + 4k\frac{x^+_{\text{QES}} - t_\infty}{t_\infty - x^-_{\text{QES}}}(t - x^+_{\text{QES}}) \\ \longrightarrow \qquad x^+_{\text{QES}} - t_\infty &\sim \frac{k}{2\pi T_1}\left(t - x^+_{\text{QES}}\right) \longrightarrow x^+_{\text{QES}} \sim t_\infty - \frac{k}{2}\left(t_\infty - t\right) , \end{aligned} \tag{3.130}$$

where the leading-order contribution $\frac{(t_\infty - x^-_{\text{QES}})^2}{t_\infty - x^-_{\text{QES}}}$ (positive) vanishes and we have to keep the next order correction $t - x^+_{\text{QES}}$ (negative). The fact that the sub-leading term has the opposite sign to the (almost vanishing) leading term is what positions the QES outside the horizon, in contrast with the cases when T_{b} is not perturbatively close to T_1. From this lesson, we also need to keep that correction for $\Gamma \sim k$ where the leading order is competing with the sub-leading order. Adding this correction to (3.112), we need to correct the right side of the second equation by

$$\frac{k}{2}\left(t_\infty - x^-_{\text{QES}}\right)\Gamma(y^-_{\text{QES}}) \quad \longrightarrow \frac{k}{2}\left(t_\infty - x^-_{\text{QES}}\right)\Gamma(y^-_{\text{QES}}) + 2k\left(t - x^+_{\text{QES}}\right) , \tag{3.131}$$

and arrive at

$$\frac{2}{x^+_{\text{QES}} - t}\left(x^+_{\text{QES}} - t_\infty\right) \approx \frac{1}{2}\left(1 - \frac{T_{\text{b}}}{T_{\text{eff}}(y^-_{\text{QES}})}\right)^2 - \frac{k}{\pi T_1} , \tag{3.132}$$

which now agrees with the results of section 3.2.

Comparing with the results of section 3.2, we can interpret the Γ term as a correction from equilibrium results, which is reinforced by the fact that Γ approaches zero as the system thermalizes. We can expect that further corrections we missed should be only at the order $\mathcal{O}(\Gamma \times k) \sim k^2$. The critical temperatures of $T_{\rm b}$ for which the QES changes position with respect to the event horizon are given by

$$\begin{aligned} T_{c_1}(u) &\approx \left(1 - \sqrt{\frac{2k}{\pi T_1}}\right) T_{\rm eff}(y^-_{\rm QES})\,, \\ T_{c_2}(u) &\approx \left(1 + \sqrt{\frac{2k}{\pi T_1}}\right) T_{\rm eff}(y^-_{\rm QES})\,, \end{aligned} \tag{3.133}$$

which define a small region of temperatures where the QES is located outside the horizon.

Lastly, we mention that since $T_{\rm eff}$ approaches $T_{\rm b}$ as the system thermalizes, even when $T_{\rm b}$ is far from T_1, the QES will eventually cross the event horizon for late enough times. This is to be expected since, as we claimed before, for $ku \to \infty$, the system behaves as the equilibrium case studied in section 3.2. Indeed, when

$$ku \gtrsim \log\left(\left|1 - \frac{T_1^2}{T_{\rm b}^2}\right| \sqrt{\frac{\pi T_1}{8k}}\right)\,, \tag{3.134}$$

the QES is located outside the event horizon. By these times, the effective temperature is very close to the bath temperature $T_{\rm eff} \approx T_{\rm b}\left(1 \pm \sqrt{\frac{2k}{\pi T_1}}\right)$, where the sign is determined by whether $T_{\rm b}$ is greater or smaller than T_1, and the correction parameter $\Gamma_{\rm eff} \approx \frac{2k}{\pi T_1}$ is perturbatively small. For bath temperatures that are very close to T_1,

$$\frac{|T_{\rm b} - T_1|}{T_1} \lesssim \sqrt{\frac{2k}{\pi T_1}} e^{\frac{T_1 - T_0}{2T_1}}\,, \tag{3.135}$$

the QES is already outside of the event horizon by the Page time in eq. (3.126).

Overheated black holes

In the previous subsections, we derived the leading order expressions of the position of QES and discussed the importance of the subleading corrections when the bath temperature approaches T_1 with $\Gamma \sim k \sim 0$ because $x^+_{\rm QES} - t_\infty$ changes its sign after the transition

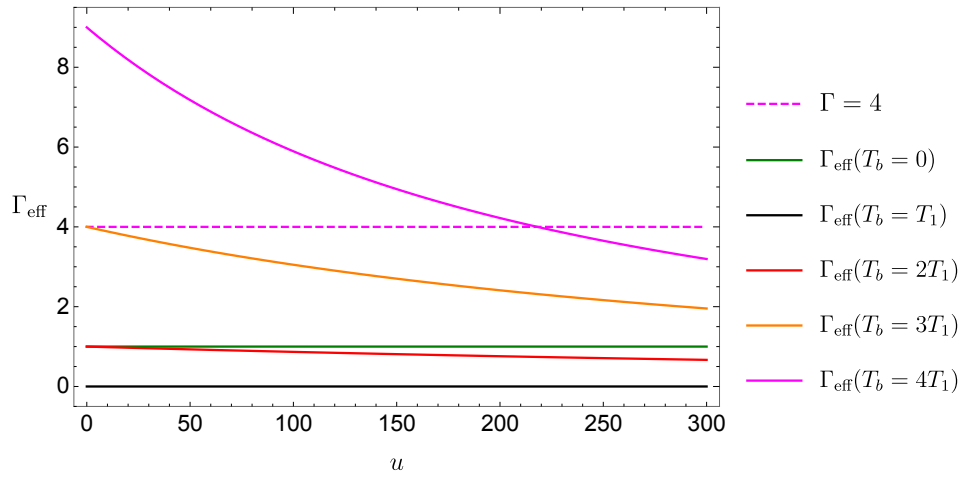

Figure 3.8: The time evolution of function $\Gamma_{\text{eff}}(u)$ for various bath temperature.

point at T_{c_1} and T_{c_2}. Although we claim our previous approximations apply for arbitrary temperatures, it is obvious that our solution (3.114) appears singular at $\Gamma = 4$ and further it appears the sign of $x^+_{\text{QES}} - t_\infty$ changes. It may appear that we have to consider next order corrections at another "critical temperature", *i.e.,*

$$T_{\text{b}} = 3T_1\,, \quad \text{with} \qquad \Gamma_0 = \left(1 - \frac{T_{\text{b}}}{T_1}\right)^2 = 4\,. \tag{3.136}$$

However, this is incorrect. The next order corrections cannot help solve this problem. Aside from x^+_{QES}, the solutions for $y^-_{\text{QES}}, x^-_{\text{QES}}$ (see eqs. (3.114) and (3.116)) show more problems because they are not well-defined when $\Gamma \geq 4$. At linear order, the generalized entropy in the late-time phase of the overheated black holes increases very rapidly, as can be seen by the coefficient of the linear term (see (3.124))

$$k\pi T_1 \left(\frac{T_{\text{b}}^2}{T_1^2} - 1\right)\,. \tag{3.137}$$

This rate of increase in generalized entropy may appears larger than that in the scrambling phase where the speed is dominated by linear term (see (3.125))

$$2k\pi(T_1 + T_{\text{b}})u \quad (ku \ll 1)\,, \qquad \text{or} \quad 4k\pi T_{\text{b}} u \quad (e^{ku} \gg 1)\,, \tag{3.138}$$

where one contribution of $(2k\pi T_{\text{b}} u)$ comes from the radiation from bath and the other $(2k\pi T_1 u$ and $2k\pi T_{\text{b}} u)$ from the black hole (for which $T_{\text{eff}} \sim T_1$ at early times and $T_{\text{eff}} \sim T_{\text{b}}$

for late times). One may wonder whether that means we can find a critical temperature T_c above which a Page transition doesn't occur because the generalized entropy in late-time phase increases faster than that from the scrambling phase. The answer is again no.

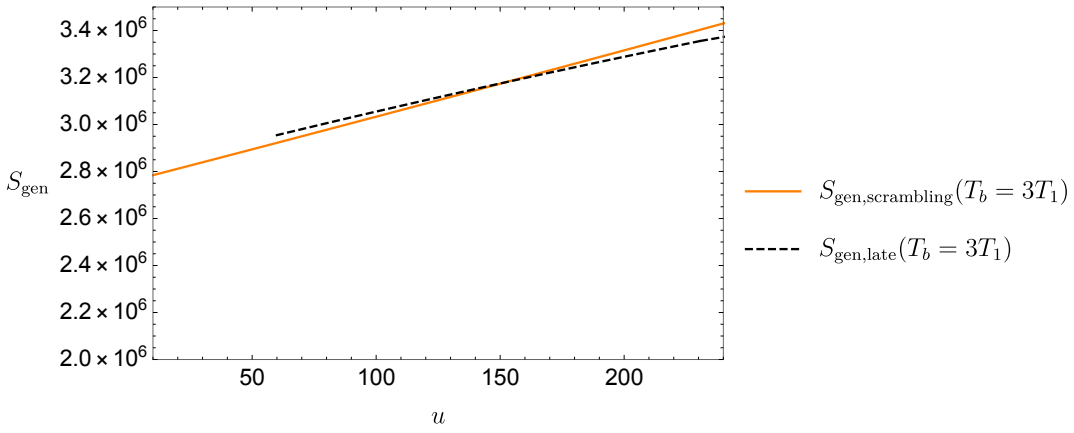

Figure 3.9: The Page transition with "critical" bath temperature at $T_{\rm b} = 3T_1$

All of the above questions or puzzles are actually due to the invalidity of the leading-order contributions in the linear region for overheated black holes. Our complete solutions are valid for arbitrary temperatures $T_{\rm b}$ outside of the critical region close to T_1 discussed in the previous section where subleading terms become important. One key ingredient to consider is that $\Gamma_{\rm eff}$ approaches zero with time, see the figure 3.8. For example, we always have $\Gamma_{\rm eff}(T_{\rm b} = 3T_1) < 4$ for $u > 0$. So there is no such new critical temperature at $T_{\rm b} = 3T_1$. Another important fact is the delay of the Page time with an increase of $|T_{\rm b} - T_1|$. Compared to the Page time at $T_{\rm b} = T_1$, the Page time with $T_{\rm b} > \# T_1$ is pushed to a later time that guarantees we have $\Gamma_{\rm eff}\,(u = u_{\rm Page}) < 4$. One might also wonder whether this time delay is really physical and why we should have a restriction on the initial time for the solutions at late-phase. Let's remark this restriction is reminiscent of what we have seen in the zero bath-temperature case and also the equilibrium case. More explicitly, the equilibrium case also presents this similar restriction on time u, *i.e.,* the inequality (3.62). The final ingredient that prevents the late time solutions in eq. (3.114) from becoming singular is the high bath-temperature itself because it creates a new and large coefficient $T_{\rm b}^2/T_1^2$ that enhances the next-order corrections to the linear region. For example, we can see those effects from the expansion of $\Gamma_{\rm eff}$, *i.e.,*

$$\Gamma_{\rm eff}(u) = \left(1 - \frac{T_{\rm b}}{T_{\rm eff}(u)}\right)^2 \approx \left(1 - \frac{T_{\rm b}}{T_1}\right)^2 - \frac{T_{\rm b}(T_1 - T_{\rm b})^2(T_1 + T_{\rm b})}{T_1^4} ku + \cdots , \qquad (3.139)$$

where the second order correction cannot be simply ignored for large T_b/T_1. To verify that there is no divergence, we show the Page transition using numerics for the "critical temperature" $T_b = 3T_1$ in figure 3.9. We also compare the position of the QES using our approximation (3.114) with numerical results and they fit well as for the small T_b cases.

Page Curve and Thermalization

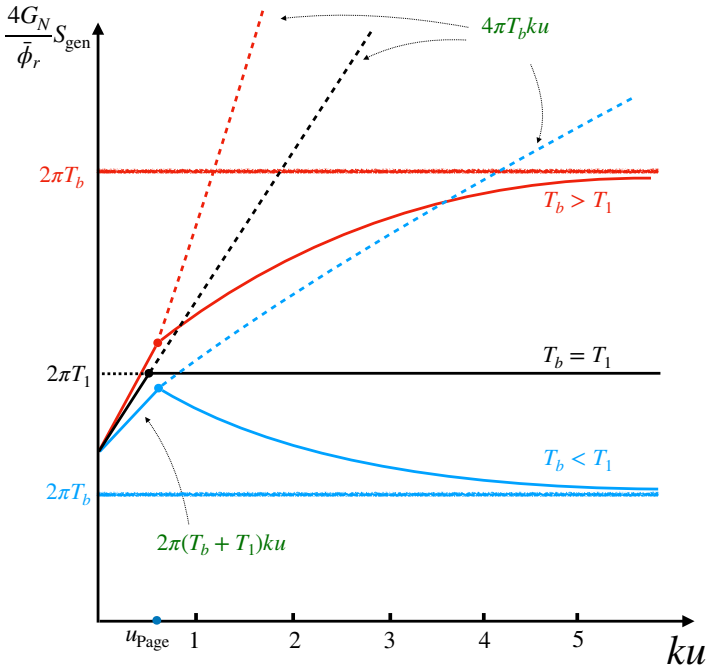

Figure 3.10: The schematic diagram for Page curve of black hole coupled with a thermal bath at different temperatures. The red, black, and blue solid lines show the Page curve for a growing black hole with $T_b > T_1$, an external black hole at equilibrium status with $T_b = T_1$, and an evaporating black hole with $T_b < T_1$, respectively. The corresponding dashed lines present the generalized entropy at the late-time region, whose behavior is dominated by the linear term $4\pi T_b ku$ as discussed around (3.138).

So far, we have focused on the evolution of the generalized entropy of the evaporating black hole up to times comparable with the Page time. As we will now show, we can also use the position of the QES in eq. (3.114), to find a full Page curve from $u = 0$ to the late time regime with $e^{ku} \gg 1$. The expected behavior of the generalized entropy $S_{\text{gen,late}}$ at late times is that the subleading corrections slow down the linear decrease ($T_b < T_1$) or

increase ($T_{\rm b} > T_1$) of the generalized entropy, which will eventually approach a constant $S_{\rm gen,late}(T_{\rm b})$ corresponding to the entropy of a black hole with temperature $T_{\rm b}$, as derived in eq. (3.64). However, we cannot simply substitute the solution into the definition of generalized entropy to derive its time evolution due to the absence of approximation for the middle value $v_{\rm QES}$ at late times.

Instead of considering the generalized entropy itself, we can take the time derivative of $S_{\rm gen,late}\left(u, x^+_{\rm QES}, x^-_{\rm QES}\right)$ as defined in (3.101)

$$\frac{4G_{\rm N}}{\bar{\phi}_r}\frac{dS_{\rm gen,late}}{du} = 2k\left(-\pi T_{\rm b}\frac{\cosh\left(\pi T_{\rm b}(y^-_{\rm QES}-u)\right)}{\sinh\left(\pi T_{\rm b}(y^-_{\rm QES}-u)\right)} - \frac{1}{2}\partial_u\left(\log f'(u)\right) + \frac{f'(u)}{t-x^+_{\rm QES}}\right)\,, \tag{3.140}$$

where we have used the facts

$$\frac{\partial S_{\rm gen,late}}{\partial x^+_{\rm QES}} = 0\,, \qquad \frac{\partial S_{\rm gen,late}}{\partial x^-_{\rm QES}} = 0\,, \tag{3.141}$$

from the definition of QES. The time derivative in eq. (3.140) can be further simplified by taking the limits

$$\begin{aligned}
\pi T_{\rm b}\coth\left(\pi T_{\rm b}(u-y^-_{\rm QES})\right) &\approx \pi T_{\rm b}\,,\\
-\frac{1}{2}\partial_u\left(\log f'(u)\right) &\approx \pi T_{\rm eff}(u) + k\frac{{T_{\rm eff}}^2 - T_{\rm b}^2}{4{T_{\rm eff}}^2}\,,\\
\frac{f'(u)}{t-x^+_{\rm QES}} &\approx -\frac{f'(u)}{t_\infty - t}\frac{4-\Gamma_{\rm eff}}{4} \approx \pi T_{\rm eff}(u)\frac{\Gamma_{\rm eff}-4}{2}\,,
\end{aligned} \tag{3.142}$$

to obtain

$$\frac{dS_{\rm gen,late}}{du} \approx -\frac{\bar{\phi}_r}{4G_{\rm N}}\left(1-\frac{T_{\rm b}^2}{{T_{\rm eff}}^2(u)}\right)k\pi T_{\rm eff}(u)\,. \tag{3.143}$$

Taking a linear approximation of eq. (3.143) agrees with the results found in the previous section – see eq. (3.124). Furthermore, since $T_{\rm eff}$ approaches $T_{\rm b}$ for late times ($e^{ku} \gg 1$) the time derivative obviously decays to zero in this limit, implying the generalized entropy in the late-time region is indeed approaching a constant. We can then rewrite our generalized entropy at time u in late time phase in integral form

$$S_{\rm gen,late}(u) \approx S_{\rm gen}(u_{\rm Page}) - \frac{\bar{\phi}_r}{4G_{\rm N}}\int_{u_{\rm Page}}^{u}\left(1-\frac{T_{\rm b}^2}{{T_{\rm eff}}^2(\tilde{u})}\right)k\pi T_{\rm eff}(\tilde{u})d\tilde{u}\,, \tag{3.144}$$

where the start point is the generalized entropy at Page time $S_{\rm gen}(u_{\rm Page})$ that has been derived at (3.127) in the linear region. Fortunately, the above integral is fully analytic and

can be performed to yield

$$\begin{aligned} S_{\text{gen,late}}(u) &\approx S_{\text{gen}}(u_{\text{Page}}) + \frac{\bar{\phi}_r}{4G_{\text{N}}}(2\pi\, T_{\text{eff}}(u) - 2\pi\, T_{\text{eff}}(u_{\text{Page}}))\,, \\ 2\pi T_{\text{eff}}\,(u_{\text{Page}}) &\approx 2\pi T_1 - k\pi T_1 \left(1 - \frac{T_{\text{b}}^2}{T_1^2}\right) u_{\text{Page}}\,. \end{aligned} \tag{3.145}$$

The dominant term is nothing but the black hole entropy with temperature T_{eff}, *i.e.,*

$$S_{\text{gen,late}}(u) \sim \frac{\phi(u)}{4G_{\text{N}}} \sim \frac{2\pi T_{\text{eff}}(u)\bar{\phi}_r}{4G_{\text{N}}}\,, \tag{3.146}$$

and the extra contributions from the leading order of the bulk entropy are all encoded in the value at Page time. Finally, combining with the generalized entropy at scrambling phase

$$S_{\text{gen,scrambling}}(u \gg 1) \approx \frac{\bar{\phi}_r}{4G_{\text{N}}}\left(2\pi T_0 + 2k\log\left(\frac{24\pi E_s}{\epsilon c}\frac{\sinh \pi(T_{\text{b}}u)}{\pi T_{\text{b}}}\frac{1}{\sqrt{f'(u)}}\right) + \kappa\right)\,, \tag{3.147}$$

we found the expected Page curve by taking eq. (3.145) as the generalized entropy for the late-time phase. After quench-phase, the generalized entropy is decided by that in the scrambling phase and then jumps to the late-time phase after Page time. Finally, we remark that the generalized entropy at scrambling phase $S_{\text{gen,scrambling}}$ represents the fine-graining entropy because its increase is dominated by the increase of entanglement entropy from the thermal radiation emitted from the thermal bath and black hole itself. The generalized entropy at the late-time phase obviously denotes the coarse-graining entropy, *i.e.,* the area of the dynamical black hole, as shown in (3.146). As a summary, we show a diagram to present the information about the Page curve derived in the last several subsections in figure 3.10.

In this subsection, we focused on the QES and generalized entropy of the subsystem consisting of QM_{L}, the complete thermal bath, and its purification. Similar to the analysis in section 3.2.1 for $T_1 = T_{\text{b}}$ (see section 2.2.1 for the case with zero bath temperature), we can consider a smaller subsystem by cutting a bath interval $[0, \sigma_1]$, corresponding to shifting the anchor point $x_1^{\pm}$ away from AdS_2 boundary into the bath with choosing $y_1^{\pm} = u \mp \sigma_1$. However, it is not easy to perturbatively solve the QES in general because our order assumption (3.106) may break. Instead, we can begin with assuming another order condition

$$0 < x_{\text{QES}}^{+} - t_\infty < t_\infty - x_1^{+} \ll t_\infty - x_{\text{QES}}^{-} \ll t_\infty\,. \tag{3.148}$$

Naively, the above condition requires that we do not put the anchor point near the shock wave in order to guarantee $x_1^+ = f(u-\sigma_1) \approx t_\infty$. In other words, we can generalize the approximations in this subsection to the case with x_1 near AdS_2 boundary. In most places, we only need to change u, t to $u-\sigma_1, x_1^+$. Finally, one can obtain the corresponding QES as

$$\begin{aligned} x^+_{\rm QES} &\approx t_\infty + \frac{\Gamma_{\rm eff}}{4-\Gamma_{\rm eff}}\left(t_\infty - x_1^+\right) , \\ x^-_{\rm QES} &\approx t_\infty - \frac{8\pi T_{\rm eff}}{k(4-\Gamma_{\rm eff})}\left(t_\infty - x_1^+\right) , \end{aligned} \tag{3.149}$$

from which we can find the $y^-_{\rm QES}$ is shifted in the way of

$$y^-_{\rm QES} \approx u - \sigma_1 - u_{\rm HP} . \tag{3.150}$$

Further, it is consistent with our numerical results and also the zero bath temperature case which is studied in section 2.2.1.

Simpler derivation of QES

In the above, we followed the analysis in chapter 2 to derive the position of QES as shown in eq. (3.114). However, there is one undetermined middle value $v_{\rm QES}$ appearing in many expressions due to integral over the dilaton profile (3.14). Comparing the results in eqs. (3.146) and (3.121), one finds the identify

$$2\pi T_{\rm eff}(u) \sim 2\pi T_{\rm eff}(y^-_{\rm QES}) \sim 2\pi T_1 + \frac{k}{2}\left(1-\frac{T_{\rm b}^2}{T_{\rm eff}^2(v_{\rm QES})}\right)\log\left(\frac{t_\infty - x^-_{\rm QES}}{t_\infty}\right) , \tag{3.151}$$

where corrections of order k are ignored. With the above approximation, we can simplify our results, *e.g.,* by using $T_{\rm eff}(y^-_{\rm QES})$ rather than $v_{\rm QES}$. To confirm our result, we can derive the position of QES in a more direct way. It is based on the observation in [70, 149] that the dilaton profile can be expressed without any integrals as

$$\phi(x^\pm) = \phi_r\left(\frac{2f'(y^-)}{x^+-x^-} + \frac{f''(y^-)}{f'(y^-)}\right) , \tag{3.152}$$

when the components of the stress tensor, $\langle T_{x^+x^+}\rangle$ and $\langle T_{x^+x^-}\rangle$ vanish. Correspondingly, we can rewrite the solution (3.103) from extremizing the generalized entropy as

$$\begin{aligned}
0 &= \frac{1}{\phi_r}\frac{\partial\phi(x^\pm_{\rm QES})}{\partial x^+_{\rm QES}} + 2k\left(\frac{1}{x^+_{\rm QES}-x^+_1}-\frac{1}{x^+_{\rm QES}-x^-_{\rm QES}}\right),\\
0 &= \frac{1}{\phi_r}\frac{\partial\phi(x^\pm_{\rm QES})}{\partial x^-_{\rm QES}} + 2k\left(\frac{\pi T_{\rm b}}{\tanh\left(\pi T_{\rm b}(y^-_{\rm QES}-y^-_1)\right)}\frac{1}{f'\left(y^-_{\rm QES}\right)}+\frac{1}{x^+_{\rm QES}-x^-_{\rm QES}}+\frac{1}{2}\frac{f''(y^-_{\rm QES})}{\left(f'(y^-_{\rm QES})\right)^2}\right).
\end{aligned} \tag{3.153}$$

Noting the small k expansion leads to the approximation $f'(y)\approx 2\pi T_{\rm eff}(y)\,(t_\infty - f(y))$ and our ordering condition (3.106), it is straightforward to find the derivatives of the dilaton are approximated by

$$\begin{aligned}
\frac{1}{\phi_r}\frac{\partial\phi(x^\pm)}{\partial x^+_{\rm QES}} &\approx \frac{4\pi T_{\rm eff}(y^-_{\rm QES})}{t_\infty - x^-_{\rm QES}},\\
\frac{1}{\phi_r}\frac{\partial\phi(x^\pm)}{\partial x^-_{\rm QES}} &\approx -4\pi T_{\rm eff}(y^-_{\rm QES})\frac{x^+_{\rm QES}-t_\infty}{(t_\infty-x^-_{\rm QES})^2}+\frac{T'_{\rm eff}(y^-_{\rm QES})}{(t_\infty-x^-_{\rm QES})T_{\rm eff}(y^-_{\rm QES})},
\end{aligned} \tag{3.154}$$

where we note the fact that $T'_{\rm eff}(y)=\partial_y T_{\rm eff}(y) = -k\frac{T^2_{\rm eff}-T^2_{\rm b}}{2T_{\rm eff}}$. Combining the above expressions with the approximations for the bulk entropy at $x^\pm_1 = t$, one can find the QES is determined by

$$\begin{aligned}
4\pi T_{\rm eff}(y^-_{\rm QES})(x^+_{\rm QES}-t) &\approx 2k(t_\infty - x^-_{\rm QES}),\\
4\pi T_{\rm eff}(y^-_{\rm QES})(x^+_{\rm QES}-t_\infty) &\approx \frac{k}{2}\Gamma_{\rm eff}(y^-_{\rm QES})(t_\infty - x^-_{\rm QES}).
\end{aligned} \tag{3.155}$$

which is exactly equivalent to our result in eq. (3.112) after substituting eq. (3.151). Finally, we can find the position of QES as

$$\begin{aligned}
x^+_{\rm QES} &\approx t_\infty + \frac{\Gamma_{\rm eff}}{4-\Gamma_{\rm eff}}(t_\infty - t),\\
x^-_{\rm QES} &\approx t_\infty - \frac{8\pi T_{\rm eff}}{k(4-\Gamma_{\rm eff})}(t_\infty - t),
\end{aligned} \tag{3.156}$$

which is the same as eq. (3.114). One can also easily find an approximation for dilaton profile

$$\phi(x^\pm_{\rm QES}) \approx \phi_r\left(\frac{2f'(y^-_{\rm QES})}{t_\infty - x^-} - 2\pi T_{\rm eff}(y^-_{\rm QES})\right) \approx 2\pi T_{\rm eff}(y^-_{\rm QES})\phi_r, \tag{3.157}$$

where we ignored the derivative term $T'_{\rm eff}(y^-_{\rm QES})$ as being order k.

3.3.2 Information flow

In the previous section, we studied the generalized entropy of $\mathrm{QM_L}$ plus the whole bath and its purification. (Of course, since the entire system is in a pure state, we could also think of this more simply as the entropy of $\mathrm{QM_R}$.) In this section, we chop parts of the (purified) bath and discuss which intervals, together with $\mathrm{QM_L}$, are essential to having the ability to recover the information in the interior of the black hole. In contrast to the semi-infinite interval case studied in the previous section where the bulk entropy is described by the two-point function on the UHP, the generalized entropy instead has one more endpoint, *i.e.*, $x_2^{\pm}$ (or $y_2^{\pm} = u \mp \sigma_2$) as the right end-point of the finite bath interval which can be used with $\mathrm{QM_L}$ to recover the black hole interior. According to the position of $x_2^{\pm}$ after or before the shock, we can divide the generalized entropy into two cases.

We begin by examining the case where the end-point $x_2^{\pm}$ is located after the shock, *i.e.*, $x_2^+ > 0$ or $y_2^+ = u - \sigma_2 > 0$. Similarly to the equilibrium case studied in section 3.2, we have two competing channels. The N-channel (where the black hole interior is non-recoverable) has the QES at the bifurcation point $x^{\pm}_{\mathrm{QES}''} = \pm\frac{1}{\pi T_0}$, and the generalized entropy for this channel shown in figure 3.3c is given by

$$\begin{aligned}\frac{4G_{\mathrm{N}}}{\bar{\phi}_r}S_{\mathrm{N}}(y_2^+ \geq 0) &\equiv \frac{4G_{\mathrm{N}}}{\bar{\phi}_r}\left(S^{\mathrm{gen}}_{\mathrm{QES}''} + S_{1-2}\right) \\ &= 2\pi T_0 + 2k\log 2 + 2k\log\left(\frac{1}{\epsilon^2}\frac{\sinh\left(\pi T_{\mathrm{b}}(y_2^- - y_1^-)\right)}{\pi T_{\mathrm{b}}}\frac{x_1^+ - x_2^+}{\sqrt{f'(y_1^+)f'(y_2^+)}}\right),\end{aligned} \tag{3.158}$$

where $\phi_{\mathrm{QES}''} = 2\pi T_0\bar{\phi}_r$. When this channel is preferred, the entanglement wedge of the bath interval plus $\mathrm{QM_L}$ does not contain the interior of the black hole. The R-channel (where the interior is recoverable) instead has the QES at the same location as the late-time phase QES. Correspondingly, the generalized entropy for this R-channel corresponding to figure 3.3c reads

$$\begin{aligned}\frac{4G_{\mathrm{N}}}{\bar{\phi}_r}S_{\mathrm{R}}(y_2^+ \geq 0) &\equiv \frac{4G_{\mathrm{N}}}{\bar{\phi}_r}\left(S^{\mathrm{gen}}_{\mathrm{QES}-1} + S_2\right) \\ &= \frac{\phi_{\mathrm{QES}}}{\bar{\phi}_r} + 2k\log\left(\frac{2}{\epsilon}\frac{\sinh\left(\pi T_{\mathrm{b}}(y^-_{\mathrm{QES}} - y_1^-)\right)}{\pi T_{\mathrm{b}}}\frac{x_1^+ - x^+_{\mathrm{QES}}}{x^+_{\mathrm{QES}} - x^-_{\mathrm{QES}}}\sqrt{\frac{f'(y^-_{\mathrm{QES}})}{f'(y_1^+)}}\right) \\ &\quad + 2k\log\left(\frac{12\pi E_s}{c\epsilon}\frac{\sinh\left(\pi T_{\mathrm{b}} y_2^-\right)}{\pi T_{\mathrm{b}}}\frac{x_2^+}{\sqrt{f'(y_2^+)}}\right).\end{aligned} \tag{3.159}$$

Evidently, when the R-channel is preferred, the entanglement wedge of the corresponding bath region plus the $\mathrm{QM_L}$ system includes the interior of the black hole. To find the transition where the bath interval (plus $\mathrm{QM_L}$) is able to reconstruct the black hole interior, we require *i.e.,*

$$\frac{4G_{\mathrm{N}}}{\bar{\phi}_r}\left(S_{\mathrm{N}}-S_{\mathrm{R}}\right)\geq 0\,, \tag{3.160}$$

or equivalently

$$2k\log\left(\frac{c}{6\pi E_s\epsilon}\frac{(x_1^+-x_2^+)\sinh\left(\pi T_{\mathrm{b}}(y_2^--y_1^-)\right)}{x_2^+\sqrt{f'(y_1^+)}\sinh(\pi T_{\mathrm{b}}y_2^-)}\right)\geq\frac{4G_{\mathrm{N}}}{\bar{\phi}_r}S_{\mathrm{gen,late}}(\sigma_1)-2\pi T_0\,, \tag{3.161}$$

where we rewrite the left side as the simple part because $S_{\mathrm{gen,late}}$ with $\sigma_1=0$ has been discussed in the last section. We will focus on analyzing the left-hand side of eq. (3.161) in the following calculations.

When the right end-point $y_2^+\leq 0$ is before the shock, we have two similar competing channels for the generalized entropy

$$\begin{aligned}\frac{4G_{\mathrm{N}}}{\bar{\phi}_r}S_{\mathrm{N}}(y_2^+\leq 0)&\equiv\frac{4G_{\mathrm{N}}}{\bar{\phi}_r}\left(S^{\mathrm{gen}}_{\mathrm{QES}''}+S_{1-2}\right)\\&=2\pi T_0+2k\log 2+2k\log\left(\frac{12\pi E_s}{c\epsilon^2}\frac{x_1^+\sinh\left(\pi T_{\mathrm{b}}(-y_2^+)\right)\sinh\left(\pi T_{\mathrm{b}}(y_2^--y_1^-)\right)}{(\pi T_{\mathrm{b}})^2\sqrt{f'(y_1^+)}}\right),\end{aligned} \tag{3.162}$$

and also

$$\frac{4G_{\mathrm{N}}}{\bar{\phi}_r}S_{\mathrm{R}}(y_2^+\leq 0)\equiv\frac{4G_{\mathrm{N}}}{\bar{\phi}_r}\left(S^{\mathrm{gen}}_{\mathrm{QES}-1}+S_2\right)\,. \tag{3.163}$$

with

$$\frac{4G_{\mathrm{N}}}{\bar{\phi}_r}S_2=2k\log\left(\frac{1}{\epsilon}\frac{\sinh\left(\pi T_{\mathrm{b}}(y_2^--y_2^+)\right)}{\pi T_{\mathrm{b}}}\right)\,. \tag{3.164}$$

The condition for the bath interval to have the ability to reconstruct the interior of black hole when the right end-point is located before the shock is then given by

$$2k\log\left(\frac{24\pi E_s}{c\epsilon}\frac{x_1^+\sinh\left(\pi T_{\mathrm{b}}(-y_2^+)\right)\sinh\left(\pi T_{\mathrm{b}}(y_2^--y_1^-)\right)}{\sqrt{f'(y_1^+)}\pi T_{\mathrm{b}}\sinh\left(\pi T_{\mathrm{b}}(y_2^--y_2^+)\right)}\right)\geq\frac{4G_{\mathrm{N}}}{\bar{\phi}_r}S_{\mathrm{gen,late}}(\sigma_1)-2\pi T_0\,. \tag{3.165}$$

Lastly, we remark that the N-channel and R-channel show the same divergence $2k\log\left(\frac{1}{\epsilon^2}\right)$, so the AdS cutoff ϵ is exactly canceled in the comparison and does not play an important role in the following calculations.

Regularization of the shock wave

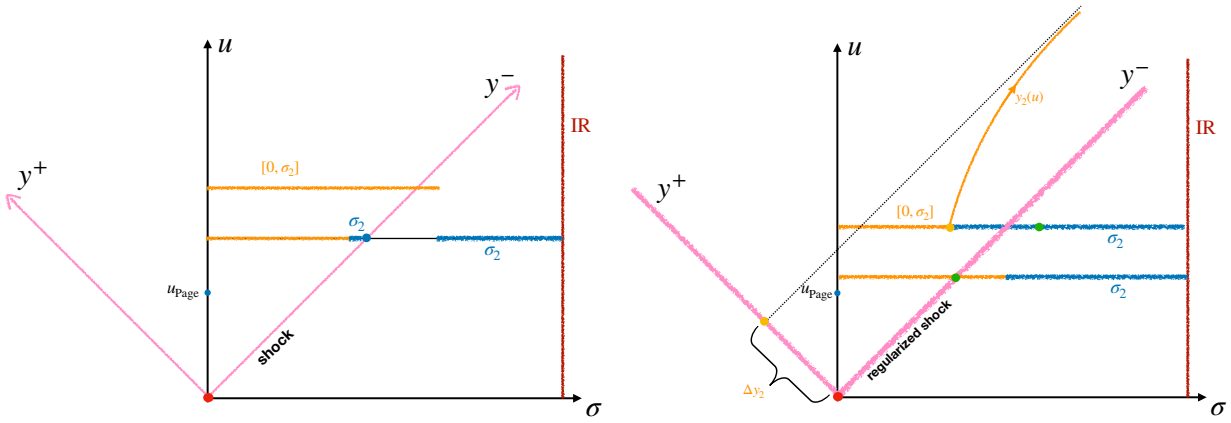

Figure 3.11: The yellow lines show the finite bath interval with $T_{\rm b} \leq T_p$ at a fixed time slice u that has the ability to reconstruct the black hole interior by including $\mathrm{QM}_{\rm L}$ but not the bath purifier. The blue shadow region presents the expected region where we can put the endpoint of the finite bath interval, *i.e.*, y_2, and make the subsystem recover the information of black hole. Left: The simple shock wave as a line. Right: The regularized shock wave as a small region indicated by the pink shadow. The yellow curve presents the endpoint y_2^+ of the minimal bath interval, which approaches a constant Δy_2 derived in eq. (3.190) with the evolution of time.

Before we discuss the condition for the finite bath-interval plus $\mathrm{QM}_{\rm L}$ (as shown in the figure 3.3c) to reconstruct the black hole interior, we can roughly estimate the region for y_2 that makes the above equalities hold by looking at the divergence structure of $S_{\rm N} - S_{\rm R}$ with endpoint y_2 at special points. We will encounter an apparent paradox that will require a careful regularization for the region of the shock wave with the help of parameter E_s/c.

Explicitly, we can take the endpoint y_2 to the IR cut-off, *i.e.*, the limit $\sigma_2 \to \infty$. It not hard to show that the two competing channels exhibit similar divergences

$$\begin{aligned} \frac{4G_{\rm N}}{\bar{\phi}_r} S_{\rm N}(y_2^+ \leq 0) \quad &\longrightarrow \quad 4k\pi T_{\rm b}\sigma_2 + 4k \log\left(\frac{1}{\epsilon \pi T_{\rm b}}\right) , \\ \frac{4G_{\rm N}}{\bar{\phi}_r} S_{\rm R}(y_2^+ \leq 0) \quad &\longrightarrow \quad 4k\pi T_{\rm b}\sigma_2 + 4k \log\left(\frac{1}{\epsilon \pi T_{\rm b}}\right) , \end{aligned} \tag{3.166}$$

for a thermal bath with nonzero $T_{\rm b}$. However, with the bath at zero temperature, the

divergences take a different form in these two channels

$$\begin{aligned}\frac{4G_{\rm N}}{\bar{\phi}_r}S_{\rm N}(y_2^+\leq 0) \quad &\longrightarrow \quad 4k\log\left(\frac{\sigma_2}{\epsilon}\right)\,,\\ \frac{4G_{\rm N}}{\bar{\phi}_r}S_{\rm R}(y_2^+\leq 0) \quad &\longrightarrow \quad 2k\log\left(\frac{2\sigma_2}{\epsilon}\right)+2k\log\left(\frac{\ell}{\epsilon}\right)\,,\end{aligned} \tag{3.167}$$

where ℓ is some finite length-scale. This difference in the divergence structure makes the R-channel preferred when y_2 is around the IR cut-off in the bath and guarantees the purification of the thermal bath is not necessary for the interior reconstruction.

Now let us consider the limit of taking y_2 near the shock wave at $\sigma_{\rm shock}=u$, *i.e.*, $y^+=0$. We have to consider approaching the shock from the region before the shock or after the shock. Under the limit $y_2^+\to 0^-$, one can find

$$\begin{aligned}\frac{4G_{\rm N}}{\bar{\phi}_r}S_{\rm N}(y_2^+\leq 0) \quad &\longrightarrow \quad 2k\log\left(\frac{-y_2^+}{\pi T_{\rm b}\epsilon^2}\right)\,,\\ \frac{4G_{\rm N}}{\bar{\phi}_r}S_{\rm R}(y_2^+\leq 0) \quad &\longrightarrow \quad 2k\log\left(\frac{\sinh\left(2\pi T_{\rm b}\sigma_2\right)}{(\pi T_{\rm b}\epsilon)^2}\right)\,,\end{aligned} \tag{3.168}$$

which implies the N-channel is preferred ($\log(-y_2^+)\to-\infty$)[25] when $y_2^+<0$ is located in the region around the shock. On the other hand, the limit $y_2^+\to 0^+$ (or $x_2^+\to 0^+$) leads us to

$$\begin{aligned}\frac{4G_{\rm N}}{\bar{\phi}_r}S_{\rm N}(y_2^+\geq 0) \quad &\longrightarrow \quad 2k\log\left(\frac{\bar{\ell}^2}{\epsilon^2}\right)\,,\\ \frac{4G_{\rm N}}{\bar{\phi}_r}S_{\rm R}(y_2^+\geq 0) \quad &\longrightarrow \quad 2k\log\left(\frac{x_2^+}{\epsilon}\right)+2k\log\left(\frac{1}{\pi T_{\rm b}\epsilon}\right)\,,\end{aligned} \tag{3.169}$$

where $\bar{\ell}$ is some finite length-scale. For the zero bath temperature case, the divergence structure is the same.[26] By considering these divergences, it is obvious that the R-channel is preferred when y_2^+ is located in the region near the shock but after the shock wave. This region for y_2 which allows the bath interval plus $\mathrm{QM_L}$ to recover the interior of the black hole is shown in the left diagram in figure 3.11. But there is an obvious paradox because we can contain a larger part of the bath by moving the right end-point of the interval from the after-shock region to the pre-shock region. The above analysis implies that adding more bath interval surprisingly makes one lose the ability to recover the black hole interior.

[25] Taken at face value, the generalized entropy in the N-channel becomes negative for sufficiently small $|y_2^+|$. This is another hint that the shockwave needs to be regularized.

[26] The $\frac{1}{\pi T_{\rm b}}$ in the last logarithm is replaced by some finite length scale $\tilde{\ell}$ when $T_{\rm b}=0$.

However, the above paradox appears just because we consider the shock-wave as a line located at $\sigma_{\text{shock}} = u$. More precisely, the generalized entropy for the R and N-channel around the shock wave is disconnected. In order to solve this problem, we have to regularize the region of the shock wave and simultaneously make the generalized entropy a continuous function. In other words, we need to consider the entropy from one-point and two-point functions

	before-shock $y_2^+ < 0$	after shock $y_2^+ > 0$
S_2	$\log\left(\frac{1}{\epsilon}\frac{\sinh\left(\pi T_{\text{b}}(y_2^- - y_2^+)\right)}{\pi T_{\text{b}}}\right)$	$\log\left(\frac{12\pi E_s}{c\epsilon}\frac{\sinh\left(\pi T_{\text{b}} y_2^-\right)}{\pi T_{\text{b}}}\frac{x_2^+}{\sqrt{f'(y_2^+)}}\right)$
S_{12}	$\log\left(\frac{12\pi E_s}{c\epsilon^2}\frac{x_1^+\sinh\left(\pi T_{\text{b}}(-y_2^+)\right)\sinh\left(\pi T_{\text{b}}(y_2^- - y_1^-)\right)}{(\pi T_{\text{b}})^2\sqrt{f'(y_1^+)}}\right)$	$\log\left(\frac{1}{\epsilon^2}\frac{\sinh\left(\pi T_{\text{b}}(y_2^- - y_1^-)\right)}{\pi T_{\text{b}}}\frac{x_1^+ - x_2^+}{\sqrt{f'(y_1^+)f'(y_2^+)}}\right)$

The identifications

$$\begin{aligned} S_{2,\text{before}}(y_2^+ \to -0) &= S_{2,\text{after}}(y_2^+ \to +0)\,, \\ S_{12,\text{before}}(y_2^+ \to -0) &= S_{12,\text{after}}(y_2^+ \to +0)\,, \end{aligned} \tag{3.170}$$

fixes the two boundaries of shock-wave region as

$$\begin{aligned} 1 &= \frac{12\pi E_s}{c}\frac{x_2^+}{f'(y_2^+)}\,, \qquad y_2^+ \to +0 \\ \frac{12\pi E_s}{c}\frac{\sinh(-\pi T_{\text{b}} y_2^+)}{\pi T_{\text{b}}} &= 1\,, \qquad y_2^+ \to -0\,. \end{aligned} \tag{3.171}$$

Recalling the property of $f(u)$ such as $f'(0) = 1, x = f(y) \sim 0 \sim y$, we can take the energy of shock wave E_s as a regulator and regularize the shock wave as a small region defined by

$$y_{\text{shock}}^+ \equiv \left[-\frac{c}{12\pi E_s}, \frac{c}{12\pi E_s}\right] = \left[-\frac{k}{(T_1^2 - T_0^2)\pi^2}, \frac{k}{(T_1^2 - T_0^2)\pi^2}\right]\,, \tag{3.172}$$

which is independent of the temperature of bath as expected.

After identifying this small region as the shock-wave, we can take out this part from the bath interval and then make the generalized entropy connected when we move the endpoint y_2 from the after-shock region to the pre-shock region. The connectivity guarantees that we do not have the paradox about the ability of bath interval to recover the information of the black hole interior anymore. More explicitly, we will discuss this problem in detail in the next subsections.

Need for the Purification

The conditions for a finite bath interval plus $\mathrm{QM_L}$ in a zero temperature bath to reconstruct the interior of the black hole were discussed in chapter 2. Moreover, we found in section 3.2 that the equilibrium case with $T_\mathrm{b} = T_1$, even the whole semi-infinite bath interval with $\mathrm{QM_L}$ does not contain the appropriate information to reconstruct the interior of the black hole. Rather we had to also include its purification (or at least a portion of the latter). In the previous section, we have seen the difference in divergence structure between a non-zero temperature bath and that with zero temperature when y_2 approaches the IR cut-off between the bath and its purification. The smaller divergence of the leading term (3.166) in a zero-temperature bath guarantees we can use the whole bath interval $y_2 \to \infty$ with $\mathrm{QM_L}$ to reconstruct the interior of the black hole. Obviously, this is expected because this subsystem as one part of the bipartite pure system will be able to reconstruct its complementary part, *i.e.,* the black hole interior, after the Page transition. A natural question is whether all bath intervals with non-zero temperature T_b require a part of the purification in order to reconstruct the black hole interior. In this subsection, we show that only the bath interval with a temperature higher than the critical temperature T_p in eq. (3.179) requires its purification.

To this end, we consider large bath intervals by putting the left end-point after the shock and the right end-point before the shock and focus on the inequality in eq. (3.165). The left-hand side of the inequality monotonically increases with $y_1^+ = u - \sigma_1$ ($u \geq u_\mathrm{Page}$) and the right-hand side decreases, so the weakest condition for that inequality is choosing $\sigma_1 = 0$, *i.e.,* anchoring the initial point of bath interval at AdS boundary, which satisfies our physical expectation. Let's move on to the condition for y_2^+ by considering figure 3.3c and the corresponding conditions in eq. (3.165), *i.e.,*

$$2k \log \left(\frac{24\pi E_s}{c\epsilon} \frac{x_1^+ \sinh\left(\pi T_\mathrm{b}(-y_2^+)\right) \sinh\left(\pi T_\mathrm{b}\sigma_2\right)}{\sqrt{f'(y_1^+)}\pi T_\mathrm{b} \sinh\left(2\pi T_\mathrm{b}\sigma_2\right)} \right) \geq \frac{4G_\mathrm{N}}{\bar{\phi}_r} S_\mathrm{gen,late} - 2\pi T_0 \,, \tag{3.173}$$

with $\sigma_1 = 0$. Again, it is straightforward to show

$$\partial_{\sigma_2} \left(\frac{\sinh\left(\pi T_\mathrm{b}(-y_2^+)\right) \sinh\left(\pi T_\mathrm{b}\sigma_2\right)}{\pi T_\mathrm{b} \sinh\left(2\pi T_\mathrm{b}\sigma_2\right)} \right) = \frac{1}{2} \frac{\cosh(\pi T_\mathrm{b} u)}{\cosh^2(\pi T_\mathrm{b}\sigma_2)} > 0 \,, \tag{3.174}$$

which implies the maximum of the left-hand side in above inequality is the value at the limit $\sigma_2 \to \infty$. As expected, the weakest condition for the bath interval plus $\mathrm{QM_L}$ to have enough information about the black hole interior is if we consider the entirety of the bath

with $\sigma_1 = 0$ and $\sigma_2 \to \infty$. The condition to recover the interior of the black hole is then given by

$$\text{Max} = 2k \log\left(\frac{12E_s}{c\epsilon T_\text{b}} \frac{f(u)e^{-\pi T_\text{b} u}}{\sqrt{f'(u)}}\right) \geq \frac{4G_\text{N}}{\bar{\phi}_r} S_{\text{gen,late}} - 2\pi T_0 \,. \tag{3.175}$$

It is useful to notice that the right-hand side decreases with time u and the left-hand side increases for $T_\text{b} < T_1$ and decreases for $T_\text{b} > T_1$.[27] As a result, the inequality cannot hold for $T_\text{b} > T_1$ because the maximum of the left-hand side is bounded by $2k \log\left(\frac{12E_s t_\infty}{c\epsilon T_\text{b}}\right)$. This implies that in the setup where the bath heats up the black hole ($T_\text{b} > T_1$), the bath and QM_L systems are never able to reconstruct the black hole interior. We now focus on the evaporating black hole model ($T_\text{b} < T_1$) and take the the late-time approximation (3.100) at $e^{ku} \gg 1$ for which the LHS gives a constant

$$2k \log\left(\frac{12E_s t_\infty}{c\epsilon T_\text{b}}\right) - k \log\left(4\pi T_\text{b} t_\infty\right) + 4\pi \left(T_1 - T_\text{b} - T_\text{b} \log\left(\frac{T_1 + T_\text{b}}{2T_\text{b}}\right)\right) . \tag{3.176}$$

Correspondingly, the RHS reaches its minimum at the same late-time limit

$$\frac{4G_\text{N}}{\bar{\phi}_r} S_{\text{gen,late}} - 2\pi T_0 \approx 2\pi \left(T_\text{b} - T_0\right) + 2k \log\left(\frac{1}{\pi T_b \epsilon}\right) . \tag{3.177}$$

The inequality from generalized entropy in eq. (3.175) then yields the condition for the temperature of bath

$$T_\text{b} \lesssim \frac{2T_1 + T_0}{3} - \frac{2T_\text{b}}{3} \log\left(\frac{T_1 + T_\text{b}}{2T_\text{b}}\right) + \frac{k}{3\pi} \log\left(\frac{6E_s}{cT_1}\sqrt{\frac{T_1}{T_\text{b}}}\right) . \tag{3.178}$$

Finally, we can find the critical temperature of bath is

$$T_p \approx T_1 - \frac{1}{2}\left(T_1 - T_0\right) + \frac{k}{2\pi} \log\left(\frac{6E_s}{cT_1}\right) , \tag{3.179}$$

which defines the lowest bath temperature for which the purification of the bath is needed to reconstruct the interior of the black hole. It is interesting to note that the critical temperature is also near T_1 due to the ansatz $T_0 \sim T_1$. However, it is different from the critical temperatures T_{c_1} and T_{c_2} in eq. (3.133) because the former depends on T_0, the temperature of original black hole, while T_{c_1} and T_{c_2} are independent of T_0.

[27] It is easy to show that from the approximation (3.99) and (3.100) because the dominated term for $k \log\left(\frac{1}{f'(u)}\right)$ involve from $2k\pi T_1 u$ to $2k\pi T_\text{b} u$.

To summarize, a bath with a temperature $T_{\rm b} < T_p$ admits finite bath intervals plus $\mathrm{QM}_{\rm L}$ to reconstruct the interior of the black hole. When the temperature of the bath increases beyond T_p, even the whole semi-infinite bath interval plus $\mathrm{QM}_{\rm L}$ does not have enough information for interior reconstruction if part of the purification is not included. Finally, we can also change the left end-point σ_1 rather than taking it to the AdS boundary ($\sigma_1 \to 0$) and do a similar late-time approximation to obtain the constraint on bath temperature. As expected, we find a stronger condition and get a smaller critical temperature

$$T_p(\sigma_1) \approx \frac{1}{2}\left(T_1 + T_0\right) - 2kT_1\sigma_1 + \frac{k}{2\pi}\log\left(\frac{6E_s}{cT_1}\right), \text{with} \quad k\sigma_1 \ll 1\,, \tag{3.180}$$

for the reconstruction of information in black hole. We should also note the chopping off too much of the bath interval by taking the initial point from $\sigma_1 = 0$ to a finite one also may make the thermal bath interval plus $\mathrm{QM}_{\rm L}$ lose essential information to reconstruct the black hole interior if σ_1 is too large. The size of the bath interval we can ignore is also restricted by

$$\sigma_1 \lesssim \frac{1}{4kT_{\rm b}}\left(2T_1 + T_0 - 3T_{\rm b} - T_{\rm b}\log\left(\frac{T_1 + T_{\rm b}}{2T_{\rm b}}\right)\right) + \frac{1}{4\pi T_{\rm b}}\log\left(\frac{6E_s}{cT_1}\sqrt{\frac{T_1}{T_{\rm b}}}\right), \tag{3.181}$$

where we have assumed the bath temperature is not too small.

Finite Bath Interval

In this subsection, we will assume the bath temperature is lower than the critical T_p and discuss how much bath interval needed in order to reconstruct the black hole interior and in particular, what is the closest we can bring the right end-point σ_2 to the AdS boundary and still reconstruct the black hole interior. The two competing channels are described in figure 3.3c. This analysis can be understood as an extension of the late-time protocol of section 2.2.2 to the thermal bath model. Let's first assume we only need the bath interval after the shock to which the radiation of black hole escapes. Taking the time slice at u after the Page time and putting the left end-point of the bath interval at the AdS boundary ($\sigma_1 = 0$), the bath interval we are looking for satisfies eq. (3.161)

$$2k\log\left(\frac{c}{6\pi E_s\epsilon}\frac{(t - x_2^+)\sinh\left(\pi T_{\rm b}\sigma_2\right)}{x_2^+\sqrt{f'(u)}\sinh(\pi T_{\rm b}(u+\sigma_2))}\right) \geq \frac{4G_{\rm N}}{\bar{\phi}_r}S_{\rm gen,late} - 2\pi T_0\,, \tag{3.182}$$

which imposes a constraint on the size of the bath interval, *i.e.,* the value of $\sigma_2(u)$. Assuming we can have $\pi T_1 y_2^+ \gg 1$ (or $f(y_2^+) \approx t_\infty$) and still stay at the linear-region with

$ku < 1$, we can recall the approximation again

$$\begin{aligned}
2k\log\left(\frac{\sinh\left(\pi T_{\rm b}\sigma_2\right)}{\sinh(\pi T_{\rm b}(u+\sigma_2))}\right) &\approx -2k\pi T_{\rm b}u \\
2k\log\left(\frac{t-x_2^+}{x_2^+}\right) &\approx \log\left(\frac{t_\infty - f(y_2^+)}{t_\infty}\right) \sim -4k\pi T_1(u-\sigma_2)\,, \\
2k\log\left(\frac{1}{\sqrt{f'(u)}}\right) &\approx 2k\pi T_1 u - k\log\left(4\pi T_1 t_\infty\right)\,, \\
\frac{4G_{\rm N}}{\bar{\phi}_r}S_{\rm gen,late} &\approx 2\pi T_1 - k\pi T_1(u-u_{\rm HP})\left(1-\frac{T_{\rm b}^2}{T_1^2}\right) + \mathcal{O}(k\log(\cdots))\,.
\end{aligned} \tag{3.183}$$

Then the above inequality leads us to

$$\sigma_2(u) \gtrsim \frac{T_1-T_0}{2kT_1} + \frac{u}{4}\left(1+\frac{T_{\rm b}}{T_1}\right)^2 + \frac{u_{\rm HP}}{4}\left(1-\frac{T_{\rm b}^2}{T_1^2}\right)\,, \tag{3.184}$$

or equivalently

$$y_2^+(u) \equiv u-\sigma_2 \lesssim \frac{u}{4}\left(3-2\frac{T_{\rm b}}{T_1}-\frac{T_{\rm b}^2}{T_1^2}\right) - \frac{T_1-T_0}{2kT_1} - \frac{u_{\rm HP}}{4}\left(1-\frac{T_{\rm b}^2}{T_1^2}\right)\,, \tag{3.185}$$

which constrains the size of the bath interval able to reconstruct the black hole interior. By setting $T_{\rm b}=0$, we recover the results reported in chapter 2 (see eq. (2.108) and eq. (2.109)). It is also clear that the thermal bath with $T_{\rm b} \gtrsim T_1$ obviously breaks the inequality, implying we cannot find a bath interval with only $\mathrm{QM}_{\rm L}$ able to recover the information in the black hole. This conclusion is consistent with that found in the previous subsection. However, we also want to stress the validity of the condition (3.185). One can find the critical value around the Page time is not physical, *i.e.*,

$$y_2^+\big|_{u_{\rm Page}} \approx \frac{T_1-T_0}{2kT_1}\left(\frac{3-2\frac{T_{\rm b}}{T_1}-\frac{T_{\rm b}^2}{T_1^2}}{3+2\frac{T_{\rm b}}{T_1}-\frac{T_{\rm b}^2}{T_1^2}}-1\right) \lesssim 0\,. \tag{3.186}$$

This invalidity implies the condition (3.185) is only valid for time slices after the Page time with $\exp\left(\pi T_1(u-u_{\rm Page})\right) \gg 1$. To be precise, the reason is we can only find a small $y_2^+ \ll \frac{1}{\pi T_1}$ instead of $y_2^+ \gg \frac{1}{\pi T_1}$ as a solution around Page time. However, the value is so small that it is actually located in the shock-wave region. As a result, it means we cannot find a bath interval able to reconstruct the black hole interior with only the region after

the shock wave at the Page time. One can look at eq. (2.106) as an example of this. The calculation is similar and we do not repeat it here because the value of small y_2^+ in that region is not really physical after the regularization of the shock-wave. After the Page time, the critical y_2^+ will exponentially increase and move quickly to the linear region as shown in eq. (3.185). The allowed region for the endpoint of y_2^+ is shown in the right plot in figure 3.11.

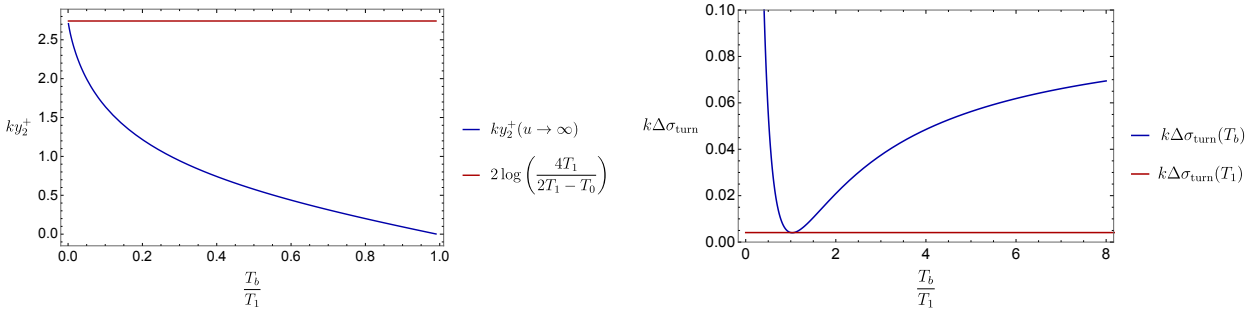

Figure 3.12: Left: the final position of the null surface y_2^+, *i.e.,* (3.190) as the endpoint of bath interval with the ability to reconstruct the information of the interior of black hole. Right: the bath temperature dependence of the minimal length $k\Delta\sigma_{\rm turn}$, *i.e.,* (3.199), that is necessary for the reconstruction of the interior of black hole.

Taking the lesson from the zero-temperature case, we can expect that the linear growth of y_2^+ is suppressed with the time evolution and finally $y_2^+(u)$ will approach a null surface. In order to show that explicitly, we should take the late-time ($e^{ku}\gg 1$) approximation in eq. (3.100) and use the following approximations

$$\begin{aligned} 2k\log\left(\frac{t-x_2^+}{x_2^+}\right)\approx\log\left(\frac{t_\infty-f(y_2^+)}{t_\infty}\right)\sim -4k\pi T_{\rm b}y_2^+ + 8\pi(T_{\rm b}-T_1)\left(1-e^{-ky_2^+/2}\right), \\ \frac{4G_{\rm N}}{\bar{\phi}_r}S_{\rm gen,late}\left(e^{ku}\gg 1\right)\approx\frac{4G_{\rm N}}{\bar{\phi}_r}S_{\rm gen,late}(T_{\rm b})\approx 2\pi T_{\rm b}+2k\log\left(\frac{1}{\pi T_{\rm b}\epsilon}\right), \end{aligned} \tag{3.187}$$

where we also keep the second-order contribution $e^{-ky_2^+/2}$ because the condition $e^{ky_2^+}\gg 1$ is not guaranteed. Combining all these approximations, the condition (3.182) becomes

$$kT_{\rm b}y_2^+ + 2\left(T_{\rm b}-T_1\right)e^{-ky_2^+/2}\lesssim -\left(T_1-\frac{T_0+T_{\rm b}}{2}+T_{\rm b}\log\left(\frac{T_1+T_{\rm b}}{2T_{\rm b}}\right)\right)-\frac{k}{2\pi}\log\left(\frac{6E_s}{cT_1}\sqrt{\frac{T_{\rm eff}}{T_1}}\right). \tag{3.188}$$

When $T_{\rm b}=0$, we get the final null surface for critical y_2^+ as

$$y_2^+\left(e^{ku}\gg 1\right)\big|_{T_{\rm b}=0}\approx\frac{2}{k}\log\left(\frac{4T_1}{2T_1-T_0}\right)\,, \tag{3.189}$$

which agrees with the result in chapter 2. For non-zero $T_{\rm b}$, the analytical solution is written as

$$y_2^+\left(e^{ku}\gg 1\right)\approx\frac{X+2T_{\rm b}\,W\left(\frac{e^{-\frac{X}{2T_{\rm b}}}(T_1-T_{\rm b})}{kT_{\rm b}}\right)}{kT_{\rm b}}=\Delta y_2\,, \tag{3.190}$$

where X represents the right side in (3.188) and $W(z)$ is the Lambert W-function or product logarithm defined by $z=W(z)e^{W(z)}$. As a summary, the time dependence of $y_2^+(u)$ is shown in the right plot in figure 3.11. It is clear that the constant Δy_2 indicates how much early radiation is not necessary in the reconstruction of black hole interior. Lastly, we show the numerical plot for position of the final null surface as a function of $T_{\rm b}/T_1$ in figure 3.12. As expected, it decays with the increase of $T_{\rm b}$ and stops at a point extremely near T_1 because the value at $T_{\rm b}=T_1$, *i.e.*, $-\frac{T_1-T_0}{T_1}$ is smaller than zero.

The Role of Purification

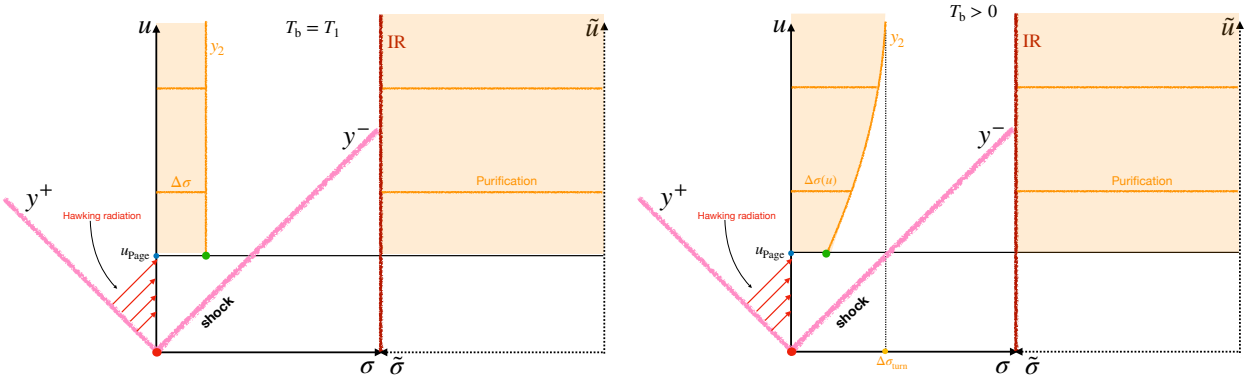

Figure 3.13: The yellow shadow denotes the minimal bath region including a full half-line as the purification of thermal bath for reconstructing the interior of the black hole. The yellow lines represent the necessary bath region at a fixed time slice after Page transition. Left: the equilibrium case with $T_{\rm b}=T_1$. Right: Non-equilibrium case where $k\,\delta\sigma(u)$ increases with the time evolution and approaches a constant $\Delta\sigma_{\rm turn}$ defined in eq. (3.199).

In the previous subsection, we focused on a finite bath interval with the bath temperature lower than the critical temperature T_p derived in eq. (3.179) because we wanted to

omit the purification of the bath itself. To reconstruct the black hole interior at higher bath temperatures, *i.e.,* to observe a Page transition, we need to include (a portion of) the purification. For simplicity, we take one endpoint of the finite bath interval on AdS boundary with $\sigma_1 = 0$ and ask how large the bath interval $[0, \sigma_2]$ needs to be to reconstruct the black hole interior. Concretely, we consider the purified bath interval with temperature $T_b > 0$ and discuss the condition for $\mathrm{QM_L}$, a finite bath interval $[0, \sigma_2]$ (where partial Hawking radiation resides) and the full purification to reconstruct the interior of the black hole.[28] Similar to the equilibrium case shown in eq. (3.65), the two competing channels showing to figure 3.3b are defined as

$$S_{\mathrm{R}} = S^{\mathrm{gen}}_{\mathrm{QES}-1} + S_{2-\mathrm{IR}}\,, \qquad S_{\mathrm{N}} = S^{\mathrm{gen}}_{\mathrm{QES}''} + S_{1-2} + S_{\frac{1}{2}\text{-line}}\,. \tag{3.191}$$

where the condition for reconstruction is decided by $S_{\mathrm{N}} - S_{\mathrm{R}} \geq 0$. Most pieces in the above two equations have been discussed in the last subsection (see eqs. (3.158) and (3.159)) in detail except for

$$\begin{aligned} S_{\frac{1}{2}\text{-line}} &= \frac{c}{6}\log\left(\frac{\sinh\left(2\pi T_{\mathrm{b}}\sigma_{\mathrm{IR}}\right)}{\pi T_{\mathrm{b}}\epsilon}\right) \approx \frac{c}{6}\left(2\pi T_{\mathrm{b}}\sigma_{\mathrm{IR}} + \log\left(\frac{1}{2\pi\epsilon T_{\mathrm{b}}}\right)\right)\,, \\ S_{2-\mathrm{IR}} &= \frac{c}{6}\log\left(\frac{12\pi E_s}{c\left(\epsilon\pi T_{\mathrm{b}}\right)^2}\frac{x_2^+\sinh\left(\pi T_{\mathrm{b}}y^+_{\mathrm{IR}}\right)\sinh\left(\pi T_{\mathrm{b}}(y_2^- - y^-_{\mathrm{IR}})\right)}{\sqrt{f'(y_2^+)}}\right)\,. \end{aligned} \tag{3.192}$$

In the limit $\sigma_{\mathrm{IR}} \to \infty$, we can rewrite that extra term as

$$S_{2-\mathrm{IR}} \approx \frac{c}{6}\left(2\pi T_{\mathrm{b}}\sigma_{\mathrm{IR}} + \log\left(\frac{1}{2\pi\epsilon T_{\mathrm{b}}}\right) - 2\pi T_{\mathrm{b}}y_2^- + \log\left(\frac{12\pi E_s}{c\epsilon}\frac{x_2^+\sinh\left(\pi T_{\mathrm{b}}y_2^-\right)}{\pi T_{\mathrm{b}}\sqrt{f'(y_2^+)}}\right)\right)\,, \tag{3.193}$$

where we pick up a time slice after the Page transition. The first two terms denoting the thermal entropy of a half-line can compensate the same divergence appearing in $S_{\frac{1}{2}\text{-line}}$ and the last term is the same as the one-point function contribution S_2 appearing in the case without purification, *i.e.,* eq. (3.159). Physically, we can explain the third term $2\pi T_{\mathrm{b}}y_2^-$ as

[28] The $T_b \to 0$ limit has some subtleties here. The "purification" of the bath with zero temperature is a pure state coupled to the bath system by direct product. Thus, the purification of the bath does not help with interior reconstruction because it is a fully unentangled region and the corresponding R-channel is defined by $S_{\mathrm{R}} = S^{\mathrm{gen}}_{\mathrm{QES}-1} + S_2 + S_{\frac{1}{2}\text{-line}}$, which cannot be derived from (3.191) by taking the limit $T_{\mathrm{b}} \to 0$. The reason is that, for $T_b = 0$, the holographic (3D) spacetime for bath interval and its purification is defined by two separated regions rather than a smooth and connected spacetime, as in the $T_b \neq 0$ case, where the entanglement between two regions glues the spacetime. However, note that the naive $T_b \to 0$ limit would leave one IR divergent term since $S_{\mathrm{N}} - S_{\mathrm{R}} \sim \frac{c}{6}\log\frac{\bar{l}}{\sigma_{\mathrm{IR}}}$.

the entanglement from the thermal radiation generated by the thermal bath. That extra term is traced back to the inclusion of the purification and the negative sign reflects the fact that the bath interval is entangled with its purification. As a result, we can expect the introduction of purification can help fulfill the condition for reconstruction as we will show below.

First, let's work on the simple linear region with $ku \ll 1$. Adding the new contributions (3.192) in eq. (3.182) and taking the linear approximations in eq. (3.183) again, the condition $S_{\rm N} - S_{\rm R} \geq 0$ can be rewritten as a restriction on the length of the finite bath interval $\Delta\sigma = \sigma_2$, *i.e.,*

$$\sigma_2(u) \gtrsim \frac{T_1 - T_0}{2k\,(T_1 + T_{\rm b})} + \frac{T_1}{4(T_1 + T_{\rm b})}\left(u\left(1 - \frac{T_{\rm b}}{T_1}\right)^2 + u_{\rm HP}\left(1 - \frac{T_{\rm b}^2}{T_1^2}\right)\right) + \frac{\log\left(\frac{6E_s}{cT_1}\right)}{2\pi(T_1 + T_{\rm b})} + \cdots\,, \tag{3.194}$$

where we also have assumed $\pi T_1 y_2^+ \gg 1$ (or $f(y_2^+) \approx t_\infty$). Comparing to the finite bath interval without purification, *i.e.,* eq. (3.184), we see that introducing the purification decreases the minimal length of the necessary bath interval for reconstructing the interior of the black hole, and also slows down the speed of its linear increase with time. More importantly, it also makes the subsystem consisting of $\mathrm{QM_L}$, a finite bath interval $[0, \sigma_2]$ (with only a fraction of the Hawking radiation) and the purification have the ability to recover the information of the black hole even when $T_b > T_p$. As with the unreliability of the linear approximations in the overheated case, we should remark that we also need to consider some corrections for the above approximate $\sigma_2(u)$ if the temperature of the thermal bath is too high, *i.e.,* $T_{\rm b} \gtrsim 3T_1$.

As one might expect, for much larger times, the linear increase of $\sigma_2(u)$ breaks down. Since the black hole eventually equilibrates with the bath, we expect qualitatively similar behavior to the equilibrium case of section 3.2, that is, we expect $\Delta\sigma = \sigma_2$ to approach half the (equilibrium) Page time as in eq. (3.69). To derive this explicitly, we focus on the time derivative of the critical length denoted by $\partial_u \sigma_2^*(u)$ directly. Noting the time evolution of the generalized entropy at late-time phase (after Page transition) has been shown in (3.143), we explicitly start from the approximation of $S_{\rm R} - S_{\rm N} = 0$ by

$$2k\left(2\pi T_{\rm b} y_2^- + \log\left(\frac{c}{6\pi E_s \epsilon}\frac{(f(u) - x_2^+)\sinh\left(\pi T_{\rm b}\sigma_2\right)}{x_2^+\sqrt{f'(u)}\sinh(\pi T_{\rm b}(u+\sigma_2))}\right)\right) \approx \frac{4G_{\rm N}}{\bar{\phi}_r} S_{\rm gen,late} - 2\pi T_0\,, \tag{3.195}$$

and obtain the differential equation

$$\begin{aligned} 4\left(T_{\text{eff}}(y_2^+)+T_{\text{b}}\right)\partial_u\sigma_2^* &\approx -T_{\text{eff}}(u)\left(1-\frac{T_{\text{b}}^2}{T_{\text{eff}}^2(u)}\right)-2T_{\text{b}}-2T_{\text{eff}}(u)+4T_{\text{eff}}(y_2^+)+\mathcal{O}(k) \\ &\approx T_{\text{eff}}(u)\left(1-\frac{T_{\text{b}}}{T_{\text{eff}}(u)}\right)^2 , \end{aligned} \tag{3.196}$$

where we denoted the solution of $S_{\text{R}}-S_{\text{N}}=0$ as $\sigma_2^*(u)$ and mainly used the approximation $f'(u)\sim 2\pi T_{\text{eff}}(u)\left(t_\infty-f(u)\right)$ and associated approximations derived in eqs. (3.98). To double check, we can focus on the linear region with $T_{\text{eff}}\approx T_1$ again and obtain

$$\partial_u\sigma_2^*(u)\approx\frac{T_1}{4\left(T_1+T_{\text{b}}\right)}\left(1-\frac{T_b}{T_1}\right)^2 , \tag{3.197}$$

which agrees with eq. (3.194) as expected. On the other hand, it is also obvious that the time derivative at late time region approaches zero, *i.e.,*

$$\partial_u\sigma_2^*\big|_{e^{ku}\gg 1}\longrightarrow 0\,, \tag{3.198}$$

because of the simple approximation $T_{\text{eff}}\left(e^{ku}\gg 1\right)\approx T_{\text{b}}$ for the effective temperature. In other words, the evolution towards equilibrium pushes the minimal length $\Delta\sigma_2$ to be a constant, which exactly matches what was shown in the equilibrium case in eq. (3.69). As a result, we can find the minimal length $\Delta\sigma_2$ with purification should approach a constant whereas the lightcone coordinate $y_2^+=u-\sigma_2$ reaches a constant as indicated in eq. (3.190) if we do not include the purification. We sketch a plot to illustrate the time dependence of $\Delta\sigma_2(u)$ when the purification is included in figure 3.13. More explicitly, we apply the late-time approximation with $e^{ku}\gg 1$ on $S_{\text{N}}-S_{\text{R}}\geq 0$ and derive the constraint

$$\sigma_2\left(e^{ku}\gg 1\right)\gtrsim\frac{1}{4kT_{\text{b}}}\left(2T_1-T_{\text{b}}-T_0-2T_{\text{b}}\log\left(\frac{T_1+T_{\text{b}}}{2T_{\text{b}}}\right)\right)+\frac{\log\left(\frac{6E_s}{cT_1}\sqrt{\frac{T_{\text{b}}}{T_1}}\right)}{4\pi T_{\text{b}}}\equiv\Delta\sigma_{\text{turn}}\,. \tag{3.199}$$

As expected, it returns to the result shown in eq. (3.69) for the equilibrium case by setting $T_{\text{b}}=T_1$. As a final remark, we point out that the minimum of the dimensionless length scale $k\Delta\sigma_{\text{turn}}$ (at leading-order) is realized at the near-equilibrium case with $T_{\text{b}}=T_1\left(2\frac{T_1}{T_0}-1\right)$. A simple numerical plot is also shown in the right figure 3.12. The interesting feature we want to highlight is that when the black hole is evaporating, we need more bath interval to recover the interior of the black hole, while a thermalized black hole requires less bath interval in which less of the outgoing Hawking radiation is located.

In the above, we have seen how including the entire purification of the thermal bath allows for the reconstruction of the black hole interior. The next natural question is how much of purifier is really necessary for this reconstruction, as was considered in section 3.2.3 for the equilibrium case. In order to investigate that question, we consider a subsystem with QM_{L}, a bath interval $[0,\sigma_2]$ and a finite interval $[0,\tilde{\sigma}_3]$ in the purification (on the time slice $\tilde{u}_3$). As shown in figure 3.3d, the generalized entropy for the two competing channels are defined as

$$S_{\mathrm{R}} = S^{\mathrm{gen}}_{\mathrm{QES}-1} + S_{2-3}\,, \qquad S_{\mathrm{N}} = S^{\mathrm{gen}}_{\mathrm{QES}''} + S_{1-2} + S_3\,, \tag{3.200}$$

where the three endpoints are taken as a point on the AdS boundary with $y_1^{\pm} = u$ (*i.e.,* $\sigma_1 = 0$), the bath point $y_2^{\pm} = u \mp \sigma_2$ in the region II and the point with $\tilde{y}_3^{\pm} = \tilde{u}_3 \pm \tilde{\sigma}_3$ in the purification region, respectively. As before, the two terms $S^{\mathrm{gen}}_{\mathrm{QES}-1}$, $S^{\mathrm{gen}}_{\mathrm{QES}''} + S_{1-2}$ are given by eqs. (3.159) and (3.158), respectively. We only need to consider two new ingredients, *i.e.,*

$$\begin{aligned} S_3 &= \frac{c}{6}\log\left(\frac{\sinh\left(2\pi T_{\mathrm{b}}\tilde{\sigma}_3\right)}{\pi T_{\mathrm{b}}\epsilon}\right)\,, \\ S_{2-3} &= \frac{c}{6}\log\left(\frac{12\pi E_s}{c\left(\epsilon\pi T_{\mathrm{b}}\right)^2}\frac{x_2^+\cosh\left(\pi T_{\mathrm{b}}\tilde{y}_3^+\right)\cosh\left(\pi T_{\mathrm{b}}(y_2^- + \tilde{y}_3^-)\right)}{\sqrt{f'(y_2^+)}}\right)\,. \end{aligned} \tag{3.201}$$

which can be derived from the counterparts with point $y_3^{\pm}$ in the region IV by the map $\pi T_{\mathrm{b}}\tilde{y}_3^{\pm} = \frac{i\pi}{2} - \pi T_{\mathrm{b}} y_3^{\pm}$. First of all, it is easy to find that we can retrieve the results in the last subsection (see eq. (3.192)) where we include the full purification region, by pushing the third point $\tilde{\sigma}_3$ to the IR cut-off surface with $\tilde{\sigma}_3 \to \sigma_{\mathrm{IR}} \sim +\infty$ (*i.e.,* approaching the null surface in the spacetime of bath's purifier). More explicitly, we can define the difference due to the finite $\tilde{\sigma}_3$, *i.e.,*

$$\left(S_{\mathrm{N}} - S_{\mathrm{R}}\right) - \left(S_{\mathrm{N}} - S_{\mathrm{R}}\right)\big|_{\tilde{\sigma}_3\to\infty} = \frac{c}{6}\log\left(\frac{\sinh\left(2\pi T_{\mathrm{b}}\tilde{\sigma}_3\right)}{2e^{\pi T_{\mathrm{b}} y_2^-}\cosh\left(\pi T_{\mathrm{b}}(\tilde{y}_3^+)\right)\cosh(\pi T_{\mathrm{b}}(y_2^- + \tilde{y}_3^-))}\right)\,, \tag{3.202}$$

as $\Delta S_{\text{NR-NR}}$. Equipped with the above difference for the two configurations in figures 3.3c and 3.3d , we can discuss the result of cutting part of the purification in the reconstruction. Noting that the dependence on $\tilde{\sigma}_3$ only appears on $\Delta S_{\text{NR-NR}}$, one can easily find the derivative of $S_{\mathrm{N}} - S_{\mathrm{R}}$ satisfies

$$\begin{aligned} &\frac{\partial\left(S_{\mathrm{N}} - S_{\mathrm{R}}\right)}{\partial\tilde{\sigma}_3} = \frac{\partial\left(\Delta S_{\text{NR-NR}}\right)}{\partial\tilde{\sigma}_3} \\ &= \frac{c}{6}\left(2\coth(2\pi T_{\mathrm{b}}\tilde{\sigma}_3) - \tanh\left(\pi T_{\mathrm{b}}(\tilde{y}_3^+)\right) + \tanh\left(\pi T_{\mathrm{b}}(y_2^- + \tilde{y}_3^-)\right)\right) \geq 0\,, \end{aligned} \tag{3.203}$$

due to the simple facts that $\coth x \geq 1$ for $x \geq 0$ and $|\tanh x| \leq 1$. The above positive derivative shows that $S_{\rm N} - S_{\rm R}$ monotonically increases with the increase of σ_2, implying that it is easier to reconstruct the black hole interior by including a larger interval in the bath. We can then rewrite the condition for this subsystem to reconstruct the black hole interior as

$$S_{\rm N} - S_{\rm R} = (S_{\rm N} - S_{\rm R})\big|_{\tilde{\sigma}_3 \to \infty} + \Delta S_{\text{NR-NR}} \geq 0\,, \tag{3.204}$$

where $(S_{\rm N} - S_{\rm R})\big|_{\tilde{\sigma}_3 \to \infty}$ is positive if and only if the condition in eq. (3.184) or (3.199) is satisfied. Because the maximum of $\Delta S_{\text{NR-NR}}$ is defined as $\tilde{\sigma}_3 \to \infty$ and is zero, we always have $\Delta S_{\text{NR-NR}} < 0$ for a finite $\tilde{\sigma}_3$, indicating that we need to include more bath interval than the critical length $\sigma_2^*(u)$ (derived in eq. (3.184) or (3.199)) in order to make the channel with a finite portion of the purification recoverable. Recalling the σ_2-dependence of eq. (3.195), we can find the following decomposition

$$S_{\rm N} - S_{\rm R} \approx \frac{c}{6}\left(2\pi T_{\rm b} y_2^- + \log\left(\frac{c}{6\pi E_s \epsilon}\frac{(f(u) - x_2^+)\sinh(\pi T_{\rm b}\sigma_2)}{x_2^+\sqrt{f'(u)}\sinh(\pi T_{\rm b}(u+\sigma_2))}\right)\right) + \Delta S_{\text{NR-NR}} + \cdots\,, \tag{3.205}$$

where we ignored the extra terms without dependence on $\sigma_2, \tilde{\sigma}_3$. Then we can simply take the results in the above subsection to derive the necessary conditions for σ_2 and $\tilde{\sigma}_3$. However, it is more convenient to define the length of the finite bath interval beyond the critical value as[29]

$$\delta\sigma_2 = \sigma_2 - \sigma_2^*(u)\,, \tag{3.206}$$

which helps us to show the effect of including more bath interval and cutting part of the bath purifier. It is straightforward to rewrite the necessary condition (3.204) to support the recoverable channel for the linear region ($ku \ll 1$) as

$$2\pi\,(T_1 + T_{\rm b})\,\delta\sigma_2 + \log\left(\frac{\sinh(2\pi T_{\rm b}\tilde{\sigma}_3)}{2e^{\pi T_{\rm b} y_2^-}\cosh\left(\pi T_{\rm b}(\tilde{y}_3^+)\right)\cosh(\pi T_{\rm b}(y_2^- + \tilde{y}_3^-))}\right) \geq 0\,, \tag{3.207}$$

by noting the approximation (3.183) and its result $(S_{\rm N} - S_{\rm R})\big|_{\tilde{\sigma}_3 \to \infty} = \frac{c}{3}\pi(T_1 + T_{\rm b})\delta\sigma_2$. Noticing the other approximation (3.100) and the simple relation $(S_{\rm N} - S_{\rm R})\big|_{\tilde{\sigma}_3 \to \infty} = \frac{2c\pi}{3}\pi T_{\rm b}\delta\sigma_2$ in the late-time region, one can find the condition for reconstructing the interior of black hole reads

$$4\pi T_{\rm b}\delta\sigma_2 + \log\left(\frac{\sinh(2\pi T_{\rm b}\tilde{\sigma}_3)}{2e^{\pi T_{\rm b} y_2^-}\cosh\left(\pi T_{\rm b}(\tilde{y}_3^+)\right)\cosh(\pi T_{\rm b}(y_2^- + \tilde{y}_3^-))}\right) \geq 0\,, \tag{3.208}$$

[29] We hide the complicated expressions which are not shown in (3.205) by using $\sigma_2^*(u)$. For the equilibrium case discussed in section 3.2.3, we considered a more general set-up with $\delta\sigma_2 = \sigma_2 - \sigma_1 - \Delta_{\rm turn}$ where the critical value is just the constant $\Delta_{\rm turn}$.

whose further reductions depend on the sign of the terms inside cosh functions and are similar to what have done in section 3.2.3. For example, if we assume all length scales on the above are larger than $\frac{1}{\pi T_{\rm b}}$, we can simply find the length of extra bath interval $[\sigma_2^*(u), \sigma_2]$ is constrained by

$$\delta\sigma_2 \gtrsim \begin{cases} \frac{T_{\rm b}}{2(T_1+T_{\rm b})}\left(|\tilde{y}_3^+| + |y_2^- + \tilde{y}_3^-| + y_2^- - 2\tilde{\sigma}_3\right) , & \text{if} \quad ku \ll 1 \\ \frac{1}{4}\left(|\tilde{y}_3^+| + |y_2^- + \tilde{y}_3^-| + y_2^- - 2\tilde{\sigma}_3\right) , & \text{if} \quad e^{ku} \gg 1 \end{cases} . \tag{3.209}$$

Then it is easy to find that the RHS of the above equation can be reduced to four cases where one of them vanishes, implying we need to consider the regime with $2\pi(T_1+T_{\rm b})\delta\sigma_2 \ll 1$, and other three cases at late-time region retrieve the results derived in eq. (3.86). Finally, we also comment the above linear dependence would like appear for the time region between the two limits due to the complicate dependence of entropy on σ_2. However, if we only focus on a small perturbation with $\delta\sigma_2/\sigma_2^* \ll 1, (T_{\rm eff}+T_{\rm b})\delta\sigma_2 \gg 1$, we can calculate the derivative of $(S_{\rm N} - S_{\rm R})\big|_{\tilde{\sigma}_3\to\infty}$ with respect to σ_2 and find the following expected result

$$2(T_{\rm eff}(y_2^+) + T_{\rm b})\delta\sigma_2 \gtrsim T_{\rm b}\left(|\tilde{y}_3^+| + |y_2^- + \tilde{y}_3^-| + y_2^- - 2\tilde{\sigma}_3\right) , \tag{3.210}$$

where the two terms on the RHS describe the entropy of radiation located on the small region $[\sigma_2^*, \sigma_2]$ and emitted from the black hole and the thermal bath, respectively.

Starting from the subsystem with $\mathrm{QM}_{\rm L}$, bath interval with the critical bath length σ_2^* and all purification, the above inequalities in eqs. (3.209) and (3.210) tell us how much bath interval we need to include if we want to exclude part of the purification in $\tilde{\sigma} = [\tilde{\sigma}_3, \tilde{\sigma}_{\rm IR}]$. Needless to say, we can interpret these inequalities in the opposite way, *e.g.,* [30]

$$2\tilde{\sigma}_3 \gtrsim |\tilde{y}_3^+| + |y_2^- + \tilde{y}_3^-| + y_2^- - 2\frac{T_{\rm eff}(y_2^+) + T_{\rm b}}{T_{\rm b}}\delta\sigma_2 . \tag{3.211}$$

Then we can learn how much bath purifier is necessary for reconstruction for a fixed bath interval $[0, \sigma_2]$ plus $\mathrm{QM}_{\rm L}$. In particular, we specify an interval in the purifier by both its length $\tilde{\sigma}_3$ and the time slice $\tilde{u}_3$ on which it is placed in the spacetime of purification region. First, we observe from eq. (3.211) if $|\tilde{u}_3|$ is very large both of the two expressions with absolute values on the right-hand side would be very large. That is, for very large $|\tilde{u}_3|$, we would need a large interval in the purifier with $\tilde{\sigma}_3 \sim |\tilde{u}_3|$ to recover the black hole interior.

[30] Although eqs. (3.86) and (3.211) look very similar, it is important to keep in mind that the assumptions leading to the two results are different. While for eq. (3.86) we simply needed to assume that all lengths we are dealing with are larger than the thermal scale, for eq. (3.211) we further needed to restrict to the cases where $\delta\sigma_2 \ll \sigma_2$.

Varying over the time slice $\tilde{u}_3$, we find that the "optimal purifier" with smallest length is determined by

$$\tilde{\sigma}_3 \approx \frac{1}{2}y_2^- - \frac{T_{\text{eff}}(y_2^+)+T_{\text{b}}}{2T_{\text{b}}}\delta\sigma_2\,, \quad \text{with} \quad \left|\tilde{u}_3 + \frac{1}{2}y_2^-\right| \leq \frac{T_{\text{eff}}(y_2^+)+T_{\text{b}}}{2T_{\text{b}}}\delta\sigma_2\,. \tag{3.212}$$

We note that this expression simply reduces to the equilibrium case shown in the second case in eq. (3.86) after taking either the late-time limit or setting $T_{\text{b}} = T_1$. Hence the present results are analogous to those illustrated for the equilibrium case in figure 3.4. That is, from eq. (3.212), the optimal purifier lies anywhere on a band of time slices centered at $\tilde{u}_3 = -y_2^-/2$ and with width $\Delta\tilde{u}_3 = \frac{T_{\text{eff}}(y_2^+)+T_{\text{b}}}{2T_{\text{b}}}\delta\sigma_2$. In this band, the length of the purifier interval is given by the expression above. Therefore when $\delta\sigma_2/\sigma_2$ is small, the optimal purifier is simply an interval of length $\tilde{\sigma}_3 = y_2^-/2$ on the time slice $\tilde{u}_3 = -y_2^-/2$.

In this subsection, we have discussed the necessity of the thermal bath's purification when the bath temperature is beyond the critical temperature and also the constraint on the length of the bath interval and its purifier. To complete the explorations on the role of purification, the last question we ask is what is the minimal length of the bath's purifier. Of course, we have shown it is zero when $T_{\text{b}} \leq T_p$. For a bath system with higher temperature, it is natural to expect that the length of the bath's purifier is minimal when the entire bath interval is included in the subsystem for reconstruction. Making some more effort, one can find that that expectation is true by showing $\partial_{\sigma_1}(S_{\text{N}} - S_{\text{R}}) \leq 0$ and $\partial_{\sigma_2}(S_{\text{N}} - S_{\text{R}}) \geq 0$. It means that the best for reconstruction is including all the bath interval with $\sigma \in [0, \sigma_{\text{IR}}]$. In the limit $\sigma_2 \to \sigma_{\text{IR}} \sim +\infty$, one can read the entropy two completing channels as

$$S_{\text{R}} = S^{\text{gen}}_{\text{QES}-1} + S_{3-\text{IR}}\,, \qquad S_{\text{N}} = S^{\text{gen}}_{\text{QES}''} + S_{1-\text{IR}} + S_3\,, \tag{3.213}$$

where the entropy for the two-point function $S_{1-\text{IR}}$ is defined in eq. (3.162) taking $\sigma_1 = 0, \sigma_2 = \sigma_{\text{IR}}$ and the last new ingredient $S_{3-\text{IR}}$ is derived as

$$S_{3-\text{IR}} = \frac{c}{3}\log\left(\frac{\sinh\left(\pi T_{\text{b}}(\tilde{\sigma}_{\text{IR}} - \tilde{\sigma}_3)\right)}{\pi T_{\text{b}}\epsilon}\right)\,. \tag{3.214}$$

Similar to the calculations for critical temperature, one can find the condition $S_{\text{N}} - S_{\text{R}}$ is rewritten as

$$\begin{aligned} &2k\left(\log\left(\frac{6E_s}{c}\frac{x_1^+\sinh(\pi T_{\text{b}}(-y_{\text{IR}}^+))\sinh(\pi T_{\text{b}}(y_{\text{IR}} - y_1^-))}{\sqrt{f'(y_1^+)}}\right) + 4\pi T_{\text{b}}\tilde{\sigma}_3 - 2\pi T_{\text{b}}\tilde{\sigma}_{\text{IR}}\right) \\ &\gtrsim 2\pi\left(T_{\text{eff}}(u) - T_0\right)\,, \end{aligned} \tag{3.215}$$

where we can easily see that more purification interval is more helpful for the reconstruction. Taking $\sigma_1 = 0$ and late-time limit $e^{ku} \gg 1$, we can finally find the minimal purifier is constrained by

$$\tilde{\sigma}_3 \gtrsim \frac{1}{4kT_{\rm b}}\left(3T_{\rm b} - 2T_1 - T_0 + 2T_{\rm b}\log\left(\frac{T_1+T_{\rm b}}{2T_{\rm b}}\right)\right) - \frac{1}{4\pi T_{\rm b}}\log\left(\frac{6E_s}{cT_1}\sqrt{\frac{T_1}{T_{\rm b}}}\right) + \cdots , \tag{3.216}$$

which is irrelevant to the choice of $\tilde{u}_3$. And note that the RHS is positive when $T_{\rm b} \gtrsim T_p$ as we illustrated around eq. (3.179).

3.4 Discussion

In this chapter, we continued our investigation of the AEM^{4}Z model [1, 11] describing a joining quench in a doubly holographic framework. The most interesting questions concern the two-dimensional dynamics describing black hole evaporation (or growth). Invoking holographic duality (twice), the generalized entropy becomes purely geometric and its evaluation is tractable in this dynamical setup. In the three-dimensional holographic dual, the black hole geometry contains a Planck brane where Jackiw-Teitelboim gravity is localized. At finite temperature, there is a new ingredient: a horizon in the three-dimensional bulk, beyond which the second asymptotic boundary purifies the two-dimensional thermal state in the bath. Despite this difference, we have shown that the Page curve still exhibits three distinct phases (quench, scrambling, and late-time equilibration), as in the zero-temperature case. However, there are several new qualitative features in both the scrambling and late-time phase.

As in the zero temperature case, the quantum extremal surface remains at the bifurcation point in the initial quench phase and then jumps out from the original horizon in the scrambling phase where the generalized entropy shows a(n almost) linear increase with the physical time. From the first holographic level, the increase in entropy is due to the two-way exchange of quanta between the bath and black hole, which is why the linear increase is proportional to $T_1 + T_b$. From the perspective of the doubly holographic model, the increase in generalized entropy is related to the end-of-the-world brane falling deeper into the bulk towards the horizon of the three-dimensional black hole.

After the Page time, the system enters the late-time phase in which the black hole approaches an equilibrium state with the bath. However, the evolution of the black hole is determined by the temperature of the thermal bath. For a bath with a temperature which matches that of the post-quench black hole $T_{\rm b} = T_1$, this equilibration is immediate and

the generalized entropy is constant throughout this phase. For a lower temperature bath with $T_{\rm b} < T_1$, the black hole evaporates and loses some of its mass, similar to the zero temperature case in chapter 2. Since the black hole not only emits Hawking radiation but also receives the thermal radiation from the bath, the black hole can also grow when the bath temperature satisfies $T_{\rm b} > T_1$. At extremely late times, the system will finally equilibrate with the bath temperature, and the entanglement entropy approaches its equilibrium value. Figure 3.10 illustrates these three possible scenarios.

We also found that the position of the late-time extremal surface relative to the event horizon of the black hole depends on the temperature of the bath. In the evaporating black hole models (with a bath at zero temperature) of chapter 2, the late-time extremal surface lies inside the horizon – in fact, it lies inside the horizon throughout the entire evolution of the black hole. Correspondingly, the information of the region outside of the black hole could not be reconstructed by $\mathrm{QM_L}+$ bath. On the other hand, in the equilibrium configuration studied in [62], the extremal surface is located outside of the event horizon. The equilibrium case studied in section 3.2 reproduces this behavior with the QES located outside the event horizon – see eq. (3.55). Hence in these cases, the information just outside of the event horizon could be reconstructed by $\mathrm{QM_L}+$ bath after the Page time. Moreover, at any temperature, the black hole eventually equilibrates with the bath, and the system is qualitatively similar to the equilibrium case. Indeed, for any temperature, after a time of $ku \geq \log\left(\left|1-\frac{T_1^2}{T_b^2}\right|\sqrt{\frac{\pi T_1}{8k}}\right)$, the late-time extremal surface crosses the horizon and stays outside as the system equilibrates. Furthermore, for black hole temperatures T_1 very close to the bath temperature $T_{\rm b}$, *i.e.,* $\frac{|T_{\rm b}-T_1|}{T_1} \leq \sqrt{\frac{2k}{\pi T_1}}\exp\left[\frac{T_1-T_0}{2T_1}\right]$, the QES is already outside of the event horizon at the Page time. One may ask why the behaviour of our black holes where only one side is in equilibrium with the bath matches that of the eternal two-sided black holes studied in [62], where there is an equilibrium with a thermal bath on both sides. However, this is relatively obvious from the holographic perspective since the HRT surfaces are really probing identical portions of the three-dimensional bulk geometry in the island phase for both cases.

As noted above, the appearance of QES outside of the horizon was first found in [62] for an eternal AdS_2 black hole coupled with a thermal bath. This same behavior was also seen in higher dimensional holographic systems [60, 97]. A similar phenomenon is also found at black holes in asymptotically flat spacetime, *e.g.,* [65, 69]. A dynamical QES crossing the horizon (similar to our present results) was also found for an evaporating black hole in JT gravity [70]. As discussed around eq. (3.56), while the QES may extend outside of the horizon, it is never very far from the horizon. These results may imply that we should consider some quantum corrections to the event horizon in order to extend the boundary of

the interior of black hole, *e.g.,* taking the stretched horizon [150] as a surrogate for the event horizon. Then the QES can be seen to stay outside the classical event horizon but inside the stretched horizon [65]. However, let us add that in the higher dimensional holographic systems studied in [59, 60], this effect can be understood in terms of entanglement wedge nesting [133, 151]

After deriving the Page curve with three phases as shown in figure 3.10, we further focused on investigating the ability of various subsystems consisting of QM_{L} and different parts of the bath interval to reconstruct the black hole interior – see figure 3.3 for the competing channels for every case. As we first demonstrated in the equilibrium case of section 3.2, the reconstruction of black hole interior always requires at least part of the purification of the bath. Of course, the key difference from the scenario with the evaporating black hole coupled to a zero temperature bath is that our bath here begins in a mixed state before the quench whereas in the previous studies the bath begins in a pure state (*i.e.,* the CFT vacuum). Hence, part of the purification of the bath becomes essential for interior reconstruction when the bath temperature is higher than the critical temperature $T_p \sim \frac{1}{2}(T_1 + T_0) \lesssim T_1$, as given in eq. (3.179). This requirement arises for two reasons: First, the thermal bath radiation in the interval containing the Hawking radiation must be purified to distill information about the black hole interior. Second, after the quench, thermal radiation from the bath falls into the black hole entangling the black hole interior with radiation in the purifier. That is, part of the entanglement initially shared between the bath and its purifier is transferred to the black hole interior and the purifier. So information about the black hole interior is spread to the purification although, of course, none of the Hawking radiation enters this region.

A simple example where the importance of the purifier was seen was the case where the black hole and the bath were in equilibrium, *i.e.,* with $T_{\mathrm{b}} = T_1 > T_p$. In this case, the reconstruction of the black hole interior with QM_{L}, a finite bath interval $[\sigma_1, \sigma_2]$ at some time u, and a restricted portion $[0, \tilde{\sigma}_3]$ of the purifier at another time $\tilde{u}_3$ was considered in section 3.2.3. There, the bound (3.86) on the purifier interval size $\tilde{\sigma}_3$ necessary for reconstruction can be given a physical interpretation in figure 3.4 as the requirement that $[0, \tilde{\sigma}_3]$ captures purifier quanta entangled with out-going thermal bath radiation in $0 < y^- < y_2^-$, shown in red in the left panel of figure 3.4. Given the thermofield double preparation of the bath and purifier, the relevant purifier quanta are those marked by dashed wavy lines in the right panel of figure 3.4. The bound (3.86) then corresponds to the minimal interval in the purifier which captures these quanta. Namely, if the bath interval has a length that is only above-critical by a few thermal lengths, then the requisite purifier interval must capture essentially all of the quanta marked in the right panel of figure 3.4, *e.g.,* see the blue interval. If the bath interval exceeds the critical length with

a large margin $\sigma_2 - \sigma_1 - \Delta_{\text{turn}}$, then the amount of the marked quanta that must be captured by the purifier interval is reduced proportionately, *e.g.,* see the green interval. This discussion, however, leaves open the question of why the $0 < y^- < y_2^-$ section of bath thermal radiation is important to begin with. One might argue that the bath radiation in $y_1^- < y^- < y_2^-$ obfuscates the Hawking radiation captured by the bath interval $[\sigma_1, \sigma_2]$, so that purifying this section of bath thermal radiation is beneficial. One may also argue that $0 < y^- < y_{\text{QES}}^-$ contains thermal bath radiation eaten by the quantum extremal island, so its purifier would contain information about the island. But, it also seems that the bath radiation in the in-between range $y_{\text{QES}}^- < y^- < y_1^-$ is not pertinent. In particular, if one is free to discard the purifier quanta for this radiation, then it should be possible to reduce the interval length of $[0, \tilde{\sigma}_3]$ beyond what is allowed by (3.86) in some cases where $\sigma_2 - \sigma_1$ exceeds Δ_{turn} by many thermal lengths.

One may ask why the previous effects are not always important. That is, why is there a critical bath temperature T_p below which no portion of the purifier is needed to recover the black hole interior. Certainly, there are many physical effects that come into play here, *e.g.,* the redundancy of the encoding of the black hole interior in the Hawking radiation (see section 2.2.3), but remarkably the critical temperature T_p can be derived with the following simple intuitive argument:[31] Recall that in the usual black hole evaporation (with $T_{\text{b}} = 0$), the Page phase arises when the naive entropy of the Hawking radiation exceeds the Bekenstein-Hawking entropy of the black hole. Of course, we now understand that this conflict is resolved by the formation of a quantum extremal island, and hence a portion of the black hole interior is reconstructible in this phase. When the black hole is coupled to a finite temperature bath, the appearance of the critical temperature T_p indicates that islands form for lower bath temperatures but not for higher temperatures, when keeping track of modes in the mixed state of the bath (along with QM_{L}). But in turn, we can understand this as indicating that for $T_{\text{b}} < T_p$, one reaches an inconsistency where the naive entropy of the bath (including the Hawking radiation and also QM_{L}) exceeds the entropy of the black hole and the bath purifier. But no such inconsistency arises for $T_{\text{b}} > T_p$. Examining this latter perspective in more detail below then allows us to derive the critical temperature T_p.

That is, we consider the necessity of islands at late times in the evolution of the system. First, we observe that the (coarse-grained) Bekenstein-Hawking entropy provides a bound

[31] This argument and the following calculations are similar in spirit to the calculations in Appendix B of [10]. We thank Geoff Penington for discussing this point with us.

on the (fine-grained) entropy of $\mathrm{QM_R}$, with[32]

$$S_{\mathrm{QM_R}} \lesssim S_{\mathrm{UV}} + S_{\mathrm{BH}}(T_{\mathrm{eff}}) \xrightarrow[u\to\infty]{} S_{\mathrm{UV}} + S_{\mathrm{BH}}(T_{\mathrm{b}})\,. \tag{3.217}$$

Here, S_{UV} denotes a UV-divergent contribution due to the separation between $\mathrm{QM_R}$ and the bath, T_{eff} is the effective temperature (3.92) of the JT black hole on the right, and S_{BH} is the Bekenstein-Hawking entropy (3.45). The argument now proceeds as follows: Purity of the complete system, including the bath's purifier, demands

$$S_{\mathrm{QM_L}\cup\mathrm{bath}} = S_{\mathrm{QM_R}\cup\overline{\mathrm{bath}}} \leq \; S_{\mathrm{QM_R}} + S_{\overline{\mathrm{bath}}}\,, \tag{3.218}$$

where $\overline{\mathrm{bath}}$ denotes the bath's purifier. Here, the inequality follows from the subadditivity of entanglement entropy. Now let us begin by assuming the absence of any islands, in which case,

$$S_{\mathrm{QM_L}\cup\mathrm{bath}} \approx \; S_{\mathrm{BH}}(T_0) + S_{\mathrm{bath}}\,. \tag{3.219}$$

Note that here, we are implicitly including the entire bath region and so we must regulate the size of the latter to avoid having an IR divergence in S_{bath}. Further, combining the bound (3.217) with the subadditivity inequality in eq. (3.218), we also have

$$S_{\mathrm{QM_R}\cup\overline{\mathrm{bath}}} \leq S_{\mathrm{QM_R}} + S_{\overline{\mathrm{bath}}} \lesssim S_{\mathrm{UV}} + S_{\mathrm{BH}}(T_{\mathrm{b}}) + S_{\overline{\mathrm{bath}}}\,. \tag{3.220}$$

It remains to approximate the difference $S_{\mathrm{bath}} - S_{\overline{\mathrm{bath}}}$. Just after the joining quench, S_{bath} can be expressed as the sum of three contributions: $S_{\overline{\mathrm{bath}}}$, the UV contribution S_{UV}, and a shock contribution,[33] *i.e.,*

$$S_{\mathrm{bath}}(u=0) = S_{\overline{\mathrm{bath}}} + S_{\mathrm{UV}} + S_{\mathrm{shock}}\,, \quad \text{where} \;\; S_{\mathrm{shock}} \approx \frac{c}{6}\log\frac{E_S}{c\,T_1}\,. \tag{3.221}$$

Now while $S_{\overline{\mathrm{bath}}}$ remains constant, S_{bath} changes[34] due both to the absorption of Hawking radiation at temperature T_{eff} and the loss of thermal radiation to the black hole (purified

[32] Violation of the Bekenstein area bound in the island region is a necessary condition for the appearance of QEIs [152]. In the following argument, we begin by assuming that it holds and so no QEI forms, even in the far future.

[33] To obtain the following expression for S_{shock}, we may compare, for example, the $x^{\pm} \in$ II and $x^{\pm} \in$ IV cases of eq. (3.32). Further, we have chosen $1/T_1$ to be a 'typical' length scale for the x^+ coordinate. Other choices differing by $O(1)$ factors from this will not significantly modify the result of this argument.

[34] Alternatively, one may discard from this argument, all of the 'bystander' thermal quanta entangled to each other in the bath and purifier regions, which have not yet fallen into the black hole. In this case, S_{bath} and $S_{\overline{\mathrm{bath}}}$ both increase, respectively due to the absorption of Hawking radiation and being entangled with bath radiation lost to the black hole. What is important is that the difference $\partial_u(S_{\mathrm{bath}} - S_{\overline{\mathrm{bath}}})$ evolves according to the RHS of (3.222).

by quanta in $S_{\overline{\text{bath}}}$) at temperature T_b. To be precise, we have

$$\partial_u S_\text{bath} \approx \frac{\pi c}{6} \left(T_\text{eff} - T_\text{b}\right) . \tag{3.222}$$

Now combining eqs. (3.221) and (3.222), we find at late times

$$\begin{aligned} \lim_{u\to\infty} S_\text{bath} - S_{\overline{\text{bath}}} &\approx S_\text{UV} + S_\text{shock} + \frac{\pi c}{6}\int_0^\infty du \left(T_\text{eff} - T_\text{b}\right) \\ &\approx S_\text{UV} + \frac{c}{6}\log\frac{E_S}{cT_1} + \frac{\pi c}{6k}\left[T_1 - T_\text{b} + O\left(\frac{(T_1-T_\text{b})^2}{T_1}\right)\right] \end{aligned} \tag{3.223}$$

Finally, combining eqs. (3.219) and (3.220) together with eq. (3.223), we find that our assumption of no islands leads to

$$T_\text{b} \gtrsim \frac{T_0+T_1}{2} + \frac{k}{2\pi}\log\frac{E_S}{cT_1}, \tag{3.224}$$

where we recognize the RHS as the expression (3.179) for T_p. Thus, T_p corresponds to the bath temperature above which the inequality (3.218) can be satisfied at late times without introducing any island. Conversely, to satisfy the entropy bound (3.218) for $T_\text{b} < T_p$, an island must be introduced at sufficiently late times and as a result, the black hole interior may be reconstructed from QM_L and the bath alone, without the bath's purifier. Alternatively, for $T_\text{b} > T_p$, reconstructing the black hole interior requires additional information from the purification. This argument provides further intuition for understanding the critical temperature T_p than perhaps offered by the initial calculations leading up to (3.179) in section 3.3.2.

Furthermore, for the lower bath temperatures $T_\text{b} < T_p$, we found that with the subsystem comprising only $\text{QM}_\text{L}$and a finite bath interval, as shown in figure 3.3c, it is possible to reconstruct the black hole interior in section 3.3.2. The length of the minimal bath interval for reconstruction increases with the physical time and approaches a linear increase as shown in eqs. (3.184) and (3.190), and as summarized in figure 3.11. After including the purification in the subsystem as presented in figures 3.3b and 3.3d, we considered the reconstruction of the black hole interior in section 3.3.2 with a general bath temperature T_b, *i.e.,* interior reconstruction also becomes possible for $T_\text{b} > T_p$. We first found that the black hole interior is reconstructible with any bath interval above the shock-wave with a length larger than $\Delta_\text{turn} \sim \frac{T_1-T_0}{4kT_1}$, given in eq. (3.69) for the equilibrium case. For the evaporating and thermalized black hole, the interval length required for interior reconstruction increases with time as shown in (3.196). Since late time behavior should be similar to the equilibrium case, one finds as expected, the minimal interval length for late times

asymptotes to a finite constant which is defined as $\Delta\sigma_{\text{turn}}$ in eq. (3.199). The two above results are illustrated in figure 3.13.

Recent explorations on QES and Page curves inspire the island formula for the quantum systems coupled to gravity [1]. Although we do not explicitly apply the island formula in our analysis, it is clear that the island region emerges in the recoverable channel, as shown in figure 3.3. Without knowledge of the island formula, we can also derive the same results and desired Page curve because we can apply the RT formula in the doubly holographic models. In other words, RT formula knows about the existence of the island. On the other hand, it is also possible to get the right answer by noting the entropy of a subsystem in a *pure state* equals the entropy of its complementary part. For example, we can easily find that the entropy of QM_{R} after Page transition is defined by $S_{\text{QES}-1}$ with y_1 on the AdS boundary. Taking the pure state as the whole system, we simply know $S_{\text{QES}-1}$ also defines the generalized entropy of QM_{L}, entire bath interval, and its purification (see figure 3.3a), which implies the Page curve for that subsystem. However, this approach does not work for mixed states because the entropy of a subsystem in a *mixed state* generally does not agree with the entropy of its complementary part. Let's construct a mixed state as an example by tracing out the bath's purification. Then the complementary subsystem of QM_{R} consists of QM_{L} and only the entire bath interval. Correspondingly, the generalized entropy of this complementary system is defined by the minimal entropy between the two channels (see figure 3.3c with $\sigma_2 \to \sigma_{\text{IR}}$)

$$\begin{aligned} S_{\text{N}} &= S^{\text{gen}}_{\text{QES}''} + S_{\frac{1}{2}\text{-line}}\,, \qquad \text{No Island}\,, \\ S_{\text{R}} &= S^{\text{gen}}_{\text{QES}-1} + S_{\text{IR}}\,, \qquad \text{With Island}\,. \end{aligned} \tag{3.225}$$

It is obvious that neither of the above two terms equals the entropy of QM_{R}, *i.e.,* $S^{\text{gen}}_{\text{QES}-1}$. More importantly, we have shown S_{N} is always preferred when $T_{\text{b}} \gtrsim T_p$, which indicates the entanglement wedge of the corresponding subsystem with QM_{L} and any thermal bath interval does not contain the island region.

As a final remark, let us comment on an important lesson from our results for the reconstruction of the black hole interior. It is obvious that the emitted Hawking radiation carries out information about the black hole. Although all the Hawking radiation is only stored in the finite interval $[0, \sigma_{\text{shock}}(u))$, our studies on the reconstruction for a black hole coupled to a finite temperature bath indicate that the information describing the black hole interior is not contained solely within this part of the bath (along with QM_{L}). Rather we see that in this situation, the black hole and Hawking radiation (*i.e.,* $[0, \sigma_{\text{shock}}(u))$, the bath region) are entangled with a complicated environment comprising QM_{L}, the remaining bath interval and the bath purifier, and hence the information about the black hole interior

is distributed in a complicated way over the whole system. Of course, as identified above, the new physical mechanism contributing to the information flow in the present situation is the incoming radiation falling from the bath onto the black hole, which entangles the black hole interior with the purifier (and possibly distant regions in the finite temperature bath). For example, we found that when the bath temperature satisfies $T_{\rm b} > T_p$, reconstruction always needs the purification even if we already have all of the Hawking radiation and $\mathrm{QM}_{\rm L}$. On the other hand, we also found that the $\mathrm{QM}_{\rm L}$ plus only a smaller bath interval $[0, \sigma_2(u)]$ with $e^{\pi T_1 (u - u_{\rm Page})} \gg 1$ and $\sigma_2 < \sigma_{\rm shock}(u)$ is also sufficient to recover the information of the black hole interior when $T_b < T_p$ in section 3.3.2 (see the right panel of figure 3.11). This means that we actually do not require all of the Hawking radiation. The information inherited in the ignorable (early-time) Hawking radiation located at $[\sigma_2, \sigma_{\rm shock}]$ is shared by other parts of the system. This reflects the redundancy of the encoding of the black hole interior in the Hawking radiation discussed in chapter 2.

Chapter 4

Conclusions and outlook

The study of black holes has sparked exciting progress in our understanding of quantum field theory in curved spacetime and quantum gravity. Over the last few years, new tractable models of black hole evaporation and equilibration have allowed us to explicitly compute the Page curve during these processes. In this thesis, we employed the AEM^{4}Z model to study the structure of information during black hole equilibration and black hole evaporation. The AEM^{4}Z model consists of a doubly holographic setup in which a thermofield double state QM_L+QM_R is dual to a JT gravity black hole plus holographic CFT matter. The extra layer of holography allows for a dual description of the CFT matter in terms of a bulk AdS_3 gravity. Crucially, this simplifies the computation of the CFT corrections to the generalized entropy. Indeed, the CFT entropy in this setup is calculated via the HRT prescription in the bulk, and becomes a purely geometric calculation.

The QM_R system is then coupled to a bath consisting of the holographic CFT on a half line. The bath CFT can be prepared in the vacuum state as in chapter 2, or at finite temperature as in chapter 3. In the zero temperature case, the Hawking radiation emitted by the black hole is absorbed by the bath and the black hole evaporates until at very late times the Hawking temperature is of the order of the quantum fluctuations and the semiclassical picture breaks down. For baths with non-zero temperature, the thermal radiation coming from the bath eventually balances out the Hawking radiation to reach an equilibrium state with non-zero Hawking temperature.

In this doubly holographic model, the extra layer of holography allows for an easy computation of the generalized entropy. By comparing the generalized entropy of the different candidate quantum extremal surfaces, we were able to compute the Page curve of QM_R, or one side of the double sided black hole, and observe three phases in the

evolution of the generalized entropy: the quench phase, the scrambling phase and the late-time phase. During the quench phase, the QES remains at the bifurcation point, and the generalized entropy increases linearly, due to the Hawking quanta crossing the asymptotic boundary between the AdS_2 bulk and the bath. The intermediate phase corresponds to the scrambling phase, in which the QES jumps perturbatively away from the bifurcation surface. During this phase, the QM_L+bath system has enough information to reconstruct a very small part of the black hole interior. The evolution of the generalized entropy in this phase depends on the parameters if the problem, but in most cases exhibits a small initial decrease and then continues to grow until the Page time. After the Page time, the QES is located far away from the bifurcation surface, past the infalling shockwave caused by the quenching between black hole and bath. In this phase, a large portion of the black hole interior is encoded in QM_L+bath which indicates that most of the information required for interior reconstruction has been transfered from QM_R to the bath via Hawking radiation. The generalized entropy in this phase asymptotes towards its equilibrium value, starting off with a linear decrease (increase) for baths with temperature lower (higher) than the black hole.

Repeating the same calculations with different intervals of the bath, it is also possible to study which parts of the radiation are essential for interior reconstruction. In the evaporation model ($T_b = 0$), we began by showing that the portion of the bath past the outgoing shockwave is not important for reconstructing the black hole. Further, we also studied how much of the late-time radiation can be omitted while still being able to reconstruct in black hole interior, and found the profile of the smallest interval $[\sigma_{\text{Page}}(u), \sigma_{\text{shock}}]$ anchored at the shock that would contain enough information to reconstruct the black hole interior. A similar analysis was performed to find the smallest intervals $[0, \sigma_{\text{turn}}(u)]$ anchored at the asymptotic boundary between the bath and the bulk AdS_2. Comparing the two results, and looking at time slices of the bath that are late enough, the intervals $[0, \sigma_{\text{turn(u)}}]$ and $[\sigma_{\text{Page}}(u), \sigma_{\text{shock}}]$ don't overlap, an indication that there is a redundancy in the encoding of the black hole interior in the Hawking radiation. At later times, there are multiple disjoint intervals that contain enough information for interior reconstruction. This redundancy is an important characteristic of quantum error correcting codes and holography [137, 138, 139].

For finite temperature baths, the CFT was prepared in a thermofield double state, and the bath purifier plays an important role in the reconstruction for temperatures above a critical temperature T_p. Below the temperature T_p, the purifier is not needed to reconstruct the interior of the black hole, while for temperatures above T_p, at least some portion of the purifier is needed for interior reconstruction. In the equilibrium case ($T_b = T_1$), the QES after the Page time is static and the results agree with the setup in [62] where the bath

and the black hole are prepared in equilibrium. Notably, the QES is located outside of the event horizon, in contrast with the evaporating case of chapter 2. For a finite temperature bath, the black hole equilibrates with the bath and the results asymptote towards the equilibrium case. For example, as the temperature $T_{eff}(u)$ of the black hole approaches T_b, the QES crosses the event horizon at a critical temperature T_{c_1} (or T_{c_2}) close to T_b and remains outside of the event horizon for the remainder of the equilibration process. More generally, we repeated the analysis of which intervals of the bath (and purifier) were required to reconstruct the interior of the black hole, and the results interpolate between the zero temperature case and the equilibrium case.

In the analysis of which intervals of the bath (and bath purifier) are needed to reconstruct the interior of the black hole, the results are in line with the intuition that the information is carried by massless quasi-particles traveling at the speed of light. This can be seen for example from the profile of $\sigma_{\text{Page}}(u)$ of the earliest time at which the radiation can be ignored in the early time protocol in section 2.2.1, or the profile of the portion of the bath purifier needed for interior reconstruction in figure 3.4.

The recent studies of black hole evaporation and equilibration have brought great progress in our understanding of entanglement and geometry in quantum gravity, and have provided a partial resolution to the black hole information paradox, but there remain many open questions that are worth investigating. The evaporation and equilibration models described in this thesis rely on 2D JT gravity, but it would be worthwhile to search for other higher dimension generalizations of these models. Some progress in this direction can be found in [8, 59, 60] where higher dimensional doubly holographic setups were studied and, similar to the models studied in this thesis, quantum extremal islands naturally arise from the HRT prescription – see also [67] for an analysis of an evaporation model in three dimensions.

As was mentioned in the discussion sections, the analysis of the present work focused on the generalized entropy of the QM_{L} + (portions of the) bath system and its corresponding Page curve. A similar analysis can be done for the Page curve of the Hawking radiation without the QM_{L} system. Interestingly, the HRT prescription in this setup naturally leads to the island formula proposed more generally in [1]. Further work [14, 98] showed that the island formula can be derived from the gravitational path integral by considering wormhole geometry saddle points in the replica calculation. This surprising result indicates that the semiclassical path integral somehow contains the necessary information about non-perturbative corrections that would restore unitarity to the naive leading order entropy calculation.

Remarkably, the wormhole saddles in the gravitational path integral that are crucial to

recovering the Page curve in these doubly holographic models lead to a non-factorization of the path integral over disconnected boundaries [14, 15]. This factorization problem suggests that these gravitational models are necessarily dual to an ensemble of quantum theories, similar to the conjectured duality between SYK and pure JT gravity. Studies of the wormhole saddles of the gravitational path integral and their relation with ensemble theories have seen a resurgence since this remarkable discovery - see for example [79, 84, 153, 154, 155, 156, 157, 158, 159, 160].

Furthermore, while the current models of black hole evaporation and equilibration show that the information of the black hole interior is encoded in the radiation, so far, understanding how this information is encoded in the radiation remains to be understood. In the semiclassical models that have been studied thus far, the precise details of how the information escapes the black hole remain a mystery. In the same spirit, these semiclassical models provide no information about the black hole microstates that account for the entropy of the corresponding black hole. In the boundary perspective (see figure 1.2), the single sided black hole corresponds to the thermal state of $\mathrm{QM_R}$ after tracing out $\mathrm{QM_L}$, but the precise bulk interpretation of the states in this ensemble remains to be explored, and would likely require more than a classical bulk description to be understood - see [161] for a recent study of boundary states in BCFT and their interpretation as black hole microstates in the evaporating models.

In closing, we comment on some lessons that can be drawn by studying another important measure of entanglement that has been widely studied in holography: complexity. There are several proposals for holographic complexity, but the one we will focus on in the present discussion is the complexity=volume (CV) conjecture [162, 163]. The CV conjecture states that the complexity of the state in the boundary theory defined on a time slice $\mathbf{S}$ is dual to the volume of the maximal codimension-one bulk surface anchored to $\mathbf{S}$ on the asymptotic boundary,

$$\mathcal{C}_V(\mathbf{S}) = \max_{\partial\mathcal{B}=\mathbf{S}} \left[\frac{V(\mathcal{B})}{G_{\mathrm{N}}\,\ell}\right] , \tag{4.1}$$

where G_{N} is the Newton's constant of bulk gravity theory and ℓ is some undetermined length scale. For boundary subregions, the subregion-CV conjecture [164, 165] proposes that the complexity of the quantum state defined on a boundary subregion $\mathbf{R}$ is given by the volume of a maximal codimension-one bulk surface extending from $\mathbf{R}$ on the asymptotic boundary to the corresponding Ryu-Takayanagi (RT) surface $\Sigma_{\mathbf{R}}$ in the bulk,

$$\mathcal{C}_{\mathrm{V}}^{\mathrm{sub}}(\mathbf{R}) = \max_{\partial\mathcal{B}=\mathbf{R}\cup\Sigma_{\mathbf{R}}} \left[\frac{V(\mathcal{B})}{G_{\mathrm{N}}\,\ell}\right] . \tag{4.2}$$

In the setting of the AEM^{4}Z model, the subregion complexity of the $\mathrm{QM_L}$+intervals of

the bath (and purifier) would correspond to the volume of the minimal surface anchored at the RT surfaces and the intervals. These maximal volume surfaces correspond to the shaded regions in, *e.g.,* figures 2.1 and 3.1. A quick glance at these figures shows that at the phase transitions, there is a discontinuity in the complexity of the Hawking radiation. Indeed, the complexity of QM_{L} + bath increases at the transitions between each of the phases, while the complexity of QM_{R} decreases. This is an indication that the information of the black hole interior has transfered from QM_{R} to the bath at that point in time. Moreover, it was shown in [8] that the discontinuity in subregion complexity is precisely the complexity of the island, or in this case, of the region of the interior of the black hole which is reconstructable by QM_{L} and the bath (and purifier) intervals in question. Clearly, there are lessons to be learned by carefully studying complexity in the black hole evaporation and equilibration setups provided by the $\mathrm{AEM}^4\mathrm{Z}$ model.

References

[1] A. Almheiri, R. Mahajan, J. Maldacena and Y. Zhao, *The Page curve of Hawking radiation from semiclassical geometry*, *JHEP* **03** (2020) 149 [1908.10996].

[2] H. Z. Chen, Z. Fisher, J. Hernandez, R. C. Myers and S.-M. Ruan, *Information Flow in Black Hole Evaporation*, *JHEP* **03** (2020) 152 [1911.03402].

[3] H. Z. Chen, Z. Fisher, J. Hernandez, R. C. Myers and S.-M. Ruan, *Evaporating Black Holes Coupled to a Thermal Bath*, *JHEP* **01** (2021) 065 [2007.11658].

[4] M. Guo, J. Hernandez, R. C. Myers and S.-M. Ruan, *Circuit Complexity for Coherent States*, *JHEP* **10** (2018) 011 [1807.07677].

[5] A. Bernamonti, F. Galli, J. Hernandez, R. C. Myers, S.-M. Ruan and J. Simón, *First Law of Holographic Complexity*, *Phys. Rev. Lett.* **123** (2019) 081601 [1903.04511].

[6] E. Caceres, S. Chapman, J. D. Couch, J. P. Hernandez, R. C. Myers and S.-M. Ruan, *Complexity of Mixed States in QFT and Holography*, *JHEP* **03** (2020) 012 [1909.10557].

[7] A. Bernamonti, F. Galli, J. Hernandez, R. C. Myers, S.-M. Ruan and J. Simón, *Aspects of the first law of complexity*, *Journal of Physics A: Mathematical and Theoretical* **53** (2020) 294002.

[8] J. Hernandez, R. C. Myers and S.-M. Ruan, *Quantum Extremal Islands Made Easy, Part III: Complexity on the brane*, *JHEP* **02** (2021) 173 [2010.16398].

[9] M. Ammon, S. Grieninger, J. Hernandez, M. Kaminski, R. Koirala, J. Leiber et al., *Chiral hydrodynamics in strong external magnetic fields*, *JHEP* **04** (2021) 078 [2012.09183].

[10] G. Penington, *Entanglement Wedge Reconstruction and the Information Paradox*, 1905.08255.

[11] A. Almheiri, N. Engelhardt, D. Marolf and H. Maxfield, *The entropy of bulk quantum fields and the entanglement wedge of an evaporating black hole*, *JHEP* **12** (2019) 063 [1905.08762].

[12] S. W. Hawking, *Particle creation by black holes*, *Commun. Math. Phys.* **43** (1975) .

[13] S. Hawking, *Breakdown of Predictability in Gravitational Collapse*, *Phys. Rev. D* **14** (1976) 2460.

[14] G. Penington, S. H. Shenker, D. Stanford and Z. Yang, *Replica wormholes and the black hole interior*, 1911.11977.

[15] D. Marolf and H. Maxfield, *Transcending the ensemble: baby universes, spacetime wormholes, and the order and disorder of black hole information*, 2002.08950.

[16] S. Bowyer, E. T. Byram, T. A. Chubb and H. Friedman, *Cosmic X-ray Sources*, *Science* **147** (1965) 394.

[17] H. L. Shipman, *The Implausible History of Triple Star Models for Cygnus X-1: Evidence for a Black Hole*, *Astrophysical Letters* **16** (1975) 9.

[18] LIGO Scientific, Virgo collaboration, *Observation of Gravitational Waves from a Binary Black Hole Merger*, *Phys. Rev. Lett.* **116** (2016) 061102 [1602.03837].

[19] Event Horizon Telescope collaboration, *First M87 Event Horizon Telescope Results. I. The Shadow of the Supermassive Black Hole*, *Astrophys. J. Lett.* **875** (2019) L1 [1906.11238].

[20] S. Carlip, *Black Hole Thermodynamics*, *Int. J. Mod. Phys. D* **23** (2014) 1430023 [1410.1486].

[21] J. D. Bekenstein, *Black holes and the second law*, *Nuovo Cim. Lett.* **4** (1972) 737.

[22] J. D. Bekenstein, *Black holes and entropy*, *Phys. Rev. D* **7** (1973) .

[23] S. W. Hawking, *Black hole explosions*, *Nature* **248** (1974) 30.

[24] S. W. Hawking, *Black holes and thermodynamics*, *Phys. Rev. D* **13** (1976) 191.

[25] J. D. Bekenstein, *Holographic bound from second law of thermodynamics*, *Phys. Lett.* **B481** (2000) 339 [hep-th/0003058].

[26] J. D. Bekenstein, *Holographic bound from second law*, gr-qc/0007062.

[27] L. Susskind, *The world as a hologram*, *J. Math. Phys.* **36** (1995) 6377.

[28] G. 't Hooft, *The holographic principle*, http://arXiv.org/abs/hep-th/0003004.

[29] R. Bousso, *The holographic principle*, *Rev. Mod. Phys.* **74** (2002) 825 [http://arXiv.org/abs/hep-th/0203101].

[30] D. N. Page, *Information in black hole radiation*, *Phys. Rev. Lett.* **71** (1993) 3743 [hep-th/9306083].

[31] D. N. Page, *Time Dependence of Hawking Radiation Entropy*, *JCAP* **1309** (2013) 028 [1301.4995].

[32] J. Preskill, *Do black holes destroy information?*, hep-th/9209058.

[33] S. B. Giddings, *The Black hole information paradox*, in *PASCOS / HOPKINS 1995 (Joint Meeting of the International Symposium on Particles, Strings and Cosmology and the 19th Johns Hopkins Workshop on Current Problems in Particle Theory)*, 8, 1995, hep-th/9508151.

[34] A. Almheiri, D. Marolf, J. Polchinski and J. Sully, *Black Holes: Complementarity or Firewalls?*, *JHEP* **02** (2013) 062 [1207.3123].

[35] A. Almheiri, D. Marolf, J. Polchinski, D. Stanford and J. Sully, *An Apologia for Firewalls*, *JHEP* **09** (2013) 018 [1304.6483].

[36] S. D. Mathur, *The Information paradox: A Pedagogical introduction*, *Class. Quant. Grav.* **26** (2009) 224001 [0909.1038].

[37] S. D. Mathur, *What the information paradox is not*, 1108.0302.

[38] J. Maldacena, *The large N limit of superconformal field theories and supergravity*, *Adv. Theor. Math. Phys.* **2** (1998) 231.

[39] P. Calabrese and J. L. Cardy, *Entanglement entropy and quantum field theory*, *J.Stat.Mech.* **0406** (2004) P06002 [hep-th/0405152].

[40] P. Calabrese and J. Cardy, *Entanglement entropy and conformal field theory*, *J.Phys.* **A42** (2009) 504005 [0905.4013].

[41] S. Ryu and T. Takayanagi, *Aspects of holographic entanglement entropy*, *JHEP* **08** (2006) 045 [hep-th/0605073].

[42] S. Ryu and T. Takayanagi, *Holographic derivation of entanglement entropy from ads/cft*, *Phys. Rev. Lett.* **96** (2006) 181602 [hep-th/0603001].

[43] M. Rangamani and T. Takayanagi, *Holographic Entanglement Entropy*, *Lect. Notes Phys.* **931** (2017) pp.1 [1609.01287].

[44] H. Araki and E. H. Lieb, *Entropy inequalities*, *Commun. Math. Phys.* **18** (1970) 160.

[45] V. E. Hubeny, M. Rangamani and T. Takayanagi, *A covariant holographic entanglement entropy proposal*, *JHEP* **07** (2007) 062 [0705.0016].

[46] T. Faulkner, A. Lewkowycz and J. Maldacena, *Quantum corrections to holographic entanglement entropy*, *JHEP* **11** (2013) 074 [1307.2892].

[47] N. Engelhardt and A. C. Wall, *Quantum extremal surfaces: Holographic entanglement entropy beyond the classical regime*, *JHEP* **01** (2015) 073 [1408.3203].

[48] S. D. Mathur, *The Information paradox and the infall problem*, *Class. Quant. Grav.* **28** (2011) 125010 [1012.2101].

[49] S. D. Mathur and C. J. Plumberg, *Correlations in Hawking radiation and the infall problem*, *JHEP* **09** (2011) 093 [1101.4899].

[50] J. M. Maldacena, *Eternal black holes in anti-de Sitter*, *JHEP* **04** (2003) 021 [hep-th/0106112].

[51] L. Randall and R. Sundrum, *An alternative to compactification*, *Phys. Rev. Lett.* **83** (1999) 4690 [http://arXiv.org/abs/hep-th/9906064].

[52] L. Randall and R. Sundrum, *A large mass hierarchy from a small extra dimension*, *Phys. Rev. Lett.* **83** (1999) 3370 [http://arXiv.org/abs/hep-ph/9905221].

[53] G. R. Dvali, G. Gabadadze and M. Porrati, *4-D gravity on a brane in 5-D Minkowski space*, *Phys. Lett.* **B485** (2000) 208 [hep-th/0005016].

[54] T. Takayanagi, *Holographic dual of bcft*, *Phys. Rev. Lett.* **107** (2011) 101602 [1105.5165].

[55] N. Engelhardt and A. C. Wall, *Quantum extremal surfaces: Holographic entanglement entropy beyond the classical regime*, *JHEP* **1501** (2015) 073 [1408.3203].

[56] T. Faulkner, A. Lewkowycz and J. Maldacena, *Quantum corrections to holographic entanglement entropy*, *JHEP* **1311** (2013) 074 [1307.2892].

[57] S. Ryu and T. Takayanagi, *Holographic derivation of entanglement entropy from ads/cft*, *Phys.Rev.Lett.* **96** (2006) 181602 [hep-th/0603001].

[58] V. E. Hubeny, M. Rangamani and T. Takayanagi, *A covariant holographic entanglement entropy proposal*, *JHEP* **0707** (2007) 062 [0705.0016].

[59] H. Z. Chen, R. C. Myers, D. Neuenfeld, I. A. Reyes and J. Sandor, *Quantum Extremal Islands Made Easy, Part I: Entanglement on the Brane*, 2006.04851.

[60] H. Z. Chen, R. C. Myers, D. Neuenfeld, I. A. Reyes and J. Sandor, *Quantum Extremal Islands Made Easy, Part II: Black Holes on the Brane*, *JHEP* **12** (2020) 025 [2010.00018].

[61] J. Maldacena and L. Susskind, *Cool horizons for entangled black holes*, *Fortsch. Phys.* **61** (2013) 781 [1306.0533].

[62] A. Almheiri, R. Mahajan and J. Maldacena, *Islands outside the horizon*, 1910.11077.

[63] A. Almheiri, R. Mahajan and J. E. Santos, *Entanglement islands in higher dimensions*, *SciPost Phys.* **9** (2020) 001 [1911.09666].

[64] Y. Chen, *Pulling Out the Island with Modular Flow*, *JHEP* **03** (2020) 033 [1912.02210].

[65] F. F. Gautason, L. Schneiderbauer, W. Sybesma and L. Thorlacius, *Page Curve for an Evaporating Black Hole*, *JHEP* **05** (2020) 091 [2004.00598].

[66] T. Anegawa and N. Iizuka, *Notes on islands in asymptotically flat 2d dilaton black holes*, *JHEP* **07** (2020) 036 [2004.01601].

[67] V. Balasubramanian, A. Kar, O. Parrikar, G. Sárosi and T. Ugajin, *Geometric secret sharing in a model of Hawking radiation*, *JHEP* **01** (2021) 177 [2003.05448].

[68] T. Hartman, E. Shaghoulian and A. Strominger, *Islands in Asymptotically Flat 2D Gravity*, *JHEP* **07** (2020) 022 [2004.13857].

[69] K. Hashimoto, N. Iizuka and Y. Matsuo, *Islands in Schwarzschild black holes*, *JHEP* **06** (2020) 085 [2004.05863].

[70] T. J. Hollowood and S. P. Kumar, *Islands and Page Curves for Evaporating Black Holes in JT Gravity*, 2004.14944.

[71] M. Alishahiha, A. Faraji Astaneh and A. Naseh, *Island in the Presence of Higher Derivative Terms*, 2005.08715.

[72] H. Geng and A. Karch, *Massive Islands*, 2006.02438.

[73] T. Li, J. Chu and Y. Zhou, *Reflected Entropy for an Evaporating Black Hole*, 2006.10846.

[74] V. Chandrasekaran, M. Miyaji and P. Rath, *Islands for Reflected Entropy*, 2006.10754.

[75] A. Almheiri, T. Hartman, J. Maldacena, E. Shaghoulian and A. Tajdini, *The entropy of Hawking radiation*, 2006.06872.

[76] D. Bak, C. Kim, S.-H. Yi and J. Yoon, *Unitarity of Entanglement and Islands in Two-Sided Janus Black Holes*, 2006.11717.

[77] T. J. Hollowood, S. P. Kumar and A. Legramandi, *Hawking Radiation Correlations of Evaporating Black Holes in JT Gravity*, 2007.04877.

[78] Y. Ling, Y. Liu and Z.-Y. Xian, *Island in Charged Black Holes*, *JHEP* **03** (2021) 251 [2010.00037].

[79] D. Marolf and H. Maxfield, *Observations of Hawking radiation: the Page curve and baby universes*, *JHEP* **04** (2021) 272 [2010.06602].

[80] K. Goto, T. Hartman and A. Tajdini, *Replica wormholes for an evaporating 2D black hole*, *JHEP* **04** (2021) 289 [2011.09043].

[81] J. Kumar Basak, D. Basu, V. Malvimat, H. Parihar and G. Sengupta, *Islands for Entanglement Negativity*, 2012.03983.

[82] E. Caceres, A. Kundu, A. K. Patra and S. Shashi, *Warped Information and Entanglement Islands in AdS/WCFT*, 2012.05425.

[83] G. K. Karananas, A. Kehagias and J. Taskas, *Islands in linear dilaton black holes*, *JHEP* **03** (2021) 253 [2101.00024].

[84] V. Balasubramanian, A. Kar and T. Ugajin, *Entanglement between two disjoint universes*, *JHEP* **02** (2021) 136 [2008.05274].

[85] V. Balasubramanian, A. Kar and T. Ugajin, *Entanglement between two gravitating universes*, 2104.13383.

[86] C. F. Uhlemann, *Islands and Page curves in 4d from Type IIB*, 2105.00008.

[87] D. Neuenfeld, *Double Holography as a Model for Black Hole Complementarity*, 2105.01130.

[88] R. Bousso and A. Shahbazi-Moghaddam, *Island Finder and Entropy Bound*, *Phys. Rev. D* **103** (2021) 106005 [2101.11648].

[89] E. Verheijden and E. Verlinde, *From the BTZ black hole to JT gravity: geometrizing the island*, 2102.00922.

[90] H. Geng, Y. Nomura and H.-Y. Sun, *An Information Paradox and Its Resolution in de Sitter Holography*, 2103.07477.

[91] L. Anderson, O. Parrikar and R. M. Soni, *Islands with Gravitating Baths*, 2103.14746.

[92] X. Wang, R. Li and J. Wang, *Islands and Page curves for a family of exactly solvable evaporating black holes*, 2104.00224.

[93] A. Bhattacharya, A. Bhattacharyya, P. Nandy and A. K. Patra, *Islands and complexity of eternal black hole and radiation subsystems for a doubly holographic model*, *JHEP* **05** (2021) 135 [2103.15852].

[94] T. J. Hollowood, S. Prem Kumar, A. Legramandi and N. Talwar, *Islands in the Stream of Hawking Radiation*, 2104.00052.

[95] A. Miyata and T. Ugajin, *Evaporation of black holes in flat space entangled with an auxiliary universe*, 2104.00183.

[96] K. Ghosh and C. Krishnan, *Dirichlet Baths and the Not-so-Fine-Grained Page Curve*, 2103.17253.

[97] M. Rozali, J. Sully, M. Van Raamsdonk, C. Waddell and D. Wakeham, *Information radiation in BCFT models of black holes*, *JHEP* **05** (2020) 004 [1910.12836].

[98] A. Almheiri, T. Hartman, J. Maldacena, E. Shaghoulian and A. Tajdini, *Replica Wormholes and the Entropy of Hawking Radiation*, *JHEP* **05** (2020) 013 [1911.12333].

[99] R. Bousso and M. Tomašević, *Unitarity From a Smooth Horizon?*, 1911.06305.

[100] C. Akers, N. Engelhardt and D. Harlow, *Simple holographic models of black hole evaporation*, 1910.00972.

[101] J. Sully, M. Van Raamsdonk and D. Wakeham, *BCFT entanglement entropy at large central charge and the black hole interior*, 2004.13088.

[102] Y. Chen, X.-L. Qi and P. Zhang, *Replica wormhole and information retrieval in the SYK model coupled to Majorana chains*, *JHEP* **06** (2020) 121 [2003.13147].

[103] S. B. Giddings and G. J. Turiaci, *Wormhole calculus, replicas, and entropies*, 2004.02900.

[104] I. Kim, E. Tang and J. Preskill, *The ghost in the radiation: Robust encodings of the black hole interior*, *JHEP* **20** (2020) 031 [2003.05451].

[105] H. Verlinde, *ER = EPR revisited: On the Entropy of an Einstein-Rosen Bridge*, 2003.13117.

[106] H. Liu and S. Vardhan, *A dynamical mechanism for the Page curve from quantum chaos*, 2002.05734.

[107] D. Harlow and E. Shaghoulian, *Global symmetry, Euclidean gravity, and the black hole information problem*, *JHEP* **04** (2021) 175 [2010.10539].

[108] Y. Nomura, *Black Hole Interior in Unitary Gauge Construction*, *Phys. Rev. D* **103** (2021) 066011 [2010.15827].

[109] P.-S. Hsin, L. V. Iliesiu and Z. Yang, *A violation of global symmetries from replica wormholes and the fate of black hole remnants*, 2011.09444.

[110] N. Gaddam and N. Groenenboom, *Soft graviton exchange and the information paradox*, 2012.02355.

[111] S. Pasterski and H. Verlinde, *HPS meets AMPS: How Soft Hair Dissolves the Firewall*, 2012.03850.

[112] S. Raju, *Lessons from the Information Paradox*, 2012.05770.

[113] R. Bousso and E. Wildenhain, *Gravity/Ensemble Duality*, 2006.16289.

[114] P. Cheng and Y. An, *Soft BHIP: Page curve from Maxwell soft hair of black hole*, 2012.14864.

[115] K. Su, P. Zhang and H. Zhai, *Page Curve from Non-Markovianity*, 2101.11238.

[116] E. E. Flanagan, *An order-unity correction to Hawking radiation*, 2102.04930.

[117] H. Geng, S. Lüst, R. K. Mishra and D. Wakeham, *Holographic BCFTs and Communicating Black Holes*, 2104.07039.

[118] F. Pastawski and J. Preskill, *Code properties from holographic geometries*, *Phys. Rev.* **X7** (2017) 021022 [1612.00017].

[119] P. Hayden and J. Preskill, *Black holes as mirrors: quantum information in random subsystems*, *JHEP* **09** (2007) 120 [0708.4025].

[120] J. Maldacena, D. Stanford and Z. Yang, *Conformal symmetry and its breaking in two dimensional Nearly Anti-de-Sitter space*, *PTEP* **2016** (2016) 12C104 [1606.01857].

[121] A. Almheiri and J. Polchinski, *Models of AdS_2 backreaction and holography*, *JHEP* **11** (2015) 014 [1402.6334].

[122] J. L. Cardy, *Conformal Invariance and Surface Critical Behavior*, *Nucl. Phys.* **B240** (1984) 514.

[123] P. Calabrese and J. Cardy, *Quantum Quenches in Extended Systems*, *J. Stat. Mech.* **0706** (2007) P06008 [0704.1880].

[124] A. Coser, E. Tonni and P. Calabrese, *Entanglement negativity after a global quantum quench*, *J. Stat. Mech.* **1412** (2014) P12017 [1410.0900].

[125] I. Affleck and A. W. W. Ludwig, *The fermi edge singularity and boundary condition changing operators*, *Journal of Physics A: Mathematical and General* **27** (1994) 5375.

[126] T. Takayanagi, *Holographic Dual of BCFT*, *Phys. Rev. Lett.* **107** (2011) 101602 [1105.5165].

[127] M. Fujita, T. Takayanagi and E. Tonni, *Aspects of AdS/BCFT*, *JHEP* **11** (2011) 043 [1108.5152].

[128] T. Hartman, *Entanglement Entropy at Large Central Charge*, 1303.6955.

[129] S. Leichenauer and M. Moosa, *Entanglement Tsunami in (1+1)-Dimensions*, *Phys. Rev.* **D92** (2015) 126004 [1505.04225].

[130] R. Bousso, Z. Fisher, S. Leichenauer and A. C. Wall, *Quantum focusing conjecture*, *Phys. Rev. D* **93** (2016) 064044 [1506.02669].

[131] B. Czech, J. L. Karczmarek, F. Nogueira and M. Van Raamsdonk, *The gravity dual of a density matrix*, *Class. Quant. Grav.* **29** (2012) 155009 [1204.1330].

[132] M. Headrick, V. E. Hubeny, A. Lawrence and M. Rangamani, *Causality & holographic entanglement entropy*, *JHEP* **12** (2014) 162 [1408.6300].

[133] A. C. Wall, *Maximin surfaces, and the strong subadditivity of the covariant holographic entanglement entropy*, *Class. Quant. Grav.* **31** (2014) 225007 [1211.3494].

[134] D. L. Jafferis, A. Lewkowycz, J. Maldacena and S. J. Suh, *Relative entropy equals bulk relative entropy*, *JHEP* **06** (2016) 004 [1512.06431].

[135] X. Dong, D. Harlow and A. C. Wall, *Reconstruction of Bulk Operators within the Entanglement Wedge in Gauge-Gravity Duality*, *Phys. Rev. Lett.* **117** (2016) 021601 [1601.05416].

[136] J. Cotler, P. Hayden, G. Penington, G. Salton, B. Swingle and M. Walter, *Entanglement Wedge Reconstruction via Universal Recovery Channels*, *Phys. Rev.* **X9** (2019) 031011 [1704.05839].

[137] A. Almheiri, X. Dong and D. Harlow, *Bulk Locality and Quantum Error Correction in AdS/CFT*, *JHEP* **04** (2015) 163 [1411.7041].

[138] F. Pastawski, B. Yoshida, D. Harlow and J. Preskill, *Holographic quantum error-correcting codes: Toy models for the bulk/boundary correspondence*, *JHEP* **06** (2015) 149 [1503.06237].

[139] D. Harlow, *The Ryu–Takayanagi Formula from Quantum Error Correction*, *Commun. Math. Phys.* **354** (2017) 865 [1607.03901].

[140] B. Yoshida, *Soft mode and interior operator in the Hayden-Preskill thought experiment*, *Phys. Rev.* **D100** (2019) 086001 [1812.07353].

[141] B. Yoshida, *Firewalls vs. Scrambling*, *JHEP* **10** (2019) 132 [1902.09763].

[142] B. Yoshida and A. Kitaev, *Efficient decoding for the Hayden-Preskill protocol*, 1710.03363.

[143] T. Ugajin, *Two dimensional quantum quenches and holography*, 1311.2562.

[144] T. Shimaji, T. Takayanagi and Z. Wei, *Holographic Quantum Circuits from Splitting/Joining Local Quenches*, *JHEP* **03** (2019) 165 [1812.01176].

[145] M. Fujita, T. Takayanagi and E. Tonni, *Aspects of ads/bcft*, *JHEP* **11** (2011) 043 [1108.5152].

[146] P. Di Francesco, P. Mathieu and D. Senechal, *Conformal Field Theory*, Graduate Texts in Contemporary Physics. Springer-Verlag, New York, 1997, 10.1007/978-1-4612-2256-9.

[147] J. Engelsy, T. G. Mertens and H. Verlinde, *An investigation of AdS_2 backreaction and holography*, *JHEP* **07** (2016) 139 [1606.03438].

[148] M. Abramowitz and I. A. Stegun, *Handbook of Mathematical Functions with Formulas, Graphs, and Mathematical Tables*. Dover, New York, ninth dover printing, tenth gpo printing ed., 1964.

[149] U. Moitra, S. K. Sake, S. P. Trivedi and V. Vishal, *Jackiw-Teitelboim Model Coupled to Conformal Matter in the Semi-Classical Limit*, *JHEP* **04** (2020) 199 [1908.08523].

[150] L. Susskind, L. Thorlacius and J. Uglum, *The Stretched horizon and black hole complementarity*, *Phys. Rev. D* **48** (1993) 3743 [hep-th/9306069].

[151] M. Headrick, *General properties of holographic entanglement entropy*, *JHEP* **03** (2014) 085 [1312.6717].

[152] T. Hartman, Y. Jiang and E. Shaghoulian, *Islands in cosmology*, 2008.01022.

[153] M. Van Raamsdonk, *Comments on wormholes, ensembles, and cosmology*, 2008.02259.

[154] V. Balasubramanian, A. Kar, S. F. Ross and T. Ugajin, *Spin structures and baby universes*, *JHEP* **09** (2020) 192 [2007.04333].

[155] T. Numasawa, *Four coupled SYK models and Nearly AdS_2 gravities: Phase Transitions in Traversable wormholes and in Bra-ket wormholes*, 2011.12962.

[156] S. Colin-Ellerin, X. Dong, D. Marolf, M. Rangamani and Z. Wang, *Real-time gravitational replicas: Formalism and a variational principle*, *JHEP* **05** (2021) 117 [2012.00828].

[157] D. Marolf and J. E. Santos, *AdS Euclidean wormholes*, 2101.08875.

[158] E. Casali, D. Marolf, H. Maxfield and M. Rangamani, *Baby Universes and Worldline Field Theories*, 2101.12221.

[159] P. Saad, S. H. Shenker, D. Stanford and S. Yao, *Wormholes without averaging*, 2103.16754.

[160] H. Verlinde, *Wormholes in Quantum Mechanics*, 2105.02129.

[161] M. Miyaji, T. Takayanagi and T. Ugajin, *Spectrum of End of the World Branes in Holographic BCFTs*, 2103.06893.

[162] L. Susskind, *Computational Complexity and Black Hole Horizons*, *Fortsch. Phys.* **64** (2016) 24 [1403.5695].

[163] D. Stanford and L. Susskind, *Complexity and Shock Wave Geometries*, *Phys. Rev. D* **90** (2014) 126007 [1406.2678].

[164] M. Alishahiha, *Holographic Complexity*, *Phys. Rev. D* **92** (2015) 126009 [1509.06614].

[165] D. Carmi, R. C. Myers and P. Rath, *Comments on Holographic Complexity*, *JHEP* **03** (2017) 118 [1612.00433].